


Springer Optimization and Its Applications 169

Ilias S. Kotsireas
Anna Nagurney
Panos M. Pardalos
Arsenios Tsokas *Editors*

Dynamics of Disasters

Impact, Risk, Resilience, and Solutions

 Springer

Springer Optimization and Its Applications

Volume 169

Series Editors

Panos M. Pardalos , *University of Florida*

My T. Thai , *University of Florida*

Honorary Editor

Ding-Zhu Du, *University of Texas at Dallas*

Advisory Editors

Roman V. Belavkin, *Middlesex University*

John R. Birge, *University of Chicago*

Sergiy Butenko, *Texas A&M University*

Vipin Kumar, *University of Minnesota*

Anna Nagurney, *University of Massachusetts Amherst*

Jun Pei, *Hefei University of Technology*

Oleg Prokopyev, *University of Pittsburgh*

Steffen Rebennack, *Karlsruhe Institute of Technology*

Mauricio Resende, *Amazon*

Tamás Terlaky, *Lehigh University*

Van Vu, *Yale University*

Michael N. Vrahatis, *University of Patras*

Guoliang Xue, *Arizona State University*

Yinyu Ye, *Stanford University*

Aims and Scope

Optimization has continued to expand in all directions at an astonishing rate. New algorithmic and theoretical techniques are continually developing and the diffusion into other disciplines is proceeding at a rapid pace, with a spot light on machine learning, artificial intelligence, and quantum computing. Our knowledge of all aspects of the field has grown even more profound. At the same time, one of the most striking trends in optimization is the constantly increasing emphasis on the interdisciplinary nature of the field. Optimization has been a basic tool in areas not limited to applied mathematics, engineering, medicine, economics, computer science, operations research, and other sciences.

The series **Springer Optimization and Its Applications (SOIA)** aims to publish state-of-the-art expository works (monographs, contributed volumes, textbooks, handbooks) that focus on theory, methods, and applications of optimization. Topics covered include, but are not limited to, nonlinear optimization, combinatorial optimization, continuous optimization, stochastic optimization, Bayesian optimization, optimal control, discrete optimization, multi-objective optimization, and more. New to the series portfolio include Works at the intersection of optimization and machine learning, artificial intelligence, and quantum computing.

Volumes from this series are indexed by Web of Science, zbMATH, Mathematical Reviews, and SCOPUS.

More information about this series at <http://www.springer.com/series/7393>

Ilias S. Kotsireas • Anna Nagurney
Panos M. Pardalos • Arsenios Tsokas
Editors

Dynamics of Disasters


Impact, Risk, Resilience, and Solutions

 Springer

Editors

Ilias S. Kotsireas
Department of Physics & Computer Science
Wilfrid Laurier University
Waterloo, ON, Canada

Anna Nagurney
Isenberg School of Management
University of Massachusetts Amherst
Amherst, MA, USA

Panos M. Pardalos 
Department of Industrial
and Systems Engineering
University of Florida
Gainesville, FL, USA

Arsenios Tsokas
University of Florida
Gainesville, FL, USA

ISSN 1931-6828 ISSN 1931-6836 (electronic)
Springer Optimization and Its Applications
ISBN 978-3-030-64972-2 ISBN 978-3-030-64973-9 (eBook)
<https://doi.org/10.1007/978-3-030-64973-9>

Mathematics Subject Classification: 90, 91, 65, 93

© Springer Nature Switzerland AG 2021

This work is subject to copyright. All rights are reserved by the Publisher, whether the whole or part of the material is concerned, specifically the rights of translation, reprinting, reuse of illustrations, recitation, broadcasting, reproduction on microfilms or in any other physical way, and transmission or information storage and retrieval, electronic adaptation, computer software, or by similar or dissimilar methodology now known or hereafter developed.

The use of general descriptive names, registered names, trademarks, service marks, etc. in this publication does not imply, even in the absence of a specific statement, that such names are exempt from the relevant protective laws and regulations and therefore free for general use.

The publisher, the authors, and the editors are safe to assume that the advice and information in this book are believed to be true and accurate at the date of publication. Neither the publisher nor the authors or the editors give a warranty, expressed or implied, with respect to the material contained herein or for any errors or omissions that may have been made. The publisher remains neutral with regard to jurisdictional claims in published maps and institutional affiliations.

This Springer imprint is published by the registered company Springer Nature Switzerland AG
The registered company address is: Gewerbestrasse 11, 6330 Cham, Switzerland

Preface

This volume is a collection of thoroughly reviewed papers presented at the 4th International Conference on Dynamics of Disasters held in Kalamata, Greece, July 1–5, 2019, with additional invited papers. The conference was organized by Ilias S. Kotsireas, Anna Nagurney, and Panos M. Pardalos and gathered disaster researchers to present and to discuss their latest scientific work. This volume of 16 chapters is organized alphabetically by the first initial of the last name of the first author of each chapter with highlights of each chapter given below.

The co-editors acknowledge the chapter authors and thank the reviewers for their thorough reports. Given that the number of disasters is growing, along with the number of people affected by them, and that we are in the midst of the COVID-19 pandemic, which is a global healthcare disaster, we believe that this edited book is especially timely.

Birce Adsanver, Elvin Coban, and Burcu Balcik in the first chapter of this volume, “Drone Routing for Post-disaster Damage Assessment,” focus on rapid damage assessment operations through the use of drones, specifically after an earthquake. They note that in the past seven decades, the number and severity of disasters has risen exponentially and that earthquakes are among the deadliest disasters. It is essential to assess earthquake damage to buildings rapidly since the survival rate for people rescued from collapsed buildings decreases dramatically over time. Hence, the use of available resources, such as drones, appropriately post disaster to ascertain building damage can save many lives. The chapter presents mathematical models and a solution approach for managing drones to scan an area affected by a disaster quickly. The authors’ approach divides the disaster-affected area into grids, with the grids clustered based on their attributes. Given a set of drones and a limited time for assessments, the authors tackle the problem of determining the grids to scan by each drone and the sequence of visits to the selected grids. The goal is to maximize the total priority score collected from the assessed grids while ensuring that the prespecified coverage ratio targets for the clusters are met. Interestingly, the authors adapt formulations from the literature for electric vehicle routing problems with recharging stations and propose two alternative mixed-integer linear programming models for the problem. Using an optimization

solver to assess the computational difficulty of solving the formulations, they find that both formulations perform similarly. Since time is of the essence in humanitarian operations, the authors also propose a practical constructive heuristic for their drone routing problem, which identifies high-quality solutions quickly. With a limited literature on the use of drones in humanitarian operations, this paper makes a valuable contribution.

Fuad Aleskerov and Sergey Demin in their chapter, “DEA for the Assessment of Regions’ Ability to Cope with Disasters,” construct modifications of Data Envelopment Analysis (DEA) methods in order to take into account inaccuracies in data, which, in real life, often consist of expert estimates or approximate values. DEA is based on the idea of efficiency assessment of different decision-making units (DMUs). To date, DEA has been applied for different disasters, including floods and technological disasters, as well as the vulnerability of certain regions to typhoons. The proposed two modified DEA methods are termed IDEA (interval DEA) methods by the authors. The first IDEA method, called the best tubed IDEA, is based on the idea that some DMUs might be near the efficiency frontier. The authors’ second proposed IDEA method is based on the idea that any parameter (both input and output) might be the most important during the comparison of the DMUs. They call the second method Pareto IDEA. They then apply the basic DEA and the two IDEA methods to rank preventive measures against wildfires in 46 regions of Russia and compare the results obtained.

Gerasimos Antzoulatos, Anastasios Karakostas, Stefanos Vrochidis, and Ioannis Kompatsiaris in their chapter, “The Crisis Classification Component to Strengthen the Early Warning, Risk Assessment and Decision Support in Extreme Climate Events,” propose the open-source holistic beAWARE framework to tackle the urgent need to enhance awareness and preparedness to assess risks and to support decision-making, aiming to increase the social resilience to climate change via novelty tools. Climate change is considered as one of the most important challenges of modern times, having multiple and significant impacts on human societies and environment. The negative effects, which are revealed through extreme weather events and cause distress and loss of property and human lives, will become more intensive in the future, especially in poor countries. The authors propose the open-source holistic beAWARE framework which encompasses technological achievements that enable first responders and authorities to manage efficiently the preemergency and emergency phases of a hazardous natural event. Specifically, the Crisis Classification component of beAWARE platform consolidates functionalities to provide dual services: (a) firstly, as an Early Warning system, aiming to estimate the crisis level of the upcoming extreme conditions such as the hazard from flood, fire, or heatwave (preemergency phase); (b) secondly, as a Real-Time Monitoring and Risk Assessment system, aiming to assess the risk and support to make accurate and timely decisions when a crisis is evolved.

Buket Cilali, Nafiseh Ghorbani-Renani, Kash Barker, and Andrés D. González in their chapter, “Toward Decentralized Decision Making for Interdependent Infrastructure Network Resilience,” discuss interdependence among infrastructure and community networks, as it is an important aspect to consider when planning for

disruptive events. Further, decision-makers within different infrastructures often make decentralized decisions to protect and restore their own networks after a disruption. They extend a resilience-based optimization model in various ways to depict different decentralized decision-making structures and hierarchies: divided budget, isolation assumption, and dominance assumption. Among others, they use social vulnerability scores to show the effect of community resilience and analyze different scenarios to reveal the effect of decentralization. They illustrate the model with a system of interdependent electric power, water, and gas infrastructure networks in Shelby County, TN.

Stefania Corsaro, Pasquale Luigi De Angelis, Ugo Fiore, Zelda Marino, Francesca Perla, and Mariafortuna Pietrolungo in their chapter, “Wavelets in Multiscale Time Series Analysis: An Application to Seismic Data,” tackle the important problem in earth science of forecasting earthquakes due to their potentially devastating consequences. Specifically, the authors focus on investigating the possibility of being able to determine when an earthquake will take place. The authors formulate the problem as a multiple change-point detection problem in the time series. In particular, they make use of a multiscale formulation, where, at each stage, multiple neighboring regions which correspond to locally constant underlying signals are merged. The authors emphasize that wavelets are suitable as basis functions, due to their multiscale structure, since the coefficients of the representation contain local information. The pre-processing stage, according to the authors, includes the discrete unbalanced Haar transform, which is a wavelet decomposition of one-dimensional data with respect to an orthonormal Haar-like basis, where jumps in the basis vectors do not necessarily occur in the middle of their support. Their algorithm is tested on data from a well-characterized laboratory system.

Ugo Fiore, Zelda Marino, Francesca Perla, Mariafortuna Pietrolungo, Salvatore Scognamiglio, and Paolo Zanetti in their chapter, “Effectiveness of Investments in Prevention of Geological Disasters,” address the topic of geological disasters, which are ubiquitous, and the awareness of such disasters is also growing. Furthermore, it is thought that climate change will exacerbate geological disasters in terms of both frequency and magnitude. Specifically, the authors, in their study, investigate the relationship between the number of prevention projects and the number of subsequent geological disasters, accounting for the effect of geographical distribution. They perform their analysis on historical data provided by the Chinese Statistics Bureau. The dataset details the number of disasters that occurred and the number of prevention projects that were carried out in China between 2004 and 2017, by region. The authors utilize a recurrent neural network of the Long Short-Term Memory (LSTM) type to forecast the number of geological disasters in China. The accuracy of predictions was measured with and without including data relative to the number of prevention projects. In addition, well-known statistical methods provided a verification. The authors note that an LSTM recurrent neural network is a powerful and versatile tool in the analysis of time series data and can yield insights when it is also coupled with a module able to handle grouping information. Their results show

that it is possible to identify evidence of a connection between prevention projects and a reduction in the number of disasters.

Bernhard Garn, Klaus Kieseberg, Dominik Schreiber, and Dimitris E. Simos in their chapter, “Cyber Crises and Disaster Preparation in Austria: A Survey of Research Projects,” provide an overview and analysis of research projects within the security research-orientated KIRAS funding scheme in Austria dealing with issues of disaster preparation, giving special attention to projects concentrating on threats originating from the cyber domain. They analyze several projects dealing with crisis management and disaster response, in particular those focusing on ex-postcoordination efforts in conjunction with software supporting these activities. Regarding the cyber domain, they illustrate and exemplify how multiple research projects addressed issues arising in cyber crisis management, cyber disaster scenario generation, and cyber incident response trainings. Major parts of their chapter deal specifically with efforts conducted in Austria, but they also point out similar activities in other countries and on an international as well as European level. They conclude with a list of recommendations for the general conduct of disaster preparation activities, highlighting universal best practices and instilling motivation for future research endeavors geared towards strengthening disaster and crisis preparation efforts.

Mehdi Ghazanfari, Mohammadmehdi Hakimifar, Tina Wakolbinger, and Fuminori Toyasaki in their chapter, “Disaster Preparedness at the Municipality Level: A Scenario-Based Multi-stage Measurement Methodology,” present a framework for assessing disaster preparedness of municipalities or local governments of urban areas that can be used by policy-makers. The framework considers multi-stage aspects of disaster preparedness by integrating the pre- and post-disaster status, with preparedness being based on the four areas of hazard assessment, mitigation capabilities, resource assessment, and management performance. The authors provide a methodology incorporating several dimensions over three phases: the pre-disaster study, post-disaster prediction, and assessment. Their methodological framework differs from those reported on in the existing literature which focus on specific aspects of preparedness such as social, technical, and infrastructural. The authors discuss in detail the delineation of the three phases into further stages and the associated dimensions and their components that need to be examined. Radar diagrams for illustrative purposes are provided. The authors illustrate how the preparedness levels over different dimensions or resources or parameters in different phases for distinct disaster scenarios can be presented. Implementation of the comprehensive methodology can help municipal governments in identifying their level of disaster preparedness. Furthermore, the methodology can contribute to strengthening their readiness, as the authors note, by highlighting areas of weakness.

Yutaka Matsuno, Futaba Fukanuma, and Shigenobu Tsuruoka in their chapter, “Development of Flood Disaster Prevention Simulation Smartphone Application Using Gamification,” develop a smartphone application for simulating flood disaster evacuation that is based on gamification. Their study is inspired by the need to increase public awareness of disaster preparedness knowledge, including hazard maps, especially in the setting of Japan and its frequent flood disasters. According

to the authors, it is predicted that the frequency of heavy rain, the amount of floods, and the frequency of short-term heavy rain is expected to increase in Japan in the future due to global warming. The authors state that a hazard map is one that displays disaster-predicted areas and locations of disaster prevention facilities such as evacuation points and routes. The authors report on the design and development of a disaster prevention smartphone application with such characteristics as ease of use, continuity (users want to use it continuously), learning effects, and interest improvement. Their evaluation of the smartphone application using subject experiments with 20 participants revealed that the smartphone application is effective as compared to only using hazard maps.

John A. Mpekiaris and George D. Tsiotras in their chapter, “Natural Disasters and Their Impact on Business Units: The Greek Case,” contain the result of a survey questionnaire consisting of 45 items, with a focus on disaster types often encountered within Greece, such as floods, wildfires, and earthquakes. The study addresses the current situation in terms of Greek companies’ awareness, preparedness, and resilience against catastrophic events. The study seeks to document the implications of catastrophic events on business activities as well as the perception of entrepreneurs on business continuity and post-disaster recovery. The findings in the authors’ study reveal that crucial business continuity matters depend on particular company features. In particular, large corporations of complex legal form with many years of operation seem to be more prepared both in terms of prevention and post-disaster measures. Furthermore, the study found that only one of every four Greek entrepreneurs is aware of the nature and content of business continuity and recovery plans. The authors emphasize the clear need for governmental actions geared to emphasize the importance of business continuity planning when addressing the aftermath of a disaster.

Anna Nagurney in her chapter, “Perishable Food Supply Chain Networks with Labor in the COVID-19 pandemic,” bridges operations research and economics by constructing a supply chain generalized network optimization model for perishable food products that explicitly includes labor availability associated with the supply chain activities of production, transportation, storage, and distribution. The model is in response to the challenges of quantifying the impacts on perishable food supply chains of the COVID-19 pandemic, which was declared by the World Health Organization on March 11, 2020. The pandemic, which is a global healthcare disaster, has resulted in millions of illnesses and hundreds of thousands of deaths and has affected a plethora of food supply chains, including meat and fresh produce, due to disruptions in the labor supply, the need for social distancing to reduce contagion, losses in productivity, as well as transportation issues. The author considers a food firm that seeks to maximize profits (for its business sustainability) with the objective function including revenue and operational and discarding costs as well as costs of labor. The author utilizes linear production functions to map labor on a link to product flow. A variational inequality formulation of the problem is derived, and an algorithm is proposed that computes the optimal food product flows and the Lagrange multipliers associated with the capacities on labor. Numerical examples are presented for a fresh produce product – cantaloupes, in which the quality

deterioration is also captured. The numerical examples quantify the impacts of labor disruptions, in terms of reductions in availability as well as in productivity, on the food firm's profit, the demand market prices, product flows, and demands. They also reveal the potential positive effects of adding direct demand markets, as in the case of farm stands and farmers' markets, and enhanced marketing resulting in change in the demand market prices.

Anna Nagurney, Patrizia Daniele, and Giorgia Cappello in their chapter, "Capacitated Human Migration Networks and Subsidization," address one of the greatest challenges of the twenty-first century – that of large-scale human migration flows with drivers ranging from climate change and various disasters to wars, violence, and poverty. They build on the literature of human migration networks and construct extensions of multiclass user-optimized (U-O) and system-optimized (S-O) models to incorporate capacities associated with locations in the network economy. The authors introduce a policy framework, in the form of subsidies, that, when applied, guarantees that the system-optimized solution of the multiclass capacitated human migration network problem is also user-optimized. Such policies enable governments, and policy-making bodies, to achieve optimal societal welfare in terms of the location of the migrants in the network economy, while the migrants locate independently in a U-O manner. The authors provide alternative variational inequality formulations of the novel U-O and S-O models, which include Lagrange multipliers associated with the location capacity constraints. The values of the Lagrange multipliers at the equilibrium/optimal solutions provide valuable economic information for decision-makers. Analogies to transportation networks and associated U-O and S-O behavior are drawn, along with policies, in the form of tolls. An effective algorithm, which exploits the special network structure of the models, is detailed and applied to compute solutions to a series of examples, both uncapacitated and capacitated ones, along with the subsidies for the latter. The authors note that their modeling and computational approach allows for the investigation and evaluation of different disaster scenarios as when there are population changes and/or modifications to utility functions because of impacted infrastructure.

Stamatis Papangelou and Zinos Alexios Charalampidis in their chapter, "Land Property Data Logging on Blockchain Ledger," turn to the important problem of evaluating property risk, since there are many different types of risk that can affect properties, including wildfire risk and even excessive moisture. The underlying motivation for this work stems, in part, from the problems that arise, post-disaster, when retrieving information about damaged land properties, which may be both time consuming and may involve a lot of bureaucracy. Their goal is to combine a wide range of parameters associated with risk indexes that not only evaluate each property individually but different sub-indexes within a property in the case of different types of disasters. The different types of disasters relevant to their problem are natural disasters, man-made disasters, and types of construction. The authors, in this chapter, discuss a specific method that uses block-chain technology and specialized equipment to collect and register land property information. Such information is critical for individuals, governments, as well as insurance-based

companies for evaluating risk associated with disasters. For reasons of data integrity and transparency, all of this information is available on a public blockchain ledger. As noted by the authors, blockchain is an ordered list of records that are called blocks, which contain crypto-graphic stamps that are connected with every previous block and all the information within the block. It is a decentralized, usually public, and distributed digital ledger that is used to record transactions and data across many computers so that any involved record cannot be modified retroactively, without the modification of all subsequent blocks. The authors also describe how blockchain technology can ensure risk evaluation transparency and discuss a specific system that acquires data from the field as well as the processing of such data in the cloud.

Urmila Pyakurel and Stephan Demepe in their chapter, “Universal Maximal Flow with Intermediate Storage for Evacuation Planning,” address the important problem of evacuation modeling and solution, which is very relevant in disaster settings. In evacuation models, one wishes to shift evacuees from emergency areas (sources) to places of safety (sinks) as quickly and as efficiently as possible. The majority of the flow over time models used in evacuation planning, they note, are based on the flow conservation constraints, that is, the inflow must be equal to the outflow at each node with the exception of at the sources and sinks. The authors study, in contrast, the universal maximum flow problem with intermediate storage. In this evacuation problem type, the inflow may be greater than the outflow at intermediate nodes, which maximizes the number of evacuees leaving the emergency areas at each point of time. The authors construct efficient algorithms to solve the problem on two-terminal series-parallel and general networks. In addition, they also discuss an algorithm for the problem with arc reversal capability, as would occur in the case of contraflow, and compare these solutions without and with intermediate storage. Enabling contraflow in an evacuation network increases the outbound road capacities by reversing the direction of the flow. This chapter enriches the literature on evacuation planning for disasters.

Alexander Streicher, Rainer Schönbein, and Stefan Wolfgang Pickl in their chapter, “A General Framework and Control Theoretic Approach for Adaptive Interactive Learning Environments,” argue how disaster risk management can gain from the application of serious games as motivational and engaging tools to foster disaster response competencies through personalized or adaptive interactive learning environments. Their study proposes the transfer of adaptive control to adaptive learning systems with special focus on interactive learning environments such as educational serious games (also known as digital game based learning) or computer simulations. The general idea is to adapt systems theory and control theory to the control processes of adaptive learning systems. Adaptive learning environments should adapt to the context-related needs of the user in order to ensure and optimize learning success, especially for disaster management training. Furthermore, since the setting is that of complex systems with nonlinear and stochastic processes, they also propose to adopt adaptive control theory with reference models. This chapter is a contribution to the state of the art for adaptive games or simulations in disaster risk management.

Georgios Tsaples, Josep Maria Salanova Grau, Georgia Aifadopoulou, and Panagiotis Tzenos in their chapter, “A Simulation Model for the Analysis of the Consequences of Extreme Weather Conditions to the Traffic Status of the City of Thessaloniki, Greece,” present a decision-support tool that allows for the efficient and effective monitoring of the status of the transportation network and crisis management planning in the case of flooding. They develop a simulation model, which is combined with real-time Floating Car Data from a fleet of taxis in the city of Thessaloniki, Greece. Hence, in their study, two methodological frameworks are combined: data analytics and simulation. Thessaloniki regularly suffers from flooding that results in dire traffic conditions and obstructs the movement of vehicles. The authors emphasize that extreme weather conditions – such as flooding or snow blizzards – that were once considered events of low probability have become a recurring concern for local authorities, high-level policy-makers, and also citizens. The model was tested for two different scenarios that simulate different types of rain. The results obtained by the authors reveal that the consequences can be seen long after the rain has stopped and can last for lengthy periods resulting in a transportation system with extremely low level of service and in a state of disequilibrium. The chapter shows that policy-makers must integrate their decision-making processes regarding the transportation sector in a crisis management framework.

Waterloo, ON, Canada	Ilias S. Kotsireas
Amherst, MA, USA	Anna Nagurney
Gainesville, FL, USA	Panos M. Pardalos
Gainesville, FL, USA	Arsenios Tsokas

Contents

Drone Routing for Post-disaster Damage Assessment	1
Birce Adsanver, Elvin Coban, and Burcu Balcik	
DEA for the Assessment of Regions' Ability to Cope with Disasters	31
Fuad Aleskerov and Sergey Demin	
The Crisis Classification Component to Strengthen the Early Warning, Risk Assessment and Decision Support in Extreme Climate Events	39
Gerasimos Antzoulatos, Anastasios Karakostas, Stefanos Vrochidis, and Ioannis Kompatsiaris	
Toward Decentralized Decision-Making for Interdependent Infrastructure Network Resilience	67
Buket Cilali, Nafiseh Ghorbani-Renani, Kash Barker, and Andrés D. González	
Wavelets in Multi-Scale Time Series Analysis: An Application to Seismic Data	93
Stefania Corsaro, Pasquale Luigi De Angelis, Ugo Fiore, Zelda Marino, Francesca Perla, and Mariafortuna Pietroluongo	
Effectiveness of Investments in Prevention of Geological Disasters	101
Ugo Fiore, Zelda Marino, Francesca Perla, Mariafortuna Pietroluongo, Salvatore Scognamiglio, and Paolo Zanetti	
Cyber Crises and Disaster Preparation in Austria: A Survey of Research Projects	109
Bernhard Garn, Klaus Kieseberg, Dominik Schreiber, and Dimitris E. Simos	

Disaster Preparedness at the Municipality Level: A Scenario-Based Multistage Measurement Methodology	123
Mehdi Ghazanfari, Mohammadmehdi Hakimifar, Tina Wakolbinger, and Fuminori Toyasaki	
Development of Flood Disaster Prevention Simulation Smartphone Application Using Gamification	147
Yutaka Matsuno, Futaba Fukanuma, and Shigenobu Tsuruoka	
Natural Disasters and Their Impact on Business Units: The Greek Case	161
John A. Mpekiaris and George D. Tsiotras	
Perishable Food Supply Chain Networks with Labor in the Covid-19 Pandemic	173
Anna Nagurney	
Capacitated Human Migration Networks and Subsidization	195
Anna Nagurney, Patrizia Daniele, and Giorgia Cappello	
Land Property Data Logging on Blockchain Ledger	219
Stamatis Papangelou and Zinos Alexios Charalampidis	
Universal Maximum Flow with Intermediate Storage for Evacuation Planning	229
Urmila Pyakurel and Stephan Dempe	
A General Framework and Control Theoretic Approach for Adaptive Interactive Learning Environments	243
Alexander Streicher, Rainer Schönbein, and Stefan Wolfgang Pickl	
A Simulation Model for the Analysis of the Consequences of Extreme Weather Conditions to the Traffic Status of the City of Thessaloniki, Greece	259
Georgios Tsaples, Josep Maria Salanova Grau, Georgia Aifadopoulou, and Panagiotis Tzenos	

Drone Routing for Post-disaster Damage Assessment



Birce Adsanver, Elvin Coban, and Burcu Balcik

Abstract We consider drones to support post-disaster damage assessment operations when the disaster-affected area is divided into grids and grids are clustered based on their attributes. Specifically, given a set of drones and a limited time for assessments, we address the problem of determining the grids to scan by each drone and the sequence of visits to the selected grids. We aim to maximize the total priority score collected from the assessed grids while ensuring that the pre-specified coverage ratio targets for the clusters are met. We adapt formulations from the literature developed for electric vehicle routing problems with recharging stations and propose two alternative mixed-integer linear programming models for our problem. We use an optimization solver to evaluate the computational difficulty of solving different formulations and show that both formulations perform similarly. We also develop a practical constructive heuristic to solve the proposed drone routing problem, which can find high-quality solutions rapidly. We evaluate the performance of the heuristic with respect to both mathematical models in a variety of instances with the different numbers of drones and grids.

Keywords Post-disaster · Drone · Routing · Damage assessment · Constructive heuristic

1 Introduction

In the last 70 years, the number and severity of disasters have risen exponentially [39]. The Emergency Events Database (EM-DAT) reports 3,751 natural disasters that occurred between 2008 and 2017 [24], and the average number of deaths is about 60,000 per year [22]. Effective and efficient disaster response operations are essential to delivering relief supplies at the right places and times to minimize

B. Adsanver (✉) · E. Coban · B. Balcik
Industrial Engineering Department, Ozyegin University, Cekmekoy, Istanbul, Turkey
e-mail: birce.adsanver@ozu.edu.tr; elvin.coban@ozyegin.edu.tr; burcu.balcik@ozyegin.edu.tr

© Springer Nature Switzerland AG 2021

I. S. Kotsireas et al. (eds.), *Dynamics of Disasters*, Springer Optimization and Its Applications 169, https://doi.org/10.1007/978-3-030-64973-9_1

human suffering and death [25]. Moreover, the overall success of disaster operations is highly dependent on the speed of rapid needs and damage assessment phases, during which the extent of disaster's impact on people and infrastructure is evaluated [5].

In this study, we focus on rapid damage assessment operations conducted by using drones. While drones can be used to assess the damages on the built infrastructure in the aftermath of other disasters such as floods or hurricanes, we particularly consider a post-disaster environment after an earthquake. Earthquakes are among the deadliest disasters [22]. For instance, in 2004 and 2010, earthquakes accounted for 93% and 69% of worldwide deaths due to disasters [22]. It is critical to assess the earthquake damage on buildings rapidly since the survival rate for the people who are rescued from the collapsed buildings after an earthquake is 91% during the first 30 min, while it decreases to 81% on the first day and 36% on the second day [40]. Therefore, using available resources (such as drones or other technology) effectively after a disaster to identify the damaged buildings can save many lives.

Areas that are hit by earthquakes can be assessed by a variety of visual imaging and 3D mapping technologies, such as satellite imagery or radars. However, there are limitations to using each technology; for instance, satellite mapping may not meet high-resolution requirements due to clouds blocking the image. Recently, drones are increasingly used to assess earthquake damages [14, 48]. Drones can be deployed immediately after a disaster, and high-resolution images can be generated for the scanned regions, which would help to identify highly damaged areas quickly and direct the rescue teams to the correct spots and hence prioritize the use of relief resources effectively [29, 31]. For instance, in the aftermath of the 2015 Nepal earthquake, drones assisted in creating 3D maps through image processing software to assess the widespread damage and operate search and evacuation operations. Additionally, drones were used to identify the damaged infrastructure after an F-5 tornado in Wichita, Kansas [2]. Although drones have limited battery capacity, their flight duration can be extended by allowing them to recharge at the recharging stations (RSs) that would be positioned in the affected regions. Nevertheless, it may not be possible to assess the entire disaster-affected area rapidly by using a limited number of drones. However, the amount of useful information obtained by a limited number of drones in a restricted time period can be improved by selecting which areas to scan first. For instance, information obtained by drones that scan a part of the affected region can be used to estimate the damage status of the unscanned affected regions if different regions share similar disaster risk attributes that could affect the extent of earthquake damage. This study aims to present mathematical models and a solution approach that would support managing drones to scan a disaster-affected area quickly.

We consider a post-disaster setting, in which the drones assess the physical damage after an earthquake. The disaster-affected area is divided into grids. Each grid has a set of attributes comprising its infrastructure (e.g., construction types of the buildings), geographical (e.g., elevation), geological (e.g., soil type), and socioeconomic (e.g., wealth index) conditions. We assume that the damage level

of the built environment in a grid is highly correlated with its attribute values. The attributes can be associated with pre-disaster and post-disaster aspects. For instance, the construction types of the buildings and soil type may be specified before a disaster, while the distance to the earthquake epicenter is a post-disaster attribute [11, 46]. We assume that grids that have similar attributes are more likely to exhibit similar damage levels due to an earthquake [47]. Hence, grids can be clustered based on their similarities according to the relevant set of attributes by using various clustering methods such as k -modes clustering [47]. Since assessment of all grids in a limited amount of time may be impossible, scanning two grids belonging to different clusters may be preferred more than scanning two grids from the same cluster as information obtained from scanning a particular grid can be used to estimate the damages in the other grids of the cluster. Moreover, grids can be given different priorities based on whether a grid is densely populated and/or there is an important facility in the grid such as hospitals and schools. We focus on planning the routes of drones by considering grid clusters and priorities.

Given a set of drones and a limited time for assessments, we address the problem of determining the grids to scan and assess by each drone and the sequence of visits to the selected grids to maximize the total priority score collected from the assessed grids. We cluster grids before making routing plans based on various relevant pre- and post-disaster attributes. Then, a minimum level of coverage ratio for each cluster is targeted to achieve adequate and balanced information among all clusters, where the coverage ratio is defined as the ratio of the number of visited grids in a cluster to the total number of grids in that cluster. Nevertheless, it may not be possible to achieve the coverage target within a limited time, which may lead to infeasible solutions. To avoid infeasibilities, we penalize the maximum unfilled coverage ratio in the objective function. Moreover, if the coverage ratio is satisfied for all clusters but there is still time in the given assessment period, additional grids can still be scanned to increase the amount of collected information and hence the total priority score.

To extend drones' flight duration, we consider several RSs already positioned in the region where drones can recharge their batteries. The drone routing problem has some similarities with the electric vehicle routing problem (E-VRP) or green vehicle routing problem (G-VRP) since recharging times and locations of drones must be considered while determining the sequence of visits to the grids. However, the proposed drone routing problem is different due to its objective function and the coverage ratio constraint, which are introduced to capture the characteristics of the post-disaster damage assessment operations. We develop two mixed-integer linear programming (MILP) models, which are adapted from [19], and propose a novel heuristic to find high-quality solutions rapidly to assist decision-makers in making effective and efficient plans for drone routing during the damage assessment phase.

The rest of the paper is organized as follows. Section 2 reviews the relevant literature. Section 3 describes the system and problem in detail and presents our MILP model formulations. Section 4 describes the proposed heuristic, whereas Sect. 5 introduces the data set developed and reports the results of the computational experiments performed. Finally, we conclude in Sect. 6 and discuss future work.

2 Literature Review

Drones are relatively inexpensive and easy to deploy and use for supporting not only military applications but also civilian applications [12]. Since they can carry cameras [42], sensors [8], and mail [13], they are utilized frequently in several sectors such as agriculture, commerce, and construction. Nowadays, they are also used in humanitarian relief operations [15, 17, 33].

Drones were utilized in various past disasters to gather information about post-disaster situations, for example, to measure radiation contamination in the Daiichi nuclear power plant [43], capture the images of damaged reactors after the Japan East great earthquake in 2011 [33], monitor the affected area after the 2011 Thailand floods [34], and assess the damages after the 2016 Kumamoto earthquake [48], the 2009 L'Aquila earthquake [14], and Typhoon Haiyan in the Philippines [27]. Thus, integrating drones into the existing post-disaster operations may accelerate the information-gathering process and help rescuers to make timely and efficient decisions.

Integrating drones at the applications of commercial logistics is well studied in the literature [1, 21, 35, 36]; however, there are relatively few studies that focus on humanitarian applications. In particular, the studies that consider using drones in humanitarian settings address finding the location of relief facilities [7, 10, 20], distributing relief or medical items [26, 41], and post-disaster monitoring [9, 38].

An edge-based facility location problem where drones deliver relief items to aid recipients is studied in [20]. In this work, aid recipients are distributed along the network edges, and they can only travel to the distribution centers by using the accessible edges. The authors propose a mixed-integer non-linear programming model and metaheuristic algorithms to find the locations of facilities minimizing the aggregate traveling time for both the aid recipients and drones. Similarly, in [10], the authors determine the locations of the distribution centers, their corresponding service regions, and the number of emergency supplies to be kept in these centers by proposing a continuous approximation model to minimize the overall distribution cost of trucks and drones. The authors consider various drone-specific aspects such as accelerating, decelerating, and velocity changes while calculating the transportation cost. Additionally, a facility coverage problem is studied in [7] considering drone energy consumption and drone flight range limitations. A location-allocation problem for positioning recharging stations is addressed by [45]. In [41], the authors focus on drone routing decisions for last-mile distribution, where energy consumption is dependent on the weight of the payload. The authors develop a MILP model to minimize the total traveling distance while considering several priority policies on the locations. A MILP and metaheuristics are proposed to scan the post-disaster-affected areas to minimize the total assessment costs in [9]. In [38], the authors study a post-disaster damage assessment strategy that focuses on population points (nodes) and road segments (arcs), where the damage level of nodes and arcs is assessed by drones and motorcycles. The authors consider the drones' battery time as a time limit for damage assessment operations, such that all vehicles must

return to the depot before the time limit. Drones can assess the roads that are covered by debris; however, the motorcycles are restricted by the debris. Additionally, the authors prioritize the critical nodes and arcs in the affected network and present a multi-objective MILP model to maximize the total profit collected by visiting nodes and traversing arcs.

In [37], a post-earthquake relief distribution system is proposed where drones are used to serve areas that are inaccessible by ground transportation. In the proposed system, there is a data analysis center, where the information from different sources (e.g., social media, rescue employees, police reports, satellite images, and drone monitoring) must be analyzed thoroughly. After analyzing the information, the data analysis center shares relevant information with the other centers that manage the response stage. In our study, we consider a similar information-sharing system, in which the damage information of the disaster-affected region is gathered in a single operation center after drones scan the area.

To extend the flight duration of drones, we allow drones to visit recharging stations (RS) along their routes. In this respect, the drone routing problem is similar to the electric vehicle routing problems (E-VRP), which are addressed by a large number of studies (e.g., [3, 19, 28, 30, 32, 44]). Schneider et al. [44] formulate an electric vehicle routing problem with time windows and cargo capacity constraints. The vehicles are fully charged at an RS, and the recharging time is linearly dependent on the battery level at the RS. Froger et al. [19] allow partial charging and non-linear charging functions and present three formulations by utilizing different decision variables: node-based, arc-based, and path-based. The arc-based formulation is shown to perform better than the node-based formulation due to the tighter linear relaxation [19]. However, both the node-based and the arc-based formulations require dummy RSs (i.e., recharging station copies) to allow multiple visits; and deciding the number of dummy RSs has a critical impact on the solution [19, 32]. While a large number of dummy RSs increase the computational time, few dummy RSs may cut off the optimal solutions. On the other hand, the path-based formulation is not limited by the number of RS replications [19].

In this study, we adapt arc-based and path-based formulations from [19] for our drone routing problem that addresses post-disaster damage assessment operations. There are several differences between our problem and the existing E-VRPs. Specifically, we maximize the total priority scores collected by visiting the grids, while the objective in [19] is to minimize the total time including the traveling time and recharging time. Besides, we consider a grid network, where the disaster-related attributes of the grids are utilized to assign each grid to a cluster, and only a subset of grids may be visited under a limited assessment period. We additionally consider a pre-specified coverage target for each cluster. Our study contributes to the literature by presenting a new routing problem as well as formulations and a practical heuristic to support decision-making in managing post-disaster damage assessment operations via drones.

3 Problem Definition

We consider a post-disaster setting, in which the drones assess the physical damage in the built environment after an earthquake. The disaster-affected area is divided into grids, and we address the problem of determining the grids to scan and assess by each drone and the sequence of visits to the selected grids given a set of identical drones and a limited time for assessments. We aim to maximize the total priority score collected from the assessed grids.

Grids may have different priorities, reflecting the urgency of visiting this grid, based on whether a grid is densely populated and/or there is an important facility, such as hospitals. Moreover, we propose to utilize the disaster-related characteristics, *attributes*, of the grids to make an inference about the physical damage without covering the entire set of grids as rapid coverage of the entire set of grids may not be possible. First, grids are clustered according to their attributes so that grids in the same clusters have similar attributes. Thus, gathering information about a finite number of grids from a cluster may allow us to predict the damage level of the remaining grids in that cluster. We also define a coverage ratio target for each cluster, where *the coverage ratio* equals the ratio of the number of visited grids in a cluster to the total number of grids in that cluster. However, it may not be possible to achieve the pre-specified coverage ratio target for each cluster in a limited time. Therefore, the coverage ratio constraint is transformed into a soft constraint, such that the maximum unfulfilled coverage is penalized in the objective function with a very large number. Thus, we aim to achieve balanced and adequate information among all clusters with this single objective function.

We assume a single operation center where the scanned images are analyzed. Each drone has a battery capacity and a maximum tour duration, T_{\max} . Hence, drones that leave the operation center have to return within T_{\max} time units. Drones are recharged at the RSs to extend their flight time, and the recharging time is calculated by assuming a linear battery charging rate. We assume that drones leave the operation center and the RSs fully charged. In addition, we assume that the RSs are located at the center of grids and the travel time between two grids is equivalent to the travel time between the center of these grids. Figure 1 illustrates an area of 16 grids, which belong to 5 clusters indicated by different shapes on the figure. For example, grids #1, #6, and #7 are in the same cluster. There exist three RSs located at the center of grids #2, #5, and #11. The priority scores of each grid are also shown on the figure in parenthesis. We present an example route, in which the drone scans and assesses seven grids in total and is recharged at the RS located at grid #2.

We model this drone routing problem by maximizing the total priority score collected from the assessed locations while ensuring sufficient coverage for each cluster by two MILP formulations, (i) an arc-based formulation and (ii) a path-based formulation, presented in Sects. 3.1 and 3.2, respectively.

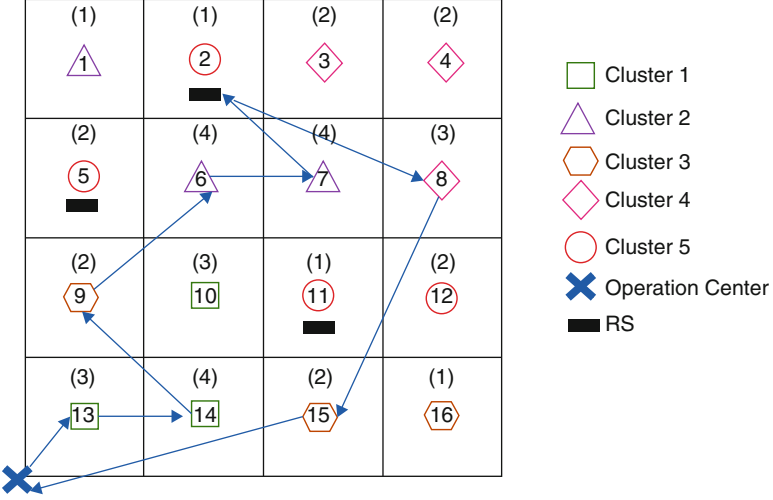


Fig. 1 Representation of a disaster-affected area divided into 16 grids and a drone's route

3.1 Arc-Based Formulation

The proposed drone routing problem is first formulated by an arc-based formulation, adapted from [19]. In the arc-based formulation, vertices represent the grid centers, and arcs connect these vertices. Let I represent the set of grids, and V_R specifies the set of RSs. V'_R defines the set of dummy RSs generated to allow multiple visits to each RS. 0 and $N + 1$ denote the operation center, such that each route starts at 0 and ends at $N + 1$. Let $V_0 = I \cup V'_R \cup \{0\}$ be the set of departure vertices and $V_1 = I \cup V'_R \cup \{N + 1\}$ be the set of arrival vertices. $V' = I \cup V'_R$ denotes the set of vertices except the operation center. We define the drone routing problem on a directed graph $G = (V, A)$, where $V = I \cup V'_R \cup \{0\} \cup \{N + 1\}$ and A is the set of arcs $A = \{(i, j) : i, j \in V, i \neq j\}$. C denotes the set of clusters.

Let s_j denote the survey time of grid j ; and t_{ij} is travel time when a drone travels on arc (i, j) . We represent energy consumption on arc (i, j) in terms of travel time. B specifies the battery capacity, i.e., maximum flight time, and r represents the recharging rate. The route duration limit is denoted by T_{\max} , such that each drone must return to the operation center within T_{\max} time units. Additionally, the number of available drones is indicated by D . ρ_j represents the priority score assigned to the grid j . Moreover, ϕ_{jc} is the coverage parameter that equals 1 if grid j is assigned to cluster c and 0 otherwise. Additionally, we define τ_c which indicates the total number of grids in cluster c . μ is the coverage ratio target, and M is a sufficiently large number used to allow the model to report a feasible solution when there exists an infeasibility related to the coverage ratio target.

Let the binary variable x_{ij} equals to 1 if a drone travels on arc (i, j) and 0 otherwise. The continuous variables a_{ij} and y_{ij} denote the time and the battery level,

respectively, when a drone departs from vertex $i \in V_0$ and travels on arc $(i, j) \in A$. The binary variable z_j takes the value of 1 if and only if the grid $j \in I$ is surveyed. The continuous variable q_j denotes the remaining battery when the drone arrives at RS $j \in V'_R$. The continuous variable θ_j denotes the amount of time required to fully charge a drone at RS j . The continuous variables β_c and γ denote the coverage ratio of cluster $c \in C$ and the minimum coverage ratio overall clusters, respectively. Finally, the continuous variable Δ is defined as the difference between the achieved coverage ratio and the coverage ratio target. If the coverage ratio target is satisfied, Δ equals zero.

The parameters and variables of the arc-based formulation provided below are summarized in Appendix 1.

$$\max \sum_{j \in I} \rho_j z_j - M \Delta \quad (1)$$

subject to

$$\sum_{\substack{j \in V_1 \\ j \neq i}} x_{ij} \leq 1 \quad \forall i \in I \quad (2)$$

$$\sum_{\substack{j \in V_1 \\ j \neq i}} x_{ij} \leq 1 \quad \forall i \in V'_R \quad (3)$$

$$\sum_{\substack{j \in V_1 \\ j \neq i}} x_{ij} - \sum_{\substack{j \in V_0 \\ j \neq i}} x_{ij} = 0 \quad \forall i \in V' \quad (4)$$

$$\sum_{j \in V_1} x_{0j} = D \quad (5)$$

$$\sum_{i \in V_0} x_{i,N+1} = D \quad (6)$$

$$z_j - \sum_{\substack{i \in V_0 \\ i \neq j}} x_{ij} = 0 \quad \forall j \in I \quad (7)$$

$$y_{0j} = Bx_{0j} \quad \forall j \in V_1 \quad (8)$$

$$\sum_{\substack{i \in V_0 \\ i \neq j}} y_{ij} - \sum_{\substack{i \in V_0 \\ i \neq j}} (t_{ij} + s_j)x_{ij} = \sum_{\substack{l \in V_1 \\ l \neq j}} y_{jl} \quad \forall j \in I \quad (9)$$

$$\sum_{\substack{i \in V_0 \\ i \neq j}} y_{ij} - \sum_{\substack{i \in V_0 \\ i \neq j}} t_{ij} x_{ij} = q_j \quad \forall j \in V'_R \quad (10)$$

$$\sum_{\substack{l \in V_1 \\ l \neq j}} y_{jl} = \sum_{\substack{l \in V_1 \\ l \neq j}} Bx_{jl} \quad \forall j \in V'_R \quad (11)$$

$$y_{ij} \leq Bx_{ij} \quad \forall i \in V_0, j \in V_1, (i \neq j) \quad (12)$$

$$q_j \leq \sum_{\substack{i \in V_0 \\ i \neq j}} Bx_{ij} \quad \forall j \in V'_R \quad (13)$$

$$a_{0j} = 0 \quad \forall j \in V_1 \quad (14)$$

$$\sum_{\substack{i \in V_0 \\ i \neq j}} a_{ij} + (t_{ij} + s_j)x_{ij} = \sum_{\substack{l \in V_1 \\ l \neq j}} a_{jl} \quad \forall j \in I \quad (15)$$

$$\sum_{\substack{i \in V_0 \\ i \neq j}} (a_{ij} + (t_{ij} + rB)x_{ij}) - rq_j = \sum_{\substack{l \in V_1 \\ l \neq j}} a_{jl} \quad \forall j \in V'_R \quad (16)$$

$$a_{ij} \leq (T_{\max} - t_{ij} - s_j - t_{j,N+1})x_{ij} \quad \forall i \in V_0, j \in I, (i \neq j) \quad (17)$$

$$a_{ij} \leq (T_{\max} - t_{ij} - t_{j,N+1} - rB)x_{ij} + rq_j \quad \forall i \in V_0, j \in V'_R, (i \neq j) \quad (18)$$

$$a_{ij} \leq Tx_{ij} \quad \forall i \in V_0, j \in V_1, (i \neq j) \quad (19)$$

$$y_{ij} \geq \left(t_{ij} + \min_{l \in V'_R \cup \{N+1\}} \{t_{jl}\} \right) x_{ij} \quad \forall i \in V', j \in V_1 \quad (20)$$

$$\sum_{j \in I} \phi_{jc} z_j / \tau_c = \beta_c \quad \forall c \in C \quad (21)$$

$$\gamma \leq \beta_c \quad \forall c \in C \quad (22)$$

$$\gamma + \Delta \geq \mu \quad (23)$$

$$a_{ij} \geq 0, \quad y_{ij} \geq 0 \quad \forall i \in V_0, j \in V_1 \quad (24)$$

$$q_j \geq 0 \quad \forall j \in V'_R \quad (25)$$

$$x_{ij} \in \{0, 1\} \quad \forall i \in V_0, j \in V_1 \quad (26)$$

$$z_j \in \{0, 1\} \quad \forall j \in I \quad (27)$$

$$\beta_c \geq 0 \quad \forall c \in C \quad (28)$$

$$\gamma \geq 0, \quad \Delta \geq 0 \quad (29)$$

The objective function (1) maximizes the total priority scores of the visited grids and penalizes the maximum unfulfilled coverage ratio target. Constraints (2) and (3) imply that each grid and dummy RSs can be visited at most once. Constraints (4) are flow balance equations. Constraints (5) and (6) ensure that the number of drones that departs from and arrives at the operation center equals the number of available drones, respectively. Constraints (7) link the x_{ij} and the z_j variables. Constraints (8) set drones to be fully charged when they depart from the operation center. Constraints (9) denote the remaining battery after a drone traverses the arc (i, j) and surveys the grid j . Constraints (10) indicate the remaining battery level at the dummy RS j after traversing the arc (i, j) . Constraints (11) guarantee that drones leave the RSs as fully charged. Constraints (12) couple the variables x_{ij} and y_{ij} , and constraints (13) link the variables x_{ij} and q_j . Constraints (14) specify the operation starting time. Constraints (15) and (16) track the departure time from the grids and the RSs, respectively. Constraints (17) and (18) ensure that drones return to the operation center within T_{\max} time units. Constraints (19) link the a_{ij} and the x_{ij} variables. Constraints (20) serve as valid inequalities to strengthen the formulation [19], such that the drone must have sufficient battery to arrive at the nearest RS or the operation center after traversing arc (i, j) . Constraints (21) denote the coverage ratio for each cluster. Constraints (22) indicate the minimum coverage ratio among all clusters. Constraint (23) specifies whether the coverage ratio target is satisfied by the visited grids and calculates Δ , which is the difference between the achieved and targeted coverage ratio. Note that the unsatisfied coverage ratio is penalized in the objective function. Finally, constraints (24)–(29) define the domains of the decision variables.

3.2 Path-Based Formulation

The arc-based formulation introduced in Sect. 3.1 requires one to generate several dummy RS nodes to allow multiple visits at each RS. However, increasing the number of dummy RSs increases the computational difficulty of the model. Moreover, calculating the exact number of required dummy RSs is not possible without solving the problem. To overcome these obstacles in the arc-based formulation, a path-based formulation is introduced in [19], which we adapt to the drone routing problem in this subsection.

In the path-based formulation, a path corresponds to a set of arcs between two vertices, which are not RS nodes, including or excluding possible visits to the RSs. More specifically, the starting and ending points of a path can only be the grid

centers to be scanned or the operation center, and any number of RS visits can be included between the starting and the ending points of a path.

We define the drone routing problem on a directed multi-graph $\hat{G} = (\hat{V}, \hat{A})$, with the set of arcs $\hat{A} = \{(i, j) : i, j \in \hat{V}, i \neq j\}$ where $\hat{V} = I \cup \{0\} \cup \{N + 1\}$. $\hat{V}_0 = I \cup \{0\}$ denotes the set of arrival vertices and $\hat{V}_1 = I \cup \{N + 1\}$ denotes the set of departure vertices. A path represents an arc between two vertices, such that path p starts at the center of grid $i \in I \cup \{0\}$ and ends at the center of grid $j \in I \cup \{N + 1\}$. A path may include varying number of visits to RSs. In other words, a path may include no visits to any RS. Then, the set of paths on the arc (i, j) is defined by P_{ij} , and the set of all paths is indicated by P . The starting and ending points on path p are $o(p)$ and $d(p)$, respectively. The number of RSs in path p equals n_p . The ordered set of RSs in p is represented by $L_p = \{0, 1, \dots, n_p - 1\}$. $\pi_p(l)$ denotes the RS at position $l \in L_p$. If $L_p = \emptyset$, then the drone doesn't visit any RS on path p . Traveling time of $p \in P$ is represented by t_p that is equal to drone's energy consumption.

The binary variable x_p is equal to 1 if a drone travels on path $p \in P$ and 0 otherwise. The continuous variables a_p and y_p represent the time and remaining battery level, respectively, before the drone travels on path $p \in P$. The continuous variable q_{pl} denotes the remaining battery level after the drone travels on path $p \in P$ and visits $\pi_p(l)$.

The parameters and variables of the path-based formulation are summarized in Appendix 1. We next present the path-based formulation

$$\max \sum_{j \in I} \rho_j z_j - M \Delta \quad (30)$$

subject to

$$(21) - (23), (27) - (29)$$

$$\sum_{\substack{i \in \hat{V}_0 \\ i \neq j}} \sum_{p \in P_{ij}} x_p \leq 1 \quad \forall j \in I \quad (31)$$

$$\sum_{\substack{j \in \hat{V}_1 \\ i \neq j}} \sum_{p \in P_{ij}} x_p - \sum_{\substack{j \in \hat{V}_0 \\ i \neq j}} \sum_{p \in P_{ji}} x_p = 0 \quad \forall i \in I \quad (32)$$

$$\sum_{j \in \hat{V}_1} \sum_{p \in P_{0j}} x_p = D \quad (33)$$

$$\sum_{i \in \hat{V}_0} \sum_{p \in P_{i, N+1}} x_p = D \quad (34)$$

$$\sum_{\substack{k \in \hat{V}_1 \\ k \neq j}} \sum_{p \in P_{jk}} y_p = \sum_{\substack{i \in \hat{V}_0 \\ i \neq j}} \sum_{p \in P_{ij}} \left(y_p - (t_p + s_j)x_p + \sum_{\substack{l \in L_p \\ |L_p| \neq 0}} (Bx_p - q_{pl}) \right) \quad \forall j \in I \quad (35)$$

$$y_p - t_{o(p), \pi_p(0)}x_p = q_{p0} \quad \forall p \in P : |L_p| \neq 0 \quad (36)$$

$$Bx_p - t_{\pi_p(l-1), \pi_p(l)}x_p = q_{pl} \quad \forall p \in P : |L_p| \neq 0, l \in L_p \setminus \{0\} \quad (37)$$

$$y_p = Bx_p \quad \forall i \in \hat{V}_1, p \in P_{0i} \quad (38)$$

$$y_p \leq Bx_p \quad \forall p \in P \quad (39)$$

$$q_{pl} \leq Bx_p \quad \forall p \in P, l \in L_p \quad (40)$$

$$y_p - t_p x_p + \sum_{l \in L_p} (Bx_p - q_{pl}) \geq 0 \quad \forall i \in I, p \in P_{i, N+1} \quad (41)$$

$$\sum_{j \in \hat{V}_1} \sum_{p \in P_{0j}} a_p = 0 \quad (42)$$

$$\sum_{\substack{k \in \hat{V}_1 \\ k \neq j}} \sum_{p \in P_{jk}} a_p = \sum_{\substack{i \in \hat{V}_0 \\ i \neq j}} \sum_{p \in P_{ij}} \left(a_p + (t_p + s_j)x_p + \sum_{\substack{l \in L_p \\ |L_p| \neq 0}} r(Bx_p - q_{pl}) \right) \quad \forall j \in I \quad (43)$$

$$a_p \leq T_{\max} - (t_p + s_{d(p)} + t_{d(p), N+1})x_p - \sum_{\substack{l \in L_p \\ |L_p| \neq 0}} r(Bx_p - q_{pl}) \quad \forall p \in P \quad (44)$$

$$x_p \in \{0, 1\} \quad \forall p \in P \quad (45)$$

$$a_p \geq 0, y_p \geq 0 \quad \forall p \in P \quad (46)$$

$$q_{pl} \geq 0 \quad \forall p \in P, l \in L_p \quad (47)$$

The objective function (30) is the same as the arc-based formulation (Sect. 3.1). Constraints (31) indicate that each grid can be surveyed at most once. Constraints (32) are for balancing the flows. Constraints (33) and (34) ensure that the number of drones that depart from and return to the operation center equals to the number of available drones. Constraints (35) track the drone's battery level at each grid. Constraints (36) and (37) indicate the remaining battery level when the drone arrives at the first RS and departs to the next RS on path $p \in P$, respectively.

Constraints (38) ensure that drones leave the operation center with a full charge. Constraints (39) and (40) link the battery level variables. Constraints (41) guarantee the path feasibility, such that the drone can arrive at its destination with a sufficient battery level. Constraints (42) define the operation start time. Constraints (43) track the time at each grid. Constraints (44) indicate the operation duration. Finally, constraints (45)–(47) indicate the domain of decision variables.

In Sect. 5.2, we compare the computational times of the proposed arc-based and path-based MILP formulations and show that both MILP models may require high computational times, especially for large instances. Similar formulations are also proposed for E-VRPs that are shown to be NP-hard [19]. However, relief agencies may not be able to access any advanced tools, and the decisions must be applied immediately after the disaster [4]. To compute reasonable solutions quickly, we develop a constructive heuristic (CH) in Sect. 4.

4 A Constructive Heuristic (CH)

Our CH developed to solve the proposed drone routing problem consists of three moves in the main phase: (i) initial route generation, (ii) insertion, and (iii) exchange. Additionally, we consider two sub-phase moves: (iv) repair and (v) improvement. The improvement sub-phase includes several operators, which are performed after every main phase move. The repair sub-phase move is performed only if the initial route generation produces a solution that does not satisfy the coverage ratio target. An overview of the CH is provided in Algorithm 1.

Initial solution generation step aims to generate a set of routes that satisfies the targeted coverage ratio. In other words, our aim in this step is not to maximize the collected priority scores, but to construct routes that minimize the route duration while satisfying the coverage ratio target. Therefore, the first step terminates when the coverage ratio target is satisfied by visiting a set of grids. In this step, a new route (drone) is initiated when the previous route cannot survey any additional grid due to time limitations. A drone route starts at the operation center, and we identify a candidate grid to survey next. The candidate grid is set as the grid that has the minimum operation time where the operation time is defined as the summation of survey time and travel time depending on the current position of the drone. If there

Algorithm 1: An Overview of the CH

Step 0: Generate an initial solution.

If the initial solution satisfies the coverage ratio target, go to Step 2; otherwise go to Step 1.

Step 1: Apply the repair move, go to Step 2;

Step 2: Apply the insertion move, followed by the improvement operators.

Step 3: Apply the exchange move, followed by the improvement operators.

If the solution is improved and there are any unvisited grids, go to Step 2; otherwise terminate the algorithm.

are multiple grids with the same operation time, the grid with the highest priority score is selected as the next candidate grid. If the remaining battery is not enough to visit the candidate grid, the drone visits the nearest RS, and the next candidate grid to visit is selected dependent on the position of the visited RS. We present the pseudocode of the initial solution generation step in Algorithm 2. Each time a grid is appended to the route of the drone, we apply the improvement sub-phase.

The *improvement* sub-phase, whose overview is presented in Algorithm 3, includes four operators: 1-opt, 2-opt, swap, and RS removal. The 1-opt operator changes the position of one grid in the route. The 2-opt operator removes two links and replaces them with two different links. The swap operator exchanges the order of two grids in the route. Note that the previously visited RSs may need to be updated when routes are modified by these improvement operators. Therefore, after an operator terminates, we apply the RS removal operator, which removes the redundant RSs to reduce the total charging time in a route. Each operator applies the first-improvement strategy; that is, we terminate searching for a new solution once a battery-feasible solution with a lower route duration is achieved. We apply the improvement operators in the following order, which are set based on preliminary experiments: 2-opt, RS removal, 1-opt, RS removal, swap, and RS removal. We apply the improvement sub-phase iteratively following this order of operators until no improving solution is found in the last iteration. We apply the improvement operators on each drone route sequentially.

The initial solution generation step terminates once routes that satisfy the coverage ratio target are generated. However, if the initial step does not generate any feasible solutions satisfying the coverage ratio target within T_{\max} , the repair sub-phase is implemented, involving a remove-add operator which aims to decrease the duration of each route and an insertion operator which aims to improve coverage by inserting grids, and hence it attains a feasible solution. Specifically, we pick each cluster with unsatisfied coverage ratio targets sequentially and attempt removing a grid from the solution and insert an unvisited candidate grid to the position of the removed grid to improve the route duration. If we attain a feasible solution that yields a lower route duration, we update the route. Note that while applying the remove-add move, the feasibility of the route with respect to the battery constraint must be checked. For the battery feasibility check, we evaluate three options for each candidate grid to be added to the solution: only the candidate grid and adding the candidate grid with its nearest RS. Specifically, let i be a candidate grid, and RS_N is the nearest RS to the center of i . Then the options are $\{i\}$, $\{i, RS_N\}$, and $\{RS_N, i\}$. We select the option with the least route duration in evaluating candidate grid i 's insertion to the route. The remove-add operator does not change the coverage ratios directly, but it allows to increase the number of visited grids and the coverage ratios by reducing the route duration. Hence, an insertion operator is implemented sequentially for each cluster that is covered less than the coverage ratio target. The unvisited grids in the regarding cluster are sorted in descending order according to their priority scores, and three options including the grid-RS combinations are generated. We try to insert additional grids to the routes until a cluster satisfies the coverage ratio target or there is no any feasible option to be inserted.

Algorithm 2: Initial Solution Generation

```

Initialization;
 $S_+$  = Set of surveyed grids
 $S_0$  = Set of candidate grids
 $\tau_k$  = Route duration of drone k
 $A$  = Minimum coverage ratio
 $T_{\max}$  = Route duration limit
while  $A < \text{Coverage ratio target}$  and  $\exists \tau_{k'} \leq T_{\max}$  do
  if  $S_+ == \emptyset$  or  $\tau_k == T_{\max}$  and  $\exists \tau_{k'} == 0$  then
    % Start a new route
    k:= an unused drone;
    z:= candidate grid yielded the minimum operation time;
    if insertion of z to the route of k is time-feasible and battery-feasible then
      Add z to the route of k;
      Do improvement
      Update  $S_+, S_0, A, \tau_k$ ;
    else
      if Surveying an updated z is time-feasible after recharging then
        Visit the nearest RS, update z;
        Add z to the route of k;
        Do improvement
        Update  $S_+, S_0, A, \tau_k$ ;
      else
        % Return to the operation center
         $\tau_k = T_{\max}$ ;
      end
    end
  end
  else
    while  $\tau_k \leq T_{\max}$  do
      % Add to the current route
      z:= candidate grid yielded the minimum operation time;
      if insertion of z to the route of k is time-feasible and battery-feasible then
        Add z to the route of d;
        Do improvement
        Update  $S_+, S_0, A, \tau_k$ ;
      else
        if Surveying an updated z is time-feasible after recharging then
          Visit the nearest RS, update z;
          Add z to the route of k;
          Do improvement
          Update  $S_+, S_0, A, \tau_k$ ;
        else
          % Return to the operation center
           $\tau_k = T_{\max}$ ;
        end
      end
    end
  end
end

```

Algorithm 3: Improvement Phase

```

Initialization;
x:=route
 $O_i := i$ th operator for  $i=1,\dots,6$ 
impr:=1
while impr  $\neq$  6 do
  Generate a candidate solution  $x'$  by  $O_i(x)$ ;
  if  $x'$  is battery-feasible and better than  $x$  then
     $x = x'$ ;
    impr = 1;
  else
    if  $i \neq 6$  then
       $i = i + 1$ ;
      impr = impr + 1
    else
       $i = 1$ ;
      impr = impr + 1
    end
  end
end

```

If there is any unvisited grid after the initial step terminates, the *insertion* move tries to insert them into the current solution to maximize the total priority score. First, we sort the unvisited grids in descending order according to their priority scores. Then we generate three insertion options for each candidate grid-RS combination, as explained in the repair sub-phase. If an insertion option can be feasibly applied and the grid can be inserted in an existing or a new route (if an unrouted drone exists), the grid is inserted, and then the improvement sub-phase is performed. The insertion is performed until no new feasible insertions can be identified.

The *exchange* move searches for an improved solution in terms of priority scores. If there are unvisited grids in the network after implementing the insertion phase, and their priority scores are higher than the visited ones, we attempt to exchange the candidate grid that has the highest priority score with a visited grid with a lower priority score. While inserting a grid in a route, in this procedure, the three insertion options explained above are considered. If an exchange attempt produces a feasible solution in terms of route duration, battery, and coverage ratio target levels, we perform the exchange move, which is followed by the improvement. We apply the exchange move only for the non-empty routes (i.e., routes that visit at least one grid).

5 Numerical Analysis

In this section, we describe the results of the numerical study conducted based on a set of test instances. The objectives of our numerical study are to understand the impact of the total number of grids and the number of drones on the quality of

the solutions and to analyze the sensitivity of system performance to changes in the generation of grid attributes. We solve the proposed MILP formulations by an optimization solver, CPLEX, and compare their performance with respect to solution quality and computational time. To evaluate the heuristic performance, we compare the solution time and the objective value achieved by the proposed algorithm relative to the best-found CPLEX solution.

We describe test instances in Sect. 5.1 and evaluate the performance of the alternative formulations and the CH in Sect. 5.2.

5.1 Test Instances

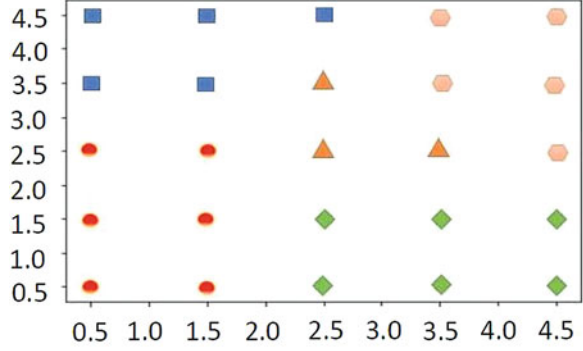
We generate 54 instances with 16, 25, and 36 equal-sized grids. The instances differ in how we assign attributes to the grids and the number of drones. We assume that the affected area is divided into square grids with a 1 kilometer side length. The operation center is assumed to be located at the left bottom corner of each instance (as in Fig. 1).

Although the area of each grid is equal, we consider different survey times since the density of buildings in each grid may vary. For instance, the grids may include areas without any built infrastructure, such as forests and lakes, and these areas do not require surveying. Thus, the survey times are randomly generated between [10,17] minutes; here, we consider an eBee drone as a benchmark, which can cover 1 km^2 in 17 min [6]. The priority score of each grid is randomly generated between [1,5].

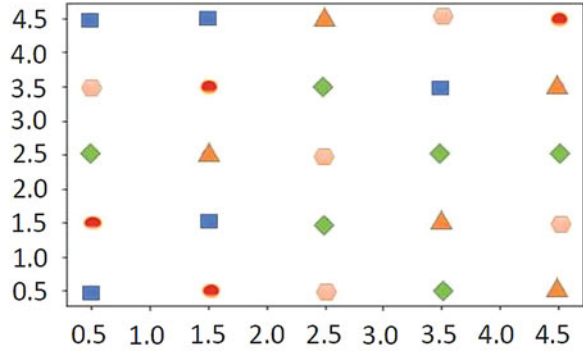
We generate 6 different instances for each network that contains 16, 25, or 36 grids where each instance is differentiated based on the assignment of a set of attributes to the grids. We consider six different attributes, with each one having a different number of levels (e.g., four levels for the soil type attribute such as hard rock, rock, stiff soil, and soft soil; three levels for the wealth index attribute, which are high, moderate, and low). We assign the attributes to the grids following two policies: (i) assign similar attribute levels based on the geographical proximity of grids, which produce C-type instances, C1, C2, and C3, and (ii) assign attribute levels randomly, which generate R-type instances: R1, R2, and R3 instances. We then use k -modes algorithm and assign the grids into five clusters [23]. Figure 2 illustrates exemplary areas of C1 and R1 instances for the area of 25 km^2 where there are five clusters represented by different shapes: a rectangle, a diamond, a triangle, a circle, or a hexagon. Thus, grids represented by the same shape belong to the same cluster.

We define the target coverage ratio as 0.25 and the battery capacity (i.e., maximum flight time) as 50 min. Similar to [9], we assume that a drone that is completely out of charge is fully charged in 5 min. Accordingly, we set the recharging time required to fill the battery for a 1-min flight time as 0.1 min. The speed of a drone is set at 60 km/h. T_{\max} is assumed to be 180 min, and the number of RSs equals three for each instance. Moreover, to solve the arc-based MILP

Fig. 2 Illustrative example of two types of instances for a 25 km² area



(a) C1 instance with 25 grids



(b) R1 instance with 25 grids

formulation, we set the number of dummy RSs to 3, 5, and 7 for the instances with 16, 25, and 36 grids, respectively. We consider using one, two, and four drones. Finally, we set the penalty weight “M” for the maximum unfulfilled coverage ratio target to 10,000 in the objective function. Here, we aim to dominate the objective function by the coverage penalty and distinguish the total priority score and the resultant penalty in the objective function value by setting M to a very large number. In our instances, total priority score can be at most 180 for the instances with 36 grids, and setting M to 10,000 causes a penalty more than 180 for any possible amount of unfulfilled coverage ratio.

In our instances, the locations of the RSs are set via solving a p -median problem. Let I be the set of grids in the affected region. J denotes the set of candidate RS locations. Let s_j be the time required to survey grid j . The travel time t_{ij} between grid i and grid j is computed by the Euclidean distance between the center of grids, and p is the number of RSs to be located. The binary variable x_j equals 1 if an RS is located to the center of grid j , and the binary variable y_{ij} equals 1 if grid i is assigned to RS at grid j . The p -median formulation computing the locations of the RSs is as follows.

$$\min \sum_{i \in I} \sum_{j \in J} s_i t_{ij} y_{ij} \quad (48)$$

subject to

$$\sum_{j \in J} y_{ij} = 1 \quad \forall i \in I \quad (49)$$

$$\sum_{j \in J} x_j = p \quad \forall i \in I \quad (50)$$

$$y_{ij} - x_j \leq 0 \quad \forall i \in I, j \in J \quad (51)$$

$$x_j \in \{0, 1\} \quad \forall j \in J \quad (52)$$

$$y_{ij} \in \{0, 1\} \quad \forall i \in I, j \in J \quad (53)$$

The objective (48) is to minimize the demand weighted total distance, where the demand equals the survey time. Constraint (49) implies that all grids must be assigned to exactly one RS. Constraint (50) specifies the number of RSs to be located. Constraint (51) couples the x_j and y_{ij} variables. Constraints (52) and (53) define the domains of the decision variables.

5.2 Results

We solve 54 test instances by using the proposed formulations and the CH. CPLEX 12.8.0 is used to solve the proposed mathematical models by imposing a 30-min time limit. The CH is coded in Python 3.6. All the numerical analyses are conducted on a HP 8th Generation Intel Core i7 processor with 8 GB of RAM in 64-bit mode.

As explained before, the arc-based formulation requires introducing dummy RS nodes. Considering a large number of dummy RSs increases the computation time immensely, whereas setting an insufficient number of RSs may cut off the optimal solution. Since it is impossible to compute the minimum sufficient number of dummy RSs in advance, we make experiments by setting a different number of dummy RSs. Specifically, we consider 3, 5, and 7 dummy RSs for instances with 16, 25, and 36 grids, respectively.

The path-based formulation requires generating all possible paths in advance. The paths are generated in 3, 20, and 95 s on average for the instances with 16, 25, and 36 grids, respectively. While we do not apply any strategies to eliminate the redundant paths in this study, one may strengthen the path-based formulation by identifying dominance rules (see [19]).

Tables 1 and 2 represent the computational results obtained by CPLEX for both arc-based and path-based formulations. The objective function values are denoted

Table 1 Computational results of the arc-based and path-based formulations for R-type and C-type instances with 16 grids

Ins.	# of drones	# of grids	Arc-based formulation					Path-based formulation				
			# of visits	CR %	Z^{Arc}	Gap %	Comp. time(s)	# of visits	CR %	Z^{path}	Gap %	Comp. time(s)
R1	1	16	11	34	40	0.0	25.8	11	34	40	0.0	15.5
R1	2	16	16	100	51	0.0	0.6	16	100	51	0.0	1.5
R1	4	16	16	100	51	0.0	0.6	16	100	51	0.0	1.4
R2	1	16	11	33	40	0.0	1.2	11	33	39	0.0	7.9
R2	2	16	16	100	51	0.0	0.6	16	100	51	0.0	1.5
R2	4	16	16	100	51	0.0	0.6	16	100	51	0.0	1.3
R3	1	16	10	25	41	0.0	1.2	10	25	40	0.0	1.5
R3	2	16	16	100	51	0.0	0.6	16	100	51	0.0	1.4
R3	4	16	16	100	51	0.0	0.6	16	100	51	0.0	1.3
C1	1	16	10	25	41	0.0	1.7	10	25	40	0.0	2.1
C1	2	16	16	100	51	0.0	0.6	16	100	51	0.0	1.5
C1	4	16	16	100	51	0.0	0.6	16	100	51	0.0	1.4
C2	1	16	10	50	41	0.0	2.0	10	50	41	0.0	2.2
C2	2	16	16	100	51	0.0	0.6	16	100	51	0.0	1.6
C2	4	16	16	100	51	0.0	0.6	16	100	51	0.0	1.4
C3	1	16	10	25	40	0.0	30.8	10	50	40	0.0	34.3
C3	2	16	16	100	51	0.0	0.6	16	100	51	0.0	1.5
C3	4	16	16	100	51	0.0	0.6	16	100	51	0.0	1.3

by Z^{arc} (Z^{path}) for the arc-based (path-based) formulation, and CR denotes the minimum coverage ratio achieved among all clusters. All instances with 16 grids are solved to optimality by both formulations within a 30-min time limit (usually within a couple of seconds), as shown in Table 1. When the number of drones is one, CR is always less than 100%. However, CR becomes 100% as more drones are used to scan the region.

For instances with 25 grids, 12 out of 18 (12 out of 18) instances are solved to optimality by the arc-based (path-based) formulation. Average computation times of the arc-based (path-based) formulation are 624 (754) and 37 (230) seconds for the all of the instances with 25 grids and for the all of the instances with 25 grids excluding the ones that cannot be solved within the computation time limit, respectively. Even if the optimality gap of the path-based formulation is higher than that of the arc-based formulation for some of the instances, the computed objective function values are all the same for both formulations. Additionally, scanning with two drones is not enough to reach 100% coverage in 25-grid instances. We observe that increasing the number of drones from two to four helps to solve these instances optimally. This implies that the problem may become easier to solve if there exist enough resources to visit all grids; that is, the problem structure may be more complicated when grid selection must be made along with routing decisions.

Similar results are observed for the instances with 36 grids. The main differences are that computed objective function values by the arc-based and path-based

Table 2 Computational results of the arc-based and path-based formulations for R-type and C-type instances with 25 and 36 grids

Ins.	# of drones	# of grids	Arc-based formulation					Path-based formulation					
			# of visits	CR %	Z ^{Arc}	Gap %	Comp. time(s)	# of visits	CR %	Z ^{path}	Gap %	Comp. time(s)	
R1	1	25	10	33	42	0.0	2.9	10	28	42	0.0	5.1	
R1	2	25	21	66	68	1.5	1800	21	66	68	2.9	1800	
R1	4	25	25	100	73	0.0	2.0	25	100	73	0.0	3.6	
R2	1	25	11	25	41	0.0	179.5	11	25	41	0.0	1093	
R2	2	25	21	66	68	1.5	1800	21	60	68	2.9	1800	
R2	4	25	25	100	73	0.0	2.3	25	100	73	0.0	3.4	
R3	1	25	10	33	40	0.0	230.5	10	33	40	0.0	1569	
R3	2	25	21	60	68	1.5	1800	21	60	68	3.0	1800	
R3	4	25	25	100	73	0.0	2.2	25	100	73	0.0	3.6	
C1	1	25	10	33	41	0.0	6.7	10	33	41	0.0	6.1	
C1	2	25	21	33	68	1.5	1800	21	33	68	3.0	1800	
C1	4	25	25	100	73	0.0	2.3	25	100	73	0.0	3.6	
C2	1	25	10	34	42	0.0	8.0	10	34	42	0.0	64	
C2	2	25	21	68	68	1.9	1800	21	80	68	2.9	1800	
C2	4	25	25	100	73	0.0	2.6	25	100	73	0.0	3.4	
C3	1	25	10	25	42	0.0	3.2	10	25	42	0.0	5.2	
C3	2	25	21	51	68	1.5	1800	21	66	68	2.9	1800	
C3	4	25	25	100	73	0.0	2.1	25	100	73	0.0	3.8	
R1	1	36	11	27	50	0.0	779.5	11	27	50	0.0	232.8	
R1	2	36	20	45	86	3.8	1800	20	34	85	3.5	1800	
R1	4	36	36	100	113	0.0	180.9	36	100	113	0.0	334	
R2	1	36	11	27	41	6.3	1800	12	28	42	0.0	1735	
R2	2	36	20	30	82	7.3	1800	20	30	82	6.1	1800	
R2	4	36	36	100	113	0.0	274.8	36	100	113	0.0	68.1	
R3	1	36	12	28	45	9.1	1800	12	28	46	0.0	829.3	
R3	2	36	20	40	85	4.6	1800	20	40	85	3.2	1800	
R3	4	36	36	100	113	0.0	282.8	36	100	113	0.0	32.8	
C1	1	36	12	33	46	6.6	1800	12	33	44	8.1	1800	
C1	2	36	20	33	85	4.7	1800	20	33	85	3.3	1800	
C1	4	36	36	100	113	0.0	260.9	36	100	113	0.0	1730	
C2	1	36	12	33	46	0.0	634.5	11	22	48-M ^a	100	1800	
C2	2	36	20	33	85	4.7	1800	20	33	85	3.3	1800	
C2	4	36	36	100	113	0.0	1076	36	100	113	0.0	64.5	
C3	1	36	12	33	45	8.0	1800	12	33	46	0.0	802	
C3	2	36	20	34	85	4.7	1800	20	34	85	3.3	1800	
C3	4	36	36	100	113	0.0	339	36	100	113	0.0	34.4	

^aCoverage ratio target cannot be met within 30 min time limit and a large negative objective function value is reported to indicate the unfulfilled coverage ratio target

formulations are not always the same. For instances with 36 grids, 8 out of 18 (10 out of 18) instances are solved to optimality by the arc-based (path-based) formulation. Similar to the instances with 25 grids, increasing the number of drones helps to solve the instances to optimality for instances. In addition, average computation times of the arc-based (path-based) formulations are 1214 (1127) and 478 (586) seconds for the all of the instances with 36 grids and for the all of the instances with 36 grids excluding the ones that cannot be solved within the computation time limit, respectively. Setting the number of dummy RSs for larger instances is nontrivial when the arc-based formulation is used; hence, one may prefer utilizing the path-based formulation as both formulations show similar performances.

Post-disaster relief operations should be organized as quickly as possible. Hence, one may not prefer waiting for the 30-min time limit. To compute a route for each drone immediately, we proposed the CH algorithm introduced in Sect. 4. Even though the proposed CH is relatively simpler than the metaheuristics proposed for E-VRP (such as [16, 18, 44]), it computes high-quality and feasible solutions for our instances within less than a second. Specifically, the CH achieves the optimal solutions in 13 (7 and 6) out of 18 instances when there are 16 (25 and 36) grids, which are presented in Tables 3 and 4.

We define the *CH gap* between the CH and the arc- and path-based mathematical formulations as the ratio of the difference between the best-computed objective function value by the mathematical formulations (denoted by Z^{BEST}) and the

Table 3 Computational results of the CH and the best solution computed by the mathematical formulations for R-type and C-type instances with 16 grids

Ins.	# of drones	# of grids	# of visits	CR %	Comp. time(s)	Z^{CH}	Z^{BEST}	CH Gap%
R1	1	16	11	34	0.3	40	40	0.0
R1	2	16	16	100	0.2	51	51	0.0
R1	4	16	16	100	0.4	51	51	0.0
R2	1	16	10	33	0.2	35	40	12.5
R2	2	16	16	100	0.1	51	51	0.0
R2	4	16	16	100	0.1	51	51	0.0
R3	1	16	10	50	0.4	39	41	4.9
R3	2	16	16	100	0.2	51	51	0.0
R3	4	16	16	100	0.2	51	51	0.0
C1	1	16	10	50	0.4	40	41	2.4
C1	2	16	16	100	0.2	51	51	0.0
C1	4	16	16	100	0.2	51	51	0.0
C2	1	16	10	25	0.3	40	41	2.4
C2	2	16	16	100	0.2	51	51	0.0
C2	4	16	16	100	0.2	51	51	0.0
C3	1	16	10	50	0.3	38	40	5.0
C3	2	16	16	100	0.2	51	51	0.0
C3	4	16	16	100	0.2	51	51	0.0

CH gap equals $(Z^{\text{BEST}} - Z^{\text{CH}}) / Z^{\text{BEST}}$ where Z^{BEST} is the best-found solution obtained by CPLEX

Table 4 Computational results of CH and the best solution computed by MILP formulations for R-type and C-type instances with 25 and 36 grids

Ins.	# of drones	# of grids	# of visits	CR %	Comp. time(s)	Z ^{CH}	Z ^{BEST}	CH Gap%
R1	1	25	11	33	0.4	36	42	14.3
R1	2	25	20	55	0.7	66	68	2.9
R1	4	25	25	100	0.3	73	73	0.0
R2	1	25	11	28	0.4	36	41	12.2
R2	2	25	21	66	0.9	68	68	0.0
R2	4	25	25	100	0.4	73	73	0.0
R3	1	25	11	36	0.4	37	40	7.5
R3	2	25	20	60	0.8	65	68	4.4
R3	4	25	25	100	0.4	73	73	0.0
C1	1	25	11	33	0.4	32	41	21.9
C1	2	25	20	33	0.8	66	68	2.9
C1	4	25	25	100	0.4	73	73	0.0
C2	1	25	11	34	0.3	34	42	19.0
C2	2	25	20	40	0.8	65	68	4.4
C2	4	25	25	100	0.3	73	73	0.0
C3	1	25	11	25	0.4	33	42	21.4
C3	2	25	20	50	0.7	66	68	2.9
C3	4	25	25	100	0.4	73	73	0.0
R1	1	36	12	27	0.5	40	50	20.0
R1	2	36	21	45	0.6	79	86	8.1
R1	4	36	36	100	0.5	113	113	0.0
R2	1	36	12	27	0.4	37	42	11.9
R2	2	36	21	30	0.6	79	82	3.7
R2	4	36	36	100	0.6	113	113	0.0
R3	1	36	12	28	0.6	31	46	32.6
R3	2	36	21	40	0.6	73	85	14.1
R3	4	36	36	100	0.6	113	113	0.0
C1	1	36	12	33	0.7	39	46	15.2
C1	2	36	22	34	0.8	75	85	11.8
C1	4	36	36	100	0.6	113	113	0.0
C2	1	36	12	33	0.6	39	46	15.2
C2	2	36	22	34	0.8	75	85	11.8
C2	4	36	36	100	0.6	113	113	0.0
C3	1	36	12	33	0.3	35	46	23.9
C3	2	36	21	34	0.7	80	85	5.9
C3	4	36	36	100	0.5	113	113	0.0

CH gap equals $(Z^{BEST} - Z^{CH})/Z^{BEST}$ where Z^{BEST} is the best-found solution obtained by CPLEX

objective function value computed by the CH (denoted by Z^{CH}), to the best-computed objective function value by the mathematical formulations. The average percentage gaps are 2, 6, and 10% for the instances with 16, 25, and 36 grids, respectively. The CH gaps decrease as the number of drones increases since limiting the number of drones makes it more difficult to satisfy the coverage ratio target. In other words, the CH first finds a feasible solution that satisfies the coverage ratio target, and then it improves the initial solution by improvement moves. If the coverage ratio target is satisfied more easily with the help of more drones, the solution quality increases since the CH focuses on increasing the collected priority scores rather than satisfying the coverage ratio target.

To sum up, the arc-based and path-based formulations result in very similar performances concerning computation times and computed objective function values. However, some instances cannot be solved to optimality within the 30-min time interval. To overcome this limitation, we propose the CH heuristic that computes a feasible solution less than a second for each instance. The quality of the CH heuristic's solution gets better as the number of drones increases and/or the number of grids decreases. One may still prefer utilizing the CH heuristic that has an average CH gap of 6%.

6 Conclusion

In this paper, we consider a post-disaster setting, in which the drones assess the physical damages on the built infrastructure caused by an earthquake. The disaster-affected area is firstly divided into grids where each grid has a set of attributes comprising its infrastructure, geographical, geological, and socioeconomic conditions. Then, grids are clustered based on their attributes. We address the problem of determining the grids to scan and assess by each drone and the sequence of visits to the selected grids given a set of drones and a limited time for assessments. We aim to maximize the total priority score collected from the assessed grids, while a minimum coverage ratio for each cluster is targeted.

We propose an arc-based and a path-based formulation and analyze 54 instances varying the way of assigning attributes to grids, as well as the number of drones and grids. We conclude that the computational performance of both formulations is very similar. However, as the number of dummy RSs affects the arc-based formulation's performance and computing the adequate number of RSs is nontrivial, using path-based formulation may be preferred. In addition to the proposed formulations, we propose a CH that computes a feasible solution that satisfies the coverage ratio target quickly, that is, in less than a second. The CH achieves a high level of performance in instances with a larger number of drones since it is easy to generate an initial feasible solution that satisfies the coverage ratio target in these cases.

Drones may play an important role in humanitarian operations by speeding up the damage assessment operations and hence supporting relief operations. There exists scarce literature that explores using drones in humanitarian logistics. Therefore, there may be several future research directions. For instance, one can extend

the proposed formulations for post-disaster damage assessment by incorporating additional aspects of drones such as different speed options which may be affected by weather conditions. Another possible extension is to consider the availability of the RS on the arrival of the drone; that is, battery charging processes can be examined in more detail. Finally, coordination of damage assessment operations and relief operations can be addressed in future research.

Appendix 1

Tables 5 and 6 demonstrate the sets, parameters, and decision variables of the arc-based and path-based formulations, respectively.

Table 5 Sets, parameters, and decision variables for the arc-based formulation

Sets and parameters
0 and $N + 1$: Same operation center for departure and arrival
I : Set of grids to be surveyed
C : Set of clusters
V_R : Set of recharging stations
V'_R : Set of dummy recharging stations
$V_0 = I \cup V'_R \cup \{0\}$: Set of departure vertices
$V_1 = I \cup V'_R \cup \{N + 1\}$: Set of arrival vertices
$V' = I \cup V'_R$: Set of vertices except the operation center
s_j : Survey time of grid j
t_{ij} : Travel time between grid i and grid j
B : Battery capacity
r : Recharging rate
T_{\max} : Route duration limit
D : Number of drones
ρ_j : Priority score of grid j
ϕ_{jc} : A coverage parameter equals to 1 if grid j is in cluster c and 0 otherwise
τ_c : Total number of grids in cluster c
μ : Coverage ratio target
M : Sufficiently large number
Decision variables
x_{ij} : 1 if a drone travels on arc $(i, j) \in A$; 0 otherwise
a_{ij} : Departure time at grid i to grid j , $(i, j) \in A$
y_{ij} : Remaining battery departing at grid i to grid j , $(i, j) \in A$
z_j : 1 if grid $j \in I$ is surveyed; 0 otherwise
q_j : Remaining battery before the charging operation at RS $j \in V'_R$
β_c : Coverage ratio of cluster $c \in C$
γ : Minimum coverage ratio
Δ : Difference between the achieved coverage ratio and the coverage ratio target

Table 6 Sets, parameters, and decision variables for the path-based formulation

Sets and parameters
0 and $N + 1$: Same operation center for departure and arrival
I : Set of grids to be surveyed
C : Set of clusters
$\hat{V} = I \cup \{0\} \cup \{N + 1\}$: Set of all vertices
$\hat{V}_0 = I \cup \{0\}$: Set of departure vertices
$\hat{V}_1 = I \cup \{N + 1\}$: Set of arrival vertices
P : Set of all paths
P_{ij} : Set of paths from i to j , $(i, j) \in \hat{A}$
s_j : Survey time of grid j
t_p : Travel time of path $p \in P$
B : Battery capacity
r : Recharging rate
T_{\max} : Route duration limit
D : Number of drones
ρ_j : Priority score of grid j
ϕ_{jc} : A coverage parameter equals to 1 if grid j is in cluster c and 0 otherwise
τ_c : Total number of grids in cluster c
μ : Coverage ratio target
M : Sufficiently large number
Decision variables
x_p : 1 if a drone travels on path $p \in P$; 0 otherwise
a_p : Time before the drone travels on path $p \in P$
y_p : Remaining battery before the drone travels on path $p \in P$
z_j : 1 if grid $j \in I$ is surveyed; 0 otherwise
q_{pl} : Remaining battery before the charging operation on path $p \in P$ at the l^{th} RS
β_c : Coverage ratio of cluster $c \in C$
γ : Minimum coverage ratio
Δ : Difference between the achieved coverage ratio and the coverage ratio target

References

1. Agatz, N., Bouman, P., Schmidt, M. (2018). Optimization approaches for the traveling salesman problem with drone. *Transportation Science*, 52(4), 965–981.
2. American Red Cross. (2015). Drones for disaster response and relief operations. Retrieved from <https://www.issuelab.org/resources/21683/21683.pdf> Accessed 17 May 2020
3. Andelmin, J., Bartolini, E. (2017). An exact algorithm for the green vehicle routing problem. *Transportation Science*, 51(4), 1288–1303.
4. Balcik, B. (2016, June). Selective routing for post-disaster needs assessments. In *International Conference on Dynamics of Disasters* (pp. 15–36). Springer, Cham.
5. Balcik, B., Beamon, B. M. (2008). Facility location in humanitarian relief. *International Journal of Logistics*, 11(2), 101–121.

6. Boccardo, P., Chiabrando, F., Dutto, F., Tonolo, F. G., Lingua, A. (2015). UAV deployment exercise for mapping purposes: Evaluation of emergency response applications. *Sensors*, 15(7), 15717–15737.
7. Chauhan, D., Unnikrishnan, A., Figliozzi, M. (2019). Maximum coverage capacitated facility location problem with range constrained drones. *Transportation Research Part C: Emerging Technologies*, 99, 1–18.
8. Chmaj, G., and Selvaraj, H. (2015). Distributed processing applications for UAV/drones: a survey. In *Progress in Systems Engineering* (pp. 449–454). Springer, Cham.
9. Chowdhury, S. (2018). Drone routing and optimization for post-disaster inspection. Mississippi State University.
10. Chowdhury, S., Emelogu, A., Marufuzzaman, M., Nurre, S. G., Bian, L. (2017). Drones for disaster response and relief operations: A continuous approximation model. *International Journal of Production Economics*, 188, 167–184.
11. Davidson, R. A., Shah, H. C. (1997). An urban earthquake disaster risk index. Stanford University: John A. Blume Earthquake Engineering Center.
12. Dhein, G., Zanetti, M. S., de Araújo, O. C. B., and Cardoso Jr, G. (2019). Minimizing dispersion in multiple drone routing. *Computers and Operations Research*, 109, 28–42.
13. Dorling, K., Heinrichs, J., Messier, G. G., and Magierowski, S. (2016). Vehicle routing problems for drone delivery. *IEEE Transactions on Systems, Man, and Cybernetics: Systems*, 47(1), 70–85.
14. Duarte, D., Nex, F., Kerle, N., Vosselman, G. (2017). Towards a more efficient detection of earthquake induced facade damages using oblique UAV imagery. *The International Archives of Photogrammetry, Remote Sensing and Spatial Information Sciences*, 42, 93.
15. Erdelj, M., Natalizio, E. (2016, February). UAV-assisted disaster management: Applications and open issues. In *2016 international conference on computing, networking and communications (ICNC)* (pp. 1–5). IEEE.
16. Erdoğan, S., and Miller-Hooks, E. (2012). A green vehicle routing problem. *Transportation Research Part E: Logistics and Transportation Review*, 48(1), 100–114.
17. Estrada, M. A. R., Ndoma, A. (2019). The uses of unmanned aerial vehicles—UAV’s-(or drones) in social logistic: Natural disasters response and humanitarian relief aid. *Procedia Computer Science*, 149, 375–383.
18. Felipe, Á., Ortuño, M. T., Righini, G., and Tirado, G. (2014). A heuristic approach for the green vehicle routing problem with multiple technologies and partial recharges. *Transportation Research Part E: Logistics and Transportation Review*, 71, 111–128.
19. Froger, A., Mendoza, J. E., Jabali, O., Laporte, G. (2019). Improved formulations and algorithmic components for the electric vehicle routing problem with nonlinear charging functions. *Computers and Operations Research*, 104, 256–294.
20. Golabi, M., Shavarani, S. M., Izbirak, G. (2017). An edge-based stochastic facility location problem in UAV-supported humanitarian relief logistics: a case study of Tehran earthquake. *Natural Hazards*, 87(3), 1545–1565.
21. Ham, A. M. (2018). Integrated scheduling of m-truck, m-drone, and m-depot constrained by time-window, drop-pickup, and m-visit using constraint programming. *Transportation Research Part C: Emerging Technologies*, 91, 1–14.
22. Ritchie, H. and Roser, M. (2020) - “Natural Disasters”. Published online at OurWorldIn-Data.org. Retrieved from: <https://ourworldindata.org/natural-disasters> Accessed 17 May 2020
23. Huang, Z. (1998). Extensions to the k-means algorithm for clustering large data sets with categorical values. *Data mining and knowledge discovery*, 2(3), 283–304.
24. IFRC (International Federation of Red Cross and Red Crescent Societies): World disasters report 2018. <https://media.ifrc.org/ifrc/wp-content/uploads/sites/5/2018/10/B-WDR-2018-EN-LR.pdf>. Accessed 12 March 2020
25. IFRC (International Federation of Red Cross and Red Crescent Societies): Humanitarian logistics and procurement. (n.d.). Retrieved from <https://www.ifrc.org/en/what-we-do/logistics/> Accessed 17 May 2020

26. Kim, S. J., Lim, G. J., Cho, J., Côté, M. J. (2017). Drone-aided healthcare services for patients with chronic diseases in rural areas. *Journal of Intelligent and Robotic Systems*, 88(1), 163–180.
27. Kim, K., Pant, P., Yamashita, E. (2015). Disasters, drones, and crowdsourced damage assessment. In *Proceedings of Computers in Urban Planning and Urban Management Conference*, Cambridge, Massachusetts.
28. Koç, Ç., and Karaoglan, I. (2016). The green vehicle routing problem: A heuristic based exact solution approach. *Applied Soft Computing*, 39, 154–164.
29. Leetaru, K., (2015). How Drones Are Changing Humanitarian Disaster Response. Retrieved from <https://www.forbes.com/sites/kalevleetaru/2015/11/09/how-drones-are-changing-humanitarian-disaster-response/> Accessed 17 May 2020
30. Leggieri, V., and Haouari, M. (2017). A practical solution approach for the green vehicle routing problem. *Transportation Research Part E: Logistics and Transportation Review*, 104, 97–112.
31. Meier, P., (2015). Crisis Mapping Nepal with Aerial Robotics. Retrieved from <https://irevolutions.org/2015/11/04/crisis-mapping-nepal-aerial-robotics/> Accessed 17 May 2020
32. Montoya, A., Guéret, C., Mendoza, J. E., and Villegas, J. G. (2017). The electric vehicle routing problem with nonlinear charging function. *Transportation Research Part B: Methodological*, 103, 87–110.
33. Motlagh, N. H., Taleb, T., Arouk, O. (2016). Low-altitude unmanned aerial vehicles-based internet of things services: Comprehensive survey and future perspectives. *IEEE Internet of Things Journal*, 3(6), 899–922.
34. Murphy, R. R., Duncan, B. A., Collins, T., Kendrick, J., Lohman, P., Palmer, T., Sanborn, F. (2016). Use of a Small Unmanned Aerial System for the SR-530 Mudslide Incident near Oso, Washington. *Journal of field Robotics*, 33(4), 476–488.
35. Murray, C. C., Chu, A. G. (2015). The flying sidekick traveling salesman problem: Optimization of drone-assisted parcel delivery. *Transportation Research Part C: Emerging Technologies*, 54, 86–109.
36. Murray, C., Raj, R. (2020). The multiple flying sidekicks traveling salesman problem: Parcel delivery with multiple drones. *The multiple flying sidekicks traveling salesman problem: Parcel delivery with multiple drones*, *Transportation Research Part C: Emerging Technologies*, 110, 368–398.
37. Nedjati, A., Vizvari, B., Izbirak, G. (2016). Post-earthquake response by small UAV helicopters. *Natural Hazards*, 80(3), 1669–1688.
38. Oruc, B. E., Kara, B. Y. (2018). Post-disaster assessment routing problem. *Transportation research part B: methodological*, 116, 76–102.
39. Özdamar, L., and Ertem, M. A. (2015). Models, solutions and enabling technologies in humanitarian logistics. *European Journal of Operational Research*, 244(1), 55–65.
40. Qi, J., Song, D., Shang, H., Wang, N., Hua, C., Wu, C., ... and Han, J. (2016). Search and rescue rotary-wing uav and its application to the lushan ms 7.0 earthquake. *Journal of Field Robotics*, 33(3), 290–321.
41. Rabta, B., Wankmüller, C., Reiner, G. (2018). A drone fleet model for last-mile distribution in disaster relief operations. *International Journal of Disaster Risk Reduction*, 28, 107–112.
42. Remondino, F., Barazzetti, L., Nex, F., Scaioni, M., and Sarazzi, D. (2011). UAV photogrammetry for mapping and 3d modeling—current status and future perspectives. *International archives of the photogrammetry, remote sensing and spatial information sciences*, 38(1), C22.
43. Sato, Y., Ozawa, S., Terasaka, Y., Kaburagi, M., Tanifuji, Y., Kawabata, K., ..., Torii, T. (2018). Remote radiation imaging system using a compact gamma-ray imager mounted on a multicopter drone. *Journal of Nuclear Science and Technology*, 55(1), 90–96.
44. Schneider, M., Stenger, A., Goeke, D. (2014). The electric vehicle-routing problem with time windows and recharging stations. *Transportation Science*, 48(4), 500–520.
45. Shavarani, S. M. (2019). Multi-level facility location-allocation problem for post-disaster humanitarian relief distribution. *Journal of Humanitarian Logistics and Supply Chain Management*.

46. Shohet, I. M., Levi, L. A. D. T., Levy, R., Salamon, A., Vilnay, O., Ornai, D., . . . , Levi, S. S. O. (2015). Analytical-Empirical Model for the Assessment of Earthquake Casualties and Injuries in a Major City in Israel—The Case of Tiberias. *Contract*, 3, 9618.
47. Sokat, K. Y., Dolinskaya, I. S., Smilowitz, K., Bank, R. (2018). Incomplete information imputation in limited data environments with application to disaster response. *European Journal of Operational Research*, 269(2), 466–485.
48. Yamazaki, F., Kubo, K., Tanabe, R., Liu, W. (2017, July). Damage assessment and 3d modeling by UAV flights after the 2016 Kumamoto, Japan earthquake. In 2017 IEEE International Geoscience and Remote Sensing Symposium (IGARSS) (pp. 3182–3185). IEEE.

DEA for the Assessment of Regions' Ability to Cope with Disasters



Fuad Aleskerov and Sergey Demin

Abstract Usually, DEA methods are used for the assessment of a region's disaster vulnerability. However, most of these methods work with precise values of all the characteristics of the regions. At the same time, in real life, quite often most of the data consists of expert estimates or approximate values. In this regard, we propose to use modified DEA methods, which will take into account inaccuracy of the data. We apply these methods to the evaluation of wildfire preventive measures in the Russian Federation regions.

Keywords Data envelopment analysis (DEA) · Efficiency assessment · Wildfire · Preventive measures

1 Introduction

Unfortunately, emergency situations, both natural and technological, are an integral part of the modern world. They constantly accompany people, threaten their lives, bring pain and suffering, damage and destroy material values, and cause huge, often irreparable, damage to the environment, society, and civilization.

The annual growth in the number of victims, by 8–9%, and material losses by 10% as a result of emergencies is a steady trend [7]. Global damage from natural disasters can amount up to about 160 billion dollars annually. In addition, the scale of anthropogenic activities in modern society and the complexity of technological processes increased, with the use of a significant amount of explosions, fire, radiation, and chemically hazardous substances. All these facts emphasize the importance of the problems associated with ensuring safety and preserving the economic potential and the environment in cases of emergency.

F. Aleskerov · S. Demin (✉)

Institute of Control Sciences of Russian Academy of Sciences, National Research University
Higher School of Economics, Moscow, Russia
e-mail: alesk@hse.ru; sdemin@hse.ru

© Springer Nature Switzerland AG 2021

I. S. Kotsireas et al. (eds.), *Dynamics of Disasters*, Springer Optimization and Its Applications 169, https://doi.org/10.1007/978-3-030-64973-9_2

31

Since it is important to predict and mitigate the consequences of disasters, the question arises how to execute this properly in certain conditions. Given that there are still no uniform rules, the only solution seems to be just a repetition of the most successful examples. For this reason, it is crucial to determine which cases are effective and which are not.

Consequently, it is necessary to apply some methods of efficiency assessment, compare the results for different examples, and choose the best alternative as a benchmark.

Since Huang et al. [8] claimed that quantitative assessment is very sensitive to the importance of various factors, it is decided to use linear programming approach for the efficiency assessment. This approach was proposed by Charnes and Cooper [3] and consists of using the linear fraction function of several features of the object as its efficiency. Later, this approach evolved into the widely used methodology known as data envelopment analysis [4]. Nowadays, it is used in different spheres and for different tasks: financial portfolio efficiency [15], for greenhouse gases control in electric power generation [12], manufacturing firm comparison [13], etc.

As mentioned above, data envelopment analysis (DEA) is based on the idea of efficiency assessment of different decision-making units (DMUs) by the fraction of DEA parameters. All objects are characterized by two vectors – inputs, such as resources spent, and outputs, which are basically interpreted as achieved results.

Considering multi-objective optimization (cost minimization and output maximization), Charnes et al. [4] proposed to calculate the efficiency of DMU as a fraction of weighted sum of outputs over the weighted sum of inputs. In addition, taking into account rationality and the meaning of the efficiency, there should be constraints, which guarantee that the efficiency of all objects lies in the interval $[0, 1]$.

As a result, the full form of the problem is written as

$$\max_{u_i, v_j} \frac{\sum_{i=1}^M u_i y_{ik}}{\sum_{j=1}^N v_j x_{jk}}$$

under the constraints $\forall i, j, k$

$$\begin{cases} \frac{\sum_{i=1}^M u_i y_{ik}}{\sum_{j=1}^N v_j x_{jk}} \leq 1 \\ u_i \geq 0 \\ v_j \geq 0 \end{cases}$$

Here, y_{ik} and x_{jk} are the outputs and inputs of the k -th DMU, while u_i, v_j are non-negative model coefficients, showing the importance of output and input parameters, respectively.

Solving this problem for each object in comparison, we get the optimal frontier, where the efficiency is equal to 1. For all DMUs lying below this frontier, the efficiency is evaluated using the distance from the benchmark frontier.

DEA has been applied for different disasters. For example, Li et al. [10] applied DEA to the flood disaster vulnerability assessment in the Dongting Lake region (China). Aleskerov and Demin [2] analyzed technological disasters in different regions of the Russian Federation. Meanwhile, Cheng and Chang [5] proposed to use it for the analysis of the effectiveness of earthquake risk reduction policy implementation, and Yu et al. [14] worked with the vulnerability of important economic Chinese regions to the typhoon disasters.

Moreover, there are some modifications of DEA. For instance, de Almada Garcia et al. [6] used DEA for the assessment of the security level at a nuclear power plant. For this purpose, it was proposed to take into account the specification of some problems. For example, it was claimed that the severity of the failure mode is much more important than all other criteria (occurrence and detectability). Therefore, it is necessary to place some restrictions on the features' weight indices. This will allow the construction of a more realistic and more precise method, which will pay attention to the ratio of importance of different criteria, which must be respected in solving some problems.

However, for the application of all aforementioned versions of DEA, it is necessary to get precise assessments of all DMUs' features. Meanwhile some characteristics, such as a region's population or GDP, are estimated roughly, because small deviations in these parameters are not so important.

Furthermore, there are some characteristics which cannot be measured directly. For instance, in the case of a region's disaster preventive measures' efficiency comparison, such features as the potential number of killed or injured people, or total economic losses, are evaluated using some simulation models. Therefore, these parameters cannot be precise because of inaccuracy of the simulation process and are usually given as approximate values.

As a result, it is clear that for application in real life, it is better to use some specific DEA modifications which can work with approximate data.

2 Framework

In our research, we propose two methods which will solve the highlighted problem.

We discard all stochastic and probabilistic approaches based on fuzzy logic, which are mainly used in modern DEA modifications for rough data [9, 11]. Indeed, in some cases it might be too demanding to request stochastic or probabilistic evaluations of parameters. That is why we propose to use simple intervals for the parameter assessment instead of single value (pair (y_{ik}^-, y_{ik}^+) instead of y_{ik}). But for the comparison of the objects, we need to clarify new methodology for the parameters' value comparison ($>_i$ – comparison according to the i -th output feature):

$$\text{object}_k >_i \text{object}_l \iff y_{ik}^- > y_{il}^+$$

In turn, if both inequalities $y_{ik}^+ > y_{il}^-$ and $y_{il}^+ > y_{ik}^-$ hold, which means that intervals (y_{ik}^-, y_{ik}^+) and (y_{il}^-, y_{il}^+) are intersecting, objects k and l are incomparable.

Using this type of data representation and parameters comparison, we can apply two IDEA (interval DEA) methods.

The first one is based on the idea that some DMUs might be near the efficiency frontier. But, in the case of basic DEA, they will not get 100% efficiency. We want to discard this drawback. Hence, we propose to assign 100% efficiency, not only to the objects on the best efficiency frontier but also to the DMUs, which are incomparable with them. As a result, the so-called best tube of 100% efficient objects is constructed (consequently, the method is called the “best tube” IDEA). Efficiency of all other DMUs is assessed by the basic DEA.

The second proposed IDEA method is based on the idea that any parameter (both input and output) might be the most important during the DMU comparison. Consequently, if one of the objects has the best value according to at least one feature, it should be considered as the best one. Technically, it means that the Pareto optimality principle should be used:

$$\text{object}_k > \text{object}_l \iff \begin{cases} y_k \geq y_l \\ x_k \leq x_l \end{cases} \iff \begin{cases} \forall i y_{ik}^- \geq y_{il}^+ \\ \forall j x_{jk}^+ \leq x_{jl}^- \end{cases}$$

This principle has some attractive properties [1] and can be efficiently applied for the comparison of the objects with interval assessments of the features.

According to the Pareto optimality principle, the set of the best objects is constructed from all objects which are not Pareto-dominated:

$$C_{\text{Pareto}}(X) = \{y \in X \mid \nexists x \in X : x > y\}$$

As a result, we propose the Pareto IDEA, according to which, in the first step, the procedure chooses all Pareto optimal DMUs and assigns 100% efficiency. Afterward, all other objects are evaluated by the basic DEA.

3 Application of the Model

Next, we compare wildfire preventive measures in different regions of the Russian Federation. Any precautionary measures definitely demand financial funds, and this is the most important input parameter. However, information about direct expenditures on fire-preventive events is not available, so we use two different money flows as input parameters: environmental protection and investments in agriculture and forestry. The first money flow directly influences the security of the forests. Meanwhile, the second money flow improves the quality of forestry. As a result, the quality and the amount of produced wood increase, and wildfire security is one of the ways of saving the forest, which can then be sold in future.

In turn, we also need to parametrize the results of precautionary measures. In this part, we consider two main characteristics: the number of wildfires in the region and the area of forest land covered by fires.

In order to conduct our research more correctly, we compare only 46 Russian regions, which face the problem of wildfires (these regions have at least 10 wildfires per year). We apply three methodologies for these DMUs: basic DEA, best tube IDEA, and Pareto IDEA.

4 Results and Analysis

As a result of applying different methodologies, we got three efficiency assessments for each region. Consequently, there are three different rankings of the Russian regions, according to each DEA modification.

As expected, the results of all methods give us almost the same order, with slight distinctions (the best regions are in Table 1 and the worst regions are in Table 2). The main difference is the fact that interval DEA shows better results (higher efficiency), because it assigns 100% result to some “additional” objects in the comparison set, which are furthermore excluded from the subsequent efficiency evaluation process. As a result, the benchmark for all inefficient DMUs becomes worse and improves their efficiency.

Moving to particular results, it is necessary to point out seven regions, which get 100% efficiency according to all methods: Novgorod Oblast, Udmurtia, Penza Oblast, Ulyanovsk Oblast, Republic of Khakassia, Kamchatka Krai, and Magadan Oblast. Good results of these regions can be explained by different reasons. The first five are just regions with small territory (less than 0.4% of the area of the Russian Federation); therefore it is not complicated to monitor and resist wildfires. Magadan Oblast mainly consists of mountainous desert, so wildfire is also not a

Table 1 Regions with the best wildfire preventive measures

	Basic DEA	Best tube IDEA	Pareto IDEA
Novgorod Oblast	1	1	1
Udmurtia	1	1	1
Penza Oblast	1	1	1
Ulyanovsk Oblast	1	1	1
Republic of Khakassia	1	1	1
Kamchatka Krai	1	1	1
Magadan Oblast	1	1	1
Vladimir Oblast	0.93	1	1
Saratov Oblast	0.82	1	1
Kemerovo Oblast	0.57	1	1
Sakhalin Oblast	0.46	0.58	1

Table 2 Regions with the worst wildfire preventive measures

	Basic DEA	Best tube IDEA	Pareto IDEA
Krasnoyarsk Krai	0.00	0.00	0.01
Irkutsk Oblast	0.00	0.00	0.02
Sverdlovsk Oblast	0.00	0.01	0.03
Chelyabinsk Oblast	0.01	0.01	0.05
Republic of Bashkortostan	0.01	0.02	0.07

serious problem for this region. Kamchatka Krai is the only region which might be characterized as a real benchmark, because more than 14.5% of the Kamchatka Krai represents the specially protected area and, according to the results of the research, protection is provided by high qualified professionals.

However, the worst regions – Krasnoyarsk Krai, Irkutsk Oblast, and Sverdlovsk Oblast – should also be mentioned, and their low ranking can be explained by the fact that these regions are at the top of the region list according to area (Krasnoyarsk Krai constitutes about 14% of the Russian Federation area). But the fact is that in every summer in the Russian Federation, huge territories in Siberia suffer from wildfires.

5 Conclusion

We applied two new methods based on data envelopment analysis to the regions of the Russian Federation. Both of them help in solving the problem of uncertainties in the data by using interval assessments of the regional parameters. Obtained rankings of preventive measures in different regions are similar to the ranking obtained by the basic DEA.

It should be mentioned that these methods may be successfully applied to similar problems.

Acknowledgments The paper was prepared within the framework of the Basic Research Program at the National Research University Higher School of Economics (HSE) and supported within the framework of a subsidy by the Russian Academic Excellence Project “5–100.” The work was conducted by the International Centre of Decision Choice and Analysis (DeCAN Lab) of the National Research University Higher School of Economics.

References

1. Aleskerov F., Multicriterial Interval Choice Models, *Information Sciences*, 80 (1994) pp. 25–41
2. Aleskerov F., Demin S., 2016: *An Assessment of the Impact of Natural and Technological Disasters Using a DEA Approach*, *Dynamics of Disasters—Key Concepts, Models, Algorithms, and Insights*. Switzerland: Springer, pp. 1–14

3. Charnes A., Cooper W., 1962: *Programming with linear fractional functional*, Naval Research Logistics Quarterly, vol. 9, pp. 181–186
4. Charnes A., Cooper W.W., Rhodes E., 1978: *Measuring the Efficiency of Decision Making Units*, European Journal of Operational Research 2, pp. 429–444
5. Cheng H.-T., Chang H.-S., 2018: *A Spatial DEA-Based Framework for Analyzing the Effectiveness of Disaster Risk Reduction Policy Implementation: A Case Study of Earthquake-Oriented Urban Renewal Policy in Yongkang, Taiwan*, Sustainability, 10: 1751
6. De Almada Garcia Adriano, P., Curty Leal Junior I., Alvarenga Oliveira M., 2013: *A weight restricted DEA model for FMEA risk prioritization*, Producao, v. 23, n. 3, pp. 500–507
7. Guha-Sapir D., Hoyols P., 2012: *Measuring the human and economic impact of disasters*, CRED, Government Office for Science
8. Huang J., Liu Y., Ma L., 2011: *Assessment of regional vulnerability to natural hazards in China using a DEA model*, Int. Journal Disaster Risk Science, 2 (2), pp. 41–48
9. Kuamr N., Singh A., 2017: *Efficiency evaluation of select Indian banks using fuzzy extended data envelopment analysis*, Int. J. Information and Decision Sciences, 9(4), pp. 334–352
10. Li C.-H., Li N., Wu L.-C., Hu A.-J., 2013: *A relative vulnerability estimation of flood disaster using data envelopment analysis in the Dongting Lake region of Hunan*, Natural hazards and earth system sciences, 13(7), pp. 1723–1734
11. Namakin A., Najafi S.E., Fallh M., Javadi M., 2018: *A New Evaluation for Solving the Fully Fuzzy Data Envelopment Analysis with Z-Numbers*, Symmetry, 10, 384
12. Sanchez L., Vasquez C., Vilorio A., 2018: *The Data Envelopment Analysis to Determine Efficiency of Latin American Countries for Greenhouse Gases Control in Electric Power Generation*, International Journal of Energy Economics and Policy, 8(3), pp. 197–208
13. Smriti T.N., Khan Md H.R., 2018: *Efficiency Analysis of Manufacturing Firms Using Data Envelopment Analysis Technique*, Journal of Data Science, 16(1), pp. 69–78
14. Yu X., Chen H., Li C., 2019: *Evaluate Typhoon Disasters in 21st Century Maritime Silk Road by Super-Efficiency DEA*, International Journal of Environmental Research and Public Health, 16(9): 1614
15. Yucel L., 2010: *Measuring the Efficiency of Portfolios with Data Envelopment Analysis*, Sosyal Bilimler Dergisi, 2, pp. 116–121

The Crisis Classification Component to Strengthen the Early Warning, Risk Assessment and Decision Support in Extreme Climate Events



Gerasimos Antzoulatos, Anastasios Karakostas, Stefanos Vrochidis, and Ioannis Kompatsiaris

Abstract Climate change is considered as being one of the most important challenges of modern times, having multiple and significant impacts on human societies and environment. The negative effects which are revealed through weather extreme events and causing distress and loss of property and human lives will become more intensive in the future, especially in poor countries. Hence, there is an urgent need to develop novelty tools to enhance awareness and preparedness, to assess risks and to support decision-making, aiming to increase the social resilience to climate changes.

The proposed open-source holistic beAWARE framework encompasses technological achievements that enables first responders and authorities to manage efficiently the pre-emergency and emergency phases of a hazardous natural event. Specifically, the Crisis Classification component of beAWARE platform consolidates functionalities to provide dual services: (a) firstly, as an Early-Warning system, aiming to estimate the crisis level of the upcoming extreme conditions such as the hazard of flood, fire or heatwave (pre-emergency phase), and (b) secondly, as a Real-Time Monitoring and Risk Assessment system aiming to assess the risk and support to make accurate and timely decisions, when a crisis has evolved.

Keywords Risk assessment · Crisis classification · Early warning systems · Risk-based decision support systems · Natural disasters

1 Introduction

The characteristics of the recent crises differ significantly compared with the past crises, as the former are unexpectedly large scale and unprecedented. Also,

G. Antzoulatos (✉) · A. Karakostas · S. Vrochidis · I. Kompatsiaris
Centre for Research and Technology Hellas (CERTH), Information Technologies Institute (ITI),
Thermi-Thessaloniki, Greece
e-mail: [gantoulatos@iti.gr](mailto:gantzoulatos@iti.gr); akarakos@iti.gr; stefanos@iti.gr; ikom@iti.gr

they exhibit an unusual combination and transboundary nature spreading across geographic borders and/or policy boundaries and may create significant economic knock-on effects [3, 6]. As Charles Baubion reported in [6], the increasing number of modern crises, often consisting of new threats, rises the complexity and requires the involvement of many actors above and beyond emergency services, resulting in the demand of effective coordination so as to confront successfully these crises. Additionally, as human societies become more and more complex and interconnected, the vulnerability and exposure at new and unforeseen crises and threats are amplified, and the cascading effects spread very fast [6].

Furthermore, due to the climate change, the characteristics of natural hazardous weather events and threats are changing as well presenting an increasing frequency and severity, resulting in cascading impacts to human societies. Climate change refers to a change in the state of the climate that can be identified (e.g. by using statistical tests) and that persists for an extended period, typically for at least a few decades or longer [27]. Climate change can be caused by natural external forcings (e.g. modulations of the solar cycles and volcanic activity) and by anthropogenic forcings (e.g. changes in the composition of the atmosphere or in land use). There is strong evidence that currently observed changes in many climate variables, including extremes, can be attributed to anthropogenic climate change [7, 49, 52].

Over the past decades Europe faced the increase in severity, duration and/or extent of many types of extreme weather- and climate-related events, and research indicates that under future climate change, this trend will persist [18, 19, 28]. Particularly, global warming is projected to intensify the hydrological cycle and increase the occurrence and frequency of flood events (including pluvial floods and flash floods) in large parts of Europe; frequency, intensity, duration and health impacts of heatwaves will increase, especially in southern and south-eastern Europe; projected increases in heatwaves, droughts and dry spells will lead to expansion of the fire-prone areas and increase the duration and severity of fire seasons across Europe, mostly in southern Europe. According to the European Environment Agency (EEA), the total reported economic losses caused by weather- and climate-related extremes in the 33 EEA member states over the years 1980–2016 over EUR 450 billion [18]. The largest share of the economic impacts was caused by floods (approximately 40%), while heatwaves were the deadliest, followed by flooding, landslides and forest fires. In this changing landscape of crises, governments, crisis managers, disaster risk management agencies, civil protection and other actors need to adapt their procedures to anticipate, respond and recover from the new hazardous crisis events effectively [6]. Thus, the crisis management processes and tools should be reconsidered and redesigned in order to cope with these new crisis challenges.

Towards this direction, the beAWARE platform aims to deploy in a unified and holistic framework, state-of-the-art methodologies and technologies in order to analyse and semantically fuse the obtained heterogeneous data through intelligent reasoning mechanisms. The ultimate objective is to assist the engaged stakeholders (authorities, first responders, crisis managers, decision-makers, etc.) to confront effectively either a forthcoming extreme event (Early-Warning phase) or the evolution of an extreme crisis. It is worth to note that in the two latest editions of Global

Risks Reports (published by the World Economic Forum), the extreme weather events were ranked first among top ten global risks in terms of likelihood and second in terms of impact, just behind weapons of mass destruction [11, 12]. This is a significant evidence that the scientific and research interest is increased to confront the extreme disruptive nature events and assess the risk in order to strengthen the resilience of our societies.

Among the other components of beAWARE platform, the *Crisis Classification* has been conceived to encompass technologies in order to provide services into two directions: (a) firstly, as an Early-Warning system aiming to notify the authorities and first responders to the upcoming extreme conditions such as the hazard of flood, fire or heatwave (pre-emergency phase) and (b), secondly, as a Real-Time Monitoring and Risk Assessment system when a crisis is evolved aiming to support local stakeholders, authorities and rescue teams to make accurate and timely decisions and actions. In this work, we focus on the Crisis Classification component and analyse its operation as an Early-Warning and recommendation system for preventing and reducing the effects from floods, wildfires and heatwaves.

The rest of this paper is structured as follows: after a brief presentation of the related work and useful background in Sect. 2, the architecture of the Crisis Classification component and its main functionalities are analysed focusing on the Early-Warning component (Sect. 3), and subsequently the application of the Early-Warning component to the three use cases is exhibited (Sects. 4.1–4.3). Finally, in Sect. 5, future directions and concluding remarks will be mentioned.

2 Related Work

Before we proceed with the analysis of the Crisis Classification architecture and methodological framework, it will be useful to present briefly the relevant background notions, approaches and methods that have been proposed in the field of decision support systems for crisis risk assessment focusing on the three use cases, namely, the flood, fire and heatwave.

2.1 Decision Support Systems for Crisis Management

Crisis management is a dynamic, complex and multidisciplinary process, that consists of consecutive sets of activities including the collection of information, the analysis of heterogeneous data and the formulation of alternative decision-making processes for implementation and monitoring of a crisis [21, 44]. As authors state, an integrated framework for extreme risk analysis should include the following four steps [44]:

1. Scenario formulation in which the collection and analysis of data related to hazards in terms of their possible origins, pathways and mitigation are defined;

2. Extreme risk assessment in which the list of potential extreme events together with their exposure or vulnerability is formulated;
3. Extreme risk management in which the development of mitigation measures and procedures based on the output from the risk characterisation should be carried out;
4. Communication by using a dedicated platform to enable a better understanding of the rationale behind the categories of risk assessment.

Furthermore, they conclude that in the modern literature, a lot of applications are presented, procedures and activities able to anticipate, prepare for, prevent and reduce different types of risks/losses associated with different types of crises, but there are only a few integrated frameworks to deal directly with these extreme events. In this case, the decision-maker needs technical assistance to support the decision-making process before, during and after extreme events [44]. Moreover, towards the direction to cover this gap, Ezzeldin [21] proposed a conceptual framework for the information elements that should be included in any effective decision support system in crisis management unit. This framework, which contains five parts, can be a basis for understanding the nature of the decision support system in a crisis situation, as claimed by authors. Generally, the concept of risk refers to the combination of the probability of a certain hazard to occur and of its potential negative impacts [20, 32, 44, 53]:

$$R = f(H \times V \times E) \quad (1)$$

where

- H denotes the hazard
- V denotes the vulnerability
- E denotes the exposure

Specifically, the *Hazard* is the occurrence of the physical event, which can happen with a certain probability and intensity. The difference between the hazard and the disaster is that a hazard may not cause any negative impact [17]. *Vulnerability* is defined as the susceptibility or predisposition for loss and damage to human beings and their livelihoods, as well as their physical, social and economic support systems when affected by hazardous physical events. Vulnerability includes the characteristics of a person or group and its situation that influences its capacity to anticipate, cope with, resist, respond to and recover from the impact of a physical event [8, 25, 48]. *Exposure* is defined in this report as the presence of people, livelihoods, environmental services and resources, infrastructure and economic, social and cultural assets in areas or places that are subject to the occurrence of physical events and that thereby are subject to potential future negative impacts [26, 53]. The first two elements, hazard and vulnerability, are characterised by probability distributions, while the latter, exposure, is measured in money. The result of R is an expected value measured in a monetary unit.

2.2 DSS for Flood Crisis Management

In the context of a natural disaster, the emergence of numerous Early-Warning systems and specialised decision support systems (DSS) plays an important role in assisting to reduce the risks resulting from the interaction of human societies and their natural environments. Especially floods can be classified among the most disastrous natural phenomena, since they can cause fatalities and severe damages to the environment and the economic development of the affected areas. Recognising these negative aspects of flood crises, the EU introduced the European Flood Directive 2007/60/EU which demands for the preparation of flood hazard and risk maps and finally flood risk management plans at the level of the river basin district from all Member States [20, 41].

By motivating this, remarkable scientific/research efforts have been made to develop decision support systems dedicated to flood risk management, serving various aspects of decision options for prevention, mitigation, preparation, response and recovery from flood impacts [1, 4, 9, 14, 24, 31, 45, 40, 55]. In [45] a classification of these systems according to their functional roles has been proposed.

Currently, the majority of these emerged tools are not capable of providing an integrated and generalised framework for formulating decision options for crisis level estimation and risk assessment. Furthermore, the advances to the Internet of things (IoT) as well as the increasing volume of heterogeneous data from multiple resources (mobile phones and Apps, sensing data, drones, etc.) generate new capabilities and opportunities to timely alerting and tackling effectively an extreme weather or natural phenomenon. The authorities, risk managers and decision-makers should confront new challenges in flood risk management by operating in a holistic and interoperable framework combining data from multiple resources. A few efforts toward this direction have been made by proposing generalised platforms combining the flood risk management-relevant science, such as the Iowa Flood Information System (IFIS) [14], FLOODSS [40] and Flood Disaster Management System (FDMS) [45].

2.3 DSS for Fire Crisis Management

In the framework of fire, noteworthy efforts have been made towards creating Early-Warning and decision support systems for fire crisis management. Specifically, a number of decision support GIS platforms have been developed which support wildfire prevention and/or control activities focusing on fire detection, fire weather, fire risk analysis and fire behaviour modelling [5, 10, 13, 23, 34, 50].

The acquired knowledge from these systems enables fire protection agencies to spatially define and identify forecasted high-risk areas and plan the necessary preventive and control actions [50]. The Firementor system primarily focuses on the provision of services for decision and operational support in fire suppression [37].

AUTO-HAZARD PRO (AHP) is a decision support system for prevention planning and emergency management of forest fire events. The system encompasses functionalities for weather data management, geographical data viewer, a priori danger forecasting and fire propagation modelling, automatic fire detection and optimal resource dispatching [30]. The major limitation of the Firementor and AHP DSS is that they are not web-based applications. On the contrary, the WFDSS [42] and European Forest Fire Information System (EFFIS) [47] operate through the web. The WFDSS provides a comprehensive, risk-informed decision-making and implementation planning, while the EFFIS aims to provide up-to-date, reliable, and harmonised information on forest fires during both pre- and post-fire phases at a European and Mediterranean level. Virtual Fire is a web-based platform which integrates advanced technologies, tools and protocols into a state-of-the-art web-based GIS application, to assist on early fire warning, fire control and coordination of firefighting forces [29].

2.3.1 Fire Weather Indices

One of the main characteristic of the above decision support systems for fire risk management systems relies on the utilisation of indices that enable to estimate the fire danger. A well-known and popular indicator is the *Canadian Forest Fire Weather Index (FWI)* [54], which comprises six standard components. The first three are fuel moisture codes that follow daily changes in the moisture contents of three classes of forest fuel with different drying rates. The last three components are fire behaviour indexes representing the rate of spread, fuel weight consumed and fire intensity. The system depends solely on weather readings taken each day at noon local standard time (LST): temperature, relative humidity, wind speed and rain during the previous 24 h. A brief description of the six components is presented below [33]:

- The *Fine Fuel Moisture Code (FFMC)* is a numeric rating of the moisture content of litter and other cured fine fuels. The FFMC is an indicator of the relative ease of ignition and flammability of fine fuels.
- The *Duff Moisture Code (DMC)* is a numeric rating of the moisture content of loosely compacted organic (duff) layers of moderate depth. The DMC is an indicator of fuel consumption in moderate duff layers and medium-sized downed woody material.
- The *Drought Code (DC)* is a numeric rating of the moisture content of deep, compact organic layers. The DC is an indicator of seasonal drought effects on forest fuels and the amount of smouldering in deep duff layers and large logs.

The two intermediate fire behaviour indexes represent fire spread rate and amount of available fuel:

- The *Initial Spread Index (ISI)* is a numeric rating of the expected rate of fire spread, which combines the effects of wind and FFMC on rate of spread without the influence of variable quantities of fuel.

Table 1 FWI ranges and the six danger classes

FWI ranges	Fire danger class
<2	Very low danger
[2, 6)	Low danger
[6, 13)	Moderate danger
[13, 26)	High danger
[26, 48)	Very high danger
≥48	Extreme danger

- The *Buildup Index (BUI)* is a numeric rating of the total amount of fuel available for combustion, which combines DMC and DC.
- The final fire behaviour index, the *Fire Weather Index (FWI)*, combines ISI and BUI to represent the intensity of a spreading fire as energy output rate per unit length of fire front.

The EFFIS developed and utilised the FWI and categorised its value into six (6) danger classes defined with simple FWI thresholding, irrespective of the fuel types (Table 1).

However, in the current EFFIS, implementation of the FWI proposed 5 fire danger classes which are determined after the study of 2000 large fires of more than 500 hectares occurred in Europe during 20 years [47].

2.4 DSS for Heatwave Crisis Management

Heatwave Early-Warning systems aim to reduce the human health consequences of heatwaves. These systems involve various functionalities including the forecasting of the heatwave event, the prediction of possible health outcomes, the triggering of effective and timely response plans targeting vulnerable populations, the notification of heatwave events, the communication of messages and the evaluation and revision of systems [15, 16, 46]. In Europe, the need to develop plans to effectively cope with extreme heatwave events emerged after several devastating heatwave crisis events. Thus, many countries implemented Heatwave Early-Warning System (HEWS) as a risk reduction strategy aiming to reduce avoidable human health consequences of heatwaves through timely notification of prevention measures to vulnerable populations [35].

In [36] an Early-Warning system exploiting the reliable sub-seasonal-to-seasonal (S2S) climate forecasts of extreme temperatures is proposed. The system aims to improve the exploitation of short-to-medium-term resource management and the incorporation into heat-health action plans aiming to protect vulnerable populations and ensuring access to preventive measures ahead of imminent heatwave events in Europe. As heatwaves have significant impacts on both ecosystems and human beings, the scientific interest focuses on understanding the phenomenon including how heatwaves are measured, their driving mechanisms observed and projected

changes, and quantifying the anthropogenic influence behind these changes. In review papers [43, 56], the authors attempt to present an overview of the advances that have been carried out to deal with these challenges.

3 High-Level Architecture of Crisis Classification Component

The Crisis Classification component is designed to provide twofold functionalities in an innovative and beneficial manner. The proposed unified and holistic framework for crisis management encapsulates services and tools which cover the pre-emergency as well as the emergency phase providing important capabilities to stakeholders. Hence, the *Early-Warning module* actively involves the communities at risk, by raising their awareness of the upcoming risk and ensuring their preparedness. Furthermore, the *Real-Time Monitoring and Risk Assessment module* enables to track and report constantly the evolvement of an ongoing extreme event, by assessing its severity/risk. Another advantage is that the Crisis Classification system combines the fused heterogeneous information acquired from individual incidents or group of incidents. Finally, Crisis Classification is flexible to adapt and handle any type of crisis event, even a compound of extreme events in a multi-hazard scenario.

The *Early-Warning module* is able to analyse heterogeneous sensory data and forecasts from weather/flood/fire prediction systems in order to estimate the potential overall crisis level supporting the authorities to evaluate the severity of the forthcoming extreme natural event (e.g. flood, forest fire, heatwave) in specific areas and/or regional level (Fig. 1). In the Data Acquisition phase, the sensing data easily is imported into the system by employing the appropriate deployed tools for this purpose. Furthermore, the Early-Warning component is able to obtain predictions from weather forecasting models, such as the High-Resolution Limited Area Model (HIRLAM), as well as estimations for river water level (i.e. AMICO model) and fire danger (e.g. the Forest Fire Weather Index from EFFIS). In the Sensor Fusion module, a data fusion algorithm, which relies on a rule-based approach, combines the obtained forecasts in order to estimate the upcoming crisis severity level. The aggregated stream data are forwarded to the control centre (public-safety answering point – PSAP) and to beAWARE dashboard so as to communicate to decision-makers and other stakeholders by using interactive and user-friendly visualisations. Also, hazard and risk/impact maps are provided to the crisis managers and people in control room aiming to assist them in the decision-making process.

During the emergency phase, when a hazardous natural event is evolving, the *Real-Time Monitoring and Risk Assessment module* is designed to analyse data from heterogeneous sources (sensory data, outcomes of multimedia and textual analytical processes in the beAWARE framework), in order to provide tractability facilities of the crisis-to-crisis management and reliable risk assessments. It integrates a multi-layer fusion approach which encompasses the data/information fusion layer and the decision fusion layer (Fig. 2). In the Information/Data Fusion phase, methodologies

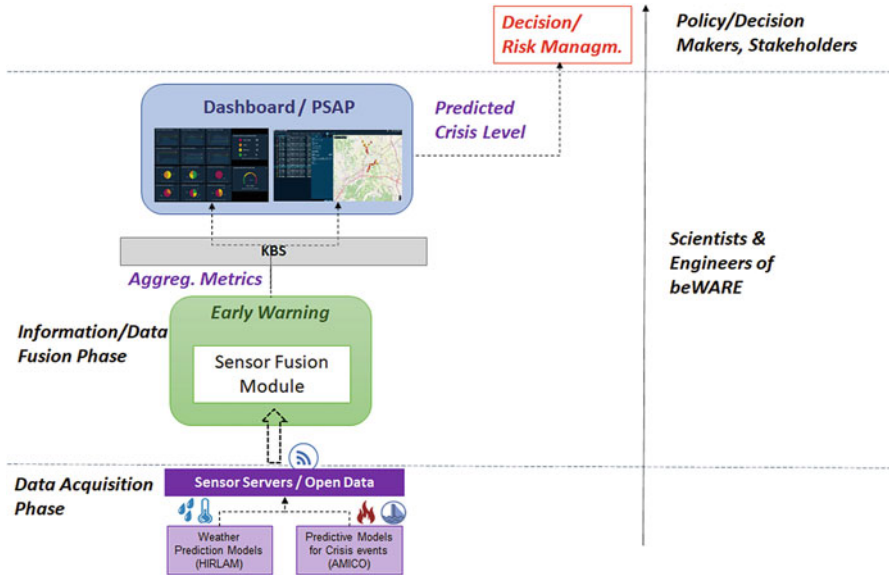


Fig. 1 High-level architecture of Early-Warning module

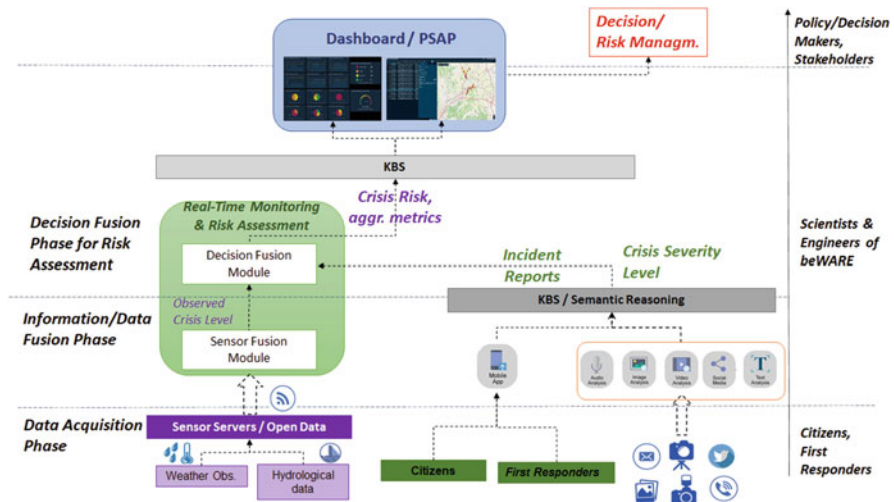


Fig. 2 High-level architecture of Real-Time Monitoring and Risk Assessment module

of information/data fusion will be employed aiming to combine the sensory real-time data and result in reliable estimates regarding the crisis level. In the Decision Fusion phase for Risk Assessment phase, methods and techniques are conceived and employed for exploiting the synthesis of the decisions, which are obtained based on individual beAWARE modalities. The goal is to make a fused decision which is analysed further to obtain a final decision about the risk of ongoing crisis event.

4 Crisis Classification Component as an Early-Warning System

The Crisis Classification component has been designed to operate as an Early-Warning system aiming to notify seamlessly and accurately the crisis managers and decision-makers for a potentially disruptive natural extreme event. It consists of the following basic steps:

- Step 1. **Data Acquisition module:** weather, flood and fire danger estimations are gathered from various prediction models in the region of interest.
- Step 2. **Sensor Fusion module:** the obtained data from the previous step feed this module, and the output is an assessment of the overall crisis level in the region of interest.
- Step 3. **Visualisation module:** the outcomes of the Sensor Fusion module are forwarded to the beAWARE dashboard and the map at PSAP, producing interactive visualisations. Furthermore, information, whenever is available, extracted from hazard and/or risk/impact maps is presented into the map, enhancing the decision-making process with historical knowledge.

Depending on the users' requirements and needs as well as the use case specifications, the application of the above steps could be customised accordingly. Generally, to evaluate and disseminate beAWARE solution in managing crisis events, there were selected three demonstration scenarios for flood, fire and heatwave use cases to be implemented in Vicenza, Valencia and Thessaloniki, respectively. The locations were selected based on the frequency of the occurrence of those events. In the following subsections, the application of the Early-Warning module in each one of the use cases is described along with the preliminary results of the evaluation process.

4.1 *Application of the Early-Warning Module in the Flood Case*

The main goal of the Early-Warning module is to enhance the preparedness of the authorities and crisis managers to face unplanned events, particularly floods and flash floods. To achieve this goal, in the pro-crisis stage, the Early-Warning module has been developed so as to aggregate and employ the available forecasts for the water river level in the Bacchiglione River Basin at Vicenza district, by attempting to estimate the crisis level of the forthcoming flood event.

In this use case, the Bacchiglione River has been divided into 304 river sections grouped into 6 main clusters (Fig. 3). The predictions for the river water level on these river sections are generated, continuously, every 6 h by the AMICO flood forecasting system. AMICO has been developed by Alto Adriatico Water Authority

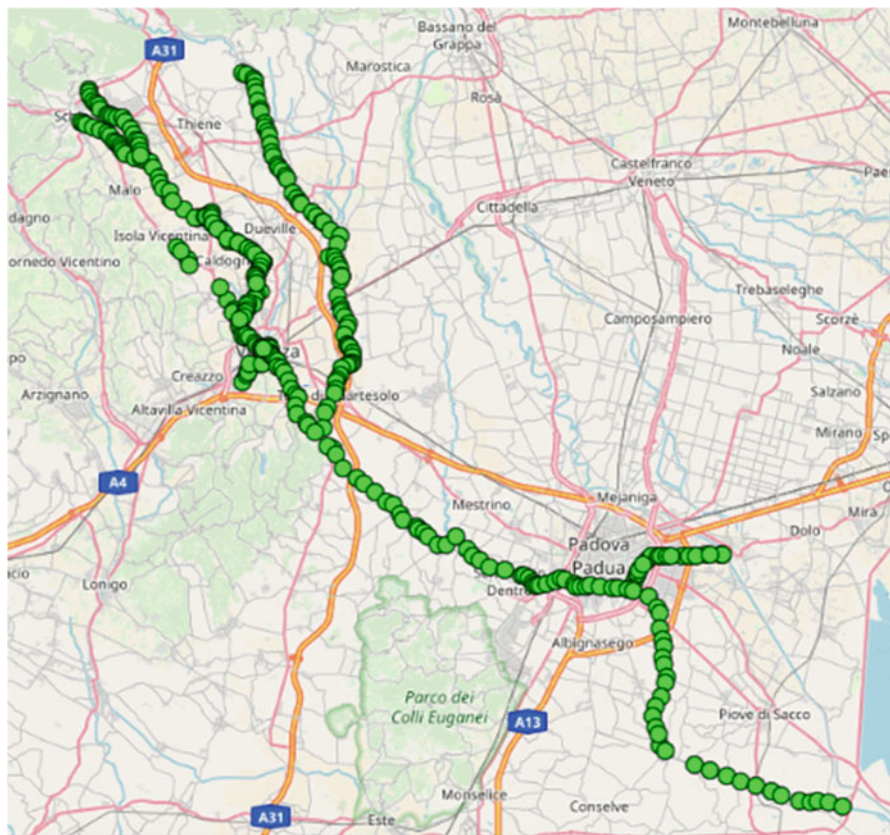


Fig. 3 Overview of 304 river sections in Vicenza district

(AAWA) for the Veneto Regional Civil Protection [22, 38]. It is an operational semi-distributed hydrological and hydraulic model enabling to provide:

- Continuous water balance simulation from the past to the nowadays
- Autocalibration and data assimilation
- Flood forecast based on several weather forecasts (e.g. HIRLAM, LAMI, ECMWF)
- Manual configuration of hydraulic structures
- Data visualisation on GIS

4.1.1 Data Fusion and Rule-Based Approach for Flood Crisis Level Assessment

The proposed data fusion and rule-based approach consists of the following steps:

Step 1. For each river section, a comparison of the predicted water level (WL) with its predefined alarm thresholds is executed. For the i -th river section, a simple rule below is applied:

```

if  $WL_i < AlarmThreshold_1$  then
   $Scale_i = 1$ 
else if  $AlarmThreshold_1 \leq WL_i < AlarmThreshold_2$  then
   $Scale_i = 2$ 
else if  $AlarmThreshold_2 \leq WL_i < AlarmThreshold_3$  then
   $Scale_i = 3$ 
else if  $AlarmThreshold_3 \leq WL_i$  then
   $Scale_i = 4$ 
end if

```

Step 2. For each group of river sections ($k = 1, \dots, 6$) the **Overall Crisis Classification Index (OCCI)** is calculated as follows:

- i. Define the number of river sections which belong to each one of the scale categories (1, 2, 3 and 4). Let's suppose that $Counts_k = [n_{1k}, n_{2k}, n_{3k}, n_{4k}]$ presents a list of categories' cardinality in the k -th group of river sections. n_{ik} denotes the number of river sections which is classified to scale i , where $i = 1, \dots, 4$.
- ii. Calculate the $OCCI_k$ using the generalised (power) mean with power $p = 4$ by the following formula:

$$OCCI_k = \left[\sqrt[p]{\frac{\sum_{sc=1}^4 n_{sc,k} * sc^p}{\sum_{sc=1}^4 n_{sc,k}}} \right] \quad (2)$$

where

$n_{sc,k}$ denotes the cardinality of the sc -th scale category at the k -th group of river sections
 $[\cdot]$ is the upper bound

Step 3. For each group of river sections ($k = 1, \dots, 6$) the **Predicted Flood Crisis Level per group (PFLCL_k)** is calculated as follows:

```

if  $OCCI_k = 1$ , meaning that the WL for the river sections of k-th
group are below the 1st alarm threshold then
     $PFLCL_k = 1$ 
else if  $OCCI_k = 2$  and  $\nexists$  river section r of the k-th group :
 $Scale_r = 4$  then
     $PFLCL_k = 2$ 
else if  $OCCI_k = 2$  and  $\exists$  river section r of the k-th group :
 $Scale_r = 4$  then
     $PFLCL_k = 2+$ 
else if  $OCCI_k = 3$  and  $\nexists$  river section r of the k-th group :
 $Scale_r = 4$  then
     $PFLCL_k = 3$ 
else if  $OCCI_k = 3$  and  $\exists$  river section r of the k-th group :
 $Scale_r = 4$  then
     $PFLCL_k = 3+$ 
else if  $OCCI_k = 4$  then
     $PFLCL_k = 4$ 
end if

```

Step 4. Estimate the overall **Predicted Flood Crisis Level** for the whole region of interest, by aggregating the corresponding flood crisis level of each group taking into consideration the significance of each group. Let us assume that $0 \leq W_k \leq 1$, $k = 1, \dots, 6$ denotes the significant level of the k-th group of river sections, where the maximum value of a weight ($W_k = 1$) presents the highest significance. The lower significance could be 0 which indicates that the particular group does not play any importance role when it is flooded. Thus, the overall Predicted Flood Crisis Level for the region of interest can be estimated by the weighted average over the groups, as follows:

$$PFCL = \frac{\sum_{k=1}^6 W_k \times PFCL_k}{\sum_{k=1}^6 W_k} \quad (3)$$

Furthermore, the Early-Warning component further enhanced by the integration of a mechanism that enables crisis managers to consider the forthcoming flood crisis level along with historical knowledge which is depicted into the appropriate generated flood hazard and risk/impact maps by AAWA. In the flood maps (map at the left in Fig. 4), the geographical areas which could be covered by floodwaters from all natural sources at several levels of probability are indicated along with the flood extent according to historical events, flood depth propagation, velocity of flooding, etc. These maps assist in flood hazard assessment as well as to emergency planning and management under extreme weather conditions.

Additionally, flood impact/risk maps encapsulate the outcomes of a quantitative analysis where the probabilities, the consequences for human health, the environ-

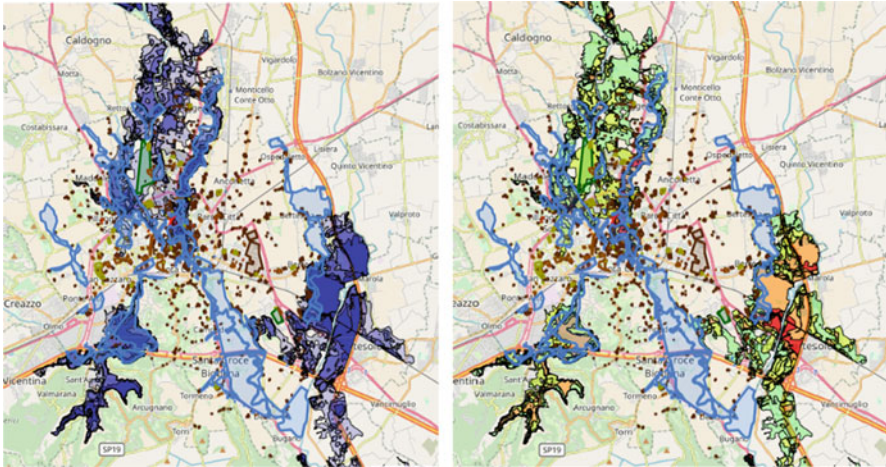


Fig. 4 Vicenza hazard map (left) and flood risk map (right) with return period of 100 years including the historical flood at November 2010 [<https://beaware.server.de/servlet/is/696/>]

ment, cultural heritage and economic activity associated with an extreme flood event are assessed and aggregated into risk number (map at the right in Fig. 4).

The Crisis Classification component acquires this data to classify the crisis event and provides early warnings followed by the estimated crisis level in local scale (identifying small areas of interest) and global scale for the whole region of interest. The results are sent to the PSAP where a metric map and a dashboard interface are displayed allowing the decision makers and crisis managers to interact in several ways.

4.1.2 Results

In the flood use case, the Early-Warning module utilises the estimations for the river water level as generated by the AMICO hydrological and hydraulic model, provided by AAWA. The AMICO model provides hourly estimations of the river water level over specific river sections in the forecasting period of 55 h ahead. From the total 304 river sections, Early-Warning module obtains forecasts and analyses the 60 most significant river sections, which have been indicated by the experts (AAWA team). Moreover, these 60 river sections have been clustered to 6 groups. In each group, one river section is considered as critical. The distribution of the river sections per group is illustrated in Fig. 5.

This series of experiments focuses to evaluate the execution time in each step of the Early-Warning component in the flood pilot. For this reason, we employ various types of real and simulated datasets. Specifically, the AMICO forecasts from the flood crisis event in the period between 31-10-2010 and 03-11-2010 are employed as real case dataset, named “Real Flood Data (2010)”. Also, three simulated datasets

Distribution of River Sections per group

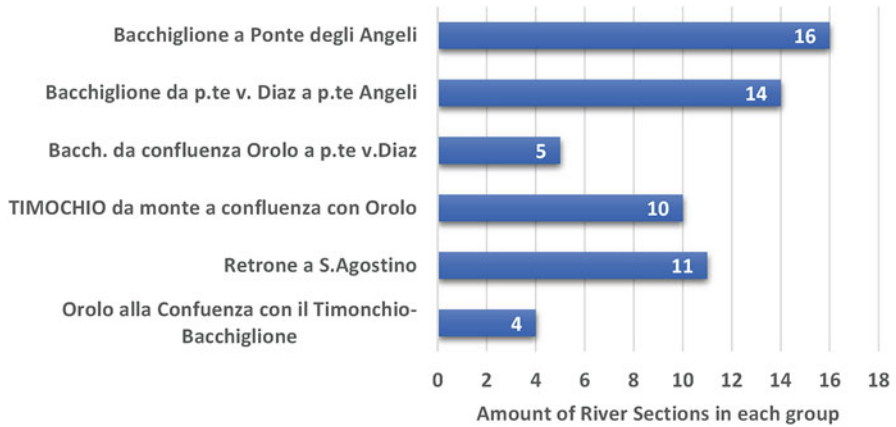


Fig. 5 Distribution of river sections per group

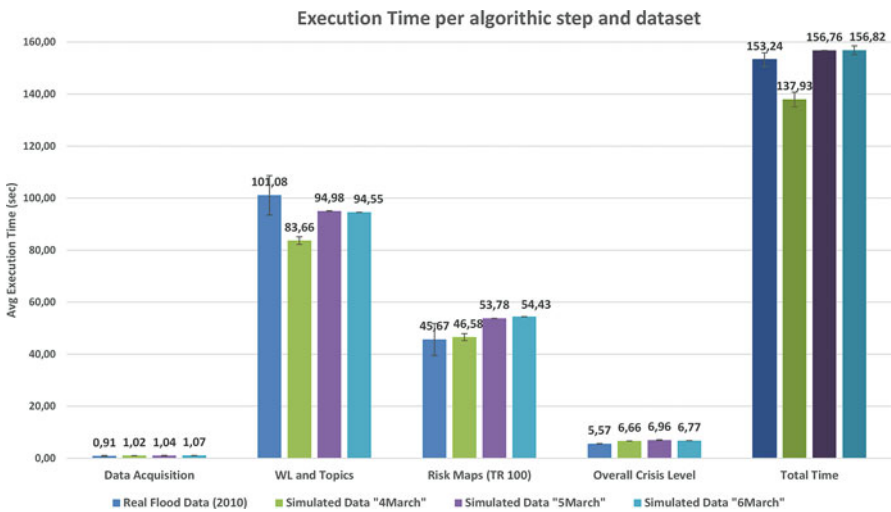


Fig. 6 Execution time per step of Early-Warning module

are utilised which corresponds to different executions of AMICO algorithm with various initial conditions. The forecasts are stored to the FROST-Server, in which all available time-series data is stored centrally for the beAWARE project, and extracted from there via appropriate queries. The number of forecasts that Early-Warning component retrieves is 3300 estimations per AMICO run. The average total execution time after five iterations of the Early-Warning algorithm is less than 3 min (156.82 ± 1.70 s) in the worst case (Fig. 6).

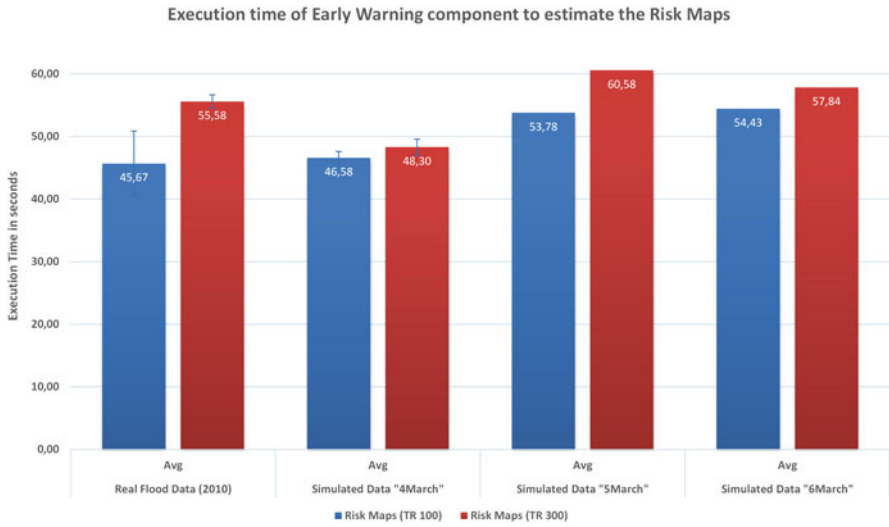


Fig. 7 Execution time of Early-Warning module for risk map estimation in return period of 100 and 300 years

It is worth to note that in the above experiment, the return period of the risk maps is 100 years. In order to examine the effect of the usage of various return periods in the performance of this component, a new set of experiments are carried out. As it is expected, there is a slight deterioration in the time that fluctuates from 1.72 s in the “Simulated Data 4March” dataset to 9.90 s in “Real Flood Data (2010)” case (Fig. 7).

Concerning the performance of the aforementioned data fusion and rule-based approach, in the real case flood event in 2010, the Early-Warning module classified the flood crisis as extreme, as 15 critical river sections which are lied in 4 groups exceeded the third alarm thresholds. The flood crisis was classified as extremely severe in three groups while in the other 3 groups as severe. In the group Retrone a S. Agostino, one critical river section is estimated that will exceed the third alarm threshold in the following hours; thus the level of severity of that group is presented a little bit higher compared with the levels of the other two (Fig. 8).

4.2 Application of the Early-Warning Module in the Fire Case

In the fire use case, the Early-Warning module employs the estimations regarding the fire danger obtained from the EFFIS system. Particularly, it utilises the Canadian Forest Fire Weather Index (FWI) in order to anticipate the fire danger in specific locations around the Parc Natural de l’Albufera in Valencia district (Fig. 9). These points of interest are located closely into popular and crowded areas which contain

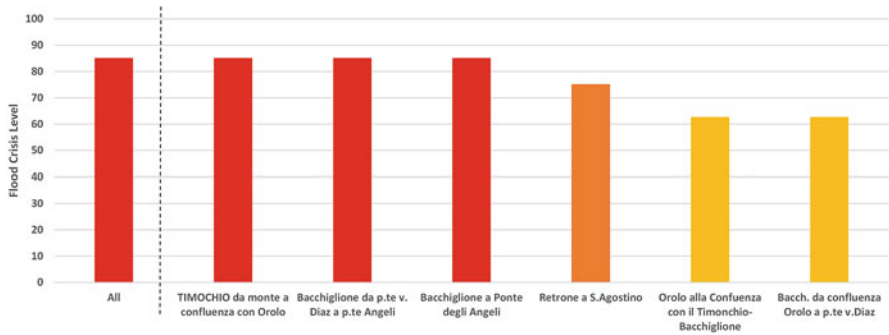


Fig. 8 Flood Crisis Level estimations in all river sections and per group of river sections, relying on water level forecasts between 31-10-2010 and 03-11-2010

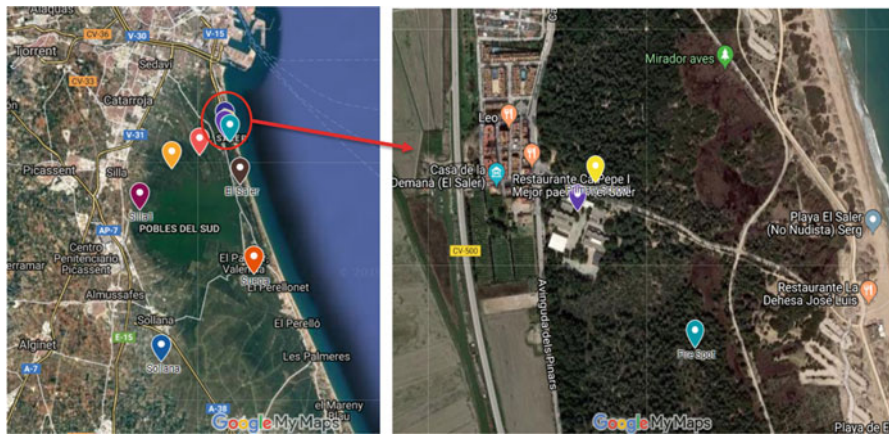


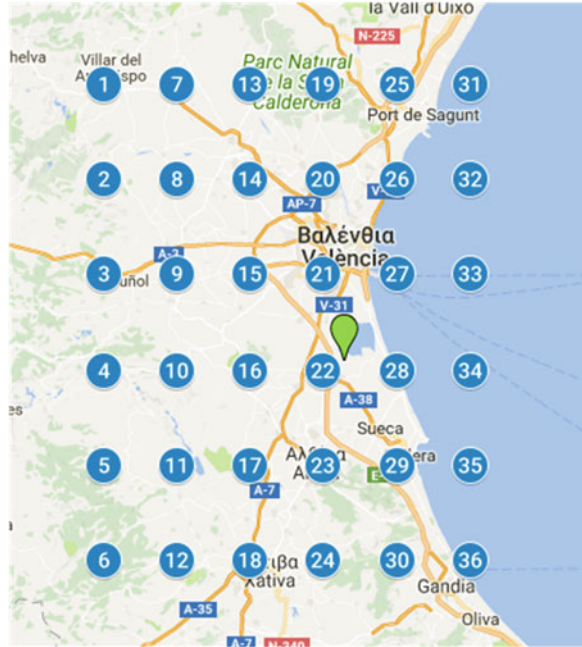
Fig. 9 Points of interest around the Parc Natural de l'Albufera in Valencia district

two schools (primary and secondary), restaurants, the fire spot, camping and other infrastructures.

To anticipate the fire danger on those preset points, the Early-Warning module applies a similar approach as in the flood case that is mentioned above, apart from the intervention of the interpolation step. Specifically, the aim is to estimate the Fire Weather Index (FWI) of the points of interest by utilising the FWI values over a district set of points. The data fusion algorithm performs the following steps:

- Step 1.** The appropriate estimations of the Fire Weather Index (FWI) extracted from the netCDF files obtained from the EFFIS system.
- Step 2.** The interpolation approach is executed for each point of interest:
 - (i) find an adjoin point for which an estimation of the Fire Weather Index exists;

Fig. 10 Distribution of the interpolation points around the Sollana’s adjoin point



- (ii) For this adjoin point, define the district set of points for which the FWI value has been estimated;
- (iii) Extract the Fire Weather Index (FWI) values for all the grid points and apply a piecewise 2D cubic, continuously differentiable interpolation algorithm.
- (iv) Set the interpolant value as a Forest Fire Weather Index for a point of interest.

As an example, let us assume that the point of interest (green pin in the map) is the “Sollana” (Fig. 10). The adjoin point in the grid is this one with label 22. For this point, 36 grid points are taken into consideration, and their FWI values are extracted.

This step is performed sequentially for each one of the points of interest in order to estimate the Fire Weather Index over the forecasting period of 10 days.

Step 3. Then, the Early-Warning module classifies each FWI value into one of the five (5) danger levels according to Table 2. The FWI ranges and the classes are presented in the following table:

Step 4. After that, Crisis Classification module calculates the overall fire crisis level, called as **Predicted Fire Crisis Level (PFRCL)**, which is estimated for each day taking into consideration all the predicted FWI values over all the points of interest, into the particular day. Thus, the following formula is employed:

Table 2 FWI ranges and the five danger classes in current EFFIS implementation

FWI ranges	Fire danger class
<5.2	Very low danger
[5.2, 11.2)	Low danger
[11.2, 21.3)	Moderate danger
[21.3, 38)	High danger
≥38	Very high danger

$$PFRCL_d = \left\lceil \sqrt[p]{\frac{\sum_{sc=1}^5 n_{sc,d} * SC^p}{\sum_{sc=1}^5 n_{sc,d}}} \right\rceil \quad (4)$$

where

- p is set to 5, due to the fact that the FWI is divided into 5 district categories
- $n_{sc,d}$ denotes the cardinality of the sc -th scale category at the d -th forecasting day
- $\lceil \cdot \rceil$ is the upper bound

It is worth to note that the Predicted Fire Crisis Level also is classified into five categories as it takes discrete values between 1 and 5. The Early-Warning module generates alerts and forwards them to the PSAP every time a fire condition is estimated, meaning that the FWI in any point of interest is classified as “high danger” or higher. Furthermore, it assesses the overall fire danger per day and notifies the authorities sending appropriate messages.

4.2.1 Results

The preliminary experiments of the proposed algorithm exhibit its efficiency in terms of the time execution and its accuracy to process and proceed with timely notifications assisting crisis managers in the decision-making process. For example, the Early-Warning module obtained the estimations for fire danger in the region of interest from the EFFIS API at 2019-07-02. It processed them and generated the appropriate results in less than 3.5 min (less than 250 s) as shown in Fig. 11. As it is expected, the most time-consuming work is to obtain and extract valuable information from the EFFIS files.

In the following two figures, the average FWI per location over the forecasting period of 9 days and the average FWI per forecasting day are exhibited (Figs. 12 and 13). The colors of the bars indicate the level of the severity of the estimated fire danger.

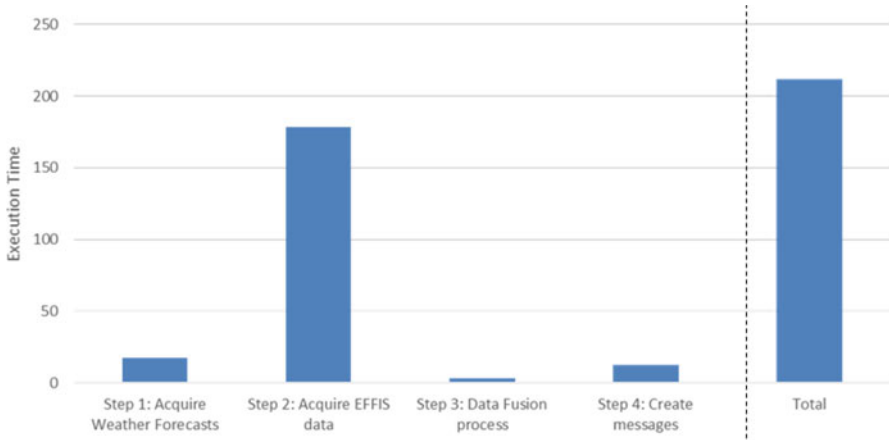


Fig. 11 Average execution time of the proposed fire algorithm by algorithmic step

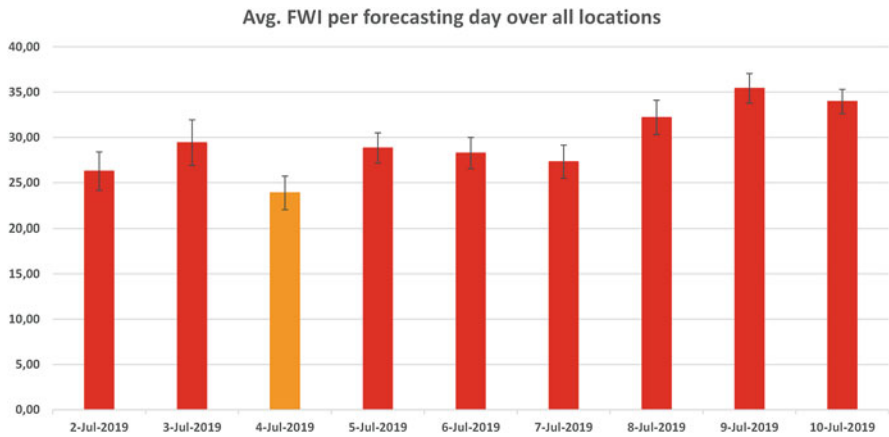


Fig. 12 Average FWI per location over the 9-day forecasting period

4.3 Application of the Early-Warning Module in the Heatwave Case

In the heatwave use case, the Early-Warning module will be triggered every time in which new forecasting weather data which are generated by HIRLAM will be available. In order to facilitate the goals of the analysis, six (6) points have been chosen by covering a wide range at Thessaloniki district and attempting to take into consideration the potential differences to climate conditions and the particular geographical relief of those landscapes (Fig. 14).

FMI provides forecasts for a series of weather parameters in the surface data such as air temperature, humidity, pressure, geopotential height, dew point, wind speed,

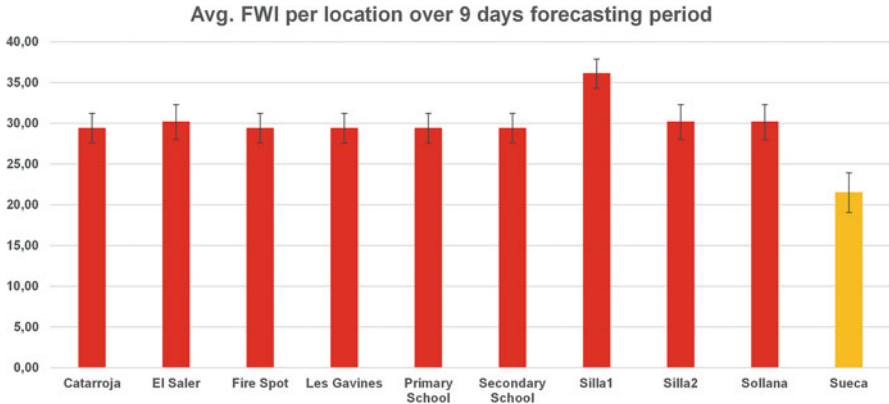


Fig. 13 Average FWI per forecasting day over the whole points of interest

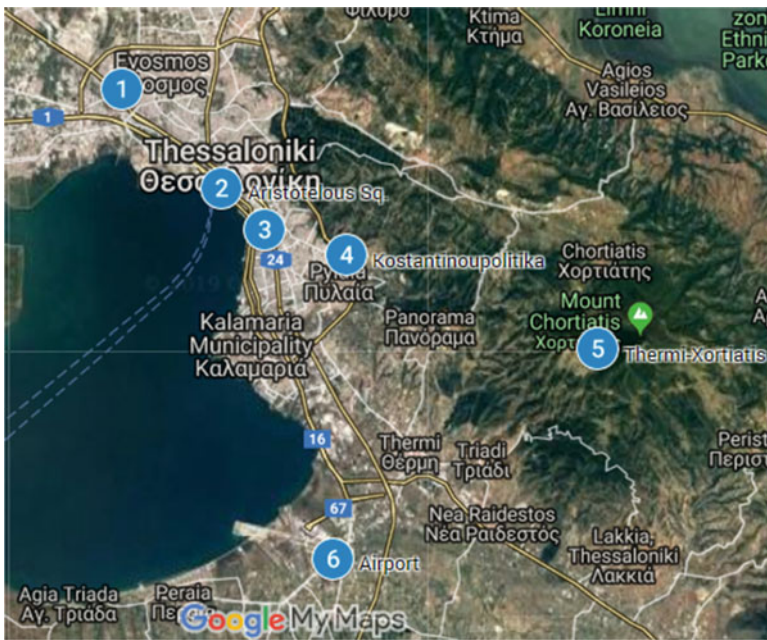


Fig. 14 Distribution of the points of interest in the Thessaloniki region

direction and gust, precipitation (instant, 1 h accumulation) and cloud covering, among others. The forecast values are updated every six (6) h and provided for a time slot of 55 h ahead. The Early-Warning module utilises the hourly predictions for air temperature and humidity and estimates the Discomfort Index (DI) for each one of the points of interest. Furthermore, it attempts to anticipate the overall heatwave

Table 3 Interpretation of Thom's Discomfort index

DI (°C)	Condition
Up to 21 °C	No discomfort
[21 °C, 25 °C)	Less than half population feels discomfort
[25 °C, 28 °C)	More than half population feels discomfort
[28 °C, 30 °C)	Most population feels discomfort and deterioration of psychophysical conditions
[30 °C, 32 °C)	The whole population feels an heavy discomfort
Over 32 °C	Sanitary emergency due to the very strong discomfort which may cause heatstrokes

crisis level per day combining the estimations of Discomfort Index as described in the following algorithm:

- Step 1.** For each point of interest, acquire forecasts hourly data for temperature and humidity
- Step 2.** Calculate the Discomfort Index per hour over all points of interest using the formula:

$$DI = T_a - 0.55 * (1 - 0.01 * RH) * (T_a - 14.5) \quad (5)$$

where

T_a denotes the hourly average of air temperature (in °C)

RH denotes the relative humidity expressed as percentage

Discomfort Index (DI) is one of the outdoor thermal comfort indexes that determine the human discomfort level based on the combination of ambient temperature and relative humidity [2, 39]. Thom's Discomfort Index (DI) [51] was used to measure the degree of human discomfort for the selected locations by the evaluation of how current temperature and relative humidity can affect the discomfort sensation and cause health danger in the population. It is divided into a discomfort sensation scale of six (6) levels, as shown in Table 3.

- Step 3.** Aggregating the DI estimations of the above step, the assessment of the heatwave overall crisis level, namely, **Predicted Heatwave Crisis Level (PHWCL)**, can be calculated using the following formula:

$$PHWCL_d = \left[\sqrt[p]{\frac{\sum_{sc=1}^4 n_{sc,d} * SC^p}{\sum_{sc=1}^4 n_{sc,d}}} \right] \quad (6)$$

where

p is set to 4, indicating the number of categories ($scale = 1, \dots, 4$) of the PHWCL index

Table 4 Interpretation of the PHWCL index

DI (°C)	Condition	
Up to 21 °C	No discomfort	Warm (1)
[21 °C, 25 °C)	Less than half population feels discomfort	
[25 °C, 28 °C)	More than half population feels discomfort	
[28 °C, 30 °C)	Most population feels discomfort and deterioration of psychophysical conditions	Hot (2)
[30 °C, 32 °C)	The whole population feels an Heavy Discomfort	Very hot (3)
Over 32 °C	Sanitary emergency due to the Very Strong Discomfort which may cause heatstrokes	Extreme (4)

$n_{sc,d}$ denotes the cardinality of the sc -th scale category at the d -th day
 $[\cdot]$ is the upper bound

It is worth to mention that due to the fact that the Early-Warning module should alert the authorities for the upcoming heatwave crisis, the most interesting classes to be considered are those which affect most of the population feeling discomfort and deterioration of psychophysical conditions. Thus, DI classes below this threshold can be merged, and the new categories for the PHWCL index are described in the following table (Table 4).

The Early-Warning module generates notifications and forwards them to PSAP every time where an imminent heatwave event has impact on the most of the population. Additionally, it assesses the overall heatwave crisis level per day and notifies the authorities sending appropriate messages if needed (greater than “hot” category).

4.3.1 Results

The preliminary experiments for the proposed algorithm exhibit its efficiency in terms of the time execution and its accuracy to estimate the DI over all locations and forecasting value and proceed with timely notifications assisting crisis managers in the decision-making process. For example, the Early-Warning module obtained the estimations for fire danger in the region of interest (Thessaloniki) from the HIRLAM of FMI at 2018-07-23 to 2018-07-25 (forecasting period). It processed them and generated the appropriate results as shown in the following figures. The color of each bar indicates the severity level of the forthcoming heatwave event, in other words the estimated discomfort level of the population. As it is expected, the most significant impact will appear in urban areas closest to the city centre and less in the suburbs or at the mountain (Fig. 15). Similar, in noon hours the upcoming heatwave crisis expects to be more severe in those areas (Fig. 16).

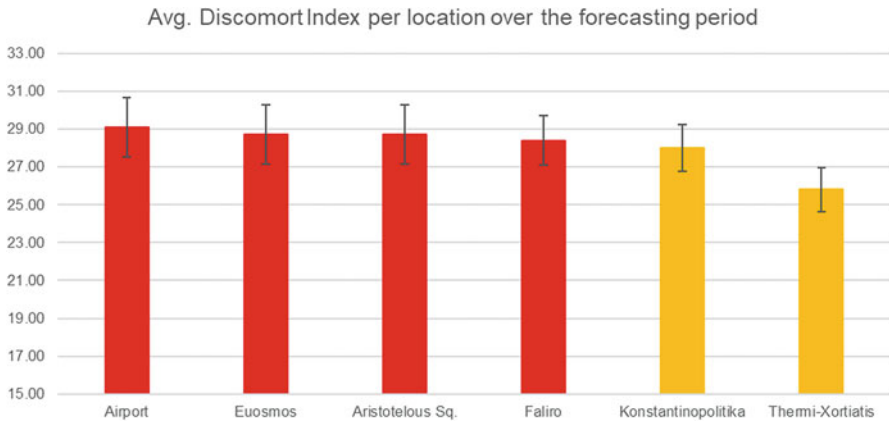


Fig. 15 Average DI per location over the forecasting period

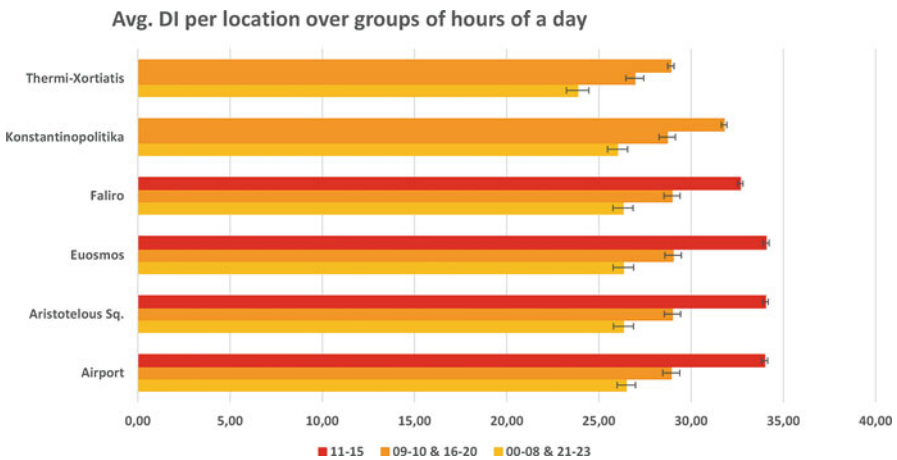


Fig. 16 Average FWI per location over the group of hours

5 Conclusion Remarks

In this work the Early-Warning module of the Crisis Classification system is presented. The objectives of the Crisis Classification component are to encapsulate the necessary technological solutions to process the available forecasts from prediction models (weather, hydrological, etc.) and sensor data as well as other heterogeneous sources to provide comprehensive operational support over the entire process of the disaster management. Relying on the results of the analysis, the Early-Warning module generates the appropriate warning alerts to timely notify the authorities as well as the meaningful metrics in order to support the visualisation tools at the beAWARE's dashboard in the pre-emergency phase as well as during the emergency

phase. The Early-Warning module enables to integrate all the available information which is generated from a single hazardous threat or from the multi-hazard threat, which can be a key tool for crisis managers, governments and authorities to prepare for a crisis, elevating warning levels for a certain threat, etc. [6]. As mentioned above, the Early-Warning module can easily adapt and deal with any natural hazardous event (e.g. flood, forest fire, heatwave, etc.). Furthermore, it can face multiple crisis events simultaneously.

However, further work should be done in the direction the Crisis Classification component will be considered as a holistic framework to support decision-making processes in crisis management. First of all, the Real-Time Monitoring and Risk Assessment component should be enhanced by functionalities to aggregate and analyse the collected data from heterogeneous sources using advanced decision fusion methodologies in order to assess the risk of an ongoing crisis event. Furthermore, various risk/impact maps should be integrated and the extracted information utilised by the Crisis Classification approaches.

Acknowledgments This work was supported by the EC-funded research and innovation program H2020 beAWARE: “Enhancing decision support and management services in extreme weather climate events” under the grant agreement No.700475.

References

1. H.W. Albrecht, S. Jaap, and S.W. Frederiek. Real-time geospatial data handling and forecasting: Examples from delft-fews forecasting platform/system. *IEEE Journal of Selected Topics in Applied Earth Observations and Remote Sensing*, 3(3):386–394, 2010.
2. V. E. Angouridakis and T. J. Makrogiannis. The discomfort-index in thessaloniki, greece. *International Journal of Biometeorology*, 26(1):53–59, Mar 1982.
3. C. Ansell, A. Boin, and Ann C. Keller. Managing transboundary crises: Identifying the building blocks of an effective response system. *Journal of Contingencies and Crisis Management*, 18(4):195–207, 2010.
4. E. Artinyan, B. Vincendon, K. Kroumova, N. Nedkov, P. Tsarev, S. Balabanova, and G. Koshinchanov. Flood forecasting and alert system for arda river basin. *Journal of Hydrology*, 541:457–470, 2016.
5. J. Barber, C. Bose, A. Bourlioux, Willard Braun, E. Brunelle, Tanya Garcia, T. Hillen, and B. Ong. Burning issues with prometheus, the canada’s wildfire growth simulator. *Canadian Applied Math Quarterly*, 16:337–378, 01 2010.
6. Charles Baubion. Strategic crisis management. *OECD Risk Management*, 23, 2013.
7. N.L. Bindoff, P.A. Stott, K.M. AchutaRao, M.R. Allen, N. Gillett, D. Gutzler, K. Hansingo, G. Hegerl, Y. Hu, S. Jain, I.I. Mokhov, J. Overland, J. Perlwitz, R. Sebbari, and X. Zhang. *Climate Change 2013: The Physical Science Basis. Contribution of Working Group I to the Fifth Assessment Report of the Intergovernmental Panel on Climate Change*, chapter Detection and Attribution of Climate Change: from Global to Regional, pages 867–952. Cambridge University Press, 2013.
8. Omar D. Cardona. *Disaster Risk and Vulnerability: Concepts and Measurement of Human and Environmental Insecurity*, pages 107–121. Springer Berlin Heidelberg, Berlin, Heidelberg, 2011.

9. E. Castellet, M. Valentin, J. Ripolles, E. Oñate, J. Piazzese, and G. Poupeau. Decision support system for flood risk assessment and management. In *Proceedings of the 7th International Conference on Hydroinformatics, HIC 2006*, Nice, FRANCE, 2006.
10. Emilio Chuvieco. *Wildland Fire Danger Estimation and Mapping*. World Scientific, 2003.
11. The Global Competitiveness and Risks Team. The global risks report 2017. Technical report, World Economic Forum, 2017.
12. The Global Competitiveness and Risks Team. The global risks report 2018. Technical report, World Economic Forum, 2018.
13. D.K. Davies, S. Ilavajhala, M.M. Wong, and C.O. Justice. Fire information for resource management system: Archiving and distributing modis active fire data. *IEEE Transactions on Geoscience and Remote Sensing*, 47(1):72–79, 2009.
14. I. Demir and W.F. Krajewski. Towards an integrated flood information system: Centralized data access, analysis, and visualization. *Environmental modelling & software*, 50:77–84, 2013.
15. K. L. Ebi, R. S. Kovats, and B. Menne. An approach for assessing human health vulnerability and public health interventions to adapt to climate change. *Environmental health perspectives*, 114(12):1930–1934, 2006.
16. Kristie L. Ebi, Thomas J. Teisberg, Laurence S. Kalkstein, Lawrence Robinson, Weiher, and Rodney F. Heat watch/warning systems save lives: Estimated costs and benefits for philadelphia 1995–98. *Bulletin of the American Meteorological Society*, 85(8):1067–1074, 2004.
17. EEA. Mapping the impacts of natural hazards and technological accidents in europe, an overview of the last decade. Technical report 13/2010, European Environment Agency, Luxembourg, 2010.
18. EEA. *Climate Change adaptation and disaster risk reduction in Europe – Enhancing coherence of the knowledge base, policies and practices*. European Environment Agency, 2017.
19. EEA. *Climate Change, impacts and vulnerability in Europe 2016 – An indicator-based report*. European Environment Agency. European Environment Agency, 2017.
20. C. E. European. Directive 2007/60/ec of the European parliament and of the council of 23 october 2007 on the assessment and management of flood risks (text with eea relevance). Retrieved from <https://eur-lex.europa.eu/legal-content/EN/TXT/PDF/?uri=CELEX:32007L0060&from=EN>, 2007. EC Brussels.
21. Abdel Moneim Ghanem Ezzeldin. Decision support system in the crisis management unit. *International Journal of Humanities and Social Science*, 4(8):169–173, 2014.
22. M. Ferri, M. Monego, D. Norbiato, F. Baruffi, C. Toffolon, and R. Casarin. Amico: La piattaforma previsionale per i bacini idrografici del nord est adriatico (i). In *Proceedings of the XXXIII Convegno Nazionale di Idraulica e Costruzioni Idrauliche*, Brescia, Italy, 2012.
23. Paolo Fiorucci, Francesco Gaetani, and Riccardo Minciardi. Development and application of a system for dynamic wildfire risk assessment in italy. *Environmental Modelling & Software*, 23(6):690–702, 2008.
24. F. Fotopoulos, C. Makropoulos, and M.A. Mimikou. Flood forecasting in transboundary catchments using the open modeling interface. *Environmental Modelling & Software*, 25(12):1640–1649, 2010.
25. J. Gaillard. Vulnerability, capacity, and resilience: perspectives for climate and development policy. *Journal of International Development*, 22:218–232, 2010.
26. D. Gasper. The idea of human security. *Climate Change, Ethics and Human Security*, pages 23–46, 01 2010.
27. IPCC. *Climate Change 2013: The Physical Science Basis. Contribution of Working Group I to the Fifth Assessment Report of the Intergovernmental Panel on Climate Change*. Cambridge University Press, Cambridge, United Kingdom, 2013.
28. IPCC. *Climate Change 2014: Synthesis Report. Contribution of Working Groups I, II and III to the Fifth Assessment Report of the Intergovernmental Panel on Climate Change*. IPCC, Geneva, Switzerland, 2014.

29. Kostas Kalabokidis, Nikolaos Athanasis, Fabrizio Gagliardi, Fotis Karayiannis, Palaiologos Palaiologou, Savas Parastatidis, and Christos Vasilakos. Virtual fire: A web-based gis platform for forest fire control. *Ecological Informatics*, 16:62–69, 2013.
30. Kostas Kalabokidis, Gavriil Xanthopoulos, Peter Moore, David Caballero, George Kallos, Juan Llorens, Olga Roussou, and Christos Vasilakos. Decision support system for forest fire protection in the euro-mediterranean region. *European Journal of Forest Research - EUR J FOR RES*, 131(3):597–608, 05 2012.
31. A. Kauffeldt, F. Wetterhall, F. Pappenberger, P. Salamon, and J. Thielen. Technical review of large-scale hydrological models for implementation in operational flood forecasting schemes on continental level. *Environmental Modelling & Software*, 75:68–76, 2016.
32. F. Klijn, K. de Bruijn, A. Ölfert, E. Penning-Rowsell, J. Simm, and M. Wallis. Flood risk assessment and flood risk management. an introduction and guidance based on experiences and findings of floodsite (an eu-funded integrated project). Technical Report T29-09-01, Deltares | Delft Hydraulics, 2009.
33. B.D. Lawson and O.B. Armitage. Weather guide for the canadian forest fire danger rating system. Technical report, Canadian Forest Service, Northern Forestry Centre, Northern Forestry Centre, Edmonton, Alberta, 2008.
34. B.S Lee, M.E Alexander, B.C Hawkes, T.J Lynham, B.J Stocks, and P Englefield. Information systems in support of wildland fire management decision making in canada. *Computers and Electronics in Agriculture*, 37(1):185–198, 2002.
35. Ebi K. L. & Fors B. Lowe, D. Heatwave early warning systems and adaptation advice to reduce human health consequences of heatwaves. *International Journal of Environmental Research and Public Health*, 8(12):4623–4648, 2011.
36. García-Díez M. Ballester J. Creswick J. Robine J.-M. Herrmann F. & Rodó X. Lowe, R. Evaluation of an early-warning system for heat wave-related mortality in europe: Implications for sub-seasonal to seasonal forecasting and climate services. *International Journal of Environmental Research and Public Health*, 13(2), 2016.
37. N. Markatos, C.T. Kiranoudis, V.C. Vescoukis, and P. Balatsos. Towards an integrated system for planning and decision support in forest fire management. In *Proceedings of the 4th International Wildland Fire Conference*, Seville, Spain, 2007.
38. Maurizio Mazzoleni, Martin Verlaan, Leonardo Alfonso, Martina Monego, Daniele Nobiato, Michele Ferri, and Dimitri P. Solomatine. Can assimilation of crowdsourced data in hydrological modelling improve flood prediction? *Hydrology and Earth System Sciences*, 21:839–861, 2017.
39. Mohd Fadhil Md Din, Yee Yong Lee, Mohanadoss Ponraj, Dilshan Remaz Ossen, Kenzo Iwao, and Shreeshivadasan Chelliapan. Thermal comfort of various building layouts with a proposed discomfort index range for tropical climate. *Journal of thermal biology*, 41:6–15, April 2014.
40. M.V. Muste and A.R. Firoozfar. Toward generalized decision support systems for flood risk management. *E3S Web Conf.*, 7, 2016.
41. C. Papathanasiou, E. Safiolea, C. Makropoulos, and M. Mimikou. The fladar project and its contribution to the implementation of the eu flood directive 2007/60. In *Proceedings of the 11th International Conference on Environmental Science and Technology*, Chania, Crete, 2009.
42. Morgan Pence and Thomas Zimmerman. The wildland fire decision support system: Integrating science, technology, and fire management. *Fire Management Today*, 71(1):18–22, 2011.
43. Sarah E. Perkins. A review on the scientific understanding of heatwaves—their measurement, driving mechanisms, and changes at the global scale. *Atmospheric Research*, 164–165:242–267, 2015.
44. Gabriela Prelipcean and Mircea Boscoianu. *Emerging Applications of Decision Support Systems (DSS) in Crisis Management*, pages 359–376. InTech, 2011.
45. Linyao Qiu, Zhiqiang Du, Qing Zhu, and Yida Fan. An integrated flood management system based on linking environmental models and disaster-related data. *Environmental Modelling & Software*, 91:111–126, 2017.

46. Hajat S., Sheridan S.C., Allen M.J., Pascal M., Laaidi K., Yagouti A., Bickis U., Tobias A., Bourque D., Armstrong B.G., and Kosatsky T. Heat-health warning systems: a comparison of the predictive capacity of different approaches to identifying dangerously hot days. *Am J Public Health*, 100(6):1137–1144, 2010.
47. Jesús San-Miguel-Ayanz, Ernst Schulte, Guido Schmuck, Andrea Camia, Peter Strobl, Giorgio Liberta, Cristiano Giovando, Roberto Boca, Fernando Sedano, Pieter Kempeneers, Daniel McInerney, Ceri Withmore, Sandra Santos de Oliveira, Marcos Rodrigues, Tracy Durrant, Paolo Corti, Friderike Oehler, Lara Vilar, and Giuseppe Amatulli. Comprehensive monitoring of wildfires in europe: The European forest fire information system (effis). In John Tiefenbacher, editor, *Approaches to Managing Disaster*, chapter 5. IntechOpen, Rijeka, 2012.
48. S. Schneider, S. Semenov, A. Patwardhan, I. Burton, C. Magadza, M. Oppenheimer, A. Pittock, A. Rahman, J. Smith, A. Suarez, and F. Yamin. *Climate change 2007: impacts, adaptation and vulnerability. Contribution of Working Group II to the Fourth Assessment Report of the IPCC*, chapter Assessing key vulnerabilities and the risk from climate change, pages 781–810. Cambridge University Press, 2007.
49. P.A. Stott, N. Christidis, F.E.L. Otto, Y. Sun, J.-P. Vanderlinden, G.J. van Oldenborgh, R. Vautard, H. von Storch, P. Walton, P. Yiou, and F.W. Zwiers. Attribution of extreme weather and climate-related events. *Wiley Interdisciplinary Reviews: Climate Change*, 7(1):23–41, 2016.
50. S.W. Taylor and Martin Alexander. Science, technology, and human factors in fire danger rating: the canadian experience. *International Journal of Wildland Fire*, 15:121–135, 03 2006.
51. E.C. Thom. The discomfort index. *Weatherwise*, 12(2):57–61, 1959.
52. K.E. Trenberth, J.T. Fasullo, and T.G. Shepherd. Attribution of climate extreme events. *Nature Climate Change*, 5(8):725–730, 2015.
53. UNISDR. *United Nations International Strategy for Disaster Reduction (UNISDR) Terminology on disaster risk reduction*. UNISDR, Geneva, Switzerland, 2009.
54. Van Wagner. Development and structure of the canadian forest fire weather index system. Technical Report Forestry Technical Report 35, Canadian Forest Service, Northern Forestry Centre, Headquarters Ottawa, 1987.
55. Z. Wan, Y. Hong, S. Khan, J. Gourley, Z. Flamig, D. Kirschbaum, and G. Tang. A cloud-based global flood disaster community cyber-infrastructure: Development and demonstration. *Environmental Modelling & Software*, 58:86–94, 2014.
56. Jian Zuo, Stephen Pullen, Jasmine Palmer, Helen Bennetts, Nicholas Chileshe, and Tony Ma. Impacts of heat waves and corresponding measures: a review. *Journal of Cleaner Production*, 92:1–12, 2015.

Toward Decentralized Decision-Making for Interdependent Infrastructure Network Resilience



Buket Cilali, Nafiseh Ghorbani-Renani, Kash Barker,
and Andrés D. González

Abstract Interdependence among infrastructure and community networks is an important aspect to consider when planning for disruptive events. Further, decision-makers within different infrastructures often make decentralized decisions to protect and restore their own networks after a disruption. As such, a resilience-based optimization model is extended in various ways to depict different decentralized decision-making structures and hierarchies: divided budget, isolation assumption, and dominance assumption. Among others, social vulnerability scores are used to show the effect of community resilience, and different scenarios are analyzed to reveal the effect of decentralization. The model is illustrated with a system of interdependent electric power, water, and gas infrastructure networks in Shelby County, TN.

Keywords Interdependent networks · Resilience · Restoration · Optimization

1 Introduction

Modern societies are dependent on infrastructure systems such as electric power, water supply, and telecommunication. With the improvements in living standards and the new Internet of Things and connected health technologies, among others, our dependence on these critical infrastructure systems continues to increase. The more dependent we become, the more important the resilience of such critical infrastructure systems has become. And dependence upon these infrastructure systems is not limited to society and our technology but also the infrastructure systems themselves: interdependencies among physical (lifeline) infrastructure systems can lead to widespread cascading effects after a disruption (e.g., a natural disaster or a malevolent attack). As such, studying the problem of infrastructure resilience

B. Cilali · N. Ghorbani-Renani · K. Barker (✉) · A. D. González
School of Industrial and Systems Engineering, University of Oklahoma, Norman, OK, USA
e-mail: Buket.cilali@ou.edu; Nafish.ghorbani@ou.edu; kashbarker@ou.edu;
andres.gonzalez@ou.edu

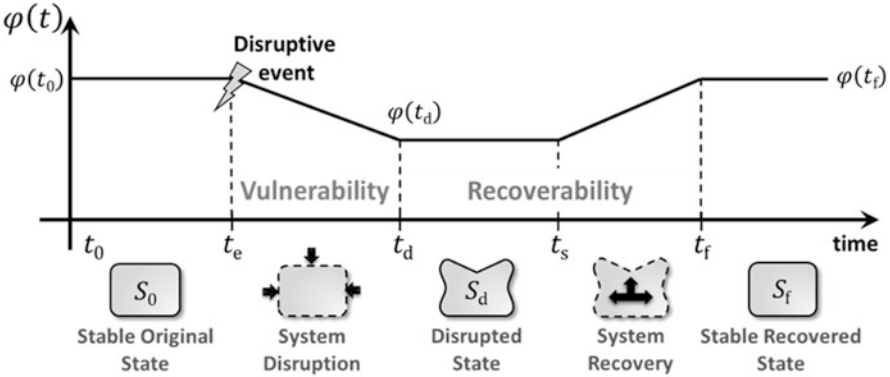


Fig. 1 System performance across system states. (Adapted from Ref. [17])

requires a societal impact perspective and an infrastructure interdependency and decision-making perspective.

The behavior of critical infrastructure networks after a disruption has become an important topic of study in recent years [1]. For the recovery of critical infrastructure networks, various studies consider different aspects such as choosing disrupted network components to restore, assigning work crews, and deciding the order of restoration [2–9]. The restoration of interdependent infrastructure networks became an especially common subject in recent studies [10–13]. Generally, previous studies propose different solution approaches in terms of different network interdependencies, definitions and measures of resilience, objectives, time aspects/order of decisions, the types of threats, numbers and roles of decision-makers (centralized/decentralized decision-making), and social vulnerability views. Some of the existing works minimize unmet demand [14] or cost [12], while others maximize total flow [15] or performance of the system [7, 13]. A variety of network interdependencies are used in different works: physical, cyber, geographic, logical, functional, spatial, geospatial, policy, informational, input, mutual, shared, exclusive, co-located, functional, budgetary, market, and economic [10, 12–14, 16].

In this chapter, the resilience model based on the system performance across system states, adapted from [17] and illustrated in Fig. 1, will be used. Resilience is measured by vulnerability, defined as the drop-in performance after a disruptive event, and recoverability, defined as the timely restoration of the system performance to the desired level. Performance of the infrastructure system at time t is represented by $\varphi(t)$.

Models developed to study interdependent network resilience (investing in reducing vulnerability or enhancing recoverability from Fig. 1) often assume that there are centralized entities making decisions at each level. However, in realistic scenarios, particularly for systems of interdependent networks, decisions are taken by multiple entities. For example, one could argue that each utility (e.g., power, water) is managed by a separate entity, which is autonomous in its decisions. Nevertheless, decisions made about building resilience in the components of one

network will have interdependent effects on the vulnerability and recovery of the other networks. Thus, it is important to model the resilience actions assuming decentralized dynamics. Sharkey et al. [13] analyze the effect of decentralized decision-making environment under optimistic assumptions, pessimistic assumptions, and iterative information sharing; and then, they show that sharing planned restoration efforts significantly decreases the negative impact of decentralization on restoration effectiveness. To improve resilience by means of increasing network connectivity, Chen and Zhu [18, 19] suggest iterative methods for the initial network design for the interdependent networks that will converge to an equilibrium solution that is close to a team/global optimal solution. However, one should be careful about the iterative nature of these studies: depending on the purpose of the model, adopted solution approach, and the number of steps until the convergence, an iterative approach may cause computational complexity or infeasibility under real-life conditions. From an interdependent network resilience perspective, an iterative approach might be more appropriate for making prior design or protection decisions rather than making real-time restoration plans. Talebiyan and Dueñas-Osorio [20] solve a decentralized interdependent network design problem by applying the judgment call method with a Bayesian hierarchical model to reflect the use of field expertise and judgment in a decentralized environment with limited communication and uncertainty.

In this chapter, we extend a tri-level optimization formulation for interdependent network resilience [14] to account for a decentralized decision-making environment. The tri-level optimization formulation solves a protection-interdiction-restoration, or defender-attacker-defender, problem that addresses the vulnerability and recoverability dimensions of resilience from Fig. 1: the first defender action reduces interdependent network vulnerability, an attacker then optimally attacks, and then the second defense action recovers the networks. The original tri-level formulation assumed a centralized decision-maker, and in this work, we design one semi-centralized and two decentralized decision-making strategies for protecting and restoring the networks given a fixed interdiction action. Further, we incorporate socioeconomic characteristics into the decision-making model to account for the social vulnerability of the communities impacted by the interdiction action.

The rest of this chapter is organized into the following sections. The formulation of the tri-level model and the solution approach that is adapted in this study are given in Sect. 2. The proposed decentralization approaches are explained in Sect. 3. The application is described and computational results are presented in Sect. 4. Concluding remarks are given in Sect. 5.

2 Tri-level Optimization Model Background

The tri-level model from [14] and the proposed formulation are explained in this section. Also discussed is the solution approach used to solve the NP-hard nature of tri-level interdiction models.

2.1 Assumptions

The tri-level model formulation is based on the following assumptions related to the interdependent network infrastructure problem [14]:

- Each infrastructure network includes a set of supply, demand, and transshipment nodes that are connected by a set of links with known flow capacities.
- The implementation of a protection or interdiction strategy for a network component is subject to a fixed cost.
- Protection and interdiction of network components are limited by the associated fixed budgets that are defined for the entire system of interdependent networks.
- When a network component is covered by the protection strategy, it is invulnerable to disruption for the rest of the planning horizon.
- Each network has a specific number of work crews responsible for repairing disrupted components in each infrastructure network.
- A work crew has a limited capacity and cannot work on more than one disrupted component simultaneously.
- Only one work crew can be assigned to a disrupted component. Once the assignment is made, the assigned work crew continuously works on that disrupted component until it is operational.
- The restoration rate for each component is known.
- The restoration time for each disrupted component depends on its failure level and restoration rate.
- The type of interdependence between infrastructure networks is assumed to be physical interdependence, meaning that all parent nodes must be operational for a child node to be operational.

2.2 Notation

The following notation was defined in [14] to develop the tri-level optimization problem (Tables 1, 2, and 3).

2.3 Model Formulation

The tri-level model proposed by Ghorbani-Renani et al. [14] aims to optimize the performance of a system of interdependent networks by minimizing the cumulative weighted fraction of unmet demand, as shown in Eq. (1), for the worst-case interdiction over time. Each level of the model has a contribution to the objective function, its own decision variables, and its own constraints. The objective function of the model is shown in Eq. (2).

Table 1 Set notation for the tri-level formulation

N	Set of nodes
A	Set of links
$G = (N, A)$	Undirected network
K	Set of networks
N^k	Set of nodes in network $k \in K$ such that $\bigcup_{k \in K} N^k = N$
N_s^k	Set of supply nodes in network $k \in K$ such that $N_s^k \cap N_d^k = \emptyset$
N_d^k	Set of demand nodes in network $k \in K$ such that $N_s^k \cap N_d^k = \emptyset$
$N^k \setminus \{N_d^k, N_s^k\}$	Set of transshipment nodes in network $k \in K$
N'^k	Set of candidate nodes in network $k \in K$
A^k	Set of links in network k such that $\bigcup_{k \in K} A^k = A$
A'^k	Set of candidate links in network $k \in K$
Ψ	Interdependency among networks such that $((i, k), (\bar{i}, \bar{k})) \in \Psi$ denotes node $i \in N^k$ in network $k \in K$ physically depends on node $\bar{i} \in N^{\bar{k}}$ in network $\bar{k} \in K$ where $N^k \cap N^{\bar{k}} = \emptyset$, $A^k \cap A^{\bar{k}} = \emptyset$ and $\forall k, \bar{k} \in K : k \neq \bar{k}$
R^k	Available work crews in network $k \in K$
T	Set of available time periods

Table 2 Parameter notation for the tri-level formulation

η_{ite}^k	Flow reaching node $i \in N_d^k$ in network $k \in K$ before the attack
w_{it}^k	Importance weight assigned to node $i \in N_d^k$ in network $k \in K$ at time $t \in T$
$C P_{ij}^k$	Cost of protecting link $(i, j) \in A'^k$ in network $k \in K$
$C P_i^k$	Cost of protecting node $i \in N'^k$ in network $k \in K$
$C I_{ij}^k$	Cost of attacking link $(i, j) \in A'^k$ in network $k \in K$
$C I_i^k$	Cost of attacking node $i \in N'^k$ in network $k \in K$
B_P	Total available budget for the protector
B_I	Total available budget for the interdictor
S_i^k	Amount of supply in node $i \in N_s^k$ in network $k \in K$
d_i^k	Amount of demand in node $i \in N_d^k$ in network $k \in K$
u_{ij}^k	Capacity of link $(i, j) \in A^k$ in network $k \in K$
λ_{ij}^k	Restoration rate of the link $(i, j) \in A'^k$ in network $k \in K$
λ_i^k	Restoration rate of the node $i \in N'^k$ in network $k \in K$
ε	An arbitrarily small positive number, $0 < \varepsilon < 1$
M	An arbitrarily large positive number

Table 3 Decision variables for the tri-level formulation

η_{it}^k	Amount of demand met at node $i \in N_d^k$ in network $k \in K$ at time $t \in T$, continuous
x_{ij}^k	Flow on link $(i,j) \in A^k$ in network $k \in K$ in time $t \in T$
y_{ij}^k	Equal to 1 if link $(i,j) \in A^k$ in network $k \in K$ is protected, binary
y_i^k	Equal to 1 if node $i \in N^k$ in network $k \in K$ is protected, binary
z_{ij}^k	Equal to 1 if link $(i,j) \in A^k$ in network $k \in K$ is interdicted, binary
z_i^k	Equal to 1 if node $i \in N^k$ in network $k \in K$ is interdicted, binary
F_{ij}^k	Equal to 1 if link $(i,j) \in A^k$ in network $k \in K$ is disrupted, binary
F_i^k	Equal to 1 if node $i \in N^k$ in network $k \in K$ is disrupted, binary
α_{ij}^k	Equal to 1 if link $(i,j) \in A^k$ in network $k \in K$ is operational, binary
α_i^k	Equal to 1 if node $i \in N^k$ in network $k \in K$ is operational, binary
α_{ijt}^{rk}	Equal to 1 if link $(i,j) \in A^k$ in network $k \in K$ is restored by work crew $r \in R^k$ in time $t \in T$, binary
α_{it}^{rk}	Equal to 1 if node $i \in N^k$ in network $k \in K$ is restored by work crew $r \in R^k$ in time $t \in T$, binary
β_{ijt}^k	Equal to 1 if link $(i,j) \in A^k$ in network $k \in K$ is reactivated at time $t \in T$, binary
β_{it}^k	Equal to 1 if node $i \in N^k$ in network $k \in K$ is reactivated at time $t \in T$, binary

$$\zeta(t) = 1 - \left(\frac{\sum_{k \in K} \sum_{i \in N_d^k} w_{it}^k \eta_{it}^k}{\sum_{k \in K} \sum_{i \in N_d^k} w_{it}^k \eta_{ite}^k} \right) \quad \forall t \in T \quad (1)$$

$$\xi = \min_y \max_z \min_{\eta, x, F, \alpha, \alpha', \beta} \sum_{t \in T} \zeta(t) \quad (2)$$

The first set of constraints shown below deal with the first and second, or protection and interdiction, levels.

$$\sum_{k \in K} \sum_{(i,j) \in A^k} C P_{ij}^k y_{ij}^k + \sum_{k \in K} \sum_{i \in N^k} C P_i^k y_i^k \leq B_P \quad (3)$$

$$\sum_{k \in K} \sum_{(i,j) \in A^k} C I_{ij}^k z_{ij}^k + \sum_{k \in K} \sum_{i \in N^k} C I_i^k z_i^k \leq B_I \quad (4)$$

$$y_{ij}^k \in \{0, 1\} \quad \forall k \in K, \forall (i, j) \in A^k \quad (5)$$

$$y_i^k \in \{0, 1\} \quad \forall k \in K, \forall i \in N^k \quad (6)$$

$$z_{ij}^k \in \{0, 1\} \quad \forall k \in K, \forall (i, j) \in A'^k \quad (7)$$

$$z_i^k \in \{0, 1\} \quad \forall k \in K, \forall i \in N'^k \quad (8)$$

Constraint (3) is related to the first/protection level of the problem and represents the budget restriction on protection investment decisions. Likewise, constraint (4) is related to the second/interdiction level of the problem and represents the budget restriction on interdiction decisions. Constraints (5)–(8) represent the binary nature of the decision variables of the first two levels of the problem.

Constraints (9)–(50) are then related to the third, or restoration, level of the problem.

$$y_{ij}^k + (1 - z_{ij}^k)(1 - y_{ij}^k) = 1 - F_{ij}^k \quad \forall k \in K, \forall (i, j) \in A'^k \quad (9)$$

$$y_i^k + (1 - z_i^k)(1 - y_i^k) = 1 - F_i^k \quad \forall k \in K, \forall i \in N'^k \quad (10)$$

$$\alpha_{ij}^k \leq 1 - F_{ij}^k \quad \forall k \in K, \forall (i, j) \in A'^k \quad (11)$$

$$\alpha_{ij}^k + F_{ij}^k \geq \varepsilon \quad \forall k \in K, \forall (i, j) \in A'^k \quad (12)$$

$$\alpha_i^k \leq 1 - F_i^k \quad \forall k \in K, \forall i \in N'^k \quad (13)$$

$$\alpha_i^k + F_i^k \geq \varepsilon \quad \forall k \in K, \forall i \in N'^k \quad (14)$$

$$\alpha_{ij}^k \leq 1 - \beta_{ijt}^k \quad \forall k \in K, \forall (i, j) \in A'^k, \forall t \in T \quad (15)$$

$$\alpha_i^k \leq 1 - \beta_{it}^k \quad \forall k \in K, \forall i \in N'^k, \forall t \in T \quad (16)$$

$$\beta_{ij1}^k = 0 \quad \forall k \in K, \forall (i, j) \in A'^k \quad (17)$$

$$\beta_{i1}^k = 0 \quad \forall k \in K, \forall i \in N'^k \quad (18)$$

$$\sum_{(i,j) \in A^k} x_{ijt}^k - \sum_{(j,i) \in A^k} x_{jit}^k \leq S_i^k \quad \forall k \in K, \forall i \in N_s^k, \forall t \in T \quad (19)$$

$$\sum_{(i,j) \in A^k} x_{ijt}^k - \sum_{(j,i) \in A^k} x_{jit}^k = 0 \quad \forall k \in K, \forall i \in N^k \setminus \{N_d^k, N_s^k\}, \forall t \in T \quad (20)$$

$$\sum_{(i,j) \in A^k} x_{ijt}^k - \sum_{(j,i) \in A^k} x_{jit}^k = -\eta_{it}^k \quad \forall k \in K, \forall i \in N_d^k, \forall t \in T \quad (21)$$

$$\eta_{it}^k \leq d_i^k \quad \forall k \in K, \forall i \in N_d^k, \forall t \in T \quad (22)$$

$$x_{ijt}^k \leq u_{ij}^k \quad \forall k \in K, \forall (i, j) \in A^k, \forall t \in T \quad (23)$$

$$x_{ijt}^k \leq u_{ij}^k \left(\alpha_{ij}^k + \beta_{ijt}^k \right) \quad \forall k \in K, \forall (i, j) \in A^k, \forall t \in T \quad (24)$$

$$x_{ijt}^k \leq u_{ij}^k \left(\alpha_i^k + \beta_{ijt}^k \right) \quad \forall k \in K, \forall (i, j) \in A^k, \forall i \in N^k, \forall t \in T \quad (25)$$

$$x_{ijt}^k \leq u_{ij}^k \left(\alpha_j^k + \beta_{ijt}^k \right) \quad \forall k \in K, \forall (i, j) \in A^k, \forall j \in N^k, \forall t \in T \quad (26)$$

$$\sum_{s=1}^t \alpha_{ijs}^{kr} \leq M \left(1 - \left(\alpha_{ij(t+1)}^{kr} - \alpha_{ijt}^{kr} \right) \right) \quad \forall k \in K, \forall (i, j) \in A^k, \quad \forall t \in T, \forall r \in R^k \quad (27)$$

$$\sum_{r \in R^k} \sum_{t \in T} \alpha_{ijt}^{kr} \geq \frac{F_{ij}^k}{\lambda_{ij}^k} - M \alpha_{ij}^k \quad \forall k \in K, \forall (i, j) \in A^k \quad (28)$$

$$\sum_{r \in R^k} \sum_{t \in T} \alpha_{ijt}^{kr} < \left(\frac{F_{ij}^k}{\lambda_{ij}^k} + 1 \right) + M \alpha_{ij}^k \quad \forall k \in K, \forall (i, j) \in A^k \quad (29)$$

$$\sum_{s=1}^t \alpha_{is}^{kr} \leq M \left(1 - \left(\alpha_{i(t+1)}^{kr} - \alpha_{it}^{kr} \right) \right) \quad \forall k \in K, \forall i \in N^k, \forall t \in T, \forall r \in R^k \quad (30)$$

$$\sum_{r \in R^k} \sum_{t \in T} \alpha'_{it}{}^{kr} \geq \frac{F_i^k}{\lambda_i^k} - M\alpha_i^k \quad \forall k \in K, \forall i \in N'^k \quad (31)$$

$$\sum_{r \in R^k} \sum_{t \in T} \alpha'_{it}{}^{kr} < \left(\frac{F_i^k}{\lambda_i^k} + 1 \right) + M\alpha_i^k \quad \forall k \in K, \forall i \in N'^k \quad (32)$$

$$\frac{\sum_{r \in R^k} \sum_{s=1}^{t-1} \alpha'_{ijs}{}^{kr}}{F_{ij}^k / \lambda_{ij}^k} \geq \beta_{ijt}^k \quad \forall k \in K, \forall (i, j) \in A'^k, \forall t \in T \mid t \neq 1 \quad (33)$$

$$\frac{\sum_{r \in R^k} \sum_{s=1}^{t-1} \alpha'_{is}{}^{kr}}{F_i^k / \lambda_i^k} \geq \beta_{it}^k \quad \forall k \in K, \forall i \in N'^k, \forall t \in T \mid t \neq 1 \quad (34)$$

$$\sum_{\substack{s \in R^k \\ s \neq r}} \sum_{t \in T} \alpha'_{ijt}{}^{ks} \leq M \left(1 - \alpha'_{ijt}{}^{kr} \right) \quad \forall k \in K, \forall (i, j) \in A'^k, \forall t \in T, \forall r \in R^k \quad (35)$$

$$\sum_{\substack{s \in R^k \\ s \neq r}} \sum_{t \in T} \alpha'_{it}{}^{ks} \leq M \left(1 - \alpha'_{it}{}^{kr} \right) \quad \forall k \in K, \forall i \in N'^k, \forall t \in T, \forall r \in R^k \quad (36)$$

$$\sum_{r \in R^k} \alpha'_{ijt}{}^{kr} \leq 1 \quad \forall k \in K, \forall (i, j) \in A'^k, \forall t \in T \quad (37)$$

$$\sum_{r \in R^k} \alpha'_{it}{}^{kr} \leq 1 \quad \forall k \in K, \forall i \in N'^k, \forall t \in T \quad (38)$$

$$\sum_{(i,j) \in A'^k} \alpha'_{ijt}{}^{kr} + \sum_{i \in N'^k} \alpha'_{it}{}^{kr} \leq 1 \quad \forall k \in K, \forall t \in T, \forall r \in R^k \quad (39)$$

$$x_{ijt}^k \leq u_{ij}^k \left(\alpha_{\bar{i}}^k + \beta_{\bar{i}}^k \right) \quad \forall k, \bar{k} \in K, \forall (i, j) \in A^k, \forall \bar{i} \in N^{\bar{k}} \mid \\ ((i, k), (\bar{i}, \bar{k})) \in \Psi \text{ or } ((j, k), (\bar{j}, \bar{k})) \in \Psi, \forall t \in T \quad (40)$$

$$\eta_{it}^k \geq 0 \quad \forall k \in K, \forall i \in N_d^k, \forall t \in T \quad (41)$$

$$x_{ijt}^k \geq 0 \quad \forall k \in K, \forall (i, j) \in A^k, \forall t \in T \quad (42)$$

$$F_{ij}^k \in \{0, 1\} \quad \forall k \in K, \forall (i, j) \in A^k \quad (43)$$

$$F_i^k \in \{0, 1\} \quad \forall k \in K, \forall i \in N'^k \quad (44)$$

$$\alpha_{ij}^k \in \{0, 1\} \quad \forall k \in K, \forall (i, j) \in A^k \quad (45)$$

$$\alpha_i^k \in \{0, 1\} \quad \forall k \in K, \forall i \in N'^k \quad (46)$$

$$\alpha_{ijtr}^{'kr} \in \{0, 1\} \quad \forall k \in K, \forall (i, j) \in A'^k, \forall t \in T, \forall r \in R^k \quad (47)$$

$$\alpha_{itr}^{'kr} \in \{0, 1\} \quad \forall k \in K, \forall i \in N'^k, \forall t \in T, \forall r \in R^k \quad (48)$$

$$\beta_{ijt}^k \in \{0, 1\} \quad \forall k \in K, \forall (i, j) \in A^k, \forall t \in T \quad (49)$$

$$\beta_{it}^k \in \{0, 1\} \quad \forall k \in K, \forall i \in N'^k, \forall t \in T \quad (50)$$

Constraints (9) and (10) provide the failure status for the candidate components according to the related protection and interdiction decisions. Constraints (11)–(14) provide the operability status for the candidate components such that the component will be operational if it is protected or not interdicted. Constraints (15) and (16) ensure that the restoration status will always be 0 for the operational components. Constraints (17) and (18) ensure that the restoration status will be 0 for all components at period 1 since at least one time period is required for the restoration. Constraints (19)–(22) are the flow balance constraints. Constraint (23) is the link capacity constraint. Constraints (24)–(26) ensure that a link can have a positive flow only when both ends of the link are operational or restored. Constraints (27) and (30) require that the restoration of a disrupted component will continue without a break once it starts. Constraints (28), (29), (31), and (32) provide the total assignment durations of the work crews for the disrupted components. Constraints (33) and (34) ensure that once the nonoperational component is restored, its restoration status will be 0 for the remaining time periods. Constraints (35) and (36) require that once the restoration of a disrupted component is started by a work crew, that specific work crew completes the restoration process. Constraints (37)

and (38) ensure that only a single work crew can work on a specific disrupted component at a specific time period. Constraint (39) ensures that a work crew can be assigned at most one disrupted component at a time. Constraint (40) establishes the interdependence among the nodes from the different networks. Constraints (41) and (42) represent the nonnegative nature of the decision variables related to satisfied demand and amount of flow. Constraints (43)–(50) represent the binary nature for the decision variables for the third level of the problem.

Ghorbani-Renani et al. [14] linearize the nonlinear constraints (9), (10), (33), and (34) by replacing them with the equivalent sets of linear constraints. Constraint (9) is replaced with the constraints (51)–(53).

$$y_{ij}^k + (1 - z_{ij}^k) + F_{ij}^k \geq 1 \quad \forall k \in K, \forall (i, j) \in A'^k \quad (51)$$

$$F_{ij}^k \leq z_{ij}^k \quad \forall k \in K, \forall (i, j) \in A'^k \quad (52)$$

$$y_{ij}^k \leq 1 - F_{ij}^k \quad \forall k \in K, \forall (i, j) \in A'^k \quad (53)$$

Constraint (10) is replaced with the constraints (54)–(56).

$$y_i^k + (1 - z_i^k) + F_i^k \geq 1 \quad \forall k \in K, \forall i \in N'^k \quad (54)$$

$$F_i^k \leq z_i^k \quad \forall k \in K, \forall i \in N'^k \quad (55)$$

$$y_i^k \leq 1 - F_i^k \quad \forall k \in K, \forall i \in N'^k \quad (56)$$

Constraints (33) and (34) are replaced with the constraints (57) and (58).

$$1 - \left(\frac{\frac{F_{ij}^k}{\lambda_{ij}^k} - \sum_{r \in R^k} \sum_{s=1}^{t-1} \alpha'^{kr}_{ijs}}{M}} \right) \geq \beta_{ijt}^k \quad \forall k \in K, \forall (i, j) \in A'^k, \forall t \in T \mid t \neq 1 \quad (57)$$

$$1 - \left(\frac{\frac{F_i^k}{\lambda_i^k} - \sum_{r \in R^k} \sum_{s=1}^{t-1} \alpha'^{kr}_{is}}{M}} \right) \geq \beta_{it}^k \quad \forall k \in K, \forall i \in N'^k, \forall t \in T \mid t \neq 1 \quad (58)$$

2.4 Solution Approach

To solve the model to optimality, a decomposition-based solution method is utilized in which the original tri-level model is divided into two bi-level formulations: (i) master problem and (ii) subproblem. By iteratively solving the smaller bi-level problems, the final solution for the tri-level model is obtained.

To construct the master problem, the attacker decision variables are fixed, $z \leftarrow \hat{z}$, in the original model. As a result, the resilience interdiction model is transformed into the bi-level min-min formulation represented in Eqs. (59)–(65). Note that since the master problem is a relaxed formulation relative to the complete tri-level model, it provides a valid lower bound value for the entire tri-level model [21, 22].

$$\min_y \min_{\eta, x, F, \alpha, \alpha', \beta} \sum_{t \in T} \zeta(t) \quad (59)$$

$$\sum_{k \in K} \sum_{(i, j) \in A'^k} CP_{ij}^k y_{ij}^k + \sum_{k \in K} \sum_{i \in N'^k} CP_i^k y_i^k \leq B_P \quad (60)$$

$$y_i^k \in \{0, 1\} \quad \forall k \in K, \forall i \in N'^k \quad (61)$$

$$y_{ij}^k \in \{0, 1\} \quad \forall k \in K, \forall (i, j) \in A'^k \quad (62)$$

$$y_{ij}^k + (1 - \hat{z}_{ij}^k) (1 - y_{ij}^k) = 1 - F_{ij}^k \quad \forall k \in K, \forall (i, j) \in A'^k \quad (63)$$

$$y_i^k + (1 - \hat{z}_i^k) (1 - y_i^k) = 1 - F_i^k \quad \forall k \in K, \forall i \in N'^k \quad (64)$$

$$\text{Constraints (11)–(50)} \quad (65)$$

On the other hand, by fixing the protector decision variables, $y \leftarrow \hat{y}$, the subproblem is constructed as a bi-level max-min formulation including the interdiction and restoration levels as represented in Eqs. (66)–(72). Like the master problem, the subproblem is a relaxed problem, providing a valid upper bound value for the original tri-level model.

$$\max_z \min_{\eta, x, F, \alpha, \alpha', \beta} \sum_{t \in T} \zeta(t) \quad (66)$$

$$\sum_{k \in K} \sum_{(i, j) \in A'^k} CI_{ij}^k z_{ij}^k + \sum_{k \in K} \sum_{i \in N'^k} CI_i^k z_i^k \leq B_I \quad (67)$$

$$z_i^k \in \{0, 1\} \quad \forall k \in K, \forall i \in N^k \quad (68)$$

$$z_{ij}^k \in \{0, 1\} \quad \forall k \in K, \forall (i, j) \in A^k \quad (69)$$

$$\hat{y}_{ij}^k + (1 - z_{ij}^k) (1 - \hat{y}_{ij}^k) = 1 - F_{ij}^k \quad \forall k \in K, \forall (i, j) \in A^k \quad (70)$$

$$\hat{y}_i^k + (1 - z_i^k) (1 - \hat{y}_i^k) = 1 - F_i^k \quad \forall k \in K, \forall i \in N^k \quad (71)$$

$$\text{Constraints (11)–(50)} \quad (72)$$

However, both the master problem and subproblem are bi-level formulations that often cannot be solved directly with available optimization solvers; therefore further manipulation is required. To convert the master-problem—the bi-level min-min formulation—into the single minimization problem, we implement Benders decomposition method [21, 22]. On the other hand, the bi-level max-min model generated through the subproblem can be transformed into a single-level model by utilizing a set-covering approach [23, 24]. Therefore, the solution algorithm is constructed by integrating Benders decomposition and set-covering approach in which the master problem and subproblem are iteratively solved to deliver lower-bound and upper-bound values for the model, respectively. The algorithm is terminated and the final solution for the original tri-level model is returned when the gap between the two bounds becomes zero or sufficiently small enough (i.e., the optimality tolerance gap set by the user). Note that by solving the master problem, the protection plan is determined, $y \leftarrow \hat{y}$, which will be the input of the subproblem. By solving the subproblem on the other hand, the interdiction plan is determined, $z \leftarrow \hat{z}$, and serves as the input of the master problem. The algorithm is initialized by the preliminary feasible solution $z \leftarrow 0$, meaning that no components are interdicted at this step. The algorithm finds the final solution in a finite number of iterations, and the convergence proof is provided in [22].

Based on the above discussion for constructing the master problem and subproblem, the implementation steps of the solution algorithm are represented in Table 4. Note that ε is the solution gap set by the decision-maker as the stopping criterion of the algorithm. *LB*, *UB*, *obj_{MP}*, and *obj_{SP}* refer to the lower-bound, upper-bound, master problem (MP), and subproblem (SP) objective values, respectively. The best protection and interdiction decisions are denoted with y^* and z^* , respectively.

Table 4 Implementation steps of the solution algorithm

Step 1	Initialization: $LB \leftarrow -\infty$, $UB \leftarrow +\infty$ and $z \leftarrow 0$
Step 2	While $\frac{UB-LB}{LB} > \varepsilon$ do:
Step 3	Solve MP, obtain its value obj_{MP} and protection decision \hat{y}
Step 4	$y^* \leftarrow \hat{y}$, $LB \leftarrow obj_{MP}$
Step 5	Solve SP, obtain its value obj_{SP} and interdiction decision \hat{z}
Step 6	$z^* \leftarrow \hat{z}$, $UB \leftarrow \min \{UB, obj_{SP}\}$
Step 7	Update MP by generating a new set of variables and constraints
Step 8	Exit (protection decision y^* and interdiction decision z^* are returned)

2.5 Accounting for Social Vulnerability

Social vulnerability is defined as “the characteristics of a person or group and their situation that influence their capacity to anticipate, cope with, resist and recover from the impact of a natural hazard” [25]. One means to measure social vulnerability is in terms of socioeconomic characteristics of a community in such a way that it will represent the differences in the ability of that community to respond to a similar disruptive event [26]. As a result, including the effect of social vulnerability in the optimization formulation will help decision-makers account for vulnerable populations when making protection and interdiction investment actions.

To quantify social vulnerability, Cutter et al. [27] reduce 42 socioeconomic variables into 11 social vulnerability dimensions for counties in the USA and calculate a social vulnerability index (SoVI) score for each county as an equal-weight additive model of the 11 dimensions. A subsequent iteration of the SoVI approach was reduced SoVI-Lite algorithm, which uses a smaller subset of demographic information without full principal component analysis [28]. Karakoc et al. [26] use the SoVI-Lite along with population density to prioritize the restoration of disrupted components in interdependent infrastructure networks according to the social impacts of the important services provided by those networks. Karakoc et al. [29] develop restoration-driven component importance measures that account for the multiple socioeconomic dimensions from the SoVI-Lite algorithm.

To add the effect of social vulnerability in the tri-level protection-interdiction-restoration model decisions, an approach similar to that in [26] is used. An overview of this approach is provided in Fig. 2. Further, the social vulnerability weights provide a means to select the subset of nodes to consider for protection and interdiction, rather than the topological characteristic chosen in [14].

3 Proposed Decentralized Approaches

Four different strategies to decentralized decision-making were developed and implemented by different extensions to the tri-level optimization problem discussed

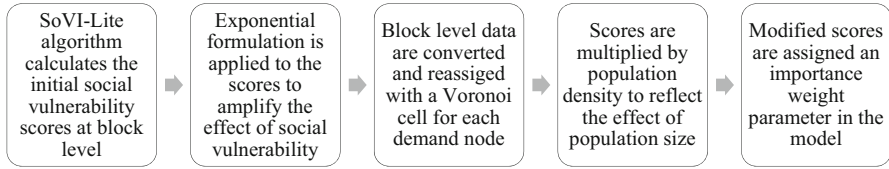


Fig. 2 The process of assigning importance weights to demand nodes in the interdependent networks based on social vulnerability characteristics

Table 5 Decentralized decision-making strategies

		Protection budget	Decisions	Interdiction plan
Case 0	Base model	Shared	Centralized	Optimal
Case 1	Divided protection budget	Divided	Centralized	Optimal
Case 2	Isolated decisions	Divided	Decentralized	Given
Case 3	Dominant decisions	Divided	Decentralized	Given

previously. These four strategies represent different decision environments, as discussed in subsequent subsections and summarized in Table 5.

Cases are designed to simulate possibilities for how the system of interdependent networks behave in real life. Even though the cases as designed may exhibit similarities to competition rather than cooperation among utility decision-makers, there is no intended competition or cooperation between the networks. Decision-makers from each network seek to maximize their own objective function without actively seeking a lower performance on the other networks. Only in Case 3 do decision-makers *expect* a one-sided cooperation, but in reality we do not intend or observe such cooperation.

3.1 Case 0: Base Model

Case 0 represents the baseline centralized optimization result from the original tri-level optimization model from [14] with the addition of SoVI-driven weights and candidate nodes to prioritize protection and interdiction decisions based on the effect on more socially vulnerable communities. The protection budget is shared by all decision-makers across the infrastructure networks, and the interdiction plan results from the optimization problem. Case 0 is suitable to represent centralized decisions where all included parties are managed by one decision authority.

3.2 Case 1: Divided Protection Budget

Case 1 represents an intermediate step between centralized and decentralized designs. While decisions continue to be centralized, the total protection budget is distributed to the networks in direct proportion to network sizes (i.e., the network with the highest number of network components commands the biggest share from the total protection budget). We need this approach in order to observe the effect of budget decentralization, and it is especially beneficial for analyzing the decisions under crises where there is a temporary central decision-maker in control for different institutions with different financial tables or when there is legal enforcement that force independently owned companies to work together for the sake of society. To reflect this change in the formulation, constraint (3) from the reference model is replaced with constraints (73) and (74), where S^k represents the ratio of the size of network $k \in K$ to the size of the total system.

$$B_p^k = B_p S^k \quad \forall k \in K \quad (73)$$

$$\sum_{(i,j) \in A^k} C P_{ij}^k y_{ij}^k + \sum_{i \in N^k} C P_i^k y_i^k \leq B_p^k \quad \forall k \in K \quad (74)$$

Case 1 is suitable to represent the situations where included parties are separate entities that must act together under one decision authority but with separate resources. Considering Case 1 is beneficial when there is a crisis and separate utility or service providers should collaborate due to government encouragement or enforcement, when there is one assigned decision-maker for separate companies or departments that need to work together, or when there is one utility network that is decentralized either for the ease of daily operations or due to different types of sources on a common service platform (e.g., an electricity supply network fed by hydro power, wind power, and solar power).

Starting from Case 1, a divided protection budget is used for all the remaining cases.

3.3 Case 2: Isolated Decisions

Case 2 describes a decentralized decision-making process where decisions are made in isolation: each decision-maker considers only its own network and makes decisions (protection and restoration) for their own network without considering any interdependence. That is, decision-makers assume that if there is no interdiction in their network, their network is not affected. The interdiction plan from Case 1 is used, as it is assumed that the attacker decisions are centralized, and the attacker will continue to focus on causing the highest possible disruption to the overall system.

To apply Case 2, objective calculation is kept same as in Eq. (1) but the objectives are updated as Eq. (75) to reflect only the recovery and restoration levels.

$$\xi = \min_y \min_{\eta, x, F, \alpha, \alpha', \beta} \sum_{t \in T} \zeta(t) \quad (75)$$

All inputs and the formulations are updated to reflect only the current network. Also, the constraint related to the independence in the system, constraint (40), is removed. Since the interdiction decisions are assumed to be centralized, and hence the optimal interdiction plan from Case 1 is valid for Case 2 as well, the interdiction level is removed, and a fixed interdiction plan is defined. The protection and the restoration problems are solved for each network separately. Final/real system performance is calculated by solving the restoration problem again by aggregating all individual protection and restoration decisions from each network and testing them against the given attack plan with all interdependence relationships defined in the real system.

3.4 Case 3: Dominant Decisions

In Case 3, each decision-maker makes separate decisions for their own network, but here decision-makers consider the entire system of networks and the interdependent impacts that disruptions in other networks might cause. Even though decision-makers consider the entire system, they do not try to maximize the overall system performance: each decision-maker tries to maximize the performance of their own network. As such, they make protection and restoration decisions that cater to their own performance needs and assume that other networks will assist in that objective. While making decisions, decision-makers assume that they dominate the other networks.

To apply Case 3, objective formulation is kept same as Eq. (1) but updated with Eq. (75) to reflect only the recovery and restoration levels.

Importance weights are updated in a way that only the candidates from the current network will have social vulnerability scores assigned as the importance weights and the remaining importance weights are given the value zero. The interdiction level is removed, and a fixed interdiction plan is defined from Case 1. The protection and the restoration problems are solved for each network separately.

Final/real system performance is calculated by solving the restoration problem again by aggregating all individual protection and restoration decisions from each network and testing them against the given attack plan with all interdependence relationships defined in the real system. Even though decision-makers make decisions with the entire system of networks in mind, only the decisions related to their own network are transferred into final decisions.

Case 2 and Case 3 are suitable to represent situations where included parties are separate entities owned or governed by different decision authorities. These cases

represent the general situation in any industry where there is an interaction but no cooperation among the players. There is no information sharing, and hence, included parties must make their own assumptions to react against adverse events happening in other parties. The nature of these assumptions differentiates Case 2 and Case 3 from each other. In Case 2, there is a perhaps more naïve approach where each party acts as if there exist no interdependencies. In Case 3, each party sees itself as the most important party and, hence, expects unconditional assistance from others.

In addition to the interdependent system of utility networks discussed here, another potential application of these two cases may be the management of resources, time, and risk in companies with different projects sponsored by different departments but under the same project management office.

4 Illustrative Example

Given its location in the New Madrid Seismic Zone, the interdependent infrastructure network case study of Shelby County, TN, has become something of a benchmark data set [12, 30–33]. Figure 3 depicts the water, gas, and power networks from Shelby County [12] that are used to illustrate the decentralized decision-making strategies described previously.

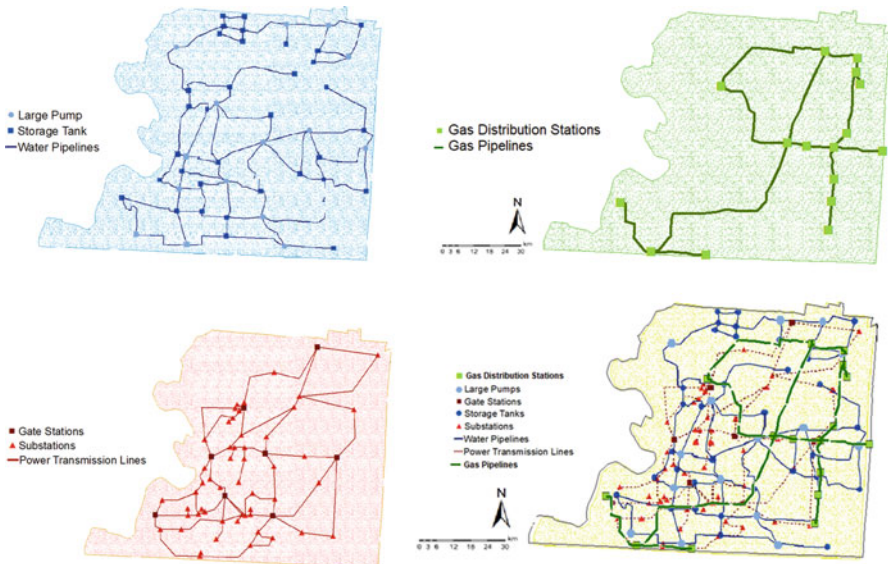


Fig. 3 General depiction of the (a) water, (b) gas, (c) power networks, and (d) the interdependence among networks in Shelby County, TN, respectively. (Adapted from Ref. [12])

The proposed model considers the physical interdependence in the system of networks, meaning that the functionality of a node in one network depends on the output or functionality of another node in another network [34]. In this Shelby County application, the physical interdependencies are defined between the power and the water networks. While it is possible to observe the interdependence in either direction between power and water networks, this does not require a two-way interdependence within power node-water node couples. For example, a water pump may depend on power in order to deliver water, or a power station may depend on water for cooling, but these interdependencies do not have to be symmetrical [35].

For this study, it is assumed that among 125 nodes and 164 links in the system of networks, only nodes can be interdicted. As a result, only the following illustrated in Fig. 3 are subject to interdiction: pumps and storage tanks from the water network, distribution stations from the gas network, and gate stations and substations from the power network. Moreover, only the critical nodes are subject to interdiction and, hence, protection. To choose these critical nodes that are candidates for potential interdiction or protection, importance weights based on modified social vulnerability scores are used, meaning that candidate nodes are selected among more socially vulnerable areas. For each network, the number of candidate nodes is decided with respect to network size. Then, that amount of demand nodes with the highest importance from each network are added to the candidate set since importance weights are defined only for the demand nodes. To see the effect of interdependence on protection decisions, parent nodes (even if they are not demand nodes or not as important in terms of social vulnerability scores) from the interdependence relationships are added to the set for each critical demand node in the candidate set. The list of the candidate nodes selected for implementation is presented in Table 6.

Figure 4 shows the topology of the interdependent system of water, gas, and power networks in Shelby County, TN, where the notation w, g, and p refer to water, gas, and power networks, respectively. The dashed lines represent the interdependency relationship between water and power networks in this case study.

The Shelby County data provides the information related to the demand/supply parameter for each node and maximum capacity parameter for each arc. On the other hand, protection costs, interdiction costs, and the restoration rates for candidate

Table 6 Candidate nodes for protection and interdiction based on social vulnerability

	Demand nodes	Supply nodes	Transshipment nodes	Total number of selected nodes
Water	2, 4, 5, 6	–	–	4
Water ^a	–	21, 23, 25, 29, 30	–	5
Gas	4, 15	–	–	2
Power	1, 2, 3, 4, 5	–	–	5
Power ^a	–	10, 16, 27, 32	–	4

^aParent nodes of the critical demand nodes from the interdependence relationship

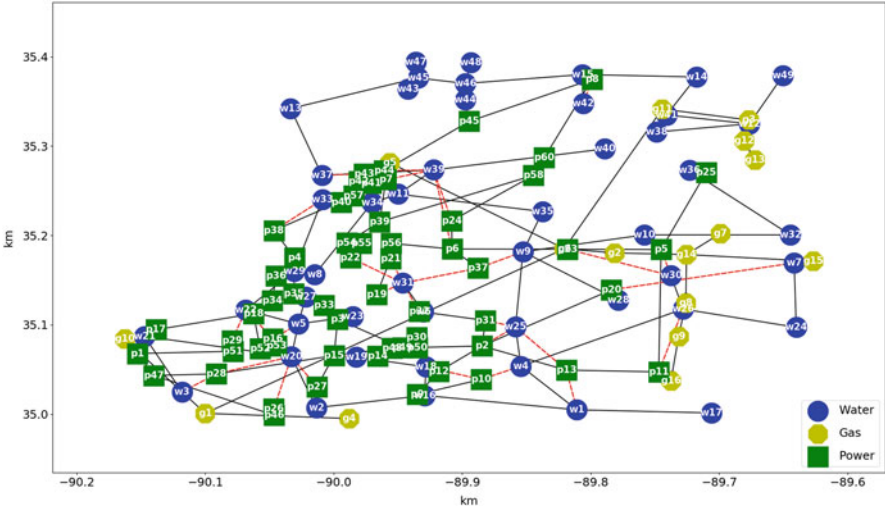


Fig. 4 The topology of the interdependent system of water, gas, and power networks in Shelby County, TN, USA

components are generated specifically for this implementation according to the following distributions [10]: $CP_{ij}^k, CP_i^k \sim U(20, 40)$, $CI_{ij}^k, CI_i^k \sim U(50, 70)$, and $\lambda_{ij}^k, \lambda_i^k \sim U(0.1, 1)$, respectively.

4.1 Computational Results

There were 20 different scenarios tested concerning five interdiction budgets ($B_I = 70, 140, 210, 280, 350$) and four protection budgets ($B_P = 0, 80, 160, 240$) for each one of the four decision-making cases. Protection and interdiction budgets are set in a fictitious way that the amount of increase for the next higher budget guarantees the coverage of one more node.

System performance is evaluated according to ξ , the cumulative fraction of weighted unmet demand over the planning horizon, meaning that a higher ξ value indicates a lower performance for the system of networks. The relationship between ξ and budget constraints is depicted in Fig. 5.

Results in Fig. 5 suggest that the system of networks responds better under Case 0 than Case 1 as a result of having an undivided budget. However, these results also suggest that the system performs better under decentralized cases, Case 2 and Case 3, compared to the centralized ones, Case 0 and Case 1. While this is an unexpected result, it can be explained by the usage of a fixed interdiction plan for Case 2 and Case 3. Results in Fig. 4, also, suggest that the system of networks responds the same both under Case 2 and Case 3. The reason is that the main difference between Case 2

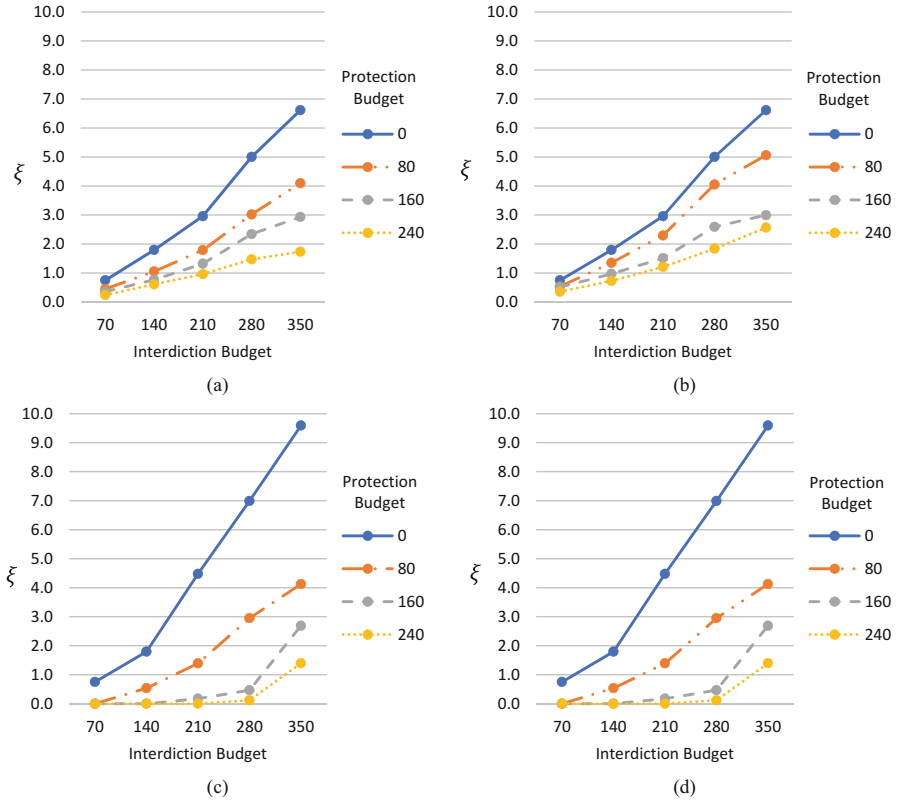


Fig. 5 The cumulative weighted fraction of unmet demand over time under different scenarios: (a) Case 0, (b) Case 1, (c) Case 2, and (d) Case 3

and Case 3 is the interdependence assumption, and these results show that the level of interdependence defined in the system is not enough to see the interdependence effect in the results. Even though being aware of the interdependencies helps each network to make more effective decisions both for itself and the other networks, only the decisions related to their own network are transferred to the general system decisions. This implies that only some of the decisions that are expected to contribute to the system are taken into consideration for the general system performance. Furthermore, all the parent nodes in the independence relationships are supply nodes, meaning that they have minor importance for the networks they belong to since they don't have importance weights. As a result, they are not prioritized in their own networks. Nevertheless, when the individual network expectations and decisions are analyzed, it is seen that the decision-makers make more realistic plans in Case 3. An example of this situation can be seen in Table 7.

In Table 7, the first major difference between the two cases is the expected objective values for the water network. Since the interdependencies are ignored in Case 2, no interruption is expected for the water network when there is no

Table 7 Individual expectations and decisions under Case 2 and Case 3 when $B_p = 80$ and $B_l = 280$

	Case 2	Case 3
Attacked nodes	(3, 2) (3, 4) (3, 10) ^a (3, 16) ^a (3, 27) ^a	(3, 2) (3, 4) (3, 10) ^a (3, 16) ^a (3, 27) ^a
Protected nodes	(3, 4)	(3, 4)
Suggested by water	–	(3, 16) ^a
Suggested by gas	–	(3, 4)
Suggested by power	(3, 4)	(3, 4)
Time until recovery	10	10
For water	0	5
For gas	0	0
For power	10	10
Objective value	2.95	2.95
Expected for water	0.00	1.09
Observed for water	5.07	5.07
Expected for gas	0.00	0.00
Observed for gas	0.00	0.00
Expected for power	0.63	0.63
Observed for power	0.63	0.63

^aParent node from an interdependence relationship

disruption in the water network itself. However, in reality, the performance of the water network will be negatively affected due to the disruption of the nodes (3, 10), (3, 16), and (3, 27) in the power network. As a result, there is a significant gap between the expected and observed objective values of the water network. On the other hand, there is an expected interruption in the water network under Case 3. In Case 3, the effect of the interdependencies is considered by the water network. Since the budget reserved for the protection of the power nodes is limited, node (3, 16) is selected among three power nodes that affect the performance of the water network and suggested to be protected by the water network. However, there is still a difference between expected and observed objective values of the water network under Case 3. This difference is observed because, during the consolidation, decisions for the power nodes are gathered from the power network (ignoring the suggestions from the other networks) and the power network suggests protecting node (3, 4).

Due to the given interdiction plan, both the covering and the restoration run times were faster for Case 2 and Case 3 compared to the Case 0 and Case 1. Equivalent of 88.36 days of total run time was spent for the implementation of all four cases with respect to 20 different budget scenarios. Approximately 64.91% of this run time was spent for Case 0 and 35.09% of this run time was spent for Case 1.¹

¹The solution algorithm was implemented in Python 3.7.3 with the Gurobi optimizer 8.1.1. Computational results were conducted on a 64-bit operating system, Intel[®] Core™ i7-6700 CPU @ 3.40GHz 3.41GHz desktop computer.

In general, results indicate the following outcomes:

- As expected, an increase in the protection budget improves the system performance, while an increase in the interdiction budget worsens it in each case.
- Based on the difference in the usage of the protection budget, the performance of the system when the protection budget is split is at least as good as the performance of the system with the shared budget for all the scenarios.
- Splitting the protection budget among networks decreases the system performance due to:
 - *The decrease in the total number of protected nodes*
When the protection budget is split between different networks, each network ends up with a (potential) residual budget that could have been joined and used in order to protect one more node in the case of a shared budget.
 - *The shift in the focus, the change in the idea of an important node, and hence the protection set*
When the protection budget is split between different networks, each network tries to protect its most important nodes which may not be the top priority for the overall system.
- In the case of isolation or domination, it had been expected that the overall system would have performed worse than the cases where the decisions are centralized since the decision-makers will lose their holistic view and power over the interdependent system. Nevertheless, decentralized cases resulted in better system performances due to
 - *The design of the cases*
The decentralized cases are designed under the assumption that the system will encounter an optimal attack scenario from the perspective of an attacker which regards the system of interdependent networks as a whole. Including the attack scenario as given provided an additional advantage to the decentralized cases. While the cases with the centralized decisions required to consider all possibilities for all of the critical nodes and spend the protection budget both for the attacked and unattacked nodes, it was possible/enough to focus on only the attacked nodes and use the protection budget more efficiently for the cases with the decentralized decisions.
- In the case of isolation or domination, actual system performances observed for each network are worse than the individual network performances expected for those networks under the specific assumptions related to the case design such as:
 - *Assuming that a network will not experience any interruption as long as there is no disruption within its own components*
 - *Assuming that the priorities of a network will be regarded with the same importance by the other networks*

- Even though final performances seem similar, individual decisions made for each network under the dominance assumption are more realistic than the decisions made under the isolation assumption through the consideration of the interdependence between different networks.

5 Concluding Remarks

While our dependence on critical infrastructure networks and the interdependence among them is growing, the economic and social impacts of disruptions to interdependent infrastructure networks are increasing drastically. As a result, ensuring the interdependent infrastructure resilience has become a major concern. The critical infrastructure resilience includes so many aspects to consider. To be prepared for real-life problems, situations that are not ideal such as social vulnerability and decentralized environments should also be considered.

In this study, social vulnerability scores are utilized by the selection of the candidate nodes and the assignment of the importance weights in order to give priority to the socially vulnerable areas and to decrease the negative effects of disruption not only on the infrastructure network but also on the society in general. Moreover, four different cases are designed to analyze the response of the interdependent system of networks when faced with the challenges of decentralization.

For this study, especially for the Case 0 and Case 1, where all three levels are simultaneously considered, the biggest limitation was the computational time. It prevented the inclusion of more nodes to the candidate list. This is an area open to improvement that currently requires careful attention to selecting nodes to include in the candidate list.

For the future work, the proposed model can be enhanced further by assigning importance weights to the supply nodes and considering supply nodes, in addition to the demand nodes, in the objective function. This approach may also help with highlighting the different effects of the isolation and dominance assumptions. Furthermore, forcing Case 2 and Case 3 protection plans to utilize all the given protection budget, and then, studying the response and performance of each case under random attack plans may help the potential decision-makers to simulate the issues related to prior planning and to derive lessons.

One of the major contributions of this study is to show the consequences of operating under different types of assumptions in a decentralized environment with multiple decision-makers. However, cases are designed such that all networks operate under the same type of assumptions in each case. Thus, future work could focus on studying systems where each network can describe different decision hierarchies and dynamics. Another area of future work includes testing the effects of having different assumptions for different parties in one system of interdependent networks, which would further improve the applicability of the proposed methods in a realistic context. For example, an isolationist management may adopt the isolated

decision assumptions, while an aggressive management may adopt dominated decision assumptions.

Acknowledgment This work was supported in part by the National Science Foundation through award 1541165. The research reported herein was supported, in part, by the Center for Risk-Based Community Resilience Planning, funded by the National Institute of Standards and Technology (NIST) under Cooperative Agreement No. 70NANB15H044. Any opinions, findings, and conclusions or recommendations expressed in this material are those of the authors and do not necessarily reflect the views of the NSF, the NIST, or the US Department of Commerce.

References

1. S. Hosseini, K. Barker, and J. E. Ramirez-Marquez, "A review of definitions and measures of system resilience," *Reliab. Eng. Syst. Saf.*, vol. 145, pp. 47–61, Jan. 2016.
2. D. Tuzun Aksu and L. Ozdamar, "A mathematical model for post-disaster road restoration: Enabling accessibility and evacuation," *Transp. Res. Part E Logist. Transp. Rev.*, vol. 61, pp. 56–67, 2014.
3. Y. P. Fang, N. Pedroni, and E. Zio, "Resilience-Based Component Importance Measures for Critical Infrastructure Network Systems," *IEEE Trans. Reliab.*, vol. 65, no. 2, pp. 502–512, Jun. 2016.
4. S. Kamamura, D. Shimazaki, K. Genda, K. Sasayama, and Y. Uematsu, "Disaster recovery for transport network through multiple restoration stages," *IEICE Trans. Commun.*, vol. E98B, no. 1, pp. 171–179, 2015.
5. T. C. Matisziw, A. T. Murray, and T. H. Grubestic, "Strategic network restoration," *Networks Spat. Econ.*, vol. 10, no. 3, pp. 345–361, 2010.
6. N. Morshedlou, A. D. González, and K. Barker, "Work crew routing problem for infrastructure network restoration," *Transp. Res. Part B Methodol.*, vol. 118, pp. 66–89, Dec. 2018.
7. S. G. Nurre, B. Cavdaroglu, J. E. Mitchell, T. C. Sharkey, and W. A. Wallace, "Restoring infrastructure systems: An integrated network design and scheduling (INDS) problem," *Eur. J. Oper. Res.*, vol. 223, no. 3, pp. 794–806, Dec. 2012.
8. E. D. Vugrin, M. A. Turnquist, and N. J. K. Brown, "Optimal recovery sequencing for enhanced resilience and service restoration in transportation networks," *Int. J. Crit. Infrastructures*, vol. 10, no. 3–4, pp. 218–246, 2014.
9. N. Xu, S. D. Guikema, R. A. Davidson, L. K. Nozick, Z. Çağnan, and K. Vaziri, "Optimizing scheduling of post-earthquake electric power restoration tasks," *Earthq. Eng. Struct. Dyn.*, vol. 36, no. 2, pp. 265–284, 2007.
10. Y. Almoghathawi, K. Barker, and L. A. Albert, "Resilience-driven restoration model for interdependent infrastructure networks," *Reliab. Eng. Syst. Saf.*, vol. 185, pp. 12–23, May 2019.
11. A. D. González, A. Chapman, L. Dueñas-Ororio, M. Mesbahi, and R. M. D'Souza, "Efficient Infrastructure Restoration Strategies Using the Recovery Operator," *Comput. Civ. Infrastruct. Eng.*, vol. 32, no. 12, pp. 991–1006, Dec. 2017.
12. A. D. González, L. Dueñas-Ororio, M. Sánchez-Silva, and A. L. Medaglia, "The Interdependent Network Design Problem for Optimal Infrastructure System Restoration," *Comput. Civ. Infrastruct. Eng.*, vol. 31, no. 5, pp. 334–350, May 2016.
13. T. C. Sharkey, B. Cavdaroglu, H. Nguyen, J. Holman, J. E. Mitchell, and W. A. Wallace, "Interdependent network restoration: On the value of information-sharing," in *European Journal of Operational Research*, Jul. 2015, vol. 244, no. 1, pp. 309–321.
14. N. Ghorbani-Renani, A. D. A. D. González, K. Barker, N. Morshedlou, A. D. A. D. González, and N. Morshedlou, "Protection-interdiction-restoration: Tri-level optimization for enhancing interdependent network resilience," *Reliab. Eng. Syst. Saf.*, vol. 199, p. 106907, Jul. 2020.

15. C. D. Nicholson, K. Barker, and J. E. Ramirez-Marquez, "Flow-based vulnerability measures for network component importance: Experimentation with preparedness planning," *Reliab. Eng. Syst. Saf.*, vol. 145, pp. 62–73, Jan. 2016.
16. M. Ouyang, "Review on modeling and simulation of interdependent critical infrastructure systems," *Reliability Engineering and System Safety*, vol. 121. Elsevier Ltd, pp. 43–60, 2014.
17. D. Henry and J. Emmanuel Ramirez-Marquez, "Generic metrics and quantitative approaches for system resilience as a function of time," *Reliab. Eng. Syst. Saf.*, vol. 99, pp. 114–122, Mar. 2012.
18. J. Chen and Q. Zhu, "Resilient and decentralized control of multi-level cooperative mobile networks to maintain connectivity under adversarial environment," in *2016 IEEE 55th Conference on Decision and Control, CDC 2016*, Dec. 2016, pp. 5183–5188.
19. J. Chen and Q. Zhu, "Interdependent network formation games with an application to critical infrastructures," in *Proceedings of the American Control Conference*, Jul. 2016, vol. 2016-July, pp. 2870–2875.
20. H. Talebiyan and L. Dueñas-Osorio, "Probabilistic assessment of decentralized decision-making for interdependent network restoration," in *13th International Conference on Applications of Statistics and Probability in Civil Engineering, ICASP 2019*, 2019.
21. W. Yuan, L. Zhao, and B. Zeng, "Optimal power grid protection through a defender–attacker–defender model," *Reliab. Eng. Syst. Saf.*, vol. 121, pp. 83–89, Jan. 2014.
22. B. Zeng and L. Zhao, "Solving two-stage robust optimization problems using a column-and-constraint generation method," *Oper. Res. Lett.*, vol. 41, no. 5, pp. 457–461, Sep. 2013.
23. E. Israeli and R. K. Wood, "Shortest-path network interdiction," *Networks*, vol. 40, no. 2, pp. 97–111, 2002.
24. Y. Yao, T. Edmunds, D. Papageorgiou, and R. Alvarez, "Trilevel Optimization in Power Network Defense," *IEEE Trans. Syst. Man, Cybern. Part C Applications Rev.*, vol. 37, no. 4, pp. 712–718, Jul. 2007.
25. B. Wisner, P. Blaikie, T. Cannon, and I. Davis, "At risk: natural hazards, peoples vulnerability and disasters," 2014.
26. D. B. Karakoc, Y. Almoghathawi, K. Barker, A. D. González, and S. Mohebbi, "Community resilience-driven restoration model for interdependent infrastructure networks," *Int. J. Disaster Risk Reduct.*, vol. 38, p. 101228, Aug. 2019.
27. S. L. Cutter, B. J. Boruff, and W. L. Shirley, "Social vulnerability to environmental hazards," *Soc. Sci. Q.*, vol. 84, no. 2, pp. 242–261, 2003.
28. J. Evans, M. E. Hauer, D. Hardy, and J. S. Pippin, "Assessing social vulnerability using SoVI-Lite: A demonstration study at Glynn County, GA." 2014.
29. D. B. Karakoc, K. Barker, C. W. Zobel, Y. Almoghathawi, and A. Yasser, "Social Vulnerability and Equity Perspectives on Interdependent Infrastructure Network Component Importance," *Sustain. Cities Soc.*, vol. 57, p. 102072, Jun. 2020.
30. I. Hernandez-Fajardo, & L. Dueñas-Osorio, "Network-consistent seismic risk assessment for interdependent infrastructure systems," *Earthq. Eng. Struct. Dyn.*, pp. 1–19, 2010.
31. I. Hernandez-Fajardo, & L. Dueñas-Osorio, "Sequential propagation of seismic fragility across interdependent lifeline systems," *Earthq. Spectra*, vol. 27, no. 1, pp. 23–43, 2011.
32. T. Adachi, & B. R. Ellingwood, "Serviceability assessment of a municipal water system under spatially correlated seismic intensities," *Comput. Infrastruct. Eng.*, vol. 24, no. 4, pp. 237–248, 2009.
33. T. Adachi, & B. R. Ellingwood, "Comparative assessment of civil infrastructure network performance under probabilistic and scenario earthquakes," *J. Infrastruct. Syst.*, vol. 16, no. 1, pp. 1–10, 2010.
34. S. M. Rinaldi, J. P. Peerenboom, and T. K. Kelly, "Identifying, understanding, and analyzing critical infrastructure interdependencies," *IEEE Control Syst. Mag.*, vol. 21, no. 6, pp. 11–25, 2001.
35. Y. Zhang, N. Yang, and U. Lall, "Modeling and simulation of the vulnerability of interdependent power-water infrastructure networks to cascading failures," *J. Syst. Sci. Syst. Eng.*, vol. 25, no. 1, pp. 102–118, Mar. 2016.

Wavelets in Multi-Scale Time Series Analysis: An Application to Seismic Data



Stefania Corsaro , Pasquale Luigi De Angelis , Ugo Fiore ,
Zelda Marino , Francesca Perla , and Mariafortuna Pietrolungo 

Abstract Forecasting earthquakes is one of the most important problems in Earth science because of their devastating consequences. Current scientific studies related to earthquake forecasting focus on three key points: when the event will occur, where it will occur, and how large it will be. In this work we investigate the possibility to determine when the earthquake will take place.

We formulate the problem as a multiple change-point detection in the time series. In particular, we refer to the multi-scale formulation described in Fryzlewicz (Ann Stat 46(6B): 3390–3421, 2018). In that paper a bottom-up hierarchical structure is defined. At each stage, multiple neighbor regions which are recognized to correspond to locally constant underlying signal are merged. Due to their multi-scale structure, wavelets are suitable as basis functions, since the coefficients of the representation contain local information. The preprocessing stage involves the discrete unbalanced Haar transform, which is a wavelet decomposition of one-dimensional data with respect to an orthonormal Haar-like basis, where jumps in the basis vectors do not necessarily occur in the middle of their support.

The algorithm is tested on data from a well-characterized laboratory system described in Rouet-Leduc et al. (Geophys Res Lett 44(18): 9276–9282, 2017).

Keywords First keyword · Second keyword · Another keyword

Authors acknowledge the financial support provided by the Research grant of Università Parthenope, DR no. 953, november 28th, 2016.

S. Corsaro · P. L. De Angelis · U. Fiore (✉) · Z. Marino · F. Perla · M. Pietrolungo
Parthenope University, Napoli, Italy
e-mail: stefania.corsaro@uniparthenope.it; pasqualeLuigiDe.angelis@uniparthenope.it;
ugo.fiore@uniparthenope.it; zelda.marino@uniparthenope.it; francesca.perla@uniparthenope.it;
mariafortuna.pietrolungo@uniparthenope.it

1 Introduction

Seismic signals recorded on the field result from the interaction of the original source with the process of wave propagation. Experiments where seismic phenomena are induced in laboratory create (partially) controlled environments where the dynamics of earthquakes can be studied. Statistical learning methods are increasingly being used to isolate patterns in seismic signals that cannot be easily detected with traditional waveform analysis techniques [7]. Recently, a study on data originated from laboratory friction experiments [9] has investigated the possibility that natural earthquakes could be preceded by precursory signals, so that the detection and measurement of these signals could be used in forecasting.

When applying an analysis and forecasting model to very long signals, such as those related to seismic events, the hypotheses made in the model about the data-generating process may not necessarily be valid for the whole duration of the signal. Further, adaptation of the model parameters to data may become increasingly complex and time-consuming. In this perspective, transforming batches of the original signal into compact representations and observing the variation over time of such representations could be a valid solution. An evaluation of the potential of a transformation based on bottom-up data decomposition and change-point detection through wavelets has been carried out in this study. The next section briefly recapitulates some ideas about wavelet transforms as tools to estimate change points in piecewise-constant functions. Section 3 describes the data analyzed, and Sect. 4 discusses the experiments performed and their results.

2 Background

Wavelet thresholding estimators have received much attention in literature, since wavelet functions show some relevant properties. The key property of wavelets is referred to as “localization,” which allows one to obtain sparse representation of certain functions and operators in wavelet bases. For this reason, wavelet techniques can provide insight beyond other approaches in jump detection in high-frequency data. Traditional wavelet thresholding estimation proceeds as follows. Take the discrete wavelet transform of a dataset, set to 0 those coefficients that fall below a certain threshold, and then take the inverse wavelet transform of the thresholded coefficients. The definition of wavelet is a quite general one; thus many wavelet families can be built. They are classified according to certain properties such as orthogonality, amplitude of the support, smoothness, and the number of vanishing moments. Each of these properties is important for specific purposes; thus the choice of the wavelet basis is strongly application dependent. When the focus is data compression, smoothness, and a compact, narrow support is desirable: in this case, localization is improved, so that small coefficients are obtained in smooth regions of the approximated function. They can therefore be neglected, preserving information

about sub-domains in which the gradient has high values. Wavelet thresholding has indeed successfully been applied in several fields such as signal denoising, image analysis, and finance [1, 2, 4].

Using Haar wavelets one obtains piecewise-constant estimates. Piecewise-constant estimators are easy to interpret: jumps in the estimate can be viewed as relevant changes in the mean level of the data, whereas constant intervals represent periods in which the mean of the data does not significantly change. This feature makes them attractive in the field of earthquake forecast, in terms of time. In this case, one can formulate the problem as a multiple change-point detection in the time series of acoustic data. A posteriori detection of multiple change points, sometimes referred to as segmentation, can often serve as the useful first step in the exploratory analysis of data. Moreover, piecewise-constant estimates are cheap to store, because the number of jumps is typically significantly less than the size of the analyzed time series. This is relevant in our application, since a huge volume of data is to be taken into account. Nonlinear estimators exhibit superior theoretical and practical performance with respect to linear ones when the underlying function is spatially inhomogeneous. In [3] authors use piecewise-constant approximation to control the number of local extremes. On the other hand, a disadvantage of Haar thresholding is that, due to Haar wavelet construction, jumps always occur at dyadic locations, even if it is not justified by the data. In [6] authors introduced the unbalanced Haar (UH) wavelet basis, in which unlike traditional Haar wavelets, jumps in the basis functions do not necessarily occur in the middle of their support. Thus, they are potentially useful as building blocks for piecewise-constant estimators that avoid the restriction of jumps occurring at dyadic locations. These wavelets enjoy the desirable properties of traditional wavelets, such as a multiresolution structure and an associated fast transform algorithm.

Our estimation procedure can be summarized as follows. We first take a transform of the data with respect to an UH basis. We then threshold the coefficients and take the inverse transform.

3 Data

The data used to test our model comes from a laboratory earthquake experiment described in [9]:

- The input is a chunk of 0.0375 s of seismic data (ordered in time), which is recorded at 4 MHz, hence 150,000 data points, and the output is time remaining until the following lab earthquake, in seconds;
- the seismic data is recorded using a piezoceramic sensor, which outputs a voltage upon deformation by incoming seismic waves. The seismic data of the input is this recorded voltage, in integers;
- seismic data include both a training set and a testing set, which come from the same experiment. There is no overlap between the training and testing sets, which

Table 1 Summary of the 17 blocks the data was found to be divided in. For each block, the start and end times are given, together with the number of measurements

Block no.	Time first	Time last	No. of readings
1	1.4691	0.0008	5656574
2	11.5408	0.0007	44429304
3	14.1806	0.0008	54591478
4	8.8567	0.0011	34095097
5	12.6940	0.0006	48869367
6	8.0555	0.0011	31010810
7	7.0590	0.0005	27176955
8	16.1074	0.0007	62009332
9	7.9057	0.0002	30437370
10	9.6372	0.0005	37101561
11	11.4264	0.0002	43991032
12	11.0242	0.0001	42442743
13	8.8281	0.0001	33988602
14	8.5660	0.0009	32976890
15	14.7518	0.0006	56791029
16	9.4595	0.0006	36417529
17	11.6186	9.7598	7159806

are contiguous in time. However, since no ground truth is available for the testing set, in this work n -fold cross-validation has been performed on the training set only;

- time to failure is based on a measure of fault strength (shear stress, not part of the published data). When a labquake occurs, this stress drops unambiguously;
- data is recorded in *bins* of 4096 samples. Within those bins seismic data is recorded at 4 MHz, but there is a 12-microsecond gap between each bin, an artifact of the recording device.

In addition, additional structure was found by examining the seismic data. The training set was found to be subdivided into 17 *blocks* of varying length, separated by different time gaps (see Table 1 for details).

To gain some insights about the data, an initial step involves computing and visualizing the autocorrelation. Figures 1 and 2 show, respectively, the autocorrelation and the partial autocorrelation averaged over all the bins of for the first data block. The charts for the subsequent blocks do not differ substantially and were not reported.

Recall that the autocorrelation is the correlation between y_t and y_{t-k} for different values of the lag k , while the partial autocorrelation gives the same correlation as above after the effects of the lags $1, 2, \dots, k-1$ have been removed. Autocorrelations have been averaged over all the bins to smooth out values which may be due to particular situations in each single 4096-measurement bin.

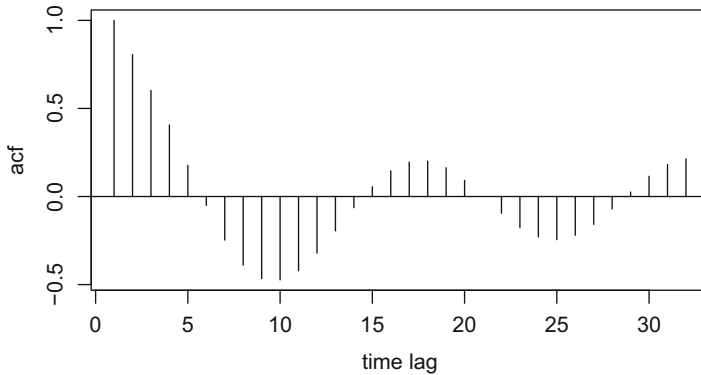


Fig. 1 Autocorrelation, computed for each of the 4096-readings bins of the first block of contiguous measurements, and then averaged

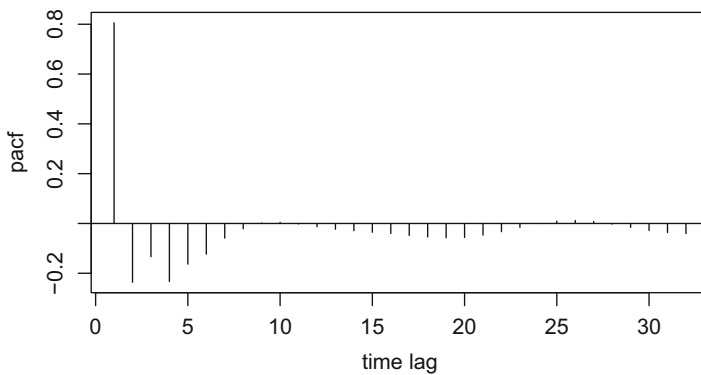


Fig. 2 Partial autocorrelation, computed for each of the 4096-readings bins of the first block of contiguous measurements, and then averaged

4 Experiments

The sheer size of the data would have had an adverse effect on the performance of training machine learning models. In addition, since data are recorded over a relatively long time with respect to the fine granularity of measurements, using a “flat” approach where each individual sample is taken separately did not look very attractive. In a hierarchical perspective, instead, if a way is found to condense each bin of readings in a representation in a small-dimension space, the evolution over time of this representation can be studied more easily.

The coefficient of a fitted AR(1) model – an autoregressive model of order one – was one of the features computed starting from a data bin. In fact, the damped sinusoidal shape of the autocorrelation, together with the presence of a spike at lag one in the partial autocorrelation, suggests [8] that fitting an AR(1) model to the data may be appropriate.

Since the transformation being sought should in some way capture the “energy” content of the observed signal, it is intuitive to think at entropy as a measure of uncertainty. The Shannon entropy of a discrete random variable Y is the expectation of the information content:

$$H(Y) = E_Y [-\log \Pr(Y)]$$

and, given a sample, it can be estimated from the observed counts. The entropy package of **R** has been used in the experiments. Note that, in all experiments, entropy was measured in bits.

The third transformation that has been used in the tests is the number of change points in the piecewise-constant mean of the noisy input vector, as described in Sect. 2. The efficient method implemented in the **R** package **breakfast** to estimate the number of change points was a critical factor in allowing the use of this technique, since computation times were reduced substantially [5].

Before going into further analysis, an interesting question that arises is at which scale the aggregation is to be performed. While the transformations can be applied to individual data bins, they could as well operate on sequences of contiguous bins (*windows*). Larger windows would tend to capture long-term effects, smoothing out fluctuations, whereas smaller windows would enable a more faithful description of short-lived variations. A preliminary calibration experiment was thus performed to select an appropriate window size. Out-of-sample correlation has been computed, after transforming the data in block number 6 (for training) and block number 7 (for testing) in different ways and for varying window sizes. Table 2 shows the results.

Entropy is seen to be the worst performer, while the number of change points obtains the best results, and the coefficient of an AR(1) model scores not too far. Moreover, a growth trend in correlation can be observed for all transformations as the window size is increased, suggesting that the accumulation of tension in the fault is a gradual process. Further experiments performed on the NCP transformation only for larger window sizes yielded correlation values as high as 0.881 for a windows size of 128 bins and even 0.945 for a window size of 256 bins. However, having the window size not exceed 32 bins – for a total of 131072 measurements – seemed to be appropriate, also in consideration that the number of 150,000 readings is used and mentioned often in [9]. A window size of 32 bins was therefore selected for the subsequent experiment.

Table 2 Out-of-sample correlation in calibration experiments for different transformations (ENT, entropy; AR1, coefficient of an AR(1) model; NCP, number of change points)

Window size (bins)	ENT	AR1	NCP
32	0.340	0.684	0.783
16	0.262	0.604	0.737
8	0.232	0.552	0.676
4	0.184	0.502	0.603
2	0.151	0.456	0.526
1	0.136	0.414	0.461

Table 3 Out-of-sample RMSE and correlation in 17-fold cross-validation experiments: training set is block i ; test set is all other blocks, $i = 1, \dots, 17$

	NCP	AR1
Mean RMSE	3.451	3.703
Mean correlation	0.603	0.501

All of the blocks in training data were used for a 17-fold cross-validation experiment. Each block was used to train a simple linear model from scratch, and all other blocks were used as testing data to verify the predictions. A linear regression model was purposely chosen as a very simple tool that would clearly expose the performance of the transformations being compared. The metrics selected to evaluate performance were the RMSE (root-mean-square error) and the correlation between the predicted data and the actual data.

Table 3 shows the results of the 17-fold cross-validation experiment. Note that n -fold cross-validation experiments are usually performed with n equal to 5 (or, less often, 10), implying a ratio between training and testing data of 1/5 (or 1/10). Here, the partitioning into 17 blocks means that the training-to-testing ratio is 1/15.84, taking into account the different sizes of the blocks.

The NCP transformation was found to outperform AR1. Finally, it was observed that using both methods in conjunction, i.e., fitting a linear model on both features, did not produce substantial improvements.

References

1. Chang, S.G., Vetterli, M.: Adaptive wavelet thresholding for image denoising and compression. *IEEE Transactions on Image Processing* **9**(9), 1532–1546 (2000). <https://doi.org/10.1109/83.862633>
2. Corsaro, S., D. Marazzina, D., Marino, Z.: A parallel wavelet-based pricing procedure for Asian options. *Quantitative Finance* **15**(1), 101–113 (2015). <https://doi.org/10.1080/14697688.2014.935465>
3. Davies, P.L., Kovac, A.: Local extremes, runs, strings and multiresolution. *The Annals of Statistics* **29**(1), 1–65 (02 2001). <https://doi.org/10.1214/aos/996986501>
4. Donoho, D.L., Johnstone, I.M.: Threshold selection for wavelet shrinkage of noisy data. In: *Proceedings of 16th Annual International Conference of the IEEE Engineering in Medicine and Biology Society*. vol. 1, pp. A24–A25 vol.1 (1994). <https://doi.org/10.1109/IEMBS.1994.412133>
5. Fryzlewicz, P.: Tail-greedy bottom-up data decompositions and fast multiple change-point detection. *The Annals of Statistics* **46**(6B), 3390–3421 (12 2018). <https://doi.org/10.1214/17-AOS1662>
6. Girardi, M., Sweldens, W.: A new class of unbalanced haar wavelets that form an unconditional basis for l_p on general measure spaces. *Journal of Fourier Analysis and Applications* **3**(4), 457–474 (Jul 1997). <https://doi.org/10.1007/BF02649107>
7. Holtzman, B.K., Paté, A., Paisley, J., Waldhauser, F., Repetto, D.: Machine learning reveals cyclic changes in seismic source spectra in geysers geothermal field. *Science advances* **4**(5) (2018)

8. Hyndman, R.J., Athanasopoulos, G.: *Forecasting: principles and practice*. OTexts (2018)
9. Rouet-Leduc, B., Hulbert, C., Lubbers, N., Barros, K., Humphreys, C.J., Johnson, P.A.: Machine learning predicts laboratory earthquakes. *Geophysical Research Letters* **44**(18), 9276–9282 (2017). <https://doi.org/10.1002/2017GL074677>, <https://agupubs.onlinelibrary.wiley.com/doi/abs/10.1002/2017GL074677>

Effectiveness of Investments in Prevention of Geological Disasters



Ugo Fiore , Zelda Marino , Francesca Perla ,
Mariafortuna Pietroluongo , Salvatore Scognamiglio ,
and Paolo Zanetti 

Abstract Research on geological disasters has made several achievements in monitoring, early warning, and risk assessment. Substantial resources are being invested in prevention projects, but, due to geographical and demographical complexity, incompleteness of data, and small number of samples, a quantitative analysis on the number of geological disasters and the entity of investments in their prevention is a difficult problem. In this work, the relation is studied between the amount of resources invested in prevention and the number of geological disasters in subsequent years. The analysis is performed on historical data, using statistical methods and a LSTM recurrent neural network.

Keywords First keyword · Second keyword · Another keyword

1 Introduction

Geological disasters are ubiquitous and people awareness about them is rising. It is also thought that mutations induced by climate change are going to exacerbate geological disasters in frequency and magnitude [8]. The availability of abundant data and ability to visualize and analyze them to understand and predict disasters is changing humanitarian operations, crisis management, and investments into prevention dramatically [1]. Studies targeting the regional heterogeneity of geological disasters, evaluating risk and the relation with factors such as direct economic losses,

Authors acknowledge the financial support provided by the Research grant of Università Parthenope, DR no. 953, november 28th, 2016.

U. Fiore (✉) · Z. Marino · F. Perla · M. Pietroluongo · S. Scognamiglio · P. Zanetti
Parthenope University, Napoli, Italy
e-mail: ugo.fiore@uniparthenope.it; zelda.marino@uniparthenope.it;
francesca.perla@uniparthenope.it; mariafortuna.pietroluongo@uniparthenope.it;
salvatore.scognamiglio@uniparthenope.it; paolo.zanetti@uniparthenope.it

frequency, and cost of prevention, attract much attention. Methods from several disciplines have been applied to this problem, ranging from hydrodynamic models [10] to gray systems [13].

Prevention has many facets, including also the assessment of the extent to which hill-slope communities are prepared [3]. In this work, the relation is studied between the number of prevention projects and the number of geological disasters in subsequent years, accounting for the effect of geographical distribution. The analysis is performed on historical data provided by the Chinese Statistics Bureau. A recurrent neural network of the long short-term memory (LSTM) type has been used to forecast the number of geological disasters in China. The accuracy of predictions was measured with and without the inclusion of data relative to the number of projects of prevention.

2 LSTM

In this work, an LSTM neural network has been used. In addition, well-known statistical methods provided a verification. In recent years, neural networks (NNs) are back on the stage. New and more powerful architectures, such as recurrent neural networks (RNNs) and convolutional neural networks (CNNs), have been proposed. Their main applications include pattern recognition, image processing, anomaly detection [4], and function approximation [5].

Among RNNs, the LSTM proposed in [6] seems to be one of the most promising candidates to analyze sequential data. The traditionally RNNs gradually lose their ability to learn from the past due to the problem of the gradient vanishing. LSTM networks overcame this problem because their structure, composed by three “gates,” respectively called input, output, and forget gate and the memory cell resulting from their interaction, allow to keep the long-term information and to combine it with short-term memory. This mechanism promotes in-depth data learning and produces excellent results in terms of performance. An extensive description of NNs and back-propagation algorithm can be found in [2] and [9].

Formally, let $\{\mathbf{x}_t, y_t\}$ a sequence of training examples, with $\mathbf{x}_t \in \mathcal{X}$ and $y_t \in \mathcal{Y}$, where $\mathcal{X} \subset \mathbb{R}^d$ is the input space and $\mathcal{Y} \subset \mathbb{R}$ the output space. According to the universal approximation theorem [7], a feed-forward network can approximate any continuous functions on compact subsets; our aim is to approximate the function g that links the elements \mathcal{Y} and \mathcal{X} :

$$y_i = g(\mathbf{x}_i) \quad (1)$$

By denoting \mathbf{i} the input gate, \mathbf{o} the output gate, \mathbf{f} the forget gate, \mathbf{z} and the intermediate state, the general mode of operation of a recurrent network with LSTM architecture with $n \in \mathbb{N}$ units can be described by the following set of equations:

$$\mathbf{i}_t = \sigma(W_i \mathbf{x}_t + U_i \mathbf{h}_{t-1} + \mathbf{b}_i) \quad (2)$$

$$\mathbf{o}_t = \sigma(W_o \mathbf{x}_t + U_o \mathbf{h}_{t-1} + \mathbf{b}_o) \quad (3)$$

$$\mathbf{f}_t = \sigma(W_f \mathbf{x}_t + U_f \mathbf{h}_{t-1} + \mathbf{b}_f) \quad (4)$$

$$\mathbf{z}_t = \tanh(W_z \mathbf{x}_t + U_z \mathbf{h}_{t-1} + \mathbf{b}_z) \quad (5)$$

$$\mathbf{c}_t = \mathbf{c}_{t-1} \odot \mathbf{f}_t + \mathbf{i}_t \odot \mathbf{z}_t \quad (6)$$

$$\mathbf{h}_t = \tanh(\mathbf{c}_t) \odot \mathbf{o}_t \quad (7)$$

where \odot denotes the Hadamard product, σ the logistic sigmoid function, and, for $k = i, o, f, z$, $W_k \in \mathbb{R}^{d \times n}$ and $U_k \in \mathbb{R}^{n \times n}$ are weight matrices and $\mathbf{b}_k \in \mathbb{R}^n$ bias vectors. Weight matrices and bias vectors are adjusted to reflect the characteristics of training data through a learning algorithm. According to equation (7), the output of the LSTM network is computed by the long-term filtered information \mathbf{c}_t . The information in the memory cell \mathbf{c}_t is updated according to equation (6). Equations (2), (3), and (4) describe how the three gates work and how they control the long-term memory. The first one filters the flow of information entering the memory cell, while the second one directs the information directly to the output step. In addition, the forget gate determines which information must be retained or removed from the long-term memory.

3 Empirical Evidence

The experiments were aimed to analyze the effectiveness of prevention projects in relation to the number of geological disasters in China. In particular, we investigate the gain in terms of accuracy, in the prediction of the number of disasters, when the information concerning the projects of preventions is included.

The data source is the China Statistics Bureau (<http://www.stat.gov.cn/>) that provides the number of disasters occurred and prevention projects carried out in the country in the years between 2004 and 2017, distinguishing by region (Fig. 1). After collecting the data, a first round of data processing was carried out. The data source does not contain the observations for 2014 which, for this reason, was excluded from the analysis. Other data were missing. Since there are only 13 years of observations, the regions for which more than three values were missing were excluded. For regions with one or two missing data, the missing values were imputed with the average value between the previous and the following observation. After this preprocessing, the number of regions included in the study, initially equal to 29, was reduced to 23. In addition, the number of disasters has been transformed into a logarithmic scale. This transformation has been also confirmed by visual inspection of the log-log scatterplots of geological disasters and projects of prevention (the year before) by region, shown in Fig. 2. A log-log chart has been chosen to enhance readability. However, in the evaluation, the number of prevention projects has not been transformed in a logarithmic scale, because (i) the range of values is not as

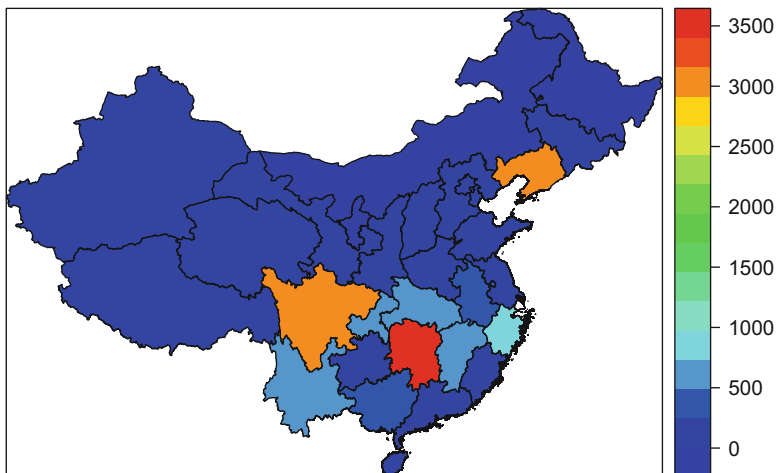


Fig. 1 Geographical distribution of geological disasters in China for the period 2004–2017

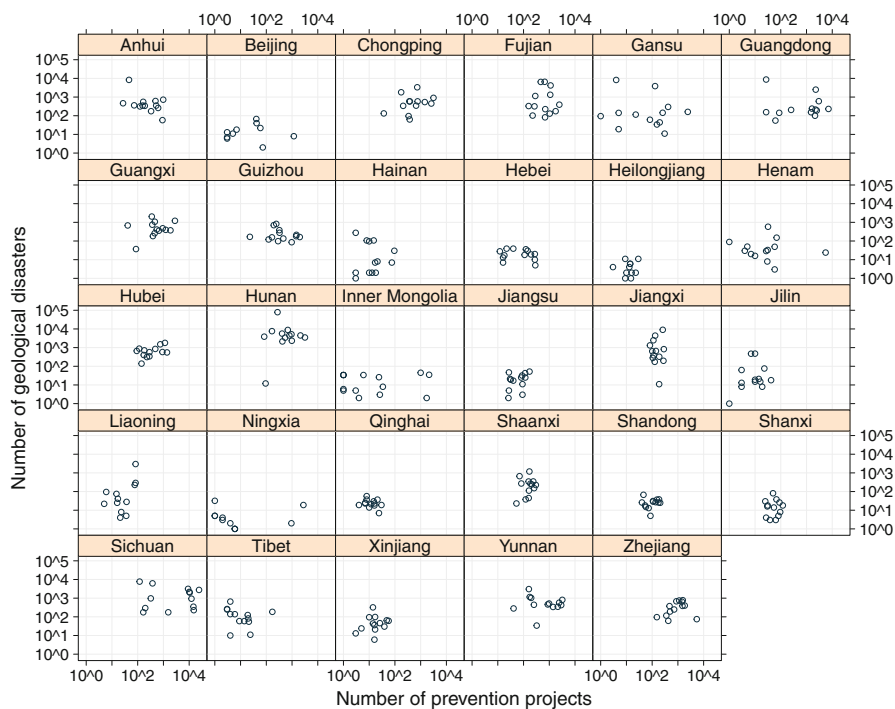


Fig. 2 Geological disasters vs. prevention projects, by region

extreme as it is the case for the number of geological disasters and (ii) the association evidenced by models is stronger when the number of prevention projects is in the original linear scale.

In order to validate the existence of a connection between the number of geological disasters and the time-lagged number of prevention projects, and to identify appropriate values for the lag, we applied statistical analysis. In the following, results of such analyses are briefly reported and then the outcomes of LSTM experiments are shown.

3.1 VAR

Since it is reasonable to think that the number of geological disasters influences and is influenced by the number of prevention projects, the vector autoregressive (VAR) [11] framework seems appealing for the analysis. In VAR models, all variables are treated symmetrically and they influence each other equally. A VAR model with lag one is specified as follows:

$$\mathbf{x}_t = \mathbf{b}_0 + \mathbf{B}_1 \mathbf{x}_{t-1} + \mathbf{u}_t \quad (8)$$

where \mathbf{x}_t is the vector of variables at time t , the components of \mathbf{u}_t are (possibly simultaneously correlated) white noise processes, and the coefficients \mathbf{B}_1 capture the influence of the lagged (at lag one) variable to itself and \mathbf{b}_0 is an intercept.

The choice of the maximum number of lags to be included is an important step in the analysis. Procedure VARselect in the var package [11] provides the best values for the maximum lag in accordance with four information criteria: Akaike information criterion (AIC), Hannan-Quinn (HQ), Schwarz criterion (SC) – more commonly known as Bayesian information criterion – and final prediction error (FPE). On the basis of that procedure, the suggested maximum lag was one, and this value has been used in the following.

VAR models were fitted for the pair (number of geological disasters, number of prevention projects) considering each region separately. Significant effects at the 5% level were found for each region. The portmanteau test did not permit to reject the null hypothesis that autocorrelations are significantly different from what would be expected from a white noise process.

3.2 Dynamical Models

We are interested in studying variation among regions and over time. Dynamical models [12] allow to estimate the size of current and future reactions of a variable \mathbf{Y} to a change in another variable \mathbf{X} . A dynamical model was fit for the number of geological disasters versus the number of prevention projects in the previous

year. The maximum lag was kept at one, as in the previous subsection. Effects were found to be highly significant ($p < 10^{-6}$). Analysis of the residuals showed that the residuals were not autocorrelated. When the region was also included, the effects were found to be highly significant for almost all regions. Again, residuals showed no autocorrelation.

3.3 LSTM

After data processing, two neural network models were calibrated: in the first one, the desired quantity y_{t+1} is the number of disasters in the next year; the predictor \mathbf{x}_t contains the number of disasters in the previous 3 years, and the region and year of interest. In the second model, the number of projects of prevention in the previous year is also included in the predictors. Hereinafter, the two models will be referred to as the “basic” and the “advanced” model.

The data are split in two parts: a training set, including the data examples before 2014, and a testing set including the observation after 2014. About the architecture, the network includes a LSTM component with 64 units to process the multivariate time series concerning the number of disasters and an additional feed-forward layer with 64 units, which further jointly processes the partial output with information relating to the region and year of interest. It is important to note that in the second model, the information concerning the projects of preventions is included in this last stage.

The results seem to show that, although the dependence between the number of geological disasters and project of prevention is very small, the use of the information concerning the project of prevention in a supervised learning model with LSTM architecture can be useful. Indeed, by introducing this additional information, the predictive power of the model increases. Table 1 shows the performances, in terms of mean absolute error (MAE), in the testing set for both models. The third column reports the ratio between the errors in the basic and advanced models. It can be seen as a gain factor in performance. It is clear that the prediction of the “advanced model” overperforms the other one in most regions. In particular, a reduction in MAE can be observed in about 70% of regions. The mean gain factor, overall, is 1.56. This evidence seems to be confirmed also by Fig. 3 that shows the residuals in the testing set for both models. In fact the residues of the advanced model seem to be closer to 0 than the others.

4 Conclusions

An LSTM recurrent neural network, a powerful and versatile tool in the analysis of time series data, can provide interesting insights when it is also coupled with a module able to handle grouping information. In this work, an LSTM has been used to assess the relationship between the number of geological disasters and the

Table 1 Mean absolute error of the two models and gain factor, by region

Region	MAE		Gain factor
	Basic model	Advanced model	
Anhui	0.9405	1.1958	0.79
Chongping	1.3894	1.2183	1.14
Fujian	1.1781	0.9725	1.21
Gansu	1.9216	0.8120	2.37
Guangdong	0.7364	0.2860	2.57
Guangxi	0.8260	0.5254	1.57
Guizhou	0.7932	0.3046	2.60
Hebei	1.0762	0.7563	1.42
Henam	0.7054	0.7905	0.89
Hubei	0.6063	0.9151	0.66
Hunan	0.3630	0.3158	1.15
Jiangsu	1.0412	1.2059	0.86
Jiangxi	0.7794	0.6102	1.28
Jilin	0.7370	0.7271	1.01
Qinghai	0.7978	0.4100	1.95
Shaanxi	1.6862	1.1783	1.43
Shandong	0.9115	0.6442	1.41
Shanxi	1.4275	1.6065	0.89
Sichuan	2.9303	2.2625	1.30
Tibet	0.9344	0.4699	1.99
Xinjiang	0.6832	1.0179	0.67
Yunnan	0.8496	0.1487	5.71
Zhejiang	0.7584	0.6898	1.10

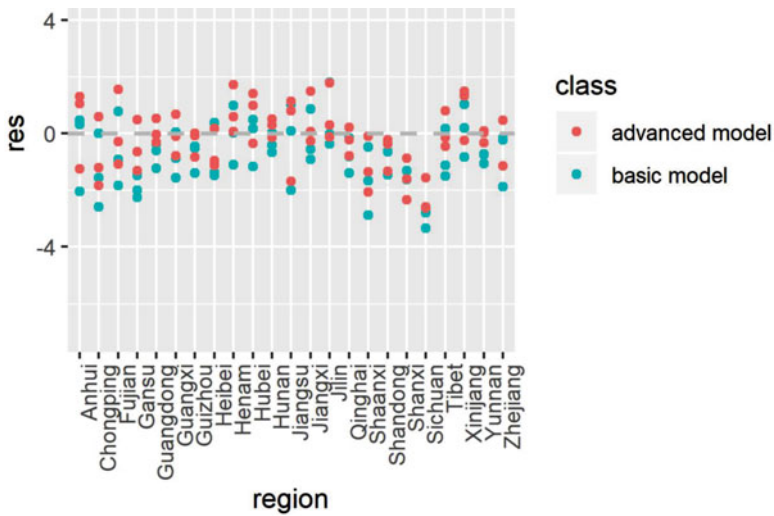


Fig. 3 Residuals of the two models in the testing set

number of prevention projects in previous years. Although discussing the results as related to the effectiveness of prevention measures goes far beyond the scope of this work, results show, in accordance with the findings of statistical methods, that it is possible to identify evidence of a connection between the prevention projects and a reduction in the number of disasters.

References

1. Akter, S., Wamba, S.F.: Big data and disaster management: a systematic review and agenda for future research. *Annals of Operations Research* pp. 1–21
2. Alpaydin, E.: *Introduction to machine learning*. MIT press (2014)
3. Chen, S.C., Ferng, J.W., Wang, Y.T., Wu, T.Y., Wang, J.J.: Assessment of disaster resilience capacity of hillslope communities with high risk for geological hazards. *Engineering geology* **98**(3-4), 86–101 (2008)
4. Fiore, U., De Santis, A., Perla, F., Zanetti, P., Palmieri, F.: Using generative adversarial networks for improving classification effectiveness in credit card fraud detection. *Information Sciences* (2017)
5. Fiore, U., Marino, Z., Passalacqua, L., Perla, F., Scognamiglio, S., Zanetti, P.: Tuning a deep learning network for solvency ii: Preliminary results. In: *Mathematical and Statistical Methods for Actuarial Sciences and Finance*, pp. 351–355. Springer (2018)
6. Hochreiter, S., Schmidhuber, J.: Long short-term memory. *Neural computation* **9**(8), 1735–1780 (1997)
7. Hornik, K., Stinchcombe, M., White, H.: Multilayer feedforward networks are universal approximators. *Neural networks* **2**(5), 359–366 (1989)
8. Huang, Y., Cheng, H.: The impact of climate change on coastal geological disasters in southeastern china. *Natural hazards* **65**(1), 377–390 (2013)
9. James, G., Witten, D., Hastie, T., Tibshirani, R.: *An introduction to statistical learning*, vol. 112. Springer (2013)
10. Li, X., Yao, J., Li, Y., Zhang, Q., Xu, C.Y.: A modeling study of the influences of yangtze river and local catchment on the development of floods in poyang lake, china. *Hydrology Research* **47**(S1), 102–119 (2016)
11. Pfaff, B.: VAR, SVAR and SVEC models: Implementation within R package vars. *Journal of Statistical Software* **27**(4) (2008), <http://www.jstatsoft.org/v27/i04/>
12. Zeileis, A.: dynlm: Dynamic Linear Regression (2019), <https://CRAN.R-project.org/package=dynlm>, r package version 0.3-6
13. Zhang, L., Li, G.j., Zhou, Z.g., WANG, Q.: Grey clustering method-based zoning assessment of regional geological disaster. *J. Nat. Disasters* **18**, 164–168 (2009)

Cyber Crises and Disaster Preparation in Austria: A Survey of Research Projects



Bernhard Garn, Klaus Kieseberg, Dominik Schreiber, and Dimitris E. Simos

Abstract In this paper, we survey some recent applied research and development projects dealing with threat analysis and disaster scenario generation, preparation, management, and training funded by the security-focused funding scheme KIRAS by the Austrian government, which include efforts for the development and execution of serious games in the respective domains. In our analysis, we found multiple lines of multiyear, multi-project activities, which consistently improve and advance the technologies and capabilities available to the affected stakeholders. Based on this review of the state of the art, we identify areas of high-potential interest to direct future applied research and development efforts.

Keywords Disaster scenario generation · Serious game · Research project survey

1 Introduction

Over the course of the last decade, various reports in the media about *cyber incidents* have alerted the public to the pivotal role that information technology is playing today, everyday, in all of our lives. These days, serious vulnerabilities in software and hardware often feature a dedicated name, logo, and explanations for the layman. Motivations behind attacks are multifaceted and can serve multiple purposes against various individuals or organizations. *Cyber security* spans all across society; individuals, businesses, and governments are all being targeted in a 24/7, highly interconnected networked world. It is noteworthy that today – among all those nefarious activities online – credit card fraud rarely makes it to the news headlines anymore or is not even mentioned anymore as a major concern explicitly. The term **comprehensive security** (*COMPRSEC*) describes the goal of permanently guaranteeing a high level of quality and security for all members of

B. Garn · K. Kieseberg · D. Schreiber · D. E. Simos (✉)

SBA Research, Vienna, Austria

e-mail: bgarn@sba-research.org; kkieseberg@sba-research.org; dschreiber@sba-research.org; dsimos@sba-research.org

© Springer Nature Switzerland AG 2021

I. S. Kotsireas et al. (eds.), *Dynamics of Disasters*, Springer Optimization and Its Applications 169, https://doi.org/10.1007/978-3-030-64973-9_7

109

society. This broad concept of security includes many domains (e.g., water, food, healthcare system), in particular the **cyber domain**. Due to the pervasiveness of today's technology, the **cyber domain** is part of or plays a part in nearly every other domain captured by *COMPRSEC*. Ergo, its *critical importance* is obvious.

To assess the research landscape in terms of activities, endeavors, and projects that have been carried out to develop, prepare, and test *civil cyber crises* operations on a national level, we survey the publicly available list of official *cyber security research projects* funded by the Austrian¹ government within the *KIRAS* funding scheme [18]. These projects showcase the synergies between academia, subject matter experts (or domain experts), and the government in applied research projects. The goals of these projects is not only to mitigate or – in the best case – prevent primary impacts but also to consider on the same level of importance secondary impacts over all different aspects of society. Several of these projects have led to simulations of disaster scenarios, with some of them being realized in the form of a serious game [54].

Contribution. In particular, this paper makes the following contributions:

- Survey-analysis of applied research projects for cyber crises and disasters within a security-focused funding scheme of the Austrian government for consortia consisting of collaborations between academia, industry, and government;
- Identification of areas and best practices for potentially promising future work for the enhancement of cyber security preparedness, resilience, and capabilities as part of *COMPRSEC*.

This paper is structured as follows. We discuss related activities in Sect. 2, both for cyber-specific serious game exercises and funding schemes. In Sect. 3, we take a look at some of the *KIRAS* research projects regarding crisis management and disaster response, which outline the current state and the direction of future research in this area. In Sect. 4, we focus our analysis on a series of projects dealing with the modeling of cyber incidents and – in particular – cyber incident scenario training exercises or simulations targeting a nationwide response. We list and comment on some of the extracted best practices in Sect. 5. Finally, with an outlook for potential promising directions future work, we conclude the paper in Sect. 6.

2 Related Activities

The importance of cyber disaster preparation and training gets more and more important, because of the ever-increasing connectivity of our world. Most countries have already witnessed that, through cyberattacks on their government or organizations, which are especially devastating if critical infrastructure is targeted. This

¹The Republic of Austria is a landlocked East Alpine country in the southern part of central Europe and a member of the European Union.

chapter presents related activities in the field of cyber disaster preparation and training from different countries, to give an overview of the state of the art.

2.1 Department of Homeland Security: Cyber Storm [27]

Cyber Storm is the name of an event, which is hosted by the Department of Homeland Security every 2 years, to exercise how to respond to cyber threats to government networks and other critical infrastructure. The scenarios are specifically crafted, so that no single organization can solve the entire situation, to promote data exchange and cooperation between participants. The last event that was held (Cyber Storm VI) brought together more than 1000 members of the private industry, government, and international partners and took place over a period of 3 days.

2.2 ENISA: Cyber Exercises [28]

ENISA is a European organization managing a wide range of exercises in the field of cyber crises management.

- **Cyber Europe:** Is an EU-level event held every 2 years, in which cyber incident and crises management exercises for both the public and private sectors from the EU and EFTA Member States are practiced. The presented incidents are inspired by real-life events and developed by European cyber security experts and involve over 1000 participants from across Europe.
- **Cyber Exercise Platform (CEP):** Is a platform to manage complex exercises and to bring closer the exercise community. It contains information about forthcoming and past exercises and an exercise playground that imitates reality.
- **Training and Exercises:** ENISA offers cyber incident training and exercises and developed a guide on planning and conducting national exercises. It also conducts surveys on global efforts on this topic.

2.3 EU Horizon [29]

EU Horizon is a research grant of the European Union with a call for proposals to enhance the resilience of our society against natural and man-made disasters, through various methods and tools. Two calls mentioning the development of scenario simulation and exercise tools are:

- Protecting the infrastructure of Europe and the people in the European smart cities.
- Security.

2.4 *European Cyber Security Organization [15]*

The European Cyber Security Organization is a fully self-financed nonprofit organization. Their goal is to develop a competitive European cyber security ecosystem, to protect the European Digital Single Market, and to provide innovative and trustworthy cyber security solutions to the public and private sector.

2.5 *EU NIS Directive [25]*

The Directive on security of network and information systems (NIS Directive) is an EU-wide legislation from 2016 that provides legal measures to enhance the overall state of cyber security in the EU. The main points that had to be passed into law by August 2018 by all European countries were:

- Member States are required to be appropriately equipped, e.g., via a Computer Security Incident Response Team (CSIRT) and a competent national NIS authority.
- Member States have to cooperate with each other by setting up a cooperation group, in order to support and facilitate strategic cooperation and the exchange of information among them. They also need to set up a CSIRT Network, for operational cooperation on specific cyber security incidents and sharing of information about risks.
- Businesses in sectors that are identified by the Member States as operators of essential services (energy, transport, water, banking, financial market infrastructures, healthcare, and digital infrastructure) have to take appropriate security measures and notify national authorities of serious incidents that get detected.

2.6 *NATO CCD CoE [3]*

The NATO Cooperative Cyber Defense Center of Excellence is a multinational and interdisciplinary cyber defense hub. They provide their members with continually improving training and exercises on the topic of cyber incident response. Some of their exercises include:

- Locked shield: a unique international cyber defense exercise offering the most complex technical live-fire challenge in the world.
- Crossed Swords: technical red teaming cyber exercise organized by the CCD-CoE since 2016.

While some of their training courses include:

- Strategic Level Training: Executive Cyber Seminar.
- Operational Level Training: Integration Cyber Considerations into Operational Planning Course, Operational Cyber Threat Intelligence Course, Critical Information Infrastructure Protection Course.
- Legal Training: International Law of Cyber Operations Course.

2.7 *CyberROAD* [13]

CyberROAD is a research project funded by the European Commission. It aims to identify the research gaps needed to enhance the security of individuals and society as a whole against forms of crime and terrorism conducted via and within cyberspace. This research addresses current technologies to some extent, but its main challenge is to anticipate tomorrow's world of interconnected living, in particular the dangers and challenges arising from the further incorporation of the digital world into our offline life.

3 General Crisis Management and Natural Disasters

The funding scheme KIRAS is focused on *security research*, whereby this expression is to be understood in the most general interpretation, taking a multidimensional, long-term, multidisciplinary, and holistic point of view. As a result, many research domains fall within this broad research program, and the list of topics of interest ranges from security and threat analysis to dedicated product developments. Critical infrastructure sectors include energy, water, and food supply; health and financial system; public safety; traffic and transportation; scientific infrastructure; and communication and information systems. The strategic goals of the KIRAS funding scheme are:

- Increase of the security and security awareness of citizens;
- Generation of required political security policy knowledge;
- Achieve a leap toward the next generation in terms of science, processes, and technology;
- Growth of national security businesses;
- Creation and expansion of excellence in the domain of *security research*.

It is important to point out that these goals are not regarded as purely technical goals, but are also considered within the context of social and humanities sciences. Hence, an additional goal is the consideration the societal impact of any aspect of *security research*.

The general problems concerning the management of critical situations as well as most aspects of natural disasters have been researched and prototypically implemented over a wide range of applied research projects in this area. These projects range from general crisis management to solutions to specific types of emergencies, for example, caused by system failures, technical defects, scarcity of vital materials, or natural disasters and cover both proactive measures like risk analysis and threat modeling and reactive measures.

In recent years, a lot of research effort has gone into the development of tools and solutions for risk assessment and risk management in critical infrastructure. The KIRAS project **MetaRisk** [20], for example, introduces a sensor-based risk analysis and management system, which, in the course of the project, is implemented in a software demonstrator [41]. Another project **Cerberus** [4] presents a novel approach to identify interdependencies potential cascading effects within a network of critical infrastructures [44].

In crisis management, effective communication and information management play an important role, and a lot of work has been conducted in ensuring and improving the distribution of information needed for a successful outcome. Here, a big challenge lies in the successful coordination of all the actors involved, especially cooperation between military and nonmilitary organizations proves often difficult, due to the different organizational structures and the use of highly specialized ICT (information and communications technology) infrastructure among armed forces [39]. The KIRAS project **INKA** [16] provides a solution for this problem, introducing an interoperability interface for authorities and organizations tasked with disaster management that supports standardized IT-supported information and communication channels. The integration of the Austrian Armed Forces in this information network helps improving the cross-organizational information exchange and aids the collaboration between civil crisis response organizations and public security organizations [33]. Assuring efficient communication between crisis management centers and the public is topic of the project **Public Warning and Alert System for Austria (PASA)** [22]. Here, the authors introduce a novel system for alerting the public via the means of different types of media [43].

Regarding disaster management, one of the biggest challenges is guaranteeing the continued supply of the area affected with goods as well as with food, power, and water. The project **Risiko- und Krisenmanagement für die Ernährungsvorsorge in Österreich (EV-A)** [23] analyzes the role of private producers and retailers in the case of disaster relief and elaborate on potential policy plans for guaranteeing food supply in Austria in case of disaster situations. Similarly, the project **Providentia** [21] provides (public) procurers with a catalog of measures which could help in ensuring the security of supply in times of crisis and natural disasters. Another project concerning the distribution of goods in disaster situations is **LMK-MUSE** [19]. Here, the authors introduce a cloud-based framework designed to help coordinate last-mile distribution of food and goods to disaster-stricken areas between multiple organizations, both private and public. A specially developed simulation and operations research toolkit allows to identify real-time schedules of relief shipments, leading to a more efficient disaster relief [26]. The toolkit also

aids decision-makers by providing a detailed overview of the situation at hand and, additionally, features an integrated agent-based simulation framework that could be used for training purposes.

4 Cyber Crises

A *cyber crisis* or a *cyber incident* belongs to the specific concept of *cyber security*, as part of the general *COMPRSEC* domain. Many different issues have also already been considered in this domain. Conducted project nearly covers the complete range of information technology that thoroughly permeates our modern society.

Activities include the behavior-based anomaly detection in cyber-physical systems [9], a study focusing on for Austria relevant stakeholders as basis for the generation of recommendations for guaranteeing cyber security in transportation systems in Austria [14]. Moreover, special attention was given to the mitigation of *social problems* in cyberspace. To this end, one goal of the project **Cyber Heroes** [12] was the specific promotion of widespread use of *counter speech*, i.e., employing targeted and selective counter messages with the goal of delegitimization of the originally problematic content online and subsequently to incite changes in the discourse norms. Furthermore, the project **(K)ein Raum** [17] aims to describe the various different forms and impacts of cyberattacks against women, who were victims of domestic abuse, often caused by ex-partners. The results of the conducted study will be used to create foundations for the demand and potential ways to support and protect affected women. To be able to illustratively quantify the prevalence of activities relevant to criminal investigations occurring in social media online, the project **Cyber Crime** [11] conducted a representative qualitative survey of Austrian social media users.

A lot of research efforts have been dedicated toward the analysis of cyber crises, responses and preparatory measures as well as the generation of training scenarios in the form of serious games with corresponding interactive simulation environments (i.e., game play infrastructure).

In 2012, the **Computer Emergency Response Team Kommunikations-Modell (CERT-Komm)** [5] project was started. It is the first project in a planned series of projects funded by the Austrian government, to analyze the current state of the art of communication between CERTs and their partners, together with their requirements and problems. Since CERTs have to react to various kinds of emergencies, affecting different kinds of industry sectors and companies, reliable and easy-to-use communication systems are of paramount importance. The results of their findings were used as a basis for follow-up projects.

Two years later in 2014, the **Computer Emergency Response Team Kommunikations-Modell II (CERT-Komm II)** [6] project began, which is the follow-up project of **CERT-Komm**. The results from the studies conducted during the first project were used to create communication models for CERTs and their partners, to efficiently persist and exchange information among each other. This collectively

managed information can then be used to detect or defend against cyber threats easier. For implementation of the communication models developed in this project, another follow-up project was planned [34, 35].

Starting in 2010, the goal of the project **Cyber Attack Information System (CAIS)** [2] was to develop two tools as foundational basis for a comprehensive cyber attack information system for the analysis and assessment of cyber attacks. The focus was on the development of a framework incorporating modeling, analysis, and simulation capabilities for IT infrastructure and – in particular – their interdependencies. This framework was designed to be able to quickly identify problems and to subsequently immediately simulate threats as guidance for the development of counter measures. In addition, another tool was developed with the capabilities for analysis and assessment of current attacks and anomalies based on multiple data sources [50, 51, 37, 38].

One year later, in 2011, the project **SCUDO** [24] started, which had the goal of testing an optimized emergency response training process, which had been specifically adapted to the requirements of Austrian businesses and to derive recommendations based upon it. Additionally, an evaluation of international standards regarding their applicability in Austria was conducted. Several emergency training scenarios were developed with project partners, which were subsequently executed with company partners representing critical infrastructures [36].

In 2012, the growing interdependencies between networks and the use of standard ICT products resulted in a increasing number of cyber security issues in critical infrastructures. In order to improve the resilience of critical systems against cyber attacks, the KIRAS project **Cyber Incident Information Sharing (CIIS)** [7] has been introduced. Its aim was the development of mechanisms used to analyze information about activities and attacks in ICT networks belonging to critical infrastructures, as well as the development of methods and technologies for the exchange of information regarding cyber-incidents across organizational borders [31, 47, 48, 32, 53, 55, 45].

Based upon a consistent fusion of existing research activities [42], the **Cyber Incident Situational Awareness (CISA)** [8] project started in 2014 to develop a process to establish cyber situational awareness as a scientifically sound concept. It was recognized that solutions – at the operational and technical level – already existed for collecting and aggregating of information concerning cyber threats, as well as for the strategic level existing research had already dealt with the assessment and subsequent handling of cyber threats based upon cyber situational awareness pictures [53]. However, it turned out that there was a knowledge gap concerning how – specifically – the technical information should be processed, presented, and integrated into the cyber situational awareness picture. Therefore, one goal of the **CISA** project was to develop a holistic definition of the expression of *cyber situational awareness* for both a military and a civilian perspective. Moreover, the involvement of legal experts will ensure a legislative view on all considered concepts and the specific demonstrators. Particular attention was given to legal implications and regulations, including issues of data protection, privacy, and liability [40].

Widespread reports about security incidents in 2016 exemplified the complexity of occurring cyber attacks (e.g., phishing, ransomware, DDoS, etc.). These events suggest that a nationwide cyber incident targeting some aspects or functionality of critical infrastructure is only a matter of time. Simultaneously, calls to enhance the cyber resilience via real-time security training simulations are being issued from various sources, including the EU NIS Directive or ENISA cyber Europe. Based on these observations, starting in 2017, the **Austrian Cyber Crises Support Activities (ACCSA) [1]** project prepared for cyber crises with comprehensive training, exercise, and evaluation concepts for all stakeholders in the cyber crisis management, thereby reducing response times and error rates in the event of a real cyber crisis [52]. The envisioned concepts, processes, and methods were supported by the implementation of an accompanying software toolbox [30]. This system for software-supported training and exercise spans over several communication levels (e.g., engineering, management, first responders, policy makers) [46, 49]. In addition, the project team included legal experts to examine and evaluate the options and actions developed or proposed in complex nationwide cyber incident scenarios and to assess whether the taken decisions actually also comply with the applicable legal framework (e.g., NIS Directive, GDPR, etc.).

Continuing the successful line of work regarding cyber security incident training and simulation, starting in 2019, the **Cyber security exercise concept and framework (CURSOR) [10]** project aims for the conception of a national cyber exercise program and their analysis. A cyber exercise platform will be specified, and a proof-of-concept exercise calendar will be implemented. The **CURSOR** project will develop a nationwide exercise program, taking into account nationwide and sector-specific program exercises. The integrative design of the exercise platform will enable the measurement and comparison of different exercises. The envisioned results of this project are expected to strengthen the strategic coordination of cyber exercises and, consequently, increase Austria's resilience against the potentially serious impacts of cyber attacks on critical infrastructures.

5 Findings & Insights

In this section, we formulate several goals as general outline for future projects and activities addressing cyber disasters. These insights are based upon the observations that have arisen as part of our survey.

Repetition: A recurrently carried out training exercise and a carefully planned evaluation of the prepared response plans is crucial to guarantee its functionality when needed.

Diversification: A diverse group of participants (regarding background, qualifications, and skills) in training exercises leads to a more representative and accurate depiction of real-life emergency cases. Including experts from multiple organizations and different business sectors will also improve

cooperation and information sharing skills. Only through cooperation of experts from different sectors can effective, technically sound, useful, and lawfully solutions be newly found in emergency situations or selected from an already available, agreed-upon, accepted, ex-ante generated list.

Level of detail: It is necessary to consider scenarios at different levels of abstraction. Although many actions on the lowest level are direct consequences of higher-level decisions, one should always be aware that ultimately actions at the lowest level have to be *performed*, which requires – at least – the formal legal authority to execute them. Even if higher-level policies are legally sound, this does not necessarily mean that all derived actions (independent of their level in the “chain of command”) inherit this justification. A failure at the lowest level should also be treated as such.

Scale and scope: Training exercises should increase in scale and scope, both in terms of participants and training scenarios, to deal with the difficulties of information exchange and the always increasing connectivity and complexity of the world.

Continuing evaluation: Training courses, scenarios, and exercises should regularly be re-evaluated to take new technologies, infrastructure, and other developments into account.

Abstract modelings: Make use of well-established modeling and formalization methods for scenario generation. Build abstract models, and use mathematical and statistical approaches both for the generation and the evaluation of results.

Automation: Automation of scenario generation and exercise environment reduces time and cost.

6 Conclusion

In this work, we surveyed some of the applied research projects carried out within the KIRAS funding scheme in Austria dealing with the preparation for cyber crises and disasters on a national level in Austria. In our analysis, we paid particular attention to disaster simulation and training efforts, as well as to the development and usage of serious games within these projects.

A key finding is that some projects together form a coherent timeline resulting in an incremental increase of knowledge via building on top of each other in terms of achieved research results, insights, and produced software artifacts.

While generally a lot has been done so far, based on the results of our conducted analysis surveying these projects, we have identified potential areas of interest to focus future efforts on, which could benefit from more research, planning, and field testing to ensure the optimal preparedness of all stakeholders involved for a better, more resilient, and safer Austria in the future.

Acknowledgments SBA Research (SBA-K1) is a COMET Center within the framework of COMET – Competence Centers for Excellent Technologies Program – and funded by BMK, BMDW, and the federal state of Vienna. The COMET Program is managed by FFG.

References

1. ACCSA. <https://www.kiras.at/gefoerderte-projekte/detail/d/accsa-austrian-cyber-crises-support-activities/>. Accessed: 2020-09-22.
2. CAIS. <https://www.kiras.at/gefoerderte-projekte/detail/d/cais-cyber-attack-information-system/>. Accessed: 2020-09-23.
3. CCDCOE - The NATO Cooperative Cyber Defence Centre of Excellence is a multinational and interdisciplinary hub of cyber defence expertise. <https://ccdcoe.org/>. Accessed: 2020-09-22.
4. Cerberus. <https://www.kiras.at/gefoerderte-projekte/detail/d/cerberus/>. Accessed: 2020-09-23.
5. CERT-Komm. <https://www.kiras.at/gefoerderte-projekte/detail/d/cert-komm/>. Accessed: 2020-09-23.
6. CERT-Komm II. <https://www.kiras.at/gefoerderte-projekte/detail/d/cert-komm-ii/>. Accessed: 2020-09-23.
7. CIIS. <https://www.kiras.at/gefoerderte-projekte/detail/d/ciis-cyber-incident-information-sharing/>. Accessed: 2020-09-22.
8. CISA. <https://www.kiras.at/gefoerderte-projekte/detail/d/cisa-cyber-incident-situational-awareness/>. Accessed: 2020-09-22.
9. CPS-Security. <https://www.kiras.at/gefoerderte-projekte/detail/d/cps-security/>. Accessed: 2020-09-22.
10. CURSOR. <https://www.kiras.at/en/financed-proposals/detail/d/cursor-cyber-security-exercise-concept-and-framework/>. Accessed: 2020-09-22.
11. Cyber Crime. <https://www.kiras.at/gefoerderte-projekte/detail/d/cyber-crime/>. Accessed: 2020-09-22.
12. Cyber Heroes. <https://www.kiras.at/gefoerderte-projekte/detail/d/cyber-heroes/>. Accessed: 2020-09-22.
13. CyberRoad: Home. <http://www.cyberroad-project.eu/>. Accessed: 2020-09-22.
14. CybSiVerkehr. <https://www.kiras.at/gefoerderte-projekte/detail/d/cybsiverkehr/>. Accessed: 2020-09-22.
15. ECSO - European Cyber Security Organisation. <https://www.ecs-org.eu/>. Accessed: 2020-09-22.
16. INKA. <https://www.kiras.at/gefoerderte-projekte/detail/d/inka/>. Accessed: 2020-09-23.
17. (K)ein Raum. <https://www.kiras.at/gefoerderte-projekte/detail/d/kein-raum-cyber-gewalt-gegen-frauen-in-ex-beziehungen/>. Accessed: 2020-09-22.
18. KIRAS - Security Research. <https://www.kiras.at/en/home/>. Accessed: 2020-09-22.
19. LMK-MUSE. <https://www.kiras.at/gefoerderte-projekte/detail/d/lmk-muse/>. Accessed: 2020-09-22.
20. MetaRisk. <https://www.kiras.at/gefoerderte-projekte/detail/d/metarisk/>. Accessed: 2020-09-23.
21. Providentia. <https://www.kiras.at/gefoerderte-projekte/detail/d/providentia-erhoehung-des-sicherheitsniveaus-oesterreichs-durch-sichere-beschaffung/>. Accessed: 2020-09-23.
22. Public Warning and Alert System for Austria. <https://www.kiras.at/gefoerderte-projekte/detail/d/pasa/>. Accessed: 2020-09-22.
23. Risiko- und Krisenmanagement für die Ernährungsvorsorge in Österreich. <https://www.kiras.at/gefoerderte-projekte/detail/d/risiko-und-krisismanagement-fuer-die-ernaehrungsvorsorge-in-oesterreich-ev-a/>. Accessed: 2020-09-22.
24. SCUDO. <https://www.kiras.at/gefoerderte-projekte/detail/d/scudo/>. Accessed: 2020-09-22.

25. The Directive on security of network and information systems (NIS Directive) | Shaping Europe's digital future. <https://ec.europa.eu/digital-single-market/en/network-and-information-security-nis-directive>. Accessed: 2020-09-22.
26. Romana Berariu, Christian Fikar, Manfred Gronalt, and Patrick Hirsch. Understanding the impact of cascade effects of natural disasters on disaster relief operations. *International Journal of Disaster Risk Reduction*, 12:350 – 356, 2015.
27. Cybersecurity & Infrastructure Security Agency, Department of Homeland Security, The White House. Cyber Storm. <https://www.cisa.gov/cyber-storm-securing-cyber-space>. Accessed: 2020-09-22.
28. ENISA. Cyber Exercises. <https://www.enisa.europa.eu/topics/cyber-exercises>. Accessed: 2020-09-22.
29. EU. Secure societies – Protecting freedom and security of Europe and its citizens. <https://ec.europa.eu/programmes/horizon2020/en/h2020-section/secure-societies-%E2%80%93-protecting-freedom-and-security-europe-and-its-citizens>. Accessed: 2020-09-22.
30. M. Frank, M. Leitner, and T. Pahi. Design considerations for cyber security testbeds: A case study on a cyber security testbed for education. In *2017 IEEE 15th Intl Conf on Dependable, Autonomic and Secure Computing, 15th Intl Conf on Pervasive Intelligence and Computing, 3rd Intl Conf on Big Data Intelligence and Computing and Cyber Science and Technology Congress (DASC/PiCom/DataCom/CyberSciTech)*, pages 38–46, 2017.
31. Ivo Friedberg, Florian Skopik, and Roman Fiedler. Cyber situational awareness through network anomaly detection: state of the art and new approaches. *e & i Elektrotechnik und Informationstechnik*, 132(2):101–105, 2015.
32. Ivo Friedberg, Florian Skopik, Giuseppe Settanni, and Roman Fiedler. Combating advanced persistent threats: From network event correlation to incident detection. *Computers & Security*, 48:35–57, 2015.
33. Ivan Gojmerac, Christoph Ruggenthaler, Maria Egly, Wolfgang Vorraber, Julia Brugger, Helmut Aschbacher, Katrin Panzenbock, and Markus Christian. Advanced information systems for enhanced civil-military interoperability in austria. pages 1–8, 12 2016.
34. Otto Hellwig, Gerald Quirchmayr, Edith Huber, Timo Mischitz, and Markus Huber. Towards a cert-communication model as basis to software assurance. In *2015 10th International Conference on Availability, Reliability and Security*, pages 481–485. IEEE, 2015.
35. Edith Huber. *Sicherheit in Cyber-Netzwerken: Computer Emergency Response Teams und ihre Kommunikation*. Springer-Verlag, 2015.
36. Peter Kieseberg. Research and innovation. *Augmented Reality*, page 28.
37. Helmut Leopold. Cyber situational awareness. *e & i Elektrotechnik und Informationstechnik*, 132(2):97–100, 2015.
38. Helmut Leopold, Florian Skopik, Thomas Bleier, Josef Schröfl, Mike Fandler, Roland Ledinger, and Timo Mischitz. Einleitung zum cyber attack information system. In *Cyber Attack Information System*, pages 1–12. Springer, 2015.
39. G. Lichtenegger, W. Vorraber, I. Gojmerac, A. Sporer, J. Brugger, E. Exner, H. Aschbacher, M. Christian, and S. Voessner. Identification of information gaps in civil-military cooperation in disaster management. In *2015 2nd International Conference on Information and Communication Technologies for Disaster Management (ICT-DM)*, pages 122–129, 2015.
40. Bernd Malle, Peter Kieseberg, Edgar Weippl, and Andreas Holzinger. The right to be forgotten: Towards machine learning on perturbed knowledge bases. In *Availability, Reliability, and Security in Information Systems*, 2016.
41. Christian Meurers, Johannes Göllner, Stefan Schauer, Stefan Schiebeck, Andreas Peer, and Martin Stierle. Meta risk model for critical infrastructures. In *European Meetings on Cybernetics and Systems Research 2014*, pages 616–621, 2014.
42. Timea Pahi, Maria Leitner, and Florian Skopik. Analysis and assessment of situational awareness models for national cyber security centers. pages 334–345, 01 2017.
43. A. Preinerstorfer, M. Egly, I. Gojmerac, C. Hochwarter, C. Schuster, and R. Stocker. Requirements for the next generation public warning and alert system for austria. In *2017 14th International Conference on Telecommunications (ConTEL)*, pages 115–122, 2017.

44. S. Schauer, S. Rass, S. König, Thomas Grafenauer, and Martin Latzenhofer. Analyzing cascading effects among critical infrastructures. In *ISCRAM*, 2018.
45. Giuseppe Settanni., Florian Skopik., Yegor Shovgenya., and Roman Fiedler. A collaborative analysis system for cross-organization cyber incident handling. In *Proceedings of the 2nd International Conference on Information Systems Security and Privacy - Volume 1: ICISSP*, pages 105–116. INSTICC, SciTePress, 2016.
46. F. Skopik and S. Filip. Design principles for national cyber security sensor networks: Lessons learned from small-scale demonstrators. In *2019 International Conference on Cyber Security and Protection of Digital Services (Cyber Security)*, pages 1–8, 2019.
47. F. Skopik, G. Settanni, R. Fiedler, and I. Friedberg. Semi-synthetic data set generation for security software evaluation. In *2014 Twelfth Annual International Conference on Privacy, Security and Trust*, pages 156–163, 2014.
48. F. Skopik, M. Wurzenberger, G. Settanni, and R. Fiedler. Establishing national cyber situational awareness through incident information clustering. In *2015 International Conference on Cyber Situational Awareness, Data Analytics and Assessment (CyberSA)*, pages 1–8, 2015.
49. Florian Skopik. The limitations of national cyber security sensor networks debunked: Why the human factor matters. In *ICCWS 2019 14th International Conference on Cyber Warfare and Security: ICCWS 2019*, page 405. Academic Conferences and publishing limited, 2019.
50. Florian Skopik, Thomas Bleier, and Roman Fiedler. Information management and sharing for national cyber situational awareness. In *ISSE 2012 Securing Electronic Business Processes*, pages 217–227. Springer, 2012.
51. Florian Skopik, Roman Fiedler, and Otmar Lendl. Cyber attack information sharing. *Datenschutz und Datensicherheit-DuD*, 38(4):251–256, 2014.
52. Florian Skopik, Tímea Páhi, and Maria Leitner. *Cyber Situational Awareness in Public-Private-Partnerships*. Springer.
53. Florian Skopik, Giuseppe Settanni, and Roman Fiedler. A problem shared is a problem halved: A survey on the dimensions of collective cyber security defense through security information sharing. *Computers & Security*, 60:154–176, 2016.
54. Aleksandra Solinska-Nowak, Piotr Magnuszewski, Margot Curl, Adam French, Adriana Keating, Junko Mochizuki, Wei Liu, Reinhard Mechler, Michalina Kulakowska, and Lukasz Jarzabek. An overview of serious games for disaster risk management – prospects and limitations for informing actions to arrest increasing risk. *International Journal of Disaster Risk Reduction*, 31:1013 – 1029, 2018.
55. M. Wurzenberger, F. Skopik, G. Settanni, and R. Fiedler. Beyond gut instincts: Understanding, rating and comparing self-learning idss. In *2015 International Conference on Cyber Situational Awareness, Data Analytics and Assessment (CyberSA)*, pages 1–1, 2015.

Disaster Preparedness at the Municipality Level: A Scenario-Based Multistage Measurement Methodology



Mehdi Ghazanfari, Mohammadmehdi Hakimifar, Tina Wakolbinger,
and Fuminori Toyasaki

Abstract This study aims to develop a methodology in the disaster management field to assist policy-makers in the evaluation of the state of disaster preparedness of a municipality considering possible disaster types and corresponding scenarios. The paper first provides an overview of selected past disaster preparedness studies and identifies the main dimensions of preparedness. Then, it integrates them into a comprehensive framework for disaster preparedness measurement. The framework considers multistage aspects of disaster preparedness by integrating the pre- and post-disaster status. Preparedness at the municipality level is evaluated with respect to the following four areas: hazard assessment, mitigation capabilities, resource preparedness, and management performance. Implementing the methodology can provide insights to governments concerning their level of disaster preparedness. By highlighting areas of weakness, it can contribute to strengthening their readiness.

Keywords Disaster preparedness · Multistage measurement · Municipality preparedness

M. Ghazanfari

Department of Industrial Engineering, Iran University of Science and Technology, Tehran, Iran
e-mail: mehdi@iust.ac.ir

M. Hakimifar · T. Wakolbinger (✉)

Institute for Transport and Logistics Management, WU (Vienna University of Economics and Business), Vienna, Austria

e-mail: mohammad.mehdi.hakimifar@wu.ac.at; tina.wakolbinger@wu.ac.at

F. Toyasaki

School of Administrative Studies, York University, Toronto, ON, Canada

e-mail: toyasaki@yorku.ca

© Springer Nature Switzerland AG 2021

I. S. Kotsireas et al. (eds.), *Dynamics of Disasters*, Springer Optimization and Its Applications 169, https://doi.org/10.1007/978-3-030-64973-9_8

1 Introduction

Governments and policy-makers try to develop and implement strategies and measures to prepare their societies for the effects of extreme natural events [32]. They spend significant amounts of money in an effort to achieve better preparedness. They need ways to assess preparedness proactively so that they know what they can expect when a disaster strikes.

Different models are presented in literature to measure disaster preparedness, which mostly consider a specific part of preparedness, e.g., social, technical, and infrastructural. A more comprehensive framework that is capable of looking at disaster preparedness from a pre- and post-disaster point of view is still lacking. The main motivation of this study is to develop a comprehensive methodology in the disaster management field to assist municipalities and related policy-makers in the evaluation of the state of disaster preparedness and to identify opportunities for improvements. The preparedness measurement framework covers multiple dimensions including risk identification, infrastructure, logistical and management resources, and capabilities. These dimensions are extracted from and inspired by various preparedness models that are presented in literature. The main characteristics of the framework are as follows:

Municipality as unit of analysis: Our research focuses on preparedness operations at the municipality level. In disaster management, a municipality (or local government) is expected to communicate with affected persons directly, coordinate relief operations, and function as an interface between affected persons and other external parties, for example, other affected local governments, the central government, and aid agencies [49]. To this end, for example, the Disaster Countermeasures Basic Act (DCBA) in Japan requires municipalities to plan and implement their own disaster preparedness operations. After the Great East Japan Earthquake in 2011, local governments recognized that sharing information on their disaster preparedness and response capacities prior to a disaster is important for effective relief operations [8]. In the USA, each county has its own emergency preparedness and response policies and procedures; however, Hurricane Katrina in Louisiana revealed that the disaster response plans that were in place did not interface effectively with each other [35]. Our comprehensive proposed framework would contribute to facilitating an interface between municipalities' disaster preparedness and response plans. Our framework focuses on large-scale urban areas where the municipalities are the main policy-makers regarding disaster preparedness.

Scenario-based and disaster-specific approach: A municipality should be prepared to react to different possible disaster scenarios. Conceivable impacts of a disaster on a municipality vary depending on possible disaster types and/or severity of the disaster. Many resilience assessment methodologies which attempt to be "multi-hazard," "all-hazard," or "disaster-independent" consider general organizational capabilities to respond to any crisis. This paper evaluates preparedness relative to the occurrence of specific disasters. It, therefore, builds

a scenario-based approach as the required resources are critically dependent on the occurrence of a disaster. The scenario sets describe impacts of large natural disasters on a municipality. They also provide a basis for further work to devise strategies for reducing disaster impacts [19].

Integration of risk assessment into preparedness measurement: Risk assessment aims to identify risks and potential threats that may affect the community. The scenario-based approach allows us to integrate well-developed research results on risk assessment into preparedness measurements. Using the scenario-based approach, we develop a multistage disaster preparedness measurement methodology that combines elements from the well-developed field of risk assessment [47, 48] with elements from preparedness assessment. This integration enables policy-makers to pursue the disaster preparedness measurement process in a systematic manner from the initial stage to the final assessment.

Pre- and post-disaster analysis: Many previous studies only measure predefined metrics before the occurrence of a disaster [2, 22, 45] and do not consider the post-disaster situation. Our scenario-based approach allows us to also consider the post-disaster situation. The model can differentiate between pre-disaster resources and resources that are available after a disaster occurs. This is of critical importance as the repositioned resources might be affected by the disaster itself.

Focus on preparedness phase: The methodology that we propose measures the short-term municipality-level readiness to respond to a disaster and considers the activities within the first 72 h after a disaster strikes. Focusing on response capabilities enables us to conduct a detailed analysis and gain comprehensive insights at the municipality level. The response capabilities are crucially dependent on the type of disaster that occurs; hence, our scenario-based approach is a good fit in this context. Hemond and Robert [28] propose to extend the concept of preparedness to resilience. Resilience measurements seek to encompass development capabilities. Our methodology covers short-term activities and does not consider its recovery capabilities. However, it could become the basis for an extended model that also encompasses the development perspective.

The paper is structured as follows: Section 2 reviews existing disaster preparedness measurement models. In Sect. 3 the proposed model including its dimensions and components is explained. Conclusions and future research directions are presented in Sect. 4.

2 Literature Review

Different models are presented in literature to measure disaster preparedness, each of which looks at the problem from a different perspective, e.g., social, technical, and infrastructural. We provide an overview of selected approaches.

Some authors and associations such Red Cross/Crescent Societies provide a list of important elements as preparedness guidelines or checklists [31]. The Federal Emergency Management Agency (FEMA) provides a guideline entitled “Are You

Ready?” including checklists for citizens and organizations [24]. The State and Local Guide (SLG-101) published by FEMA [23] includes standard operating procedures and checklists. The American Health Lawyers Association provides emergency preparedness, response, and recovery checklists (Beyond the Emergency Management Plan) [7]. The World Health Organization Regional Office for Europe [53] published the emergency response checklist for hospital administrators and emergency managers. The City of Houston Office of Emergency Management [48] provides guidelines and checklists for emergencies for households and businesses.

The abovementioned guidelines and checklist-based models focus mostly on individual and business preparedness. The main goal of this group of studies is to teach people how to protect themselves and their families against different types of hazards. Although these checklists provide a good reference for disaster preparedness, they do not include a comprehensive analysis regarding potential hazards and usually they do not consider socioeconomic parameters.

Comprehensive Preparedness Guide (CPG) 201, Third Edition [25], provides a guideline for communities to evaluate their level of preparedness, to identify and assess risks, and to estimate capability requirements [25]. The Capability Assessment for Readiness (CAR) is a self-report data collection system to measure state-level capabilities. It was developed by FEMA and the National Emergency Management Association (NEMA) and identifies 13 elements that should be addressed by states in their preparedness efforts [45]. Simpson [45] develops a multidimensional disaster preparedness measurement methodology, which considers a number of indicators to measure a community’s preparedness level and applies the weighted sum approach to yield the preparedness measurement. Using this model, the author compares the preparedness level of Sikeston, Missouri, and Carbondale, Illinois.

Alexander [4] proposes a methodology for assessing and characterizing the state of development of a civil emergency preparedness system. This paper provides the main elements of a preparedness system and provides a group of indicators to evaluate each component. In order to illustrate the methodology, a case study is presented from the town Teziutlán in Mexico. This paper suggests using a scale that extends from 0 (nonexistent) to 5 (absolute excellence) and uses an average of the scores of indicators to measure the final preparedness level. *Scandinavian Journal of Public Health* [40] provides a framework called “Preparedness process” for the development, implementation, and evaluation of the level of preparedness of the public health and medical care against disasters. This paper analyzes the preparedness level through 16 steps [40]. As measurement methodology, it presents a scaling system from 0 to 7 (0 indicates total absence or extremely low function) to compare pre-disaster and post-disaster situations.

Some other studies focus on the concept of resilience to measure communities’ preparedness. The resilience measurement approach aims to strengthen communities to cope with the risks resulting from natural disasters [3, 6, 28]. Decisions about which dimensions to include are somewhat subjective [15]. Winderl [52] conducted a review on different measurement frameworks for disaster resilience. According to this study, some measurements focus on a limited number of dimensions typically the case for measurements designed by specialized organizations with a

specific interest in a certain aspect of resilience such as climate change resilience [52]. However, other measurements provide a broader set of dimensions including measurement dimensions such as physical, human, social, political, institutional, technical, economical, food and nutrition, poverty, environmental, and ecological [26, 52]. We present some of the measurements which are close to our work in terms of having a multidimensional view and a similar unit of analysis (please refer to [52] for more resilience measurements models).

The Prevalent Vulnerability Index consists of a set of indicators that characterize prevailing vulnerability conditions reflected in exposure in disaster-prone areas. These indicators aim to measure direct (exposure and susceptibility), as well as indirect and intangible (socioeconomic fragility and lack of resilience), impacts of hazard events [9, 10 52]. The PEOPLES resilience framework is a methodology to assess, monitor, and model a community's disaster resilience [42]. This framework consists of seven general and quantitative dimensions that characterize community functionality [42]. Similarly, the Community Based Resilience Analysis (CoBRA) is a quantitative methodology for measuring and assessing the impact of community resilience [50]. This framework is based on a composite measure of five components of resilience measurement, namely, human, natural, financial, social, and physical [50]. Cutter et al. [2, 17] identified the main dimensions to measure a community's resilience, including social, economic, housing and infrastructure, institutional, community, and environmental.

3 The Proposed Framework and Model

A disaster preparedness measurement framework should consider all elements of disaster preparedness in a systematic manner. For each dimension, the appropriate components, aspects, and indicators have to be addressed. Our proposed framework consists of three phases that need to be considered sequentially. These are identified as follows: phase (I) Pre-Disaster Study, phase (II) Post-Disaster Prediction, and phase (III) Preparedness Assessments. Each phase consists of stages which are processes for data gathering and analyzing the results. Figure 1 represents the phases and stages of the proposed framework.

Phase (I) of the proposed framework, as shown in Fig. 1, has two different stages. The first one is Hazard Knowledge. This stage evaluates how well the possible risks are studied and analyzed. This stage provides useful information regarding the different scenarios of tentative disasters that may occur. The second stage is Initial Status of People and Properties which provides facts and statistics related to the current situation of people, infrastructure, administrative offices, utilities, and other facilities within the municipality under risk of a disaster.

Phase (II) of the framework, Post-disaster Prediction, consists of three different stages, Affected Status of People and Properties, Required Resources, and Available Resources. In the Affected Status stage, we need to estimate the effect of a disaster on people, facilities, and infrastructures. This stage needs to be repeated for each scenario separately. The next stage in phase (II) is Required Resources.

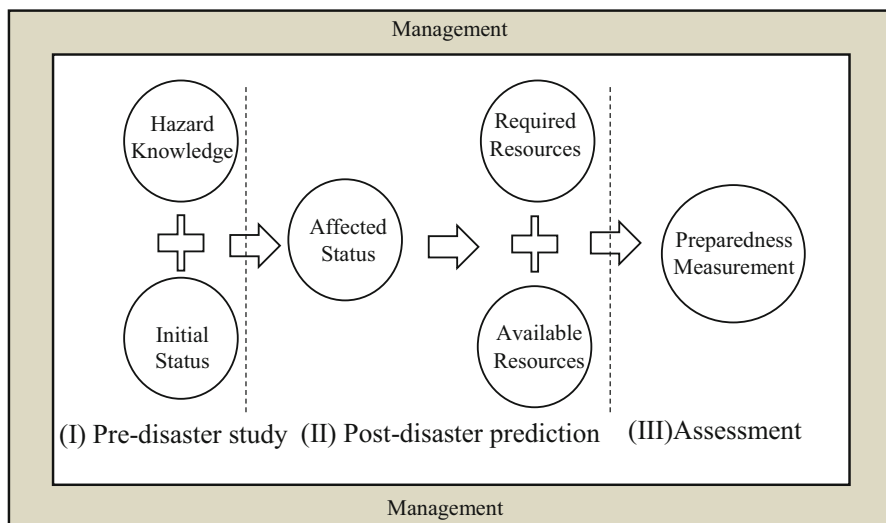


Fig. 1 The phases and stages of the proposed framework

The requirements can be determined by using a demand-supply matrix. The last stage in phase (II) is to identify the Available Resources. By Available Resources we mean all resources that have remained useful immediately after a disaster happened. Phase (III) of the framework determines the preparedness of a municipality. Efficient management is very important for the success of disaster management. As depicted in Fig. 1, efficient management is necessary for all phases of the proposed framework and is interconnecting the three phases. In the next sections, the different phases of the framework are explained in detail. For each stage, the essential class of dimensions are specified and for each dimension the components are determined.

3.1 Phase (I): Pre-disaster Study

Two stages are included in phase (I), Hazard Knowledge and Initial Status of People and Properties.

3.1.1 Hazard Knowledge

As shown in Table 1 the Hazard Knowledge stage itself has three dimensions:

- Hazard (risk) identification
- Hazard (risk) analysis and assessment
- Hazard (risk) awareness

Table 1 The dimensions and components of Hazard Knowledge Assessment

Phase	Stage	Dimensions	Components	References
(I) Pre-disaster Study	Hazard Knowledge Assessment	Hazard risk identification	Data gathering plans for hazard detection	[21, 22, 38, 47, 51]
			Data gathering tools	
			Storage and access to historical data	
		Hazard risk analysis and assessment	Hazard assessment methodologies	[11, 22, 23, 34, 51]
			Hazard maps	
		Hazard awareness	Scenario planning (predictions of occurrences)	[18, 22, 27]
Cooperation plans for public awareness and warning				

Risk identification is the first stage of risk management [47]. By hazard identification we mean data gathering plans and data gathering tools for hazard detection. This dimension uses historic data to assess the potential risk of a specific municipality.

The second dimension, hazard risk analysis and assessment, refers to methodologies and software applications to determine the nature and extent of risk by analyzing potential hazards and provide hazard maps which show the technical characteristics of hazards such as their location, intensity, frequency, and probability.

The third dimension, hazard awareness, covers scenario planning and dissemination of the results of risk analysis to governments, related organizations, and the media. By scenario planning we mean estimating the possible severities for a hazard to occur in a predetermined place. Public awareness plays a significant role in disaster risk reduction. While providing hazard maps and planning the scenarios, the potential hazards of neighboring municipalities and/or municipalities with which there is some level of interaction are also taken into account.

3.1.2 Initial Status of People and Properties

The second stage within phase (I) is Initial Status of People and Properties. As depicted in Table 2, this stage has nine dimensions: people, residential buildings, utilities, transportation, health services, government, business, sensitive facilities, and dedicated relief inventory.

In order to measure each dimension and related component, we can further break each component down to some aspects and similarly each aspect to some indicators.

Table 2 The dimensions and components of Initial Status of People and Properties

Phase	Stage	Dimensions	Components	References
(I) Pre-disaster study	Initial status	People	Total population	[42, 50]
			Demographic groups	
		Residential buildings	Physical characteristics of buildings	[1, 16, 34, 39]
			Ownership and funding situation	
		Utilities	Gas supply	[34, 42, 45]
			Water supply	
			Electricity supply	
			Telecommunication system	
			Sewage system	
		Transportation	Roads and railways	[20, 30, 34, 42]
			Land, air, and water vehicles	
			Airports and ports	
		Health services	Medical staff	[29, 37]
			Hospitals and medical centers	
			Medical devices and medicines	
		Government	Municipalities	[22, 42, 45]
			Governmental institutions	
			Public safety organizations	
		Business	Plants	[12, 33, 42, 44]
			Financial institutions and shopping centers	
			Warehouses and logistic services	
		Sensitive facilities	Crisis management rooms	[30, 34]
			Explosion potential	
			IT and ICT	
Dedicated relief inventory	Volume and quantity of relief inventories	[5, 43]		
	Location of warehouses			
	Safety of (building) warehouses			

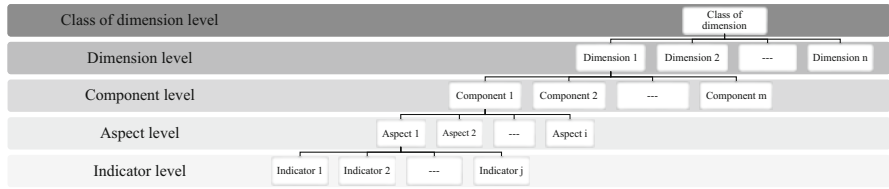


Fig. 2 A five-layer hierarchical model starting from class of dimensions to indicators

For example, in Table 2, the dimension transportation includes three components. Each of these components also can be further divided into aspects. For instance, the roads and railways component includes aspects such as highway, motorways, streets, bridges, railways, and monorails. Furthermore, each of the aspects can be broken down to some indicators which are quantifiable and easily measurable. For instance, the highway aspect can be measured by indicators such as highway length (km), number of tunnels, number of bridges, average daily traffic (h), and number of intersections [54], and similarly the railway aspect can be measured by indicators such as the length (km) of tracks, number of passenger trains, number of freight trains, and cumulative delay minutes [41].

We present a five-layer hierarchical model ranging from classes of dimension to indicators (see Fig. 2). However, to be in line with the main purpose of this paper, we limit our main focus from class of dimension to the component level and leave the definition of the lower levels to future research.

3.2 Phase (II): Post-disaster Prediction

Three stages are involved in phase (II), Affected Status of People and Properties, Required Resources, and Available Resources.

3.2.1 Affected Status of People and Properties

As shown in Table 3, the Affected Status of People and Properties has nine dimensions similar to initial status. The volume of destruction, damage, mortality, casualties, and loss depend not only on the strength of infrastructure and buildings in the city or region but also on the magnitude of a hazard. Hence, we suggest calculating this measure for each disaster scenario separately (e.g., small earthquake, medium earthquake, and large earthquake).

The result of this stage can be depicted by a radar diagram as illustrated in Fig. 3 (illustrative example). This diagram shows possible consequences of a disaster occurrence on all dimensions. It indicates the extent to which the normal situation (initial status) is going to change (affected status). One method to calculate the

Table 3 The dimensions and components of Affected Status of People and Properties

Phase	Stage	Dimensions	Components
(II) Post-disaster Prediction	Affected status	People (affected)	Affected population [dead, casualties, injured, displaced, etc.]
			Impact on demographic groups
		Residential buildings (affected)	Demolished buildings
			Buildings unfit for habitation
		Utilities (affected)	Damaged gas supply
			Damaged water supply
			Damaged electricity supply
			Damaged telecommunication systems
			Damaged sewage systems
		Transportation (in the region)	Damaged roads and railways
			Damaged vehicles
			Damaged airport and ports
		Health services (affected)	Medical staff status
			Damage ratio to hospitals, medical devices, and medicines
			Communicable diseases
		Government (in the region)	Affected municipality
			Damaged governmental institutions
			Affected public safety organizations
		Business (in the region)	Damaged plants
			Ratio of financial institutions and shopping centers unable to give services
Damaged warehouses, logistics services			
Sensitive facilities (affected)	Continuity of crisis room services		
	Explosion potential		
	Continuity of IT and ICT services		
Available relief inventory	Volume and quantity of remaining inventories		
	Access to warehouses		
	Damaged buildings		

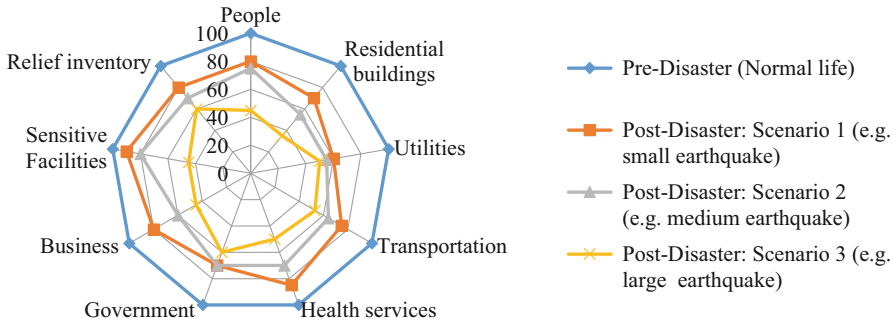


Fig. 3 The radar diagram specifying the volume of destruction and casualties after possible disaster scenarios

final values for each dimension in this radar diagram is the weighted sum approach which has been applied frequently in literature due to its simplicity for decision makers. In this approach, the assigned weights for indicators, aspects, components, and dimensions are determined by experts. See Appendix A for an example of the weighted sum calculation for the transportation dimension. The number 100 in the diagram shows the normal status of each dimension (not necessarily a perfect status). The value of indicators is calculated based on a comparison between the affected and normal situation.

The larger the area in the impacted part of the radar chart, the more vulnerable a municipality is. The diagram could be shown for each disaster scenario separately. This would highlight for which type of disaster the municipality is especially ill prepared.

3.2.2 Required Resources

After the investigation on affected status, we need to determine the resources which are required for a fast response. The data from the previous section leads to the identification of the demand for different resources. If we sum up resources, which are required for different demands, we can calculate the total requirements for that resource as shown in the example for a table format in Table 4.

3.2.3 Available Resources

Usually the government, aid agencies, municipalities, and other communities store items as safety stock for disaster occurrence. In gathering information regarding available resources, two main points have to be considered. Firstly, the investigation needs to be done about the inventories of all public and private sectors who are responsible for disaster relief operations, and secondly it has to be updated after a

Table 4 Example of a table format for calculating total required resources using a demand/resource matrix

		Required resources					
		Resource 1:	Resource 2:	Resource 3:	Resource 4:	Resource n:	
		Expert workers	Medical equipment	Building materials	Roadwork machineries	...	Funds and budget
Demands	Demand 1: injured people						
	Demand 2: displaced people						
	...						
	Demand n: destroyed vehicles						
	Total required resources						

disaster. Possible disaster occurrences may destroy some part of stored inventories. Table 5 shows an example of a table format for required and available resources. The second row of Table 5 shows the relief resources that are available after the disaster strikes. The last row of Table 5 indicates the surplus or shortage of resources by comparing required and available resources.

A detailed analysis of the underlying tables (Tables 1 to 5) can be used to identify specific improvement potentials.

3.3 Management

This paper considers three dimensions for management in pre- and post-disaster phases. These are planning and control, local/national, and international coordination. Table 6 shows both the dimensions and different components of each dimension. The effectiveness and efficiency of management is based on coordination on all levels including local and national.

3.4 Phase (III): Preparedness Assessment

To assess the disaster preparedness of a municipality, one needs to incorporate the information gathered based on the proposed framework and the embedded hierarchical model of dimensions. The method of incorporating information is shown in Fig. 4.

As depicted in Fig. 4, in order to measure the level of preparedness of a municipality, we should evaluate preparedness with respect to the following four areas:

- Preparedness for hazard assessment (*P1*) which shows the readiness of organizations involved in hazard risk identification (data gathering), hazard risk analysis and assessment, and hazard awareness
- Mitigation capabilities (*P2*) which shows the readiness of a society to eliminate or reduce the impacts and risks of hazards through proactive measures taken before an emergency or disaster occurs
- Resource preparedness (*P3*) which shows the readiness of organization and adequacy of resources to recover people and properties after a disaster
- Management performance (*P4*) which shows the quality of management and the level of coordination for pre- and post-disaster operations

At the end of this process, the policy-maker is presented with four measures. These four areas of preparedness can be represented in a radar diagram as exemplified in Fig. 5 (illustrative example).

As it was highlighted in the previous sections, this representation can be created for each disaster type (e.g., earthquake) considering different scenarios for each

Table 5 Example of a table format for required and available resources to determine surplus or shortage

	Resource 1: Expert workers	Resource 2: Medical equipment	Resource 3: Building materials	Resource 4: Roadwork machineries	...	Resource n: Funds and budget
Required resources						
Available resources						
Shortage (surplus)						

Table 6 The different dimensions and components of pre- and post-disaster management

Phase	Stage	Dimensions	Components	References
(I, II, III) All phases	Management	Planning and control	Organizers' definition	[22, 45, 46]
			Roles and responsibilities	
			Preparation exercises	
		Local/national coordination	Leading structure	[13, 22, 45]
			Coordinated plans	
			Volunteer management	
		International coordination	MOUs and agreements	[14, 36]
			Political communication	

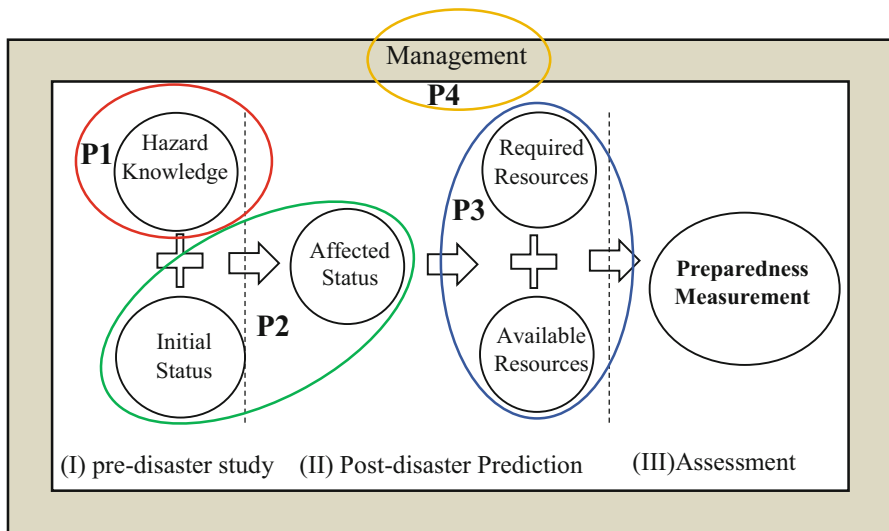


Fig. 4 Representation of different areas of preparedness assessment

disaster type (e.g., different magnitudes of earthquakes). In [Appendix B](#), we provide the weighted sum calculations for this illustrative example. As shown in [Fig. 5](#), management performance (P4) has the weakest preparedness level in all scenarios. Hence, in this illustrative example, the recommendation to policy-makers would be to focus their attention on this dimension.

4 Conclusions

This paper focuses on an important subject in the humanitarian area, disaster preparedness measurement. We provided suggestions on a classification of dimensions,

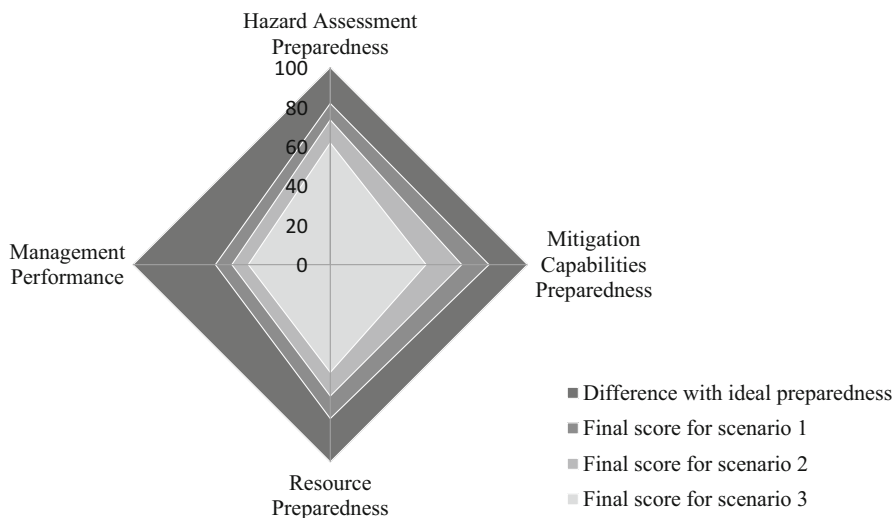


Fig. 5 The radar diagram specifying the final disaster preparedness for possible disaster

which are Hazard Knowledge, People and Properties, and Management. These classes of dimensions as a five-layer hierarchical model are later broken down to components, aspects, and indicators.

To consider multistage aspects of the disaster phenomenon, this paper develops a framework which consists of three different phases that need to be considered sequentially. These are as follows: phase (I) Pre-disaster Study, phase (II) Post-disaster Prediction, and phase (III) Preparedness Assessments. Each phase consists of stages which are processes for data gathering and analysis of results.

The framework can help policy-makers to discover weaknesses and strengths in disaster management. They could explore the preparedness for specific disasters with a range of possible strengths of occurrences as different scenarios. Furthermore, they could explore how the preparedness scores change when the disaster magnitude is increased and see if there are some critical strengths that lead to a large increase in impact. Finally, they could explore in which areas additional resources would be especially beneficial.

This methodology provides a comprehensive approach of evaluating disaster preparedness of a municipality taking the likelihood of disaster occurrence and disaster-specific impacts into consideration. As a next step, the lower layers of the model (aspect and indicator level) need to be defined. Then, the model needs to be implemented using real data. Implementing this methodology in practice is a challenging step-by-step process mainly because of two reasons; first, due to the multidimensional characteristic of our work, developing and calibrating the lower layers of the proposed model requires a wide range of knowledge and practical experiences as well as a considerable amount of time and effort. Second, the application of our model necessitates gathering and integrating data from many

different sources. Data quality is crucial issue in this context. These challenges can be overcome by close collaboration and building trust with practitioners. For example, the further development of this framework can be defined as a joint large-scale project with practitioners.

A.1 Appendices

A.1.1 Appendix A: Steps of the Weighted Sum Approach

In Fig. 3, we provided a radar diagram to show the extent to which the normal situation (initial status) is going to change after each disaster scenario. The values for each dimension in Fig. 3 are calculated using the weighted sum approach. In this section, we provide an illustrative numerical example of calculating final weighted sum values for the transportation dimension. Values of other dimensions are calculated similarly. To yield the final value of each dimension in the radar diagram, the following steps are taken. Note that this procedure is repeated separately for each scenario:

1. First, for each dimension, we assign the weights of each level, i.e., component level, aspect level, and indicator level. Note that the summation of weights at each level (node) must be 1.
2. For each indicator, the percentage ratio of post-disaster value to pre-disaster value is calculated. These percentage ratio values are used for weighted sum calculations.
3. The weighted sum calculation is done from right to left, i.e., i) for each aspect, the weighted sum of its corresponding indicator values is computed, ii) then for each component the weighted sum of its corresponding aspect values is calculated, and iii) for each dimension the weighted sum of its corresponding component values is calculated.

In Table 7, we provided only indicators for one aspect (i.e., highway). For other aspects we only provided the aggregated values. The numbers below each indicator, aspect, component, and dimension are the weighted sum values for scenarios 1, 2, and 3, respectively. In this illustrative example, we only consider a limited number of indicators for the highway aspect; however, policy-makers in practice may define a wider range of indicators. The final values for transportation are calculated as 75.73 for scenario 1, 64.72 for scenario 2, and 53.38 for scenario 3. This can be interpreted as 25 percent of transportation capacities of the municipality are affected in scenario 1.

Note that for Hazard Knowledge and Management, other scoring methods can be used since they are more qualitative.

Table 8 An illustrative example of weighted sum calculations for the final four areas of preparedness measurement

Preparedness area	Weight	Dimensions	Final score for scenario 1	Final score for scenario 2	Final score for scenario 3
Preparedness for hazard assessment (P1) (scenario 1 81.75, scenario 2 73.4, scenario 3 61.75)	0.33	Hazard risk identification	80	70	50
	0.33	Hazard risk analysis and assessment	75	70	65
	0.34	Hazard awareness	90	80	70
Mitigation capabilities (P2) (scenario 1 80.5, scenario 2 66.7, scenario 3 48.6)	0.1	People	80	73	53
	0.1	Residential buildings (affected)	90	80	70
	0.1	Utilities	80	70	60
	0.1	Transportation	75	64	53
	0.1	Health services	90	70	60
	0.1	Government	80	60	50
	0.1	Business	80	70	50
	0.1	Sensitive facilities	50	40	30
	0.2	Dedicated relief inventory	90	70	30
Resource preparedness (P3) (scenario 1 78, scenario 2 66.6, scenario 3 54.6)	0.2	Expert workers	90	80	70
	0.2	Medical equipment	50	40	30
	0.2	Building materials	90	80	70
	0.2	Roadwork machineries	80	73	53
	0.2	Funds and budget	80	60	50
Management performance (P4) (scenario 1 58.25, scenario 2 49.9, scenario 3 41.55)	0.33	Planning and control	75	70	65
	0.33	Local/national coordination	50	40	30
	0.34	International coordination	50	40	30

A.1.2 Appendix B: Weighted Sum Calculations for Preparedness Measurement

In Fig. 5, we provided a radar diagram specifying the final disaster preparedness for a possible disaster. The values of each preparedness area (i.e., P1, P2, P3, and P4) are calculated using the weighted sum approach which is explained earlier in [Appendix A](#). In Table 8, we provided the final values of each preparedness area aggregated into its dimension level. The final values of P1, P2, P3, and P4 are calculated as a weighted average of their corresponding dimension values for each scenario.

References

1. Adger, W. N. (1999). Social vulnerability to climate change and extremes in coastal Vietnam. *World Development*, 27(2), 249–269.
2. Adger, W. N., & Kelly, P. M. (1999). Social vulnerability to climate change and the architecture of entitlements. *Mitigation and Adaptation Strategies for Global Change*, 4(3–4), 253–266.
3. Ainuddin, S., & Routray, J. K. (2012). Community resilience framework for an earthquake prone area in Baluchistan. *International Journal of Disaster Risk Reduction*, 2, 25–36.
4. Alexander, DE (2015). Evaluation of civil protection programs, with a case study from Mexico. *Disaster Prevention and Management*, 24 (2), 263–283.
5. Balcik, B., & Beamon, B. M. (2008). Facility location in humanitarian relief. *International Journal of Logistics*, 11(2), 101–121.
6. Bastaminia, A., Rezaei, M. R., & Dastoorpoor, M. (2017). Identification and evaluation of the components and factors affecting social and economic resilience in city of Rudbar, Iran. *International Journal of Disaster Risk Reduction*, 22, 269–280.
7. Belmont, E., Fried, B. M., Gonen, J. S., Murphy, A. M., Sconyers, J. M., Zinder, S. F., . . . & American Health Lawyers Association. (2004). Emergency preparedness, response & recovery checklist: beyond the emergency management plan. *Journal of Health Law*, 37(4), 503.
8. Cabinet Office, Government of Japan “Saigai kihon hou tou no ichibu wo kaiseisuru houritsu” (in English “A partial amendment of the Disaster Countermeasure Basic Act in 2012”) http://www.bousai.go.jp/taisaku/kihonhou/kihonhou_h24_01.html
9. Cardona, O. D. (2007). *Indicators of disaster risk and risk management*. Inter-American Development Bank.
10. Cardona, O. D., & Carreño, M. L. (2011). Updating the indicators of disaster risk and risk management for the Americas. *IDRiM Journal*, 1(1), 27–47.
11. Cardona, O. D., Ordaz, M. G., Mora, M. G., Salgado-Gálvez, M. A., Bernal, G. A., Zuloaga-Romero, D., . . . & González, D. (2014). Global risk assessment: A fully probabilistic seismic and tropical cyclone wind risk assessment. *International Journal of Disaster Risk Reduction*, 10, 461–476.
12. Castillo, C. (2005). Disaster preparedness and business continuity planning at Boeing: An integrated model. *Journal of Facilities Management*, 3(1), 8–26.
13. Connors, T. D. (Ed.). (1995). *The volunteer management handbook* (Vol. 42). New York, NY: Wiley.
14. Coppola, D.P. (2011) Introduction to international disaster management, 2nd edn. Boston: Butterworth-Heinemann.
15. Cumming, G. S., Barnes, G., Perz, S., Schmink, M., Sieving, K. E., Southworth, J., . . . & Van Holt, T. (2005). An exploratory framework for the empirical measurement of resilience. *Ecosystems*, 8(8), 975–987.
16. Cutter, S. L., Ash, K. D., & Emrich, C. T. (2014). The geographies of community disaster resilience. *Global Environmental Change*, 29, 65–77.

17. Cutter, S. L., Barnes, L., Berry, M., Burton, C., Evans, E., Tate, E., & Webb, J. (2008). A place-based model for understanding community resilience to natural disasters. *Global Environmental Change*, 18(4), 598–606.
18. Davenport, S. S., & Waterstone, P. (1979). *Hazard Awareness Guidebook: Planning for What Comes Naturally*. Texas Coastal and Marine Council.
19. Davies, T., Beaven, S., Conradson, D., Densmore, A., Gaillard, J. C., Johnston, D., . . . & Robinson, T. (2015). Towards disaster resilience: A scenario-based approach to co-producing and integrating hazard and risk knowledge. *International journal of disaster risk reduction*, 13, 242–247.
20. Espada, R., Apan, A., & McDougall, K. (2017). Vulnerability assessment of urban community and critical infrastructures for integrated flood risk management and climate adaptation strategies. *International Journal of Disaster Resilience in the Built Environment*, 8(4), 375–411.
21. Etinay, N., Egbu, C., & Murray, V. (2018). Building urban resilience for disaster risk management and disaster risk reduction. *Procedia Engineering*, 212, 575–582.
22. Federal Emergency Management Agency (FEMA). (1997). Multi-hazard identification and risk assessment: A cornerstone of the national mitigation strategy.
23. Federal Emergency Management Agency. (1996). Guide for all-hazard emergency operations planning. *State and Local Guide (SLG) 101*.
24. FEMA (Federal Emergency Management Agency). (2004). Are You Ready? An In-depth Guide to Citizen Preparedness.
25. FEMA (Federal Emergency Management Agency). (2018). Comprehensive Preparedness Guide (CPG) 201: Threat and Hazard Identification and Risk Assessment (THIRA) and Stakeholder Preparedness Review (SPR) Guide. Retrieved from <https://www.fema.gov/media-library/assets/documents/165308>
26. Gall, M. (2013). *From social vulnerability to resilience: measuring progress toward disaster risk reduction*. UNU-EHS.
27. Hajito, K. W., Gesesew, H. A., Bayu, N. B., & Tsehay, Y. E. (2015). Community awareness and perception on hazards in Southwest Ethiopia: a cross-sectional study. *International Journal of Disaster Risk Reduction*, 13, 350–357.
28. Hémond, Y., & Robert, B. (2012). Preparedness: the state of the art and future prospects. *Disaster Prevention and Management: An International Journal*, 21(4), 404–417.
29. Hick, J. L., Hanfling, D., Burstein, J. L., DeAtley, C., Barbisch, D., Bogdan, G. M., & Cantrill, S. (2004). Health care facility and community strategies for patient care surge capacity. *Annals of Emergency Medicine*, 44(3), 253–261.
30. Ho Oh, E., Deshmukh, A., & Hastak, M. (2010). Disaster impact analysis based on inter-relationship of critical infrastructure and associated industries: a winter flood disaster event. *International Journal of Disaster Resilience in the Built Environment*, 1 (1), 25–49.
31. IFRC, (2015). The checklist on law and disaster risk reduction. <https://www.ifrc.org/PageFiles/115542/The-checklist-on-law-and-drr.pdf>
32. Jackson, B. A. (2008). The problem of measuring emergency preparedness: The need for assessing “response reliability” as part of homeland security planning. Rand Corporation.
33. Jahre, M., Pazirandeh, A., & Van Wassenhove, L. (2016). Defining logistics preparedness: a framework and research agenda. *Journal of Humanitarian Logistics and Supply Chain Management*, 6(3), 372–398.
34. JICA, C. (2000). The study on seismic microzoning of the Greater Tehran Area in the Islamic Republic of Iran. *Pacific Consultants International Report, OYO Cooperation, Japan*, 291–390.
35. Kahn, L. H., & Barondess, J. A. (2008). Preparing for Disaster: Response Matrices in the USA and UK. *Journal of Urban Health*, 85(6), 910–922.
36. Moore, Spencer, Eugenia Eng, and Mark Daniel. “International Ngos and the Role of Network Centrality In Humanitarian Aid Operations: A Case Study of Coordination During the 2000 Mozambique Floods”. *Disasters* 27.4 (2003): 305–318. Web.

37. Moy Jr, F. (1995). Facility “wellness”: Health facilities management. *Facilities*, 13(9/10), 45–48.
38. Pelling, M. (2007) ‘Learning from others: The scope and challenges for participatory disaster risk assessment’, *Disasters*, 31(4), pp. 373–385.
39. Pomonis, A., Spence, R., & Baxter, P. (1999). Risk assessment of residential buildings for an eruption of Furnas Volcano, Sao Miguel, the Azores. *Journal of Volcanology and Geothermal Research*, 92(1–2), 107–131.
40. Preparedness process. (2014). Scandinavian Journal of Public Health. https://journals.sagepub.com/toc/sjpc/42/14_suppl
41. PRIME (Platform of Railway Infrastructure Managers in Europe). (2016). Key Performance indicators for performance benchmarking. Retrieved from https://webgate.ec.europa.eu/multisite/primeinfrastructure/sites/primeinfrastructure/files/prime_kpi_catalogue_1_0_0.pdf
42. Renschler, C. S., Frazier, A. E., Arendt, L. A., Cimellaro, G. P., Reinhorn, A. M., & Bruneau, M. (2010). *A framework for defining and measuring resilience at the community scale: The PEOPLES resilience framework* (pp. 10–0006). Buffalo: MCEER.
43. Roh, S. Y., Jang, H. M., & Han, C. H. (2013). Warehouse location decision factors in humanitarian relief logistics. *The Asian Journal of Shipping and Logistics*, 29(1), 103–120.
44. Sheppard, A., Tatham, P., Fisher, R., & Gapp, R. (2013). Humanitarian logistics: enhancing the engagement of local populations. *Journal of Humanitarian Logistics and Supply Chain Management*, 3(1), 22–36.
45. Simpson, D. M. (2008). Disaster preparedness measures: a test case development and application. *Disaster Prevention and Management: An International Journal*, 17(5), 645–661.
46. Sutton, J., & Tierney, K. (2006, November). Disaster preparedness: Concepts, guidance, and research. In *Fritz Institute Assessing Disaster Preparedness Conference* (pp. 1–41).
47. Tchankova, L. (2002) ‘Risk identification – basic stage in risk management’, *Environmental Management and Health*, 13(3), pp. 290–297.
48. The City of Houston Office of Emergency Management. (2016). Disaster Preparedness Guide. <http://www.houstonoem.org/external/content/document/4027/2168878/1/COH-DPG2016-English.pdf>
49. Tufinkgi, P. (2006), Logistik im Kontext Internationaler Katastrophenhilfe: Entwicklung eines Logistischen Referenzmodells für Katastrophenhilfe, Haupt Verlag, Bern
50. UNDP Drylands Development Centre., (2013). Community Based Resilience Analysis (CoBRA): Conceptual Framework and Methodology, version May 17, 2013.
51. Velasquez, C. A., Cardona, O. D., Carreño, M. L., & Barbat, A. H. (2014). Retrospective assessment of risk from natural hazards. *International Journal of Disaster Risk Reduction*, 10, 477–489.
52. Winderl, T. (2014). Disaster resilience measurements: stocktaking of ongoing efforts in developing systems for measuring resilience.
53. World Health Organization. (2011). Hospital emergency response checklist-An all-hazards tool for hospital administrators and emergency managers. *World Health Organization (WHO) Regional Office for Europe: Copenhagen, Denmark*.
54. Yoon, C., & Sung, J. (2005). Development of Integrated Highway Management System in Korea. In *Proceedings of the Eastern Asia Society for Transportation Studies* (Vol. 5, pp. 783–790).

Development of Flood Disaster Prevention Simulation Smartphone Application Using Gamification



Yutaka Matsuno, Futaba Fukanuma, and Shigenobu Tsuruoka

Abstract In recent years, there have been many serious flood disasters. However, only a few citizens have sufficient knowledge about evacuation from the disaster. In order to reduce the damage, it is necessary for citizens to be aware of the flood risk of the residence, to prepare for disasters, and to take appropriate evacuation action at the time of disasters. For that purpose, citizens need to continuously learn disaster prevention information. Based on the above considerations, we develop a smartphone application for simulating flood disaster evacuation, based on the notion of *gamification*. In this paper, we report design and development of the disaster prevention smartphone application for citizens, focusing on easiness, continuity (wanting to use the application continuously), learning effects, and improvement of interest.

Keywords Flood disasters · Learning evacuation points · Smartphone application · Gamification

1 Introduction

In recent years, flood disasters become very serious. In Japan, there have been frequent flood disasters, such as Kanto-Tohoku Heavy Rainfall in September 2015 and heavy rains in July 2018. Japan is prone to flood damage due to its topography and weather. In addition, it is predicted that the frequency of heavy rain, the amount of floods, and the frequency of short-term heavy rain will increase in the future due to the effects of global warming [1]. In fact, there are only 60 municipalities out of

Currently in Kyodo Printing Co., Ltd.

Y. Matsuno (✉) · F. Fukanuma · S. Tsuruoka

Department of Computer Engineering, College of Science and Technology, Nihon University, Funabashi, Chiba, Japan

e-mail: matsuno.yutaka@nihon-u.ac.jp; csfu17020@g.nihon-u.ac.jp; tsuruoka3060@nifty.com

1741 Japanese municipalities that have never suffered flood damage in the 10 years from 2006 to 2015. On the other hand, the municipalities where river damage has occurred more than 10 times are 829 municipalities (47.6%), about half of the total. Although there are differences in scale, flood damage from rivers occurs in most areas [1].

Hazard maps are used as sources for mitigation of natural disasters such as floods and disaster prevention measures. A hazard map is a map that displays disaster-predicted areas, the locations of disaster prevention facilities such as evacuation points and routes, etc. The inundation area in Kurashiki City, which was affected by heavy rain in 2018, was almost the same as the expected inundation area shown in the hazard map [1].

However, public awareness of disaster prevention information (including hazard maps) is not sufficient. For example, according to an interview survey conducted by Chuo University in Japan on the flooding and evacuation situation during the Kinugawa flood, 61.0% of 516 respondents said that they did not know or had not seen the hazard map in their daily lives [1]. In addition, after the heavy rain in July 2018, 75 citizens of respondents in the questionnaire survey of 100 citizens in Kurashiki City's Manbi-cho area said that they actually knew the hazard map, but only 24 citizens had understood the content of the hazard map. According to a questionnaire conducted for residents in the heavy rain special warning announcement area during the heavy rain in July 2018, 70% of lowland residents with potential flooding risk were too optimistic about the danger of flooding [1].

In the Japanese Cabinet Office survey [1], the percentage of residents who know the meaning of the hazard map and the river water level that is the basis of evacuation judgment when flood disaster occur is very low. For successful aid from government when a flood disaster occurs, citizens must first recognize the risk of flooding in their residence area and make preparations for flooding and take appropriate evacuation actions in case of emergency.

In order for citizens to learn about disaster prevention information, citizens need to be interested in disaster prevention information. Also, continuous learning is necessary, as disasters occur not so often, but it is impossible to predict when it will happen. Furthermore, easiness of learning is important, as citizens are usually not professional of disaster prevention and need to learn it in their spare time.

Based on the above observations, we propose a method for learning with smartphone applications. In recent years, many smartphone applications that provide disaster prevention information have been developed. From a survey in Japan, such smartphone applications have been installed in about 32% of the 4156 respondents' smartphones [2]. However, due to the low level of public interest in disaster prevention information, there seem to be few applications that are used continuously.

The structure of the paper is as follows. In Sect. 2, we discuss related work. Sect. 3 explains the specification of our smartphone applications. Section 4 explains a subject experiment for evaluating the tool. In Sect. 5, we discuss the results. Section 6 concludes the paper.

2 Related Work

2.1 Gamification

Gamification is defined as the application of game design principles in non-gaming contexts [3, 4]. There are several other definitions for gamifications. In this paper, we refer to McClelland's theory of motivation (need for achievement, power, and affiliation) [5] and use the following four elements of gamification:

- Getting high score (achievement)
- Getting stamps (achievement)
- Getting high ranking (achievement and power)
- Getting high level (achievement)

Particularly, in this paper we focus on score and ranking. Incorporating need for affiliation is left as future work.

There are various works using gamification. One of the most successful examples is Pokemon GO. Pokemon GO¹ is a location information game application that allows users to get Pokemon (characters) existing in various locations using AR. Users can use their Pokemons for fighting with other Pokemons and exchanging their Pokemons. According to a survey [6] with 8859 Japanese people, over half of the people of age of 20s and over 30% of people of age of 40s have downloaded Pokemon GO, and 30% of them have been continuing to play the game. There were many reasons for the continuation, such as “killing time,” “can always do at their own pace,” “can be accompanied by commuting, shopping, walking, etc.,” and “fun.” By starting Pokemon GO, more than 60% of them said that “walking time and opportunities are increased.”

2.2 Disaster Prevention Learning Applications

There are two kinds of disaster prevention applications. One is digital applications and the other is non-digital applications. Non-digital applications include card games such as [7] and board games. The effectiveness of such games is reported in the papers. However, unfortunately, because such applications are based on classical games for which most of us would play in childhood, it is not certain that citizens really want to play the games continuously.

Recent works on digital applications often use AR (augmented reality) and VR (virtual reality) technologies. AR hazard scope [8] is a smartphone application which can display tsunami/inundation expected height of water through smartphone camera. Also, silhouettes of people are displayed on the screen. A map is displayed

¹<https://www.pokemongo.com>

to show the current position of the user and flooded area. Also, the application shows evacuation points with the names and distance. These AR and VR applications are mostly for groups in evacuation training organized by a disaster prevention organization, not for individuals, and not free. Therefore, for ordinary citizens, these applications are not easy to use continuously.

2.3 Disaster Information Applications

There are various smartphone applications for disaster information. In “goo disaster prevention application” [9], real time weather and disaster information is available in the application. Inundation degree simulation function is also available. Quizzes about evacuation and an evacuation simulation game also can be used. However, such games are designed as additional small games, and after playing them for several times, the user would lose their interests to the games.

We have reviewed related work in three subcategories: gamification, disaster prevention learning applications, and disaster information applications. Learning disaster prevention information is difficult for ordinary citizens because disasters occur not so often and it is difficult to predict when they occur. To ease the difficulty, we believe that gamification is a key solution for motivating ordinary citizens to learn disaster prevention information. Note that the gamification elements should be interesting and fun by themselves; otherwise users do not want to use the applications. Therefore gamification elements should not be based on classical and simple games in childhood. As in related work, recent technologies such as VR and AR would be effective. Also, digital applications can use actual and runtime data such as maps and flooded areas information. Use of smartphones is also important because today most of ordinary citizens use smartphones in daily lives; thus smartphone applications can be used easily and continuously. Together with conventional hazard information application, we aim to develop a flood disaster prevention simulation smartphone application using gamification.

3 Specification of Flood Disaster Prevention Smartphone Application

Our smartphone application has conventional functions for flood disaster information such as presenting weather forecast information, map, disaster prevention information. In addition, this application has river information and gaming modes. In this section we mainly explain the specifications of these two modes. Currently, only the home screen, map, game mode, and weather forecast mode have been developed. Figure 1 shows the top-level screen (left) and weather information mode as an example. From the top-level screen, users can select the six modes.

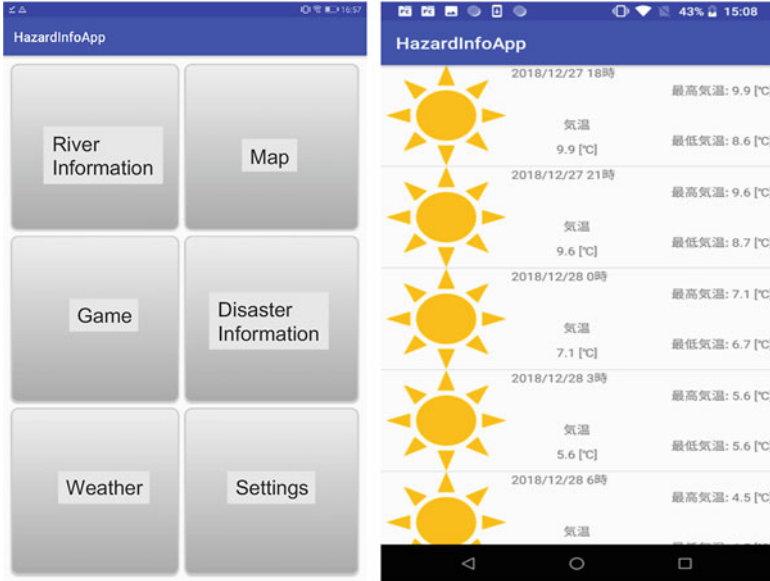


Fig. 1 Top-level screen (left) and weather information mode (right)

3.1 River Information Mode

In this mode, the water level and flow velocity of the river in the specified area can be seen with graphs and cross-sectional views. The water level can be obtained from the hydrological water quality database [10], and the flow velocity can be obtained from the flow velocity sensor [11] currently under development at Takuwa Co., Ltd. This mode is under development.

3.2 Game Mode

The game mode is set in the virtual world created by Google Street View.² We used Unity³ as the development environment, Google Maps API for field creation, and Mapbox⁴ for hazard maps.

Figure 2 shows a screenshot of the game mode.

The use steps of the evacuation game mode are as follows. First, users select a starting point listed in the screen. Currently, users can choose a starting point from

²www.google.com

³<https://unity.com>

⁴<https://www.mapbox.com>



Fig. 2 A screenshot of proposed smartphone application (Unity Technologies Japan, Mapbox, Google, Inc)

5 points in Kanagawa Prefecture, Japan (starting points can be set anywhere in the world). Next, the evacuation game starts. Finally, if the player's HP (health point, physical strength) or the timer reaches to 0, the game is over, and the result scene is displayed.

The player's purpose is to visit as many evacuation points as possible within the time limit from the starting point. However, HP decreases when passing through a flooded place on the field. Depending on the water level in the player's location point, decreasing amount of HP changes. HP of the player will be recovered when the player visits an evacuation point. Inundation areas and evacuation points data are obtained from the National Land Numerical Information of Japan,⁵ and this information and the current position of the player can be seen from the hazard map that can be displayed at the top of the screen. Figure 3 shows an example of depth of flooding area in the game screen.

3.3 Gamification Elements

We focus on "ranking" among the elements of gamification. In this game, the elapsed time, the number of discovered evacuation points, and the score are displayed at the end of the game, and then the ranking of the acquired score

⁵<http://nlftp.mlit.go.jp/ksj-e/index.html>

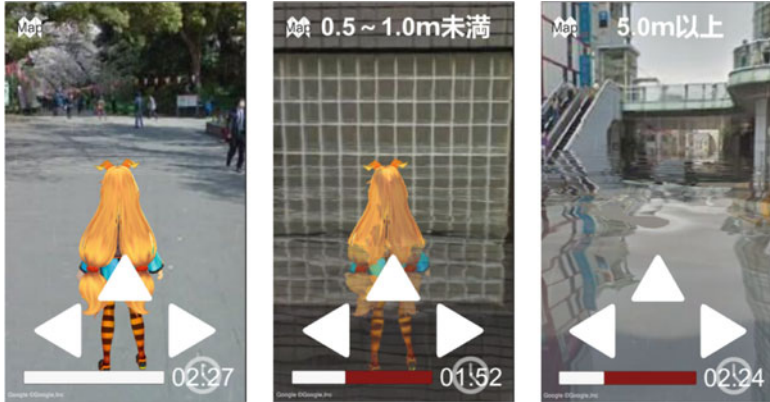


Fig. 3 Depth of flooding areas in game scenes (left, 0 m depth; middle, 0.5 to 1.0 m depth; right, over 5.0 m depth)

Fig. 4 Score and result scenes



is displayed. If the current score exceeds the existing score, the current score is highlighted as yellow. Figure 4 shows the score and the ranking scenes.

In the left of Fig. 4, it is indicated that the elapsed time is 2 min 30 s, 3 evacuation points are found, and the score is 6510. In the right of Fig. 4, the score 6510 is indicated as the top score and highlighted as yellow.

The score is determined by the following two elements, where C is an appropriate constant integer.

- Remaining HP
- Number of evacuation points found

The equation for calculating the score is basically as follows:

$$\text{Score} = C \times \text{Remaining HP} \times \text{Evacuation Points}$$

In order to get a high score, the player needs to avoid walking flooding areas. Otherwise, the HP will be decreased, and the player cannot get a high score. Also, the player needs to visit as many evacuation points as possible while avoiding dangerous places. By playing the game application, the players are expected to learn both flooding areas and evacuation points.

4 Subject Experiment

We conducted a preliminary subject experiment with ten participants. Based on the feedbacks, we conducted a subject experiment with 20 participants. The 20 participants consist of 15 undergraduate students and 5 graduate students of the College of Science and Technology, Nihon University, which is located in Tokyo, Japan. Figure 5 shows a picture of the subject experiment.

We assume that their knowledge levels of flood disaster evacuation are equal. We divide the participants to two groups:

- Group A (10 participants): Studying flood disaster evacuation with hazard maps provided by the municipalities and the smartphone application.
- Group B (10 participants): Studying flood disaster evacuation only with hazard maps.

The starting points for the game application are set to the following locations near the campus in Tokyo: Ueno Station, Okachimachi Station, Kanda-Myojin



Fig. 5 A picture of subject experiment

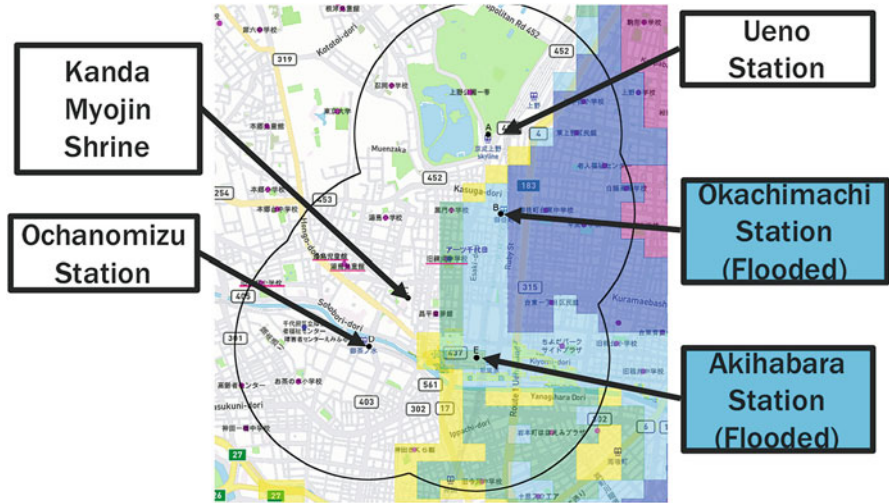


Fig. 6 Tokyo area used for the experiment with game starting points

Shrine, Ochanomizu Station, and Akihabara Station. These stations are pointed in the hazard maps used in this experiment. Figure 6 is the hazard map used in the experiment. Note that when a flood disaster occurs, Okachimachi Station and Akihabara Station will be flooded.

Each participant studies paths from the starting points to evacuation points for 30 min. The study area is within 800 meters from the starting points.

The tasks of the participants are as follows. After studying the places and names of evacuation points and flooded areas in the hazard map with (group A) or without (group B) our smartphone application in 30 min, the participants are given a map without information of evacuation points and flooded areas. They are asked to point the evacuation points, write the names, and draw flooded areas they learned. Figure 7 shows examples of answers written by the participants of groups A and B.

In Fig. 7, the participant pointed evacuation points red points. Inundation area is indicated by the curved blue line on the right.

Also, they are asked to fill questionnaires about flood disaster information. The questionnaires are 5 level evaluation (5 is higher and 1 is lower).

5 Results and Discussion

As average, the participants of group A played the game application 13.7 times (average playing time is 24 min) and read the hazard maps for 4 min and 52 s in average. The participants of group B read the hazard maps for 22 min and 30 s in average.

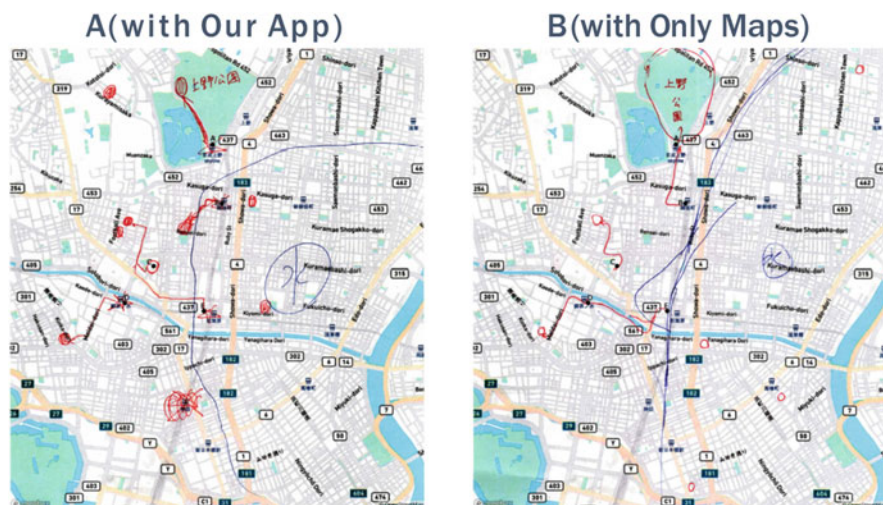


Fig. 7 Examples of answers (groups A and B)

Table 1 Evacuation points learning percentages

Group	Average	SD
A	14.50%	9.94
B	9.73%	10.7

We evaluate the results of each group A and B by accuracy of estimation of inundation areas and name and place of evacuation points.

For inundation areas, we judge the correctness by whether inundation points are checked by the participants or not. For example, Okachimachi and Akihabara Stations are inundation areas. We evaluate eight inundation areas. As a result, the average of group A is better in all eight areas.

For evacuation points, we score the number of evacuation points the participants checked. Table 1 shows the averages and the SD (standard deviation) of the scores of group A and group B. In Table 1, the average 14.50% of group A is the average percentage of checked evacuation points for all 21 evacuation points. The result of F test is that group A and group B are equal variance ($p=0.05$). The result of t test is not significantly different ($p=0.05$). The reason of this result seems that the number of the participants (20) was not enough. If the number of participants is 27 with the same average and SD, the result of t test is significantly different ($p=0.05$). However, comparing the averages, group A (with our gaming application) is indicated as better than group B.

The result for the names of evacuation points is shown in Table 2. For the result in Table 2, the result of F test is that group A and group B are not equal variance ($p=0.05$). Therefore we conducted Welch's T test. The result has not statistically significance difference. However, from the averages it is indicated that group B (learning only by hazard maps) is better than group A for learning the names of evacuation points.

Table 2 Evacuation names learning percentages

Group	Average	SD
A	4.28%	4.01
B	13.67%	10.1

Table 3 Result of questionnaires

Criteria	Question	Group	Average
Basic Knowledge	Do you know the flood information of the area?	A	2.4
		B	2.4
Easiness	Is it easy to identify evacuation points?	A	4.3
		B	2.6
Easiness	Is it easy to identify inundation area?	A	4
		B	3.3
Easiness	Is it easy to identify current point?	A	4
		B	2.3
Interest	Do you get interest in the flood information of the area?	A	3.7
		B	3
Interest	Do you get interest in studying flood evacuation?	A	4.1
		B	4
Easyness	Is the smartphone application / hazard map easy to use?	A	4.2
		B	2.3
Continuity	Do you want to continue to use the smartphone application / hazard map?	A	3.2
		B	2.6

The result of questionnaires is shown in Table 3.

The questionnaires are about basic knowledge of the participants, easiness of the smartphone application (group A) or only with hazard maps(group B), interest to the smartphone application (group A) or hazard maps (group B), easiness of the tool (group A) or hazard map (group B), and continuity of the tool (group A) or hazard map (B). The averages of basic knowledge are equal in groups A and B. This supports the assumption of equality of knowledge of groups A and B. For the other questions, the averages of group A are higher than that of group B.

We summarize the indications from results of experiments and questionnaires.

- For learning the evacuation points and inundation areas, using the smartphone application with hazard map is better than using only hazard map.
- For learning the name of evacuation points, using only hazard map is better than using the smartphone application with hazard map.
- For interest, easiness, and continuity criteria, the smartphone application has positive effects.

The limitations of above experiments and questionnaires are that the number of participants are not enough, and statistically significant difference could not be obtained. However, comparing the averages of group A and B and the results of questionnaires, the smartphone application has some positive effects for learning evacuation points. The result also indicates that using only hazard map is better than with the smartphone application for learning textual information (name of evacuation points); textual learning information would be better.

Currently, we only use two gamification elements: score and ranking. Other gamification elements such as need of level up and affiliation have not been considered. Also, although several participants of the subject experiment said the game mode is fun, the game mode should be fun as just games, as commented by the game creators of Koto Co., Ltd we interviewed. They said that even though the game mode is for learning flood disaster evacuation, the game mode itself should be fun as a game. We observe that this is a fundamental task for any application using gamification.

6 Concluding Remarks

This paper presented a smartphone application which has the flood evacuation learning mode with gamification elements, besides conventional disaster information functions such as weather forecasting. The flood evacuation learning mode uses Google Street View and Google Map. The Google Map is associated with evacuation points and inundation areas. The user character runs in the map and tries to go to evacuation points. The application has been implemented as an Android application and designed for easiness, interest, and continuity. The evaluation result by a subject experiment with 20 participants indicates that the smartphone application is effective compared with only using hazard maps.

Future steps include more improvements of the tool based on feedbacks, more integration among application modes such as river information and game mode, subject experiments involving more participants, and distributing the application through Google platform. We would like to report our progress near future.

Acknowledgments We deeply thank Professor Osamu Uchida at Tokai University for numerous comments and accepting subject experiments at his laboratory. We would like to thank Dr. Kan Shimazaki (currently at Nagoya University, Japan), Dr. Hiroko Nakajima, and Dr. Akiko Miyajima of National Research Institute for Earth Science and Disaster Resilience, Japan, and Professor Yang Ishigaki of The University of Electro-Communications for various comments on our work. Comments by people of Koto Co., Ltd. at Kyoto, Japan, from the viewpoint of game creator help us to design the application. Finally but not least, we thank the participants of DOD 2019 for fruitful discussions with them.

References

1. Japanese Cabinet Office, Disaster Prevention Information (in Japanese), <http://www.bousai.go.jp/>, accessed on 16, Feb., 2018 (2018)
2. Mobile Society Research Institutes, Disaster Prevention Report No.4 (in Japanese), http://www.moba-ken.jp/project/disaster/disaster_reduction_ict_no04.pdf, accessed on 10, Feb., 2019 (2019)
3. Huotari, K., Hamari, J., Defining Gamification A Service Marketing Perspective. Proceedings of the 16th International Academic MindTrek Conference 2012, Tampere, Finland, October. (2012)

4. Robson, K., Plangger, K., Kietzmann, J., McCarthy, I., Pitt, L., Is it all a game? Understanding the principles of gamification. *Business Horizons*. 58 (4): 411–420 (2012)
5. McClelland, D., *Human Motivation*, Cambridge University Press (1988)
6. Kao Group, Changes in behavior and consciousness brought by Pokemon GO: What makes “walking” a habit? (in Japanese), <https://www.kao.co.jp/content/dam/sites/kao/www-kao-co-jp/lifei/report/pdf/37.pdf>, accessed on 19, Feb., 2019 (2019)
7. Ministry of Land, Infrastructure, Transport and Tourism, Japan, Disaster Prevention Card Game “What will happen next?” (in Japanese), http://www.mlit.go.jp/saigai/saigai01_tk_000005.html, accessed on 18, Dec., 2018 (2018)
8. CAD CENTER, AR Hazard Scope (in Japanese), <https://www.cadcenter.co.jp/products/archives/7>, accessed on 18, Dec., 2018 (2018)
9. NTT Resonant Incorporated, goo Disaster Prevention Smartphone Application (in Japanese), <https://advance.bousai.goo.ne.jp/web/>, accessed on 19, Feb., 2019 (2019)
10. Ministry of Land, Infrastructure, Transport and Tourism, Japan, Hydrological Water Quality Database (in Japanese), <http://www1.river.go.jp>, accessed on 15, Feb., 2019 (2019)
11. Tsuruoka, S., Banepali, A., Fukanuma, F., Matsuno, Y., QUANTITY OBSERVATION SYSTEM USING IoT AND POINT CURRENT SENSOR. *Journal of Japan Society of Civil Engineers, Series F3 (Civil Engineering Informatics)*. 73. (2017)

Natural Disasters and Their Impact on Business Units: The Greek Case



John A. Mpekiaris and George D. Tsiotras

Abstract This research addresses current situation in terms of Greek companies' awareness, preparedness, and resilience against catastrophic events. Furthermore, this research aims at recording the implications of catastrophic events on business activities as well as depicting entrepreneurs' perception of business continuity and post-disaster recovery.

Keywords Natural disasters · Impact · Prevention · Business continuity planning · Disaster awareness · Preparedness

1 Introduction

Natural disasters entail a high impact on companies of all types, both in developed and developing countries. The implications of a catastrophic event on business activities may either be explicit or implicit, tangible or intangible. Enterprises – small and medium enterprises (SMEs), in particular – test their limits in cases of natural disasters. SMEs have low financial margins, poor emergency planning, and lack spatial flexibility. Moreover, only a small percentage of SMEs are insured [1].

The big challenge for every enterprise is to identify how to continue to operate in case of emergencies and to be able to successfully absorb any negative effects that might emerge. Extensive research has widely addressed the implications of natural disasters on households, people, and the macroeconomic environment. However, there is a gap in literature on the consequences of natural disasters on business and the extent to which organizations cope with catastrophic events [17].

Examples of great disasters that have affected business operations are, among others, the earthquake of March 11, 2011 in Japan – which made huge corporations, like Toyota SA and Honda SA, to cease their production activities [5, 8, 13].

J. A. Mpekiaris (✉) · G. D. Tsiotras

Business Excellence Lab, Department of Business Administration, University of Macedonia, Thessaloniki, Greece

e-mail: ibekiaris@uom.gr; ioanis.mpekiaris@nea-propontida.gr; tsiotras@uom.edu.gr

About 15 years before that, in 1995, a 7.2R earthquake in Kobe, Japan, caused multiple problems, such as water and natural gas outage and massive destructions in public infrastructure (railways, roads, ports) forcing companies that were not directly damaged by the earthquake to face malfunctions in supply, transportation, and communication networks [11].

In addition to major disasters, even a seemingly minor catastrophic event, may cause a major disruption on business operations [18]. For instance, in 2000 a production unit of Phillips S.A. was struck by a lightning that caused a fire [11].

Research on business consequences, preparedness, and short- and long-term recovery from catastrophic events has been conducted in 1993 by the Disaster Research Center of University of Delaware in Newark, USA, through five systematic, wide-scale mail surveys that collected data from over 5000 private companies located in five different states (Memphis, Tennessee, Los Angeles, California, and Florida). This research focused on three main aspects; firstly on factors that influence firms' preparedness against disasters, secondly on disaster sources causing business disruption and financial losses, and thirdly on factors influencing firms' competency to recovery from a major catastrophic event [19].

Xiao and Peacock [20] focused on firms' performance toward disaster in terms of planning, mitigation, preparedness, and impact management. They used data from Galveston, Texas, 7 months following catastrophic Hurricane Ike that made landfall on September 13, 2008. This research revealed that business planning against disasters had significantly decreased vulnerability, while the adoption and implementation of planned mitigation and preparedness measures minimized post-storm impact.

Lacho [13] explored the impact of Hurricane Katrina on small firms in Ruston, Louisiana, within a range of 400 miles around the affected area. The hurricane itself caused in Ruston only some short power outages. However, the most severe local effect was the flow of refugees from the region of New Orleans after the storm. Research findings showed that small organizations that are far less prone to serious damage yet largely affected by the mass flow of evacuees should have a management plan to handle rising business activities addressing the additional and pressing needs of refugees, particularly in terms of food and transportation.

Hayakawa et al. [10] studied the firm-level impact of the 2011 flooding in Thailand, focusing on the contracts that were signed by Japanese subsidiaries in Thailand. This research found, firstly, a higher probability for small firms to have a reduction of their local procurement share particularly the one from other Japanese-owned firms in Thailand. Secondly, young firms were found to be more prone to an increase of their share of imports from Japan whereas older firms were more likely to turn to China. These findings are useful in showing the way for multinational corporations to regulate their production networks prior and after natural disasters.

Flynn [7] used statistical data of a research conducted in 2003 and showed that there is a significantly higher percentage of companies that adopt a recovery plan among those companies that started operating following a 1997 flood in North Dakota, USA, compared to those companies that were in operation before the flood and remained in business several years afterward.

Other researchers focused on the impact of disasters on firms in different sectors using secondary data of 3500 disastrous events affecting over a hundred thousand companies for a time period of 15, years. Results showed that disasters affect industries irrespective of sector throughout their supply chains [2].

Furthermore, in a research addressing the 2009 floods in Fiji Islands, which entailed a financial damage of 24 million USD on sugar belt, it was stressed that negative impact can be reduced using a multilevel approach of risk mitigation which should meet business, social and state requirements within a basic framework based on environmental services [14].

In 1997 – 8 years after the earthquake in Loma Prieta – Disaster Research Center of Delaware University conducted a large-scale questionnaire survey in Santa Cruz, California, which was struck by the 1989 earthquake. Han and Nigg [9] have explored the influences of business and decision makers' features on disaster preparedness planning. Results showed that large companies are more likely to engage in emergency planning for the mitigation of disaster's impact. Moreover, it was found that firms belonging to the finance, insurance, and real estate sectors hold a competitive advantage over retailers and wholesalers in terms of disaster preparedness [9].

Finally, a research on damages following the 9/11 terrorist attacks showed that SMEs due to lack of business continuity planning against disasters encountered serious problems with stewardship, insurance terms in force, backup copies of legal documents, confidential data files, and critical information, in general [3].

Evidence shows that increasingly companies focus on recovery planning. Firms that had a preparedness and recovery plan in place prior to the occurrence of major catastrophic events not only survived yet they were able to return to normal operation and assure business continuity [16].

Despite its limited land coverage, Greece entails a variety of natural disaster risks, with earthquakes, floods, storms, and wildfires being some of the most common. Recent events of flooding in Mandra and wildfire in Mati, in the broader area of Attica, stressed the necessity for disaster awareness and preparedness of both people and organizations [4, 6, 15] Lasda et al. 2010). However, the limited financial resources of the governmental and regional authorities in Greece reduce the actions taken for planning and measures against disasters. This transfers the responsibility for risk management to the companies themselves. The big challenge for every enterprise is to be able to resume operation in case of emergencies. Extensive research has widely addressed the implications of natural disasters on households, people, and the macroeconomic environment. However, there is a gap in literature on the consequences of natural disasters on business and the extent to which organizations cope with catastrophic events [17]. In this train of thought, this research focuses on the Greek business context with regard to natural disaster awareness and preparedness highlighting those factors affecting business continuity planning.

2 Methodology

To serve this research purpose, a survey questionnaire was used consisting of 45 items. The measuring instrument included three sections, with the first section covering firms' demographic data, the second inquiring disaster awareness and preparedness, and the third addressing post-disaster recovery actions. The questionnaire included disaster types commonly encountered within Greek borders, such as floods, wildfires, and earthquakes. There were mostly single-answer and multiple-choice closed-type questions. Respondents' perceptions were addressed through 5-point Likert scale questions, as well. Survey has been conducted in firms throughout Greece. The majority of the responding firms were located in Macedonia, Attica, and on several islands.

Data was processed using SPSS software – version 22.0 for Windows. Data analysis was based primarily on descriptive statistics to visualize response distribution. Moreover, chi-square test of independence was used to identify any statistically significant dependencies between categorical variables.

The following research hypotheses were tested:

- Company features do not relate to the consequences of a natural catastrophic event.
- Company features do not relate to the preparedness (prevention) against a natural catastrophic event.
- Company features do not relate to the recovery (resilience) following a natural catastrophic event.
- Noncompliances – in terms of operational permits, emergency exits, safety systems, etc. – do not relate to the consequences of a natural catastrophic event and post-event recovery.

Company features refer to the type of activity (sector), company size, the years of operation, and firm ownership.

3 Summarized Results

During field survey 500 questionnaires have been distributed, out of which 331 completed questionnaires were received corresponding to a response rate of 66.2%.

Respondents are geographically distributed over Greece as follows: firms located in Thessaloniki account for 38.4%, firms located in Chalkidiki account for 37.2%, firms located in Attica account for 3.6%, and firms located in other Greek regions account for 20.8%.

In terms of legal entity, responding firms are distributed as follows: sole proprietorship firms (65.5%), general partnership companies (16%), public companies (15.4%), and limited liability companies (3.1%).

With regard to the type of activity, the sample consists of service firms (43.6%), trading firms (41.0%), manufacturing firms (10.5%), and agricultural firms (4.9%).

As far as company size is concerned, the highest percentage (76.2%) of the respondents are small enterprises with less than ten employees, while bigger firms that employ up to 50 employees cover 16.4% of the sample and large firms of more than 50 employees account for 7.4% of the sample.

In terms of years of operation, 15.3% of the respondents operate for less than 5 years, 17.8% operate from 6 to 10 years, 21.8% operate from 11 to 15 years, 12% operate from 16 to 20 years, and 33.1% operate for over 20 years.

With regard to ownership of the firm, the majority of the participating firms were owners (84.3%), while the remaining 15.7% were tenants.

As regards fixed assets ownership, 53.2% of the production facilities were owned whereas 46.8% were rented or leased.

The distribution of responses on all the questions regarding awareness, preparedness, and resilience is presented in the following tables (Tables 1, 2a, 2b, and 3).

Results indicate that the majority of the premises were built under legal construction permit. However, there is a significant percentage of companies (22.3%) that failed to fully comply whether during construction or during operation. Moreover, at almost one every five companies (18.2%) there are other plants in close vicinity that use hazardous or flammable materials. A significant percentage of companies lack safety systems (24.7%) or emergency exits (27.4%).

Furthermore, it is found that four out of ten companies (37.5%) fail to store important documents in safe location, while a high percentage (69%) lacks an alternative production site in case of damage at the main site.

The vast majority of sample firms (99.4%) holds a legal operational permit and provides a safe working environment (97.2%).

Distribution of responses on awareness and preparedness against catastrophic events is displayed in Tables 1, 2a, and 2b. It is worth noting that most companies (83.8%) are unaware of state bureaucracy when claiming financial aid. Many respondents seem to lack knowledge of potential sources of compensation and how to claim it (68.4%). According to the perception of the firms that participated in the survey, in case a disastrous event takes place, product’s demand is expected to

Table 1 Responses on awareness

Questions	Yes	No	Total
Do you have any prior experience with bureaucracy when claiming financial aid by the state?	52 (16.2%)	269 (83.8%)	321 (100%)
Do you know the source of compensation you are entitled of and how you can claim it?	103 (31.6%)	223 (68.4%)	326 (100%)
Do you know the exact definition of a business continuity plan and/or a restoration plan for a company’s operations in case a catastrophic event occurs?	84 (25.9%)	240 (74.1%)	324 (100%)

Table 2a Responses on preparedness (surroundings and legal compliance)

Questions	Yes	No	Total
Is your company located in a high seismic activity area?	142 (43%)	189 (57%)	331 (100%)
Were there any prior flood events in the vicinity of your company?	60 (18.6%)	262 (81.4%)	322 (100%)
Is there any flood protection infrastructure in the vicinity?	118 (37.6%)	196 (62.4%)	314 (100%)
Do your operational facilities operate inside an urban planning area?	261 (80.1%)	65 (19.9%)	326 (100%)
Is the land use in compliance with legislative framework in force?	299 (96.5%)	11 (3.5%)	310 (100%)
Are there any industries handling hazardous or flammable materials (i.e., refineries, gas stations, chemical plants, etc.) in the vicinity?	59 (18.2%)	266 (81.8%)	325 (100%)
Was there a construction permit issued before construction of your company's facilities?	311 (97.2%)	9 (2.8%)	320 (100%)
Have your company's facilities been built according to the issued construction permit (are facilities legally built)?	304 (95.9%)	13 (4.1%)	317 (100%)
Have any construction discrepancies occurred?	70 (22.3%)	244 (77.7%)	314 (100%)
Does your company have a legal operation permit?	323 (99.4%)	2 (0.6%)	325 (100%)
Do you provide a safe and healthy working environment for your employees in accordance to legal requirements?	312 (97.2%)	9 (2.8%)	321 (100%)

Table 2b Responses on preparedness (measures taken within companies)

Questions	Yes	No	Total
Is there an insurance contract covering the firm against catastrophic and emergency situations?	143 (44.5%)	178 (55.5%)	321 (100%)
Are there any safety systems in place?	247 (75.3%)	81 (24.7%)	328 (100%)
Are there any heavy machinery and/or sensitive equipment on site?	96 (29.4%)	230 (70.6%)	326 (100%)
Are there any emergency exits?	239 (72.6%)	90 (27.4%)	329 (100%)
Are there any backup copies of important documents stored in a safe location?	205 (62.5%)	123 (37.5%)	328 (100%)
Is there a secondary production site/location – available on demand – to host business operations in case of damage at the primary facility?	100 (31%)	223 (69%)	323 (100%)
Are there any business continuity and/or restoration plans in place for your company's operations in case of a catastrophic event?	61 (19.1%)	258 (80.9%)	319 (100%)

Table 3 Responses on resilience

Questions	Total	Not at all	Low	Medium	High	Very high
To which extent does flood protection infrastructure achieve its goal?	161 (100%)	21 (13.04%)	23 (14.3%)	51 (31.7%)	51 (31.7%)	15 (9.26%)
To which extent does your company handle hazardous materials?	328 (100%)	209 (63.7%)	65 (19.8%)	37 (11.3%)	13 (4%)	4 (1.2%)
To which extent does your company abide by safety rules?	327 (100%)	0 (0%)	28 (8.6%)	101 (30.9%)	198 (60.5%)	0 (0%)
To which extent may your facility layout expose employees at risk in case of a catastrophic event?	324 (100%)	150 (46.3%)	107 (33%)	50 (15.4%)	14 (4.3%)	3 (1.0%)
Are employees informed of which actions/procedures to follow in the event of an emergency situation?	319 (100%)	27 (8.5%)	56 (17.5%)	87 (27.3%)	101 (31.7%)	48 (15%)
In case of a catastrophic event, to which extent do you believe disruptions will occur in public networks (electricity, water, communications, etc.)	324 (100%)	17 (5.1%)	34 (10.7%)	95 (29.3%)	133 (41%)	45 (13.9%)
To which extent can you cope with an extended power loss?	328 (100%)	76 (23.2%)	86 (26.2%)	86 (26.2)	52 (15.9%)	28 (8.5%)
To which extent can you cope with an extended water supply failure?	327 (100%)	47 (14.4%)	93 (28.4%)	86 (26.3%)	70 (21.4%)	31 (9.5%)
How high will the impact of a disruption be on the equipment, raw materials, and the inventory of your company?	327 (100%)	39 (11.9%)	69 (21.1%)	95 (29.1%)	85 (26%)	39 (11.9%)
To which extent will the disruption effects allow company's operations to continue?	322 (100%)	36 (11.2%)	74 (23%)	113 (35.1%)	67 (20.8%)	32 (9.9%)
To which extent would a disruption or an interruption of company's operations compromise firm's credibility and reputation?	323 (100%)	41 (12.7%)	76 (23.5%)	89 (27.6%)	82 (25.4%)	35 (10.8%)

fluctuate (by 30.8% of the respondents), to decrease (according to 53.1% of the respondents), or to increase (perception of 32.3% of the respondents).

It is also found that 55.5% of the firms that participated in the survey are not insured against catastrophic events or other emergencies.

Finally, 74.1% of the companies are not aware of the definition of a business continuity plan, while even more (80.9%) fail to present a plan of the kind. Regretfully, it is found at a global level that small and medium enterprises stay behind in business continuity planning against catastrophic events and disaster conditions [12]. Table 3 includes respondents' perception on resilience of distinct business functions.

It is found that more than half of the respondents (54.9%) are competent of withstanding prolonged outages in public utilities' networks (see Table 3).

It has also been highlighted that at a percentage of 37.9% the consequences of a catastrophic event would seriously affect firms' equipment, inventories, and raw materials. Moreover, these consequences would allow only at three out of ten companies (30.7%) to continue their operation.

More importantly, 36.2% of the respondents believe that any interruptions or disruptions of business operations would seriously harm firm's credibility and reputation.

4 Findings and Research Hypotheses

As far as company features are concerned (legal entity, size, years of operation, ownership), they are found to relate with preparedness (prevention) for a natural catastrophic event. Particularly, when it comes to security the existence of an insurance contract seems to depend on the company's legal entity ($X^2 = 49.06$ $df = 3$ $p < 0.01$), company size ($X^2 = 51.81$ $df = 5$ $p < 0.01$), and ownership of facilities ($X^2 = 8.32$ $df = 1$ $p < 0.01$). Furthermore, security system installation depends on activity ($X^2 = 27.226$ $df = 3$ $p < 0.001$), years of operation ($X^2 = 14.019$ $df = 4$ $p < 0.01$), and company ownership ($X^2 = 4.193$ $df = 1$ $p < 0.001$). Security system installation does not depend on the ownership of facilities ($X^2 = 0.255$ $df = 1$ $p = 0.613 > 0.05$), emphasizing the awareness of companies on the significance of security measures irrespective of the entailed cost.

Moreover, emergency exit availability depends on activity ($X^2 = 15.242$ $df = 3$ $p < 0.01$), company size ($X^2 = 16.106$ $df = 5$ $p < 0.01$), and years of operation ($X^2 = 13.393$ $df = 4$ $p < 0.01$).

Prior experience with bureaucracy when claiming financial aid by the state is positively linked with companies' up-to-dateness on business continuity planning ($X^2 = 21.32$ $df = 1$ $p < 0.01$). Prior experience with bureaucracy when claiming financial aid by the state is positively linked with business continuity planning ($X^2 = 4.84$ $df = 1$ $p < 0.05$), as well.

Firms' legal entity, size, and years of operation are found to be positively correlated with the degree of preparedness (prevention measures) in the occurrence

of a catastrophic event, while ownership of the premises is found to be negatively correlated with preparedness in terms of preventive actions. This practically means that larger companies of more complex legal entity forms and more years of operation that do not own their premises show a higher degree of preparedness.

5 Discussion and Conclusions

This research highlights that there are several firms that either fail to comply with urban planning requirements and regulations or lag in preventing and coping with disaster emergencies. Smaller businesses have less developed preparedness measures and are largely unaware of continuity and recovery planning thus being more vulnerable. Moreover, this research aims to bridge the gap of relevant literature in Greece. To this end, (i) business environment is explored in terms of infrastructure, equipment, and operational compliance with legal framework in force; (ii) current conditions on disaster preventive actions are recorded; (iii) entrepreneurs' perceptions over disaster on business activities, equipment, and supplies are analyzed; and (iv) entrepreneurs' awareness level is examined in terms of business continuity planning.

The findings unveil the missing instructions for self-protection of Greek organizations and the lack of vulnerability assessment against natural risks. Vulnerability assessment is essential for the design of preventive actions leading to more resilient organizations. Furthermore, organizations should have in mind not only how to survive a catastrophic event but rather how to adjust to post-disaster conditions. In other words, crises should be prevented from happening. In case prevention is not possible, consequences of catastrophic events should be set under control.

A company's survival can be safeguarded through preparedness against disasters using business continuity planning as both the "key" and the "door" to the world of business resilience. Irrespective of their size and complexity organizations need to be adequately prepared and have a restoration and recovery plan in order to return to normal business operations following a catastrophic event. The bigger the organization, the better it copes with emerging challenges. In other words, bigger corporations enjoy better structure, more liquidity, and more effective processes of impact mitigation.

Business continuity plans for large corporations may be a costly investment, yet they are a life-saving choice for firms' survival and continuity. SMEs need to adopt this best practice of big corporations, since long-term benefits gained by such a strategy will make them less vulnerable to future disasters.

In conclusion, the better defense against disasters is vulnerability mitigation. Even if every type of risk may threaten items with different features selectively, defense mechanisms share a common denominator: resilient structures. Hence, vulnerability mitigation plans need to aim at building strong structures, resilient to risks in general, since vulnerability may be due to common causes for all risk types.

The posited research hypotheses were based on the assumption that companies' features (legal entity, size, years of operation, ownership) are irrelevant with disaster impact, prevention, and recovery. However, the findings revealed that crucial business continuity matters depend on those particular company features. More specifically, large corporations of complex legal form with many years of operation seem to be more prepared both in terms of prevention and post-disaster measures. It is found that only one in every four Greek entrepreneurs is aware of the nature and content of business continuity and recovery plans. Hence, the need is clear for governmental actions oriented to underline the significance of business continuity planning when addressing the aftermath of a disaster.

References

1. Alesch, D. J., Holly J. N., Mittler, E. & Nagy, R. (2001). Organisations at Risk: what happens when small businesses and not-for-profits encounter natural disasters? Fairfax, Public Entity Risk Institute [Avail. at: www.riskinstitute.org]
2. Altay, N. & Ramirez, A. (2010). Impact of disasters on firms in different sectors: Implications for supply chains. DePaul University and Bryant University
3. Childs D. R. & Dietrich S. (2002). Contingency Planning and Disaster Recovery. A Small Business Guide. John Wiley & Sons, Inc.
4. Diakakis, M., Priskos, G., Skordoulis, M. (2018), Public perception of flood risk in flash flood prone areas of Eastern Mediterranean: The case of Attica Region in Greece, *International Journal of Disaster Risk Reduction*, 28: 404–413. <https://doi.org/10.1016/j.ijdr.2018.03.018>
5. EEFIT (2011), The Mw9.0 Tōhoku Earthquake and Tsunami of 11th March 2011, Institution of Structural Engineers (online), www.istructe.org/resources-centre/technical-topic-areas/eeffit/eeffit-reports, Dec 2011.
6. Efthimiou, N., Psomiadis, E., Panagos, P. (2019). Fire severity and soil erosion susceptibility mapping using multi-temporal Earth Observation data: The case of Mati fatal wildfire in Eastern Attica, Greece, *CATENA*, 104320. <https://doi.org/10.1016/j.catena.2019.104320>
7. Flynn, D.T. (2007). The impact of disasters on small business disaster planning: a case study. Department of Economics, University of North Dakota, U.S.A. <https://doi.org/10.1111/j.3666.2007.01022.x>
8. Fraser, S., Raby, A., Pomonis, A., Goda, K., Chian, S. C., Macabuag, J., Offord, M., Saito, K. & Sammonds, P. (2013). Tsunami damage to coastal defences and buildings in the March 11th 2011 M w 9.0 Great East Japan earthquake and tsunami. *Bulletin of Earthquake Engineering*, 11(1), 205–239. <https://doi.org/10.1007/s10518-012-9348-9>
9. Han, Z. & Nigg, J. (2011). The influences of business and decision makers' characteristics on disaster preparedness – A study on the 1989 Loma Prieta earthquake. *International Journal of Disaster Risk Science*. 2(4): 22–31. <https://doi.org/10.1007/s13753-011-0017-4>
10. Hayakawa, K., Matsuura, T. & Okubo, F. (2015). Firm-level impacts of natural disasters on production networks: Evidence from a flood in Thailand. *Journal of the Japanese and International Economies*, 38: 244–259. <https://doi.org/10.1016/j.jipe.2015.10.001>
11. Kildow, B. A. (2011). A Supply Chain Management Guide to Business Continuity. Printed in the United States of America.
12. Kliem, R. L. & Richie, G.D. (2016). Business Continuity Planning – A Project Management Approach. Taylor & Francis Group, L.L.C. – International Standard Book Number – 13:978-1-4822-5179-1 (eBook – PDF)

13. Lacho, K.J. (2008). The Impact of Hurricane Katrina on Small Business in Ruston, Louisiana. *Academy of Strategic Management Journal*, 7. <https://www.questia.com/library/journal/1P3-1614448321/the-impact-of-hurricane-katrina-on-small-business>
14. Lal, P. (2010). Vulnerability to natural disasters: An economic analysis of the impact of the 2009 floods on the Fijian sugar belt. Australian National University. Published by Pacific Economic Bulletin
15. Lasda, O., Dikou, A., Papapanagiotou, E. (2010). Flash Flooding in Attika, Greece: Climatic Change or Urbanization?. *AMBIO*, 39, 608–611. <https://doi.org/10.1007/s13280-010-0050-3>
16. Rittinghouse, J.W. & Ransome, J.F (2006). *Disaster Recovery and Business Continuity for InfoSec Managers*. Elsevier Inc.
17. Samantha, G. (2018). The Impact of Natural Disasters on Micro, Small and Medium Enterprises (MSMEs): A Case Study on 2016 Flood Event in Western Sri Lanka. *Procedia Engineering*, 212:744–751. <https://doi.org/10.1016/j.proeng.2018.01.096>
18. Tierney, K.J. (2007). Businesses and Disasters: Vulnerability, Impacts, and Recovery. In: *Handbook of Disaster Research*, 275–296. *Handbooks of Sociology and Social Research*. Springer, New York, NY
19. Webb, G.R., Tierney, K.J. & Dahlhamer, J. M. (2000). Businesses and Disasters: Empirical Patterns and Unanswered Questions. *Natural Hazards Review*, 1(2): 83–90. [https://doi.org/10.1061/\(ASCE\)1527-6988\(2000\)1:2\(83\)](https://doi.org/10.1061/(ASCE)1527-6988(2000)1:2(83))
20. Xiao, Y. & Peacock, W.G. (2014). Do Hazard Mitigation and Preparedness Reduce Physical Damage to Businesses in Disasters? Critical Role of Business Disaster Planning. *Natural Hazards Review*, 15(3) – Permalink: [https://doi.org/10.1061/\(ASCE\)NH.1527-6996.0000137](https://doi.org/10.1061/(ASCE)NH.1527-6996.0000137)

Perishable Food Supply Chain Networks with Labor in the Covid-19 Pandemic



Anna Nagurney

Abstract The Covid-19 pandemic is a major healthcare disaster that has fundamentally transformed our daily lives and the operations of governments, businesses, healthcare operations, and educational institutions. It has elevated and expanded the role of essential workers, not only in healthcare but also in the food industry. The food industry has undergone major disruptions in the pandemic for reasons including compromised labor resources. In this paper, we develop a supply chain-generalized network optimization framework focused on perishable food. The model explicitly includes labor availability associated with the network economic activities of production, transportation, storage, and distribution in order to quantify the impacts of associated disruptions due to illnesses, physical/social distancing requirements, and decreases in labor productivity. Theoretical results are presented along with a series of numerical examples on a fresh produce product with quantification of a spectrum of pandemic-induced disruptions on product flows, demands, prices, and the profits of the food firm. We also show that including more direct demand markets for fresh produce can yield gains for the firm.

Keywords Perishable food supply chains · Labor resources · Network optimization · Disruptions · Pandemic

1 Introduction

Perishable food products including fresh produce, dairy items, meat, and fish are essential for health and well-being. The associated nutrition in such products helps to sustain life and supports a strong immune system and response to illnesses. During the Covid-19 pandemic, these vital food supply chains have been critically stressed for several reasons, including that workers are becoming ill from the

A. Nagurney (✉)

Department of Operations and Information Management, Isenberg School of Management,
University of Massachusetts, Amherst, MA, USA

e-mail: nagurney@isenberg.umass.edu

© Springer Nature Switzerland AG 2021

I. S. Kotsireas et al. (eds.), *Dynamics of Disasters*, Springer Optimization and Its Applications 169, https://doi.org/10.1007/978-3-030-64973-9_11

173

SARS-Cov-2 coronavirus with some tragically succumbing to the disease and with others reluctant to work because of fear of contagion [6]. The coronavirus has also added risk of contagion for workers engaged in supply chain network activities of production, transportation, processing, storage, and distribution since physical/social distancing may be challenging and, yet, essential to the mitigation of the spread of the virus.

Most visible, to date, as of June 2020, has been the immense negative impact of the pandemic on meat supply chains in the United States (see [14, 43]). Many of the meat supply chains for pork, beef, and chicken utilize processing plants belonging to large agribusinesses located in different states [21, 41, 38]. Close to two dozens of such plants have had to shut down due to illnesses of the workers in March and April 2020, impacting farmers and consumers alike [9]. At a time when there is growing food insecurity due to loss of jobs [26] as a consequence of the pandemic, farmers have even resorted to culling their animals when they cannot be processed [37]. Some meat processing plants, after shutting down, have undergone disinfection of their facilities, and the workers have quarantined themselves for 14 days, causing further delays and uncertainty as to the availability of fresh meat for consumers [36].

Also, with schools, restaurants, and hotels closed, the demand not only for meat but also for fresh produce as well as dairy has changed [44]. Some potato farmers, unable to get their produce processed, are resorting to discarding their ripe vegetables [3]. This dumping of food creates a huge amount of waste, results in a reduction to the farmer's incomes, and also diminishes the amount available for consumers (see, e.g., [52]). Dairy farmers also got hit early in the pandemic, and many have had to discard the milk from their cows due to processing [15]. There have also been disruptions associated with freight service provision, with truckers fearing contracting the coronavirus [8].

Furthermore, with summer approaching and the harvesting of many fresh fruits and vegetables on the horizon in the United States, migrant labor may be in short supply for picking the harvest because of reluctance to risk contracting the coronavirus [45, 35]. Clearly, we are seeing that labor is a crucial resource in perishable food supply chain networks, now compromised because of labor availability issues. Agribusiness firms and even farmers are starting to reevaluate their food supply chains even investigating possible new distribution channels and demand markets, and this is also a global issue (see [10]).

Interestingly, although economists have tackled the use of factors of production, notably, capital and labor, in production functions (see [25] and the references therein), the explicit incorporation of labor into a complete supply chain network for perishable products has not been thoroughly investigated. This is an important area of research since only when a system-wide perspective is taken can one identify the impacts of labor availability and disruptions during a pandemic on profits, costs, product waste, and consumer prices. As a side effect, there is also a quality issue since delays in a cold chain may impact the quality of the perishable product (cf. [54, 5, 31, 29]). Indeed, as noted in [54], food supply chains are different from other supply chains in that there is a continuous and significant change in the quality of the food products as they move through the pathways of entire supply chain to

points of demand and consumption. Hence, the quality of food products decreases over time, even under the best cold chain processes (see [46, 55, 40]).

Ahumada and Villalobos [1] present a review of agricultural supply chains with [13] focusing on practice and network analysis. The review of [7] details operations research applications that include agriculture and fisheries. The meat industry and, in particular, meat processing plant activities have garnered attention from operations researchers from the modeling perspective dating to 1990 [51]. For example, [2] developed an elegant mixed integer programming model focusing on meat packing operations for pork at the operational level and included worker daily hours but emphasized that they did not handle distribution. Additional recent work identifying research gaps is that of [39]. The volume edited by [4] contains a collection of articles on supply chains and finance, exemplifying a wide range of methodologies used as well as tools for risk management. Several articles therein are focused on food. Vlontzos and Pardalos [50] describe data mining and optimization issues in the food industry and note a wide range of successful case studies on fresh produce as well as processed foods. Nevertheless, a fundamental supply chain network optimization model for perishable food products that

1. includes labor on all the supply chain network economic activities;
2. can be utilized to quantify impacts of labor disruptions and
3. can be applied to different food products, with appropriate adaptations, has not, heretofore, been constructed.

In this paper, we develop a generalized supply chain network optimization model for perishable food products with the inclusion of the critical resource of labor in the supply chain network economic activities. This work extends that of [54] to include labor and its associated levels of availability. Although the literature on supply chain network optimization is rich (cf. [11, 28, 53, 31], and the references therein), it has not integrated labor into a rigorous mathematical framework for product perishability (cf. [33]). Such an integration can provide valuable insights for the management and analysis of perishable food supply chains during the pandemic and even in times when the world is not faced with a global healthcare catastrophe. This work also adds to our understanding of complex phenomena associated with dynamics of disasters (see [18, 19]). The contributions in this paper set the stage for research on other perishable product supply chains in which labor is essential and subject to disruptions as we are seeing during the Covid-19 pandemic.

This paper is organized as follows. In Sect. 2, we construct the perishable food supply chain network model with the inclusion of labor and provide the variational inequality formulation, along with the theoretical analysis. We then, in Sect. 3, propose an algorithm, which resolves the problem into closed-form expression for the product flows on the supply chain network paths at each iteration, along with the Lagrange multipliers associated with the labor availability link capacities. The algorithm is applied to compute solutions to a series of numerical examples consisting of a fresh produce product. The numerical examples quantify the impacts of labor reductions, a decrease in labor productivity, and a freight service disruption on the food firm's optimal sales, profits, labor resources, as well as the consumer

demand. We conclude with Sect. 4, in which we summarize our results and also present suggestions for future research.

2 The Perishable Food Supply Chain Network Models with Labor

We consider a single food firm, which depending upon the application can be a farm or even an agribusiness. We assume that a single perishable food product is produced (such as a meat or dairy product, fresh fruit or vegetable, etc.). The profit-maximizing food firm's supply chain network is depicted in Fig. 1. We emphasize that this topology may be adapted/modified according to the specific application. We denote the topology by the graph $G = [N, L]$, where N is the set of nodes and L is the set of links.

The top node 1 in Fig. 1 corresponds to the food firm, and the bottom nodes, w_1, \dots, w_J , correspond to the demand markets. The demand markets can be grocery stores, organizations (such as hospitals or even food banks), and/or direct consumers. We assume that there exists one directed path (or more) joining node 1 with each demand node. Note that the supply chain network topology in Fig. 1 has curved links to denote direct sales, which can even capture sales at the farm, farmers' markets, or sales direct to the other-noted demand markets above without going through storage and other shipment links. Different distribution channels are now of increasing importance to food firms because of the pandemic, as emphasized in the introduction.

As depicted in Fig. 1, the food firm is considering n_M production sites, n_C processors, and n_D distribution centers and must serve the J demand markets. The top set of links connecting the top two tiers of nodes corresponds to the food production at each of the production sites of the firm. We allow for multiple possible links connecting node 1 with its production facilities, M_1, \dots, M_{n_M} , to allow for different production technologies at different costs.

The second set of links in Fig. 1 from the production site nodes is connected to the processors of the firm and is denoted by $C_{1,1}, \dots, C_{n_C,1}$. These links correspond to the shipment links between the production sites and the processors. Different links represent different possible modes of transport. The third set of links connecting nodes $C_{1,1}, \dots, C_{n_C,1}$ to $C_{1,2}, \dots, C_{n_C,2}$ denotes the processing of the perishable food product.

The next set of nodes in Fig. 1 represents the distribution centers, and, thus, the fourth set of links connecting the processor nodes to the distribution centers is the set of shipment links. The distribution nodes are denoted by $D_{1,1}, \dots, D_{n_D,1}$. Here we also allow for multiple modes of transport. Note that faster ones may be more costly than slower ones, for example.

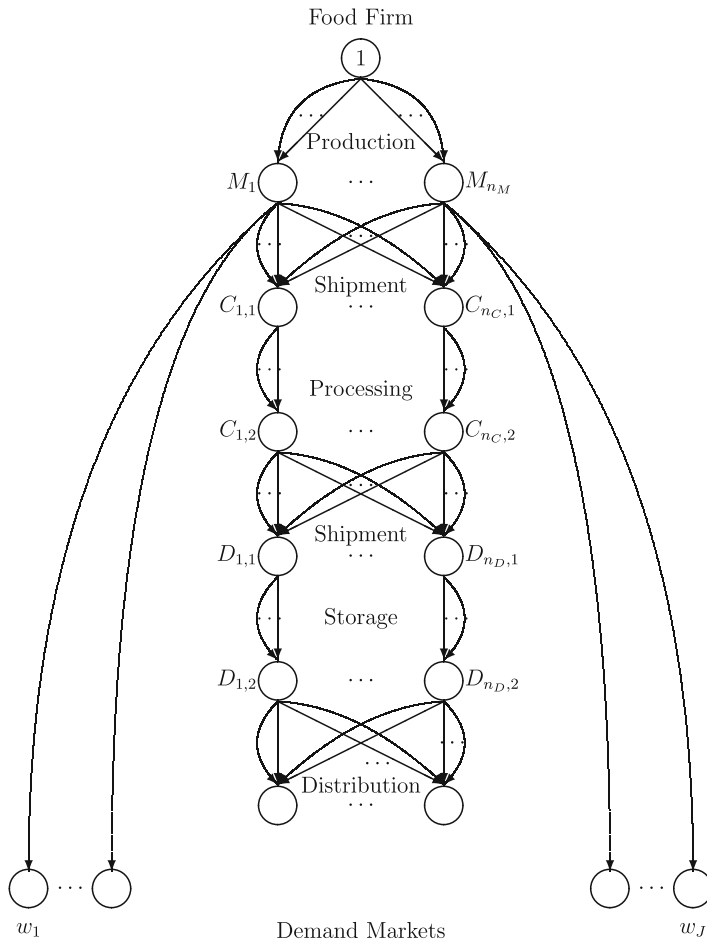


Fig. 1 The perishable food supply chain network topology

The fifth set of links in Fig. 1 connects nodes $D_{1,1}, \dots, D_{n_D,1}$ to $D_{1,2}, \dots, D_{n_D,2}$ and corresponds to the storage links. Different technologies, at associated costs, may be available for the storage network economic activity.

The final group of links in Fig. 1 connecting the two bottom tiers of the supply chain network corresponds to distribution links over which the perishable food product items are shipped from the distribution centers to the demand markets. As noted earlier, the curved links in Fig. 1 joining the upstream production nodes with the direct demand market nodes capture the possibility of on-site production and processing and direct availability, with the latter representing demand market nodes located at the farms, or at farmers' markets, or transported directly to consumers or other demand points.

A path p in the perishable food supply chain network joins node 1, which is the origin node, to a demand market node, which is a destination node. The paths are acyclic and consist of a sequence of links capturing the supply chain network activities associated with producing the perishable product and having it finally provided at the demand markets. Let P_{w_j} denote the set of paths, which represent alternative associated possible supply chain network processes, joining the pair of nodes $(1, w_j)$. P denotes the set of all paths joining node 1 to the demand market nodes. There are n_P paths in the supply chain network and n_L links. Denote a typical demand market node by w and a typical link by a . The set of all pairs of origin and demand market nodes is denoted by W .

The notation for the model is given in Table 1. All vectors are assumed to be column vectors.

The path flows must be nonnegative, that is,

$$x_p \geq 0, \quad \forall p \in P. \quad (1)$$

We handle the perishability of the product through the use of arc multipliers in a generalized network framework. Associated with each arc is an implicit time duration for completion, which can depend on the labor availability and is incorporated in the multiplier α_a for each link a . Of course, in the best scenario, one would expect full labor availability and efficient processing resulting in lower

Table 1 Notation for the perishable food supply chain network models with labor

Notation	Variables
x_p	The product flow on path p ; we group all the path flows into the vector $x \in \mathbb{R}_+^{n_P}$
f_a	The product flow on link a ; we group all the link flows into the vector $f \in \mathbb{R}_+^{n_L}$
l_a	The labor available for link a activity, $\forall a \in L$
d_{w_j}	The demand for the product at demand market w_j ; $j = 1, \dots, J$; we group the demands into the vector $d \in \mathbb{R}_+^J$
Notation	Parameters
α_a	The throughput factor on link a , which lies in the range $(0, 1]$
μ_p	The throughput on path p , where $\mu_p = \prod_{a \in p} \alpha_a$; $p \in P$
β_a	Positive factor relating inputs of labor to out of product flow on link a , $\forall a \in L$
\bar{l}_a	The upper bound on the availability of labor on link a , $\forall a \in L$
π_a	The unit cost of labor at link a , $\forall a \in L$
Notation	Functions
$\hat{z}_a(f_a)$	The discarding cost associated with link a , $\forall a \in L$
$\hat{c}_a(f)$	The total cost associated with link a , excluding the labor and discarding costs, $\forall a \in L$
$\rho_{w_j}(d)$	The demand price for the product at demand market w_j ; $j = 1, \dots, J$

food waste. Here, as argued in [54], the arc multipliers describe the decrease in quantity, which allows for the capture of the discarding of spoiled products along the pathways consisting of the supply chain links to the demand markets. Such an approach has origins in the work of [34] in studies on perishable inventory. For example, in the case of fresh produce items, such as fruits and vegetables, exponential time decay is often used. For further background on food science and food deterioration, we refer the interested reader to [48] and [12]. Here we assume that the arc multiplier α_a on production links is identically equal to 1. We now recall the definition of arc path multipliers, which were introduced for food supply chains in [54]. The multiplier, α_{ap} , which is the product of the multipliers of the links on path p that precede link a in that path, is defined as:

$$\alpha_{ap} \equiv \begin{cases} \delta_{ap} \prod_{b \in \{a' < a\}_p} \alpha_b, & \text{if } \{a' < a\}_p \neq \emptyset, \\ \delta_{ap}, & \text{if } \{a' < a\}_p = \emptyset, \end{cases} \quad (2)$$

where $\{a' < a\}_p$ denotes the set of the links preceding link a in path p and \emptyset denotes the null set. In addition, δ_{ap} is defined as equal to 1 if link a is contained in path p , and 0, otherwise. If link a is not contained in path p , then α_{ap} is set to zero. Hence, the relationship between the link flow, f_a , and the path flows can be expressed as:

$$f_a = \sum_{p \in P} x_p \alpha_{ap}, \quad \forall a \in L. \quad (3)$$

We emphasize that the above types of multipliers have also been used in other perishable product supply chain models for pharmaceuticals by [22] and for blood supply chains by [32] and [30].

In addition, here we consider the following relationship between link flows and labor:

$$f_a = \beta_a l_a, \quad \forall a \in L. \quad (4)$$

According to (4), the output on each link of product is a linear function of the labor input. This is a linear production function, according to economics (cf. [42]). Observe that with (4) we assume that the labor is applied/exerted with the product flow as at the beginning of the link a . However, what is left of f_a as the flow traverses the link, f'_a , is $\alpha_a f_a$ (see [54]).

Since we make use of a discarding cost function \hat{z}_a , for each link, we notice that:

$$f_a - f'_a = (1 - \alpha_a) f_a, \quad \forall a \in L, \quad (5)$$

so we can write that:

$$\hat{z}_a = \hat{z}_a(f_a), \quad \forall a \in L. \quad (6)$$

Also, the demand for the perishable food product at a demand market w is equal to the sum of the final product flows at the demand market, that is,

$$\sum_{p \in P_w} x_p \mu_p = d_w, \quad \forall w \in W. \quad (7)$$

Finally, the labor utilized on a supply chain network link cannot exceed the amount of labor available for that link:

$$l_a \leq \bar{l}_a, \quad \forall a \in L. \quad (8)$$

The food firm seeks to maximize its profits, which is essential for its business sustainability. The objective function faced by the firm is, hence, the difference between the revenue denoted by the sum over all the demand markets of the price the consumers are willing to pay for the product at a demand market times the demand there minus the total costs consisting of the costs associated with the links (exclusive of the labor and discarding costs), the discarding costs, and the costs associated with labor on the links:

$$\text{Maximize } \sum_{w \in W} \rho_w(d) d_w - \left(\sum_{a \in L} \hat{c}_a(f) + \hat{z}_a(f_a) \right) - \sum_{a \in L} \pi_a l_a, \quad (9)$$

subject to constraints: (1), (3), (4), (7), and (8).

We assume here that the cost functions are convex and continuously differentiable and that the demand price function is monotone decreasing and continuously differentiable. In view of (3) and (7), we can re-define the cost and demand price functions in terms of path flows as follows: $\tilde{c}_a(x) \equiv \hat{c}_a(f)$, $\forall a \in L$; $\tilde{z}_a(x) \equiv \hat{z}_a(f_a)$, $\forall a \in L$; $\tilde{\rho}_w(x) \equiv \rho_w(d)$, $\forall w \in W$.

Furthermore, in view of (3), (4), and (7), we can express objective function (9) solely in terms of path flows by incorporating these constraints directly into the objective function. Hence, the objective function (9) now becomes the following in path flows:

$$\text{Maximize } \sum_{w \in W} \tilde{\rho}_w(x) \sum_{p \in P_w} \mu_p x_p - \left(\sum_{a \in L} \tilde{c}_a(x) + \sum_{a \in L} \tilde{z}_a(x) \right) - \sum_{a \in L} \frac{\pi_a}{\beta_a} \sum_{p \in P} x_p \alpha_{ap}. \quad (10)$$

Since (3), (4), and (7) are directly incorporated into the objective function (10), we still retain the nonnegativity assumption on the path flows (1), and constraint (8) becomes, in path flows:

$$\frac{\sum_{p \in P} x_p \alpha_{ap}}{\beta_a} \leq \bar{l}_a, \quad \forall a. \quad (11)$$

Under our assumptions, the objective function (10) is convex, and the underlying feasible set is closed and convex.

2.1 Variational Inequality Formulation

In this subsection, we provide the variational inequality (VI) formulation of the above perishable food product supply chain network optimization model with labor. The solution to the supply chain network optimization model with labor is guaranteed to exist since the feasible set is bounded due to capacities on the availability of labor on the supply chain network links and, hence, also, of the product flows. This result follows from the classical theory of variational inequalities [16].

The proof of the below formulation follows from the classical theory of variational inequalities [16, 27] and the arguments as in [22] (see also [32]).

Variational Inequality Formulation

With the link labor constraint for each link a given by (11), we associate the nonnegative Lagrange multiplier λ_a and group these Lagrange multipliers into the vector $\lambda \in R_+^{nL}$. We define the feasible set $K^1 \equiv \{(x, \lambda) \in R_+^{nP+nL}\}$. The solution to the perishable food product supply chain network optimization problem is equivalent to the solution of the VI: determine $(x^*, \lambda^*) \in K^1$ such that:

$$\begin{aligned} & \sum_{w \in W} \sum_{p \in P_w} \left[\frac{\partial \hat{C}_p(x^*)}{\partial x_p} + \frac{\partial \hat{Z}_p(x^*)}{\partial x_p} + \sum_{a \in L} \frac{\pi_a}{\beta_a} \alpha_{ap} - \hat{\rho}_w(x^*) \mu_p \right. \\ & \quad \left. - \sum_{v \in W} \frac{\partial \hat{\rho}_v(x^*)}{\partial x_p} \sum_{q \in P_v} \mu_q x_q^* + \sum_{a \in L} \frac{\lambda_a^*}{\beta_a} \alpha_{ap} \right] \\ & \times \left[x_p - x_p^* \right] + \sum_{a \in L} \left[\bar{l}_a - \frac{\sum_{p \in P} x_p^* \alpha_{ap}}{\beta_a} \right] \times [\lambda_a - \lambda_a^*] \geq 0, \quad \forall (x, \lambda) \in K^1, \end{aligned} \quad (12)$$

where for each path $p \in P_w, \forall w \in W$:

$$\frac{\partial \hat{C}_p(x)}{\partial x_p} \equiv \sum_{a \in L} \sum_{b \in L} \frac{\partial \hat{c}_b(f)}{\partial f_a} \alpha_{ap}, \quad \frac{\partial \hat{Z}_p(x)}{\partial x_p} \equiv \sum_{a \in L} \sum_{b \in L} \frac{\partial \hat{z}_b(f)}{\partial f_a} \alpha_{ap}, \quad \frac{\partial \hat{\rho}_w(x)}{\partial x_p} \equiv \frac{\partial \rho_w(d)}{\partial d_w} \mu_p. \quad (13)$$

Variational inequality (12) is now put into standard form (cf. [27]): determine $X^* \in \mathcal{K}$ such that:

$$\langle F(X^*), X - X^* \rangle \geq 0, \quad \forall X \in \mathcal{K}. \quad (14)$$

where $\langle \cdot, \cdot \rangle$ denotes the inner product in n -dimensional Euclidean space.

Let $X \equiv (x, \lambda)$ and $F(X) \equiv (F_1(X), F_2(X))$ where:

$$F_1(X) = \left[\begin{aligned} & \frac{\partial \hat{C}_p(x)}{\partial x_p} + \frac{\partial \hat{Z}_p(x)}{\partial x_p} + \sum_{a \in L} \frac{\pi_a}{\beta_a} \alpha_{ap} \\ & - \hat{\rho}_w(x) \mu_p - \sum_{v \in W} \frac{\partial \hat{\rho}_v(x)}{\partial x_p} \sum_{q \in P_v} \mu_q x_q + \sum_{a \in L} \frac{\lambda_a}{\beta_a} \alpha_{ap}; w \in W; p \in P_w \end{aligned} \right],$$

$$F_2(X) \equiv \left[\bar{l}_a - \frac{\sum_{p \in P} x_p \alpha_{ap}}{\beta_a}; a \in L \right]. \quad (15)$$

3 Computational Procedure and Numerical Examples

The algorithm that we apply in this section to compute solutions to numerical examples, whose solutions satisfy VI (12), is the modified projection method of [17]. Each of the algorithm's two fundamental steps at an iteration results in closed-form expressions for the computation of the path flows as well as the Lagrange multipliers associated with the link labor capacities. Hence, the algorithm is relatively easy to implement, even in the case of a generalized network as in our perishable food product supply chain network optimization model.

Specifically, steps of the modified projection method are given below, with τ denoting an iteration counter:

The Modified Projection Method

Step 0: Initialization

Initialize with $X^0 \in \mathcal{K}$. Set the iteration counter $\tau := 1$, and let η be a scalar such that $0 < \eta \leq \frac{1}{\mathcal{L}}$, where \mathcal{L} is the Lipschitz constant (cf. (19) below).

Step 1: Computation

Compute \bar{X}^τ by solving the variational inequality subproblem:

$$\langle \bar{X}^\tau + \eta F(X^{\tau-1}) - X^{\tau-1}, X - \bar{X}^\tau \rangle \geq 0, \quad \forall X \in \mathcal{K}. \quad (16)$$

Step 2: Adaptation

Compute X^τ by solving the variational inequality subproblem:

$$\langle X^\tau + \eta F(\bar{X}^\tau) - X^{\tau-1}, X - X^\tau \rangle \geq 0, \quad \forall X \in \mathcal{K}. \quad (17)$$

Step 3: Convergence Verification

If $|X^\tau - X^{\tau-1}| \leq \epsilon$, with $\epsilon > 0$, a pre-specified tolerance, then stop; otherwise, set $\tau := \tau + 1$ and go to Step 1.

The modified projection method is guaranteed to converge to a solution of VI (13) provided that the function $F(X)$ is monotone and Lipschitz continuous (and that a solution exists). We now recall the definitions of these properties. The function $F(X)$ is said to be monotone, if:

$$\langle F(X^1) - F(X^2), X^1 - X^2 \rangle \geq 0, \quad \forall X^1, X^2 \in \mathcal{K}, \quad (18)$$

and the function $F(X)$ is Lipschitz continuous, if there exists a constant $\mathcal{L} > 0$, known as the Lipschitz constant, such that:

$$\|F(X^1) - F(X^2)\| \leq \mathcal{L}\|X^1 - X^2\|, \quad \forall X^1, X^2 \in \mathcal{K}. \quad (19)$$

These conditions we expect to hold in many reasonable applications of our model.

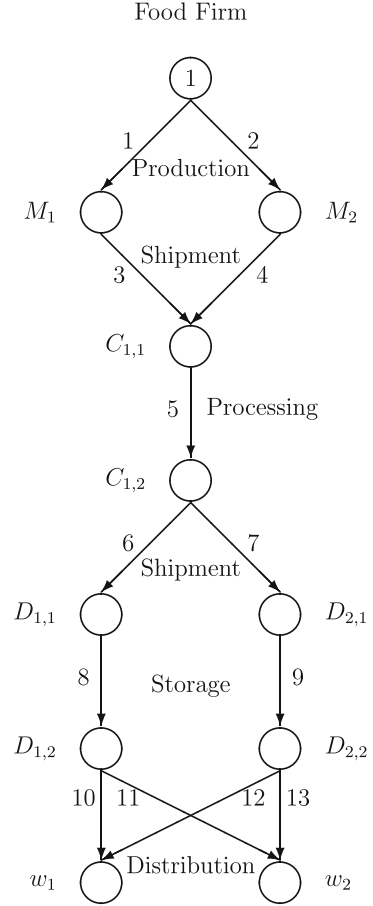
3.1 Numerical Examples

The modified projection method was implemented in FORTRAN and a Linux system at the University of Massachusetts Amherst used for the computation of solutions to the subsequent numerical examples. The numerical examples are inspired by a fresh produce application, specifically, that of cantaloupes, which are a rich source of nutrients. Cantaloupes consumed in the United States are produced in California and in Mexico and parts of Central America. Here we focus on production in the United States and consider a food firm with two production sites, a single processor, two distribution centers, and two demand markets, all of which are located in the United States. The numerical examples, hence, have the supply chain network topology depicted in Fig. 2, except where noted. The links are labeled numerically.

As noted in the introduction, perishable food products deteriorate over time even under the best conditions. Here, as in [54], from which our dataset is adapted, we assume that the temperature and other environmental conditions associated with each post-production activity/link are given and fixed. Hence, as in [34], each perishable food unit has a probability of $e^{-\gamma t}$ to survive another t units of time, where γ is the decay rate, which is given and fixed. Let N_0 denote the quantity at the beginning of the time interval (link). Then, the quantity surviving at the end of the time interval, which is implicit for each link in our supply chain network, follows a binomial distribution with parameters $n = N_0$ and probability $= e^{-\gamma t}$. Consequently, the expected quantity surviving at the end of the time interval (specific link), denoted by $N(t)$, can be expressed as:

$$N(t) = N_0 e^{-\gamma t}. \quad (20)$$

Fig. 2 The supply chain network topology for the numerical Example 1



Hence, in our application to cantaloupes, the throughput factor α_a for a post-production link a becomes:

$$\alpha_a = e^{-\gamma_a t_a}, \quad \forall a \in L, \tag{21}$$

where γ_a and t_a are the decay rate and the time duration associated with the link a , respectively; and these are given and fixed, but with the latter also adapted to factor in labor. In some cases, food deterioration follows the zero-order reactions with linear decay (see [49, 40, 5]). In that case, $\alpha_a = 1 - \gamma_a t_a$ for a post-production link.

According to [47], usually, cantaloupes can be stored for 12 through 15 days at 36 to 41 degrees Fahrenheit.

The algorithm was deemed to converge if the absolute value of the difference between each computed successive iterates was less than or equal to 10^{-7} .

Table 2 Labor costs, labor factors, labor link bounds, arc multipliers, total operational cost, and total discarding cost functions for Example 1

Link a	γ_a	t_a	α_a	β_a	π_a	\bar{l}_a	$\hat{c}_a(f)$	$\hat{z}_a(f_a)$
1	–	–	1.00	2000.00	100.00	2000.00	$.005 f_1^2 + .03 f_1$	0.00
2	–	–	1.00	3000.00	100.00	2000.00	$.006 f_2^2 + .02 f_2$	0.00
3	.150	0.20	.970	3000.00	150.00	3000.00	$.003 f_3^2 + .01 f_3$	0.00
4	.150	0.25	.963	3000.00	150.00	3000.00	$.002 f_4^2 + .02 f_4$	0.00
5	.040	0.50	.980	3000.00	110.00	4000.00	$.002 f_5^2 + .05 f_5$	$.001 f_5^2 + 0.02 f_5$
6	.015	1.50	.978	4000.00	180.00	2000.00	$.005 f_6^2 + .01 f_6$	0.00
7	.015	3.00	.956	4000.00	180.00	2000.00	$.01 f_7^2 + .01 f_7$	0.00
8	.010	3.00	.970	10000.00	120.00	3000.00	$.004 f_8^2 + .01 f_8$	$.001 f_8^2 + 0.02 f_8$
9	.010	3.00	.970	10000.00	120.00	3000.00	$.004 f_9^2 + .01 f_9$	$.001 f_9^2 + 0.02 f_9$
10	.015	1.00	.985	8000.00	170.00	20000.00	$.005 f_{10}^2 + .01 f_{10}$	$.001 f_{10}^2 + 0.02 f_{10}$
11	.015	3.00	.956	8000.00	190.00	20000.00	$.015 f_{11}^2 + .1 f_{11}$	$.001 f_{11}^2 + 0.02 f_{11}$
12	.015	3.00	.956	9000.00	180.00	20000.00	$.015 f_{12}^2 + .1 f_{12}$	$.001 f_{12}^2 + 0.02 f_{12}$
13	.015	1.00	.985	9000.00	200.00	20000.00	$.005 f_{13}^2 + .01 f_{13}$	$.001 f_{13}^2 + 0.02 f_{13}$

Example 1 (Baseline Example)

The input data for Example 1 are reported in Table 2. The decay rates reported in Table 2 are per day, and the time duration is in days. As noted in [54], the cost functions are constructed utilizing the data on the average costs available on the web (see, e.g., [23, 24] and [20]), but here we handle labor costs separately.

The demand price functions are:

$$\rho_{w_1}(d) = -.001d_{w_1} + 4, \quad \rho_{w_2}(d) = -.0001d_{w_2} + 6.$$

There are four paths for demand market w_1 : $p_1 = (1, 3, 5, 6, 8, 10)$, $p_2 = (1, 3, 5, 7, 9, 12)$, $p_3 = (2, 4, 5, 6, 8, 10)$, and $p_4 = (2, 4, 5, 7, 9, 12)$. There are also four paths for demand market w_2 : $p_5 = (1, 3, 5, 6, 8, 11)$, $p_6 = (1, 3, 5, 7, 9, 13)$, $p_7 = (2, 4, 5, 6, 8, 11)$, and $p_8 = (2, 4, 5, 7, 9, 13)$.

Since Example 1 serves as the baseline example, we set the labor bounds on the links very high for all links $a \in L$ in order to see what the food product flows, demands, prices, and profit of the food firm would be in the nonpandemic situation with many available workers for all the supply chain network economic activities.

The algorithm converges to the following optimal path flow pattern:

$$\begin{aligned} x_{p_1}^* &= 4.52, & x_{p_2}^* &= 0.00, & x_{p_3}^* &= 4.81, & x_{p_4}^* &= 0.00; \\ x_{p_5}^* &= 27.28, & x_{p_6}^* &= 38.10, & x_{p_7}^* &= 27.91, & x_{p_8}^* &= 38.15. \end{aligned}$$

The Lagrange multipliers $\lambda_a^* = 0.00$ for all links $a \in L$. The demands are $d_{w_1}^* = 8.26$ and $d_{w_2}^* = 113.86$ with prices at the demand markets of $\rho_{w_1} = 3.99$ and $\rho_{w_2} = 5.89$. These prices are reasonable for cantaloupes, a popular fruit in the

United States. The food firm earns a profit of 329.52. Note that the data for this example is on a daily basis.

Example 2 (Example with a Freight Service Disruption)

In Example 2, we consider the following scenario: The freight service providers associated with link 13 have taken ill so, in effect, that link for transport of the cantaloupes is no longer available and it is removed from the supply chain network topology of Fig. 2. All of the other data in this example remain as in Example 1. Note that paths p_6 and p_8 for demand market w_2 , therefore, no longer exist. We retain the path definitions as in Example 1.

The new optimal path flow pattern is:

$$\begin{aligned} x_{p_1}^* &= 8.71, & x_{p_2}^* &= 13.28, & x_{p_3}^* &= 8.95, & x_{p_4}^* &= 13.50; \\ x_{p_5}^* &= 32.28, & x_{p_7}^* &= 32.41. \end{aligned}$$

The Lagrange multipliers for the 12 links remain all equal to 0.00. The demand price now decreases at w_1 but increases at w_2 with $\rho_{w_1} = 3.96$ and $\rho_{w_2} = 5.94$, at the respective demands: $d_{w_1}^* = 38.12$ and $d_{w_2}^* = 55.57$. The demand at demand market w_2 has dropped by over 50% as compared to the demand in Example 1. The food firm now earns a profit of only 219.03, a 33% drop from the profit it earns in Example 1. This example demonstrates quantitatively how the lack of labor on a single link, which is a freight one may significantly negatively impact a food firm. And, during the pandemic, it has been noted that not only labor associated with food production and processing has been impacted but freight service provision has as well.

Example 3 (Example with a Freight Service Disruption and Loss of Productivity)

Example 3 has the same data as Example 2 except that now we consider even greater disruptions due to the pandemic. The disruptions affect the speed of processing due to the institution of social/physical distancing among the workers as well as the aftereffects of some having experienced the illness in themselves and/or their family units, so that workers are less productive than before.

Hence, in Example 3, we set the β_a values for all $a \in L$, to one tenth of their respective value in Table 2.

The computed optimal path flow pattern for Example 3 is:

$$\begin{aligned} x_{p_1}^* &= 0.00, & x_{p_2}^* &= 1.17, & x_{p_3}^* &= 0.00, & x_{p_4}^* &= 6.14; \\ x_{p_5}^* &= 21.38, & x_{p_7}^* &= 26.18. \end{aligned}$$

The Lagrange multipliers for the 12 links are, again, equal to 0.00.

One can see the big decrease in the cantaloupe product path flows in Example 3, as compared to the values in Example 2. Also in contrast to Example 1, now paths p_1 and p_3 are not utilized for demand market w_1 . The demand prices increase to

$\rho_{w_1} = 3.99$ and $\rho_{w_2} = 5.96$ at the demands of $d_{w_1}^* = 6.12$ and $d_{w_2}^* = 40.84$. The food firm only earns a profit of 72.96. This example emphasizes the importance of productivity in all supply chain network economic activities and the impact of a drastic reduction.

Example 4 (Example with a Freight Service Disruption, Loss of Productivity, but Increase in Price Consumers Are Willing to Pay)

Example 4 has the same data as Example 3 except that the food firm is very concerned about the loss of profits and has increased marketing so that consumers are now willing to pay a higher price for the cantaloupes at both demand markets. The fixed term in each demand price function has now doubled. Hence, the demand price functions in Example 4 are:

$$\rho_{w_1}(d) = -.001d_{w_1} + 8, \quad \rho_{w_2}(d) = -.0001d_{w_2} + 12.$$

The remainder of the data is as in Example 3.

The computed optimal path flow pattern for this example is:

$$\begin{aligned} x_{p_1}^* &= 4.46, & x_{p_2}^* &= 18.52, & x_{p_3}^* &= 7.72, & x_{p_4}^* &= 21.71; \\ x_{p_5}^* &= 59.31, & x_{p_7}^* &= 62.22. \end{aligned}$$

The Lagrange multipliers for the links are equal to 0.00.

The demands are now $d_{w_1}^* = 44.54$ and $d_{w_2}^* = 104.38$ with the demand prices 7.96 for demand market w_1 and 11.90 for demand market w_2 . We are seeing during this pandemic the escalation in prices of many perishable food products. The firm now earns a profit of 608.70, over eight times of the profit that it earns in Example 4.

Example 5 (The Cantaloupe Supply Chain Under Further Stress Because of the Pandemic)

Example 5 represents the most stressed supply chain network example.

The data for Example 5 are as in Example 4 except for the following. The availability of labor is now severely compromised so that the \bar{l}_a values are $\frac{1}{1000}$ the respective value in Example 4; that is, $\bar{l}_1 = 2.00$, $\bar{l}_2 = 2.00$, and so on. Also, the link labor factors are now $\frac{1}{10}$ their respective values in Example 4. Hence, we now have $\beta_1 = 20.00$, $\beta_2 = 30.00$, and so on. With the demand price functions as in Example 4, the solution results in all cantaloupe product flows and Lagrange multipliers being identically equal to 0.00.

The food firm is very concerned for its viability and business sustainability in the pandemic. With extraordinary, subsequent marketing efforts, the firm has influenced consumers' willingness to pay higher prices for their nutritious product. And now the demand price functions are:

$$\rho_{w_1}(d) = -.001d_{w_1} + 40, \quad \rho_{w_2}(d) = -.001d_{w_2} + 60.$$

The remainder of the data remain as immediately above. Now the optimal solution is as follows. The optimal product path flows are:

$$\begin{aligned}x_{p_1}^* &= 0.00, & x_{p_2}^* &= 0.00, & x_{p_3}^* &= 0.00, & x_{p_4}^* &= 0.00; \\x_{p_5}^* &= 24.97, & x_{p_7}^* &= 59.84.\end{aligned}$$

The Lagrange multipliers are all equal to 0.00 except that now we have that:

$$\lambda_2^* = 30.8309, \quad \lambda_5^* = 65.5255.$$

Indeed, the second production site and the storage facility are utilizing the labor at their respective bound.

Observe that the food firm has no product consumed at demand market w_1 and only at demand market w_2 where $d_{w_2}^* = 72.75$. The demand price at demand market w_2 is 31.93. The firm, by having consumers willing to pay a higher price, now garners a profit of 407.54, even under very restricted labor and impaired productivity.

Example 6 (Example with Added Direct Sale Demand Markets)

Given the results in Example 5, the food firm has decided to investigate the possibility of direct sales as depicted in Fig. 3.

There are, hence, two added demand markets w_3 and w_4 with added links 14 and 15. Path $p_9 = (1, 14)$ and path $p_{10} = (2, 15)$. The cost data on the direct demand market links are:

$$\hat{c}_{14}(f) = .0025 f_{14}^2 + .01 f_{14}, \quad \hat{c}_{15}(f) = .0025 f_{15}^2 + .02 f_{15},$$

and the waste disposal costs are:

$$\hat{z}_{14}(f) = .0005 f_{14}^2, \quad \hat{z}_{15}(f) = .0005 f_{15}^2.$$

Also, the new link data parameters and labor bounds are:

$$\begin{aligned}\beta_{14} &= 40.00, & \beta_{15} &= 40.00; \\ \pi_{14} &= 120.00, & \pi_{15} &= 120.00; \\ \alpha_{14} &= .99, & \alpha_{15} &= .99; \\ \bar{l}_{14} &= 5.00, & \bar{l}_{15} &= 5.00.\end{aligned}$$

The demand price functions at the new direct demand markets are:

$$\rho_{w_3}(d) = -.001d_{w_3} + 18, \quad \rho_{w_4}(d) = -.001d_{w_4} + 20.$$

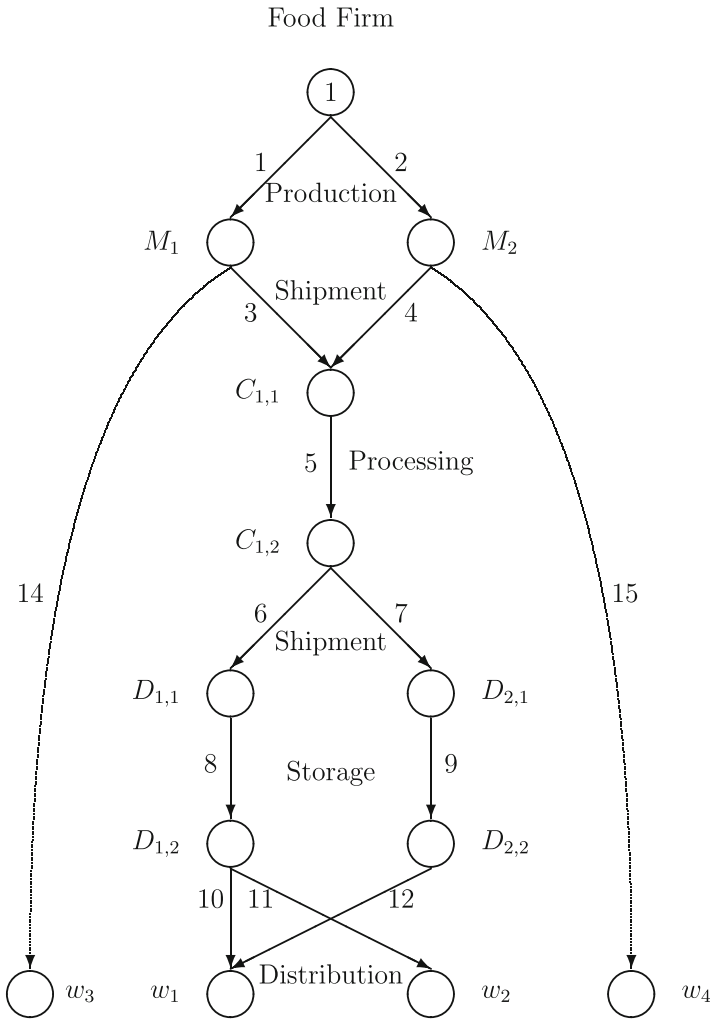


Fig. 3 The supply chain network topology for Example 6

The rest of the data remain as in Example 5.

The modified projection method yielded the following optimal solution: The optimal product flows are:

$$x_{p_1}^* = 0.00, \quad x_{p_2}^* = 0.00, \quad x_{p_3}^* = 0.00, \quad x_{p_4}^* = 0.00;$$

$$x_{p_5}^* = 0.00, \quad x_{p_7}^* = 0.00,$$

$$x_{p_9}^* = 38.93, \quad x_{p_{10}}^* = 59.63.$$

and the optimal Lagrange multipliers are:

$$\lambda_1^* = 180.76, \quad \lambda_2^* = 368.18,$$

with all other Lagrange multipliers identically equal to 0.00.

The demand for the cantaloupes is 0.00 at demand markets w_1 and w_2 . Now all sales are at the new direct demand markets with $d_{w_3}^* = 38.54$ and $d_{w_4}^* = 59.04$ at prices $\rho_{w_3} = 17.96$ and $\rho_{w_4} = 19.94$. The profit of the food firm now rises to 1,131.31.

This example is also illustrative and shows that more direct sales, whether at farmers' markets or nearby farm stands, may help a food firm in a pandemic. Many perishable product firms are now seriously considering new distribution channels with restaurants, schools, and many businesses that they would provision with food now shut down.

4 Summary and Conclusions and Suggestions for Future Research

The Covid-19 pandemic is a major healthcare disaster that has fundamentally transformed our daily lives and the operations of governments, businesses, healthcare, and educational institutions. It has brought to the fore the importance of essential workers, which now include farmers, food processors, and grocery workers. At a time when consumers need nutritious foods more than ever, there have been serious disruptions to food supply chains due, in part, to reduction of labor capacity. The reduction is occurring for multiple reasons, including Covid-19 illness, loss of life, fear to go to work, and the closure of food facilities due to the need for sanitization and even redesign because of the importance of social/physical distancing. Furthermore, many food items, including fresh produce, meat, fish, and dairy, are perishable food products, and their quality deteriorates even under the best conditions. The negative impacts of labor shortfalls and decreases in productivity are being felt in all supply chain network economic activities from production to distribution.

In this paper, we develop the first rigorous supply chain network optimization framework to explicitly include labor and bounds on labor on links for perishable food. The approach is that of a generalized network, and the food firm is interested in maximizing profits (for its business sustainability) with the objective function including revenue with the demand price functions being a function of the demand and operational and discarding costs as well as costs of labor. We utilize, in effect, linear production functions that map labor on a link to product flow. A variational inequality formulation of the problem is derived, which enables the effective computation of the solution consisting of food product flows and Lagrange multipliers associated with the capacities on labor.

A series of numerical examples is presented based on a fresh produce product, that of cantaloupes, in which the quality deterioration is also captured. We consider the impacts of labor disruptions in terms of availability as well as productivity and the potential of direct demand markets on the food firm's profit, demand market prices, product flows, and demands. We emphasize that this is just the first step in modeling labor within a general supply chain network optimization framework. Future research can include adapting the model and parameterizing it for different fresh produce items and also for meat, fish, and dairy. In addition, the possibility exists of having the arc multipliers be a function of product flow. Furthermore, since other products are perishable, such as blood, and essential in numerous medical procedures and treatments, studying the impacts of labor availability, and even donor willingness to donate during the pandemic, would merit attention.

Acknowledgments This paper is dedicated to the farmers, freight service providers, and grocery workers who sacrificed so much to sustain us with food during the Covid-19 pandemic. Thank you.

The author also acknowledges and thanks Jose Figueroa and Stephen Cumberbatch, the outstanding systems administrators in Engineering Computer Services at UMass Amherst, who even in a pandemic assisted me and kept the computer server operational.

The author thanks the three anonymous reviewers for helpful comments and suggestions on an earlier version of this paper.

References

1. Ahumada, O., Villalobos, J., 2009. Application of planning models in the agri-food supply chain: A review. *European Journal of Operational Research*, 196(1), 1–20.
2. Alborno, V.M., Gonzalez-Araya, M., Gripe, M.C., Rodriguez, S.V., 2015. A mixed integer linear program for operational planning in a meat packing plant. In: *Proceedings of the International Conference on Operations Research and Enterprise Systems (ICORES-2015)*, pp. 254–261.
3. Associated Press, 2020. Coronavirus pandemic leads to Idaho potato market woes. April 27. Available at: <https://idahonews.com/news/coronavirus/coronavirus-pandemic-leads-to-idaho-potato-market-woes>
4. Baurakis, G., Migdalas, A., Pardalos, P.M., Editors, 2004. *Supply Chain and Finance*. World Scientific Publishing Co., Singapore.
5. Besik, D., Nagurney, A., 2017. Quality in competitive fresh produce supply chains with application to farmers' markets. *Socio-Economic Planning Sciences*, 60, 62–76.
6. Bjattarai, A., Reiley, L., 2020. The companies that feed America brace for labor shortages and worry about restocking stores as coronavirus pandemic intensifies. *The Washington Post*. March 13. Available at: <https://www.washingtonpost.com/business/2020/03/13/food-supply-shortage-coronavirus/>
7. Bjorndal, T., Herrero, I., Newman, A., Romero, C., Weintraub, A., 2012. Operations research in the natural resource industry. *International Transactions in Operational Research*, 19, 39–62.
8. CBSSacramento, 2020. Trucking through coronavirus pandemic: Drivers describe new changes on the road. April 7. Available at: <https://sacramento.cbslocal.com/2020/04/07/truck-drivers-coronavirus-pandemic/>
9. Corkery, M., Yaffe-Bellany, D., 2020. The food chains weakest link: Slaughterhouses. *The New York Times*. April 18.

10. Cullen, M.T., 2020. COVID-19 and the risk to food supply chains: How to respond? Food and Agricultural Organization of the United Nations. March 29, Rome, Italy Rome. <https://doi.org/10.4060/ca8388en>
11. Geunes, J., Pardalos, P.M., 2003. Network optimization in supply chain management and financial engineering: An annotated bibliography. *Networks*, 42(2), 66–84.
12. Gustavsson, J., Cederberg, C., Sonesson, U., van Otterdijk, R., Meybeck, A., 2011. Global food losses and food waste. The Food and Agriculture Organization of the United Nations, Rome, Italy.
13. Higgins, A., Miller, C., Archer, A., Ton, T., Fletcher, C., McAllister, R., 2010. Challenges of operations research practice in agricultural value chains. *Journal of the Operational Research Society*, 61(6), 964–973.
14. Hirtzer, M., Skerrit, J., 2020. Americans on cusp of meat shortage with food chain breaking down. Bloomberg, April 27. Available at: <https://www.bloomberg.com/news/articles/2020-04-27/americans-face-meat-shortages-while-farmers-are-forced-to-cull>
15. Huffstutter, P.J., 2020. U.S. dairy farmers dump milk as pandemic upends food markets. Reuters. April 7.
16. Kinderlehrer, D., Stampacchia, G., 1980. *An Introduction to Variational Inequalities and Their Applications*. Academic Press, New York.
17. Korpelevich, G.M., 1977. The extragradient method for finding saddle points and other problems. *Matekon*, 13, 35–49.
18. Kotsireas, I.S., Nagurney, A., Pardalos, P.M., Editors, 2016. *Dynamics of Disasters: Key Concepts, Models, Algorithms, and Insights*. Springer International Publishing Switzerland.
19. Kotsireas, I.S., Nagurney, A., Pardalos, P.M., Editors, 2018. *Dynamics of Disasters: Algorithmic Approaches and Applications*. Springer International Publishing Switzerland.
20. LeBouef, J., 2002. Crop time line for cantaloupes, honeydews, and watermelons in California. AgriDataSensing, Inc., October 11. Available at: <https://ipmdata.ipmcenters.org/documents/timelines/CAmelon.pdf>
21. Little, A., 2020. A pork panic won't save our bacon. Bloomberg Opinion. April 30.
22. Masoumi, A.H., Yu, M., Nagurney, A., 2012. A supply chain generalized network oligopoly model for pharmaceuticals under brand differentiation and perishability. *Transportation Research E*, 48, 762–780.
23. Meister, H.S., 2004a. Sample cost to establish and produce cantaloupes (slant-bed, spring planted). U.C. Cooperative Extension – Imperial County Vegetable Crops Guidelines, August.
24. Meister, H.S., 2004b. Sample cost to establish and produce cantaloupes (mid-bed trenched). U.C. Cooperative Extension – Imperial County Vegetable Crops Guidelines, August.
25. Mishra, S.K., 2007. A brief history of production functions. MPRA Paper No. 5254, <http://mpra.ub.uni-muenchen.de/5254/>.
26. Morath, E., 2020. How may U.S. workers have lost jobs during coronavirus pandemic? There are several ways to count. *The Wall Street Journal*, June 3.
27. Nagurney, A., 1999. *Network Economics: A Variational Inequality Approach*, second and revised edition. Kluwer Academic Publishers, Dordrecht, The Netherlands.
28. Nagurney, A. 2006. *Supply Chain Network Economics: Dynamics of Prices, Flows and Profits*. Edward Elgar Publishing, Cheltenham, England.
29. Nagurney, A., Besik, D., Yu, M., 2018. Dynamics of quality as a strategic variable in complex food supply chain network competition: The case of fresh produce. *Chaos* 28, 043124.
30. Nagurney, A. Dutta, P., 2019. Supply chain network competition among blood service organizations: A generalized Nash Equilibrium framework. *Annals of Operations Research*, 275(2), 551–586.
31. Nagurney, A., Li, D., 2016. *Competing on Supply Chain Quality: A Network Economics Perspective*. Springer International Publishing Switzerland.
32. Nagurney, A., Masoumi, A.H., Yu, M., 2012. Supply chain network operations management of a blood banking system with cost and risk minimization. *Computational Management Science*, 9(2), 205–231.

33. Nagurney, A., Yu, M., Masoumi, A.H., Nagurney, L.S., 2013. *Networks Against Time: Supply Chain Analytics for Perishable Products*. Springer Science+Business Media, New York, NY.
34. Nahmias, S., 1982. Perishable inventory theory: a review. *Operations Research* 30(4), 680708.
35. Nickel, R., Walljasper, C., 2020. Canada, U.S. farms face crop losses due to foreign worker delays. Reuters, April 6.
36. Pitt, D., 2020. Virus is expected to reduce meat selection and raise prices. NECN, April 27. Available at: <https://www.necn.com/news/national-international/virus-is-expected-to-reduce-meat-selection-and-raise-prices/2265023/>
37. Polansek, T., Huffstutter, P.J., 2020. Piglets aborted, chickens gassed as pandemic slams meat sector. Reuters, April 27. Available at: <https://www.reuters.com/article/us-health-coronavirus-livestock-insight/piglets-aborted-chickens-gassed-as-pandemic-slams-meat-sector-idUSKCN2292YS>
38. Reiley, L., 2020. Meat processing plants are closing due to Covid-19 outbreaks. Beef shortfalls may follow. *The Washington Post*. April 16.
39. Rodriguez, S., Pla, L., Faulin, J., 2014. New opportunities in operations research to improve pork supply chain efficiency. *Annals of Operation Research*, 219, 5–23.
40. Rong, A., Akkerman, R., Grunow, M., 2011. An optimization approach for managing fresh food quality throughout the supply chain. *International Journal of Production Economics*, 131(1), 421–429.
41. Rosane, O., 2020. Meat processing plants close as working conditions encourage spread of coronavirus. *EcoWatch*. April 14.
42. Samuelson, W.F., Marks, S.G., 2012. *Managerial Economics*, seventh edition. John Wiley & Sons, Inc., Hoboken, New Jersey.
43. Scheiber, N., Corkery, M., 2020. Missouri pork plant workers way they cant cover mouths to cough. *The New York Times*. April 24.
44. Schrottenboer, B., 2020. US agriculture: Can it handle coronavirus, labor shortages and panic buying? *USA Today*. April 4.
45. Shoichet, C.E., 2020. The farmworkers putting food on America's tables are facing their own coronavirus crisis. *CNN.com*. April 11. Available at: <https://www.cnn.com/2020/04/11/us/farmworkers-coronavirus/index.html>
46. Sloof, M., Tijkskens, L.M.M., Wilkinson, E.C., 1996. Concepts for modelling the quality of perishable products. *Trends in Food Science & Technology*, 7(5), 165–171.
47. Sushow, T.V., Cantwell, M., Mitchell, J., 1997. Cantaloupe: Recommendations for maintaining postharvest quality. Department of Vegetable Crops, University of California, Davis, California.
48. Thompson, J.F., 2002. Waste management and cull utilization. In *Postharvest Technology of Horticultural Crops*, third edition, Kader, A.A., Editor, University of California Agriculture & Natural Resources, Publication 3311, Oakland, CA, pp. 81–84.
49. Tijkskens, L.M.M., Polderdijk, J.J., 1996. A generic model for keeping quality of vegetable produce during storage and distribution. *Agricultural Systems*, 51(4), 431–452.
50. Vlontzos, G., Pardalos, P.M., 2017. Data mining and optimisation issues in the food industry. *International Journal of Sustainable Agricultural Management and Informatics*, 3(1), 44–64.
51. Whitaker, D., Cammel, S., 1990. A partitioned cutting stock problem applied on the meat industry. *Journal of the Operational Research Society*, 41(9), 801–807.
52. Wootson, Jr., C.R., 2020. As produce rots in the field, one Florida farmer and an army of volunteers combat a feeling of helplessness one cucumber at a time. *Washington Post*, April 30.
53. Wu, T., Blackhurst, J., Editors, 2009. *Managing Supply Chain Risk and Vulnerability: Tools and Methods for Supply Chain Decision Makers*. Springer, London, England.
54. Yu, M., Nagurney, A., 2013. Competitive food supply chain networks with application to fresh produce. *European Journal of Operational Research*, 224(2), 273–282.
55. Zhang, G., Habenicht, W., Spiess, W.E.L., 2003. Improving the structure of deep frozen and chilled food chain with tabu search procedure. *Journal of Food Engineering*, 60, 67–79.

Capacitated Human Migration Networks and Subsidization



Anna Nagurney, Patrizia Daniele, and Giorgia Cappello

Abstract Large-scale migration flows are posing immense challenges for governments around the globe, with drivers ranging from climate change and disasters to wars, violence, and poverty. In this paper, we introduce multiclass human migration models under user-optimizing and system-optimizing behavior in which the locations associated with migration are subject to capacities. We construct alternative variational inequality formulations of the governing equilibrium/optimal conditions that utilize Lagrange multipliers and then derive formulae for subsidies that, when applied, guarantee that migrants will locate themselves, acting independently and selfishly, in a manner that is also optimal from a societal perspective. An algorithm is proposed, implemented, and utilized to compute solutions to numerical examples. Our framework can be applied by governmental authorities to manage migration flows and population distributions for enhanced societal welfare.

Keywords Human migration networks · Variational inequalities · System optimization · User optimization · Capacities · Subsidies · Societal welfare

1 Introduction

Governments of many nations are increasingly being faced with large-scale human migration flows not only within their national borders but also across their borders. The drivers of migratory flows are many, including wars, conflicts, violence and strife, and poverty, as well as challenges and disruptions posed by climate change and disasters, both sudden (earthquakes, wildfires, hurricanes, tornadoes, floods,

A. Nagurney (✉)

Department of Operations and Information Management, Isenberg School of Management, University of Massachusetts, Amherst, MA, USA
e-mail: nagurney@isenberg.umass.edu

P. Daniele · G. Cappello

Department of Mathematics and Computer Science, University of Catania, Catania, Italy
e-mail: daniele@dmf.unict.it; giorg_91@hotmail.it

tsunamis, landslides, etc.) and slow-onset (malnutrition and hunger, drought, disease epidemics, insect infestations, etc.). Migrants from time immemorial have sought a better quality of life for themselves, moving to locations to better their situations. The [53] reports that 70.8 million humans have fled their homes worldwide, the highest level of displacement ever recorded. According to the [54], since the new millennium, the number of refugees and asylum seekers has increased from 16 to 26 million, comprising about 10% of total of the international migrants. The [18] reports that there have been significant migration and displacement events during the last 2 years with such events resulting in hardship, trauma, and loss of life.

Many recent crises associated with migration have brought enhanced emphasis by both practitioners and academics on how to better address the associated challenges of migratory flows and the ultimate location of the migrants. Examples of epicenters of only a few of the migratory crises include Venezuela [23], Central America [2], Libya [50], and Syria [55], with countries such as Mexico [30], Italy [20], Greece [25], and Cyprus [52] serving as transit points for many refugees and asylum seekers in the dynamically evolving migration landscape (see also [47]).

In particular, in many reports and studies, the capacity of nations to handle migrants, and we emphasize here that there are multiple classes of migrants (cf. [22]), has risen to the fore as a critical characteristic. Examples of such studies have included even the United States in terms of migrants from Central America [43], Colombia and other countries (Costa Rica and Ecuador) because of the issues in Venezuela and Nicaragua [10], as well as multiple countries in Europe as possible destination locations of migrants [48, 17].

In this paper, we develop user-optimized (U-O) and system-optimized (S-O) multiclass models of human migration under capacities associated with the migrant classes and locations. Our work builds on that of [37], but with the generalization of the inclusion of capacities. Such a generalization is especially timely, as noted above. Moreover, to date, the majority of research on human migration networks, from an operations research and mathematical modeling perspective, has focused on the modeling of migration flows assuming user-optimizing behavior, originating with the work of [31]. In other words, it has been assumed that the migrants act selfishly and independently; see also [32, 39, 40, 45, 46, 19, 21, 9, 36, 38, 8], for a spectrum of U-O migration models. Davis et al. [15], in turn, utilize a complex network approach for human migration and utilize an international dataset for their quantitative analysis.

System optimization in multiclass human migration networks is also important since governments may wish to maximize societal welfare and hope that migrants locate accordingly. However, the latter may be extremely challenging unless proper policies/incentives are put into place. Indeed, [1] have argued for an effective cost-efficient mechanism for the distribution of refugees in the European Union, for example. Clearly, that would require some form of central control and cooperation/coordination.

Note that there are analogues to U-O and S-O network models, with a long history, in the transportation science literature (cf. [56, 3, 14, 6]). Such concepts were made explicit, for the first time, in human migration networks, by [37]. We

emphasize that in the transportation science literature, the concern is total cost minimization in the case of system optimization and individual cost minimization in the case of user optimization, along with route selection, subject to the conservation of flow equations. In the human migration network context, in contrast, we are concerned with total utility maximization in the case of S-O and individual utility maximization in the case of U-O behavior and the selection of locations.

In addition, in this paper, we provide a quantitative mechanism, in the form of subsidies, that, when applied, guarantees that the system-optimized solution of our multiclass capacitated human migration network problem is also user-optimized. This is very important, since it enables governments, and policy-making bodies, to achieve optimal societal welfare in terms of the location of the migrants in the network economy, while the migrants locate independently in a U-O manner! Our work extends that of [37] to the capacitated network economy domain. Furthermore, we provide alternative variational inequality formulations of both the new U-O and S-O models, which include Lagrange multipliers associated with the location capacity constraints as explicit variables. Their values at the equilibrium/optimal solutions provide valuable economic information for decision-makers.

This paper is organized as follows. In Sect. 2, we present the capacitated multiclass human migration network models, under S-O and under U-O behaviors. Associated with each location as perceived by a class is an individual utility function that, when multiplied by the population of that class at that location, yields the total utility function for that location and class. As in our earlier work (cf. [31], to start), the utility associated with a location and class can, in general, depend upon the vector of populations of all the classes at all the locations in the network economy. We assume a fixed population of each class in the network economy and are interested in determining the distributions of the populations among the locations under S-O and U-O behaviors. For each model, we provide alternative variational inequality formulations. We also illuminate the role that is played by the Lagrange multipliers associated with the class capacities on the locations in the network economy.

In Sect. 3, we outline the procedure for the calculation of the multiclass subsidies in order to guarantee, even in the capacitated case, that the system-optimized solution is, simultaneously, also user-optimized. Hence, once the subsidies are applied, the migrants will locate themselves individually in the network economy in a manner that is optimal from a societal perspective. As argued in [37], there are analogues of our subsidies to tolls in transportation science. In the case of congested transportation networks, the imposition of tolls (see [14, 13, 12, 29]) results in system-optimized flows also being user-optimized. In other words, once the tolls are imposed, travelers, acting independently, select routes of travel which result in a system optimum that minimizes the total cost to the society. In this paper, we construct policies for human migration networks that maximize societal welfare but in the case of capacities.

In Sect. 4, we outline the computational algorithm, which we then apply to compute solutions to numerical examples that illustrate the theoretical results in this paper in a practical format. We summarize our results and present our conclusions in Sect. 5.

2 The Capacitated Multiclass Human Migration Network Models

In this section, we construct the capacitated multiclass network models of human migration. We first present the system-optimized model and then the user-optimized one. The notation follows that in [37], where, as mentioned in the Introduction, no capacities on the populations at the locations were imposed.

We assume that the human migrants have no movement costs associated with migrating from location to location since we are concerned with the long-term population distribution behaviors under both principles of system optimization and user optimization. The network representation of the models is given in Fig. 1.

There are J classes of migrants, with a typical class denoted by k , and n locations corresponding to locations that the multiclass populations can migrate to, with a typical location denoted by i . There are assumed to be no births and no deaths in the network economy.

In the network representation, locations are associated with links. A link can correspond to a country or a region within a country, and the network economy can capture multiple countries. If a government is interested in within-country migration, exclusively, then the network economy (network) would correspond to that country.

Table 1 contains the notation for the models. All vectors here are assumed to be column vectors.

According to Table 1, there is a utility function U_i^k associated with each class k , $k = 1, \dots, J$, and location i , $i = 1, \dots, n$, which captures how attractive location i is for that class k . Observe that (see Table 1) the utility and, hence, the total utility, \hat{U}_i^k , associated with location i and class k , may, in general, depend upon the population distribution of all the classes at all the locations. The [44], for example, recognizes that different locations may be more or less attractive to distinct classes of migrants.

Fig. 1 The network structure of the multiclass human migration models

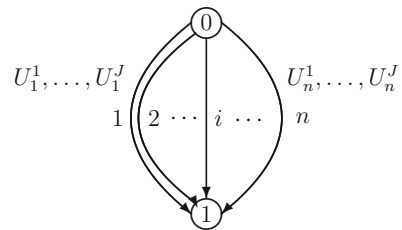


Table 1 Notation for the multiclass human migration models

Notation	Definition
p_i^k	The population of class k at location i . We group the $\{p_i^k\}$ elements into the vector $p^k \in R_+^n$. We then further group the p^k vectors, $k = 1, \dots, J$, into the vector $p \in R_+^{Jn}$
cap_i^k	The nonnegative capacity at location i for class k ; $k = 1, \dots, J; i = 1, \dots, n$
β_i^k	The Lagrange multiplier associated with capacity constraint for k at i ; $k = 1, \dots, J; i = 1, \dots, n$. We group all these Lagrange multipliers into the vector $\beta \in R_+^{Jn}$
P^k	The fixed population of class k in the network economy; $k = 1, \dots, J$
$U_i^k(p)$	The utility of individuals of class k at location i ; $i = 1, \dots, n$. We group the utility functions for each k into the vector $U^k \in R^n$ and then group all such vectors for all k into the vector $U \in R^{Jn}$
$\hat{U}_i^k(p)$	The total utility of class k at location i ; $i = 1, \dots, n$. The total utility $\hat{U}_i^k(p) = U_i^k(p) \times p_i^k; k = 1, \dots, J; i = 1, \dots, n$

We now present the constraints. The population distribution of each class among the various locations must sum up to the population of that class in the network economy, that is, for each class k ; $k = 1, \dots, J$:

$$\sum_{i=1}^n p_i^k = P^k. \tag{1}$$

Furthermore, the population of each class at each location must be nonnegative, that is,

$$p_i^k \geq 0, \quad \forall i; \forall k, \tag{2}$$

and not exceed the capacity:

$$p_i^k \leq cap_i^k, \quad \forall i; \forall k. \tag{3}$$

The feasible set $K^1 \equiv \{p \mid (1), (2), (3) \text{ hold}\}$.

We assume here that:

$$\sum_{i=1}^n cap_i^k \geq P^k, \tag{4}$$

for all classes k . In other words, we assume that the network economy has sufficient capacity to accommodate the population of each class. Hence, the feasible set K^1 is nonempty. Moreover, it is compact.

2.1 The Capacitated System-Optimized (S-O) Problem

The government (or governments), in the case of system optimization, wishes to maximize the total utility in the network economy, which reflects the societal welfare, subject to the constraints. The capacitated system-optimized (S-O) problem is:

$$\text{Maximize} \quad \sum_{k=1}^J \sum_{i=1}^n \hat{U}_i^k(p) = \sum_{k=1}^J \sum_{i=1}^n U_i^k(p) \times p_i^k \quad (5)$$

subject to constraints (1) through (3).

We assume that the total utility functions for all the classes at all the locations are concave and continuously differentiable. Then, from classical results (cf. [24] and [33]), we know that the optimal solution, denoted by p' , satisfies the variational inequality (VI) problem: determine $p' \in K^1$, such that:

$$-\sum_{k=1}^J \sum_{i=1}^n \left[\sum_{l=1}^J \sum_{j=1}^n \frac{\partial \hat{U}_j^l(p')}{\partial p_i^k} \right] \times (p_i^k - p_i^{k'}) \geq 0, \quad \forall p \in K^1. \quad (6)$$

A solution p' to VI (6) is guaranteed to exist under our imposed assumptions since the feasible set K^1 is compact and the total utility functions are continuously differentiable. Uniqueness of the solution p' then follows under the assumption that all the utility functions are strictly concave.

We now present an alternative variational inequality to the one in (6), which we utilize to compute the S-O solution in numerical examples. Furthermore, the solution of the alternative VI allows us to determine the optimal Lagrange multipliers associated with the location class capacities in the S-O context. The Lagrange multipliers at the optimal solution provide valuable economic information. We define the feasible set $K^2 \equiv \{(p, \beta) \mid (1), (2) \text{ hold and } \beta \in R_+^{Jn}\}$.

Alternative Variational Inequality Formulation of the Capacitated S-O Problem

A solution to the S-O problem also satisfies the VI: determine $(p', \beta') \in K^2$ such that:

$$\begin{aligned} -\sum_{k=1}^J \sum_{i=1}^n \left[\sum_{l=1}^J \sum_{j=1}^n \frac{\partial \hat{U}_j^l(p')}{\partial p_i^k} - \beta_i^{k'} \right] \times (p_i^k - p_i^{k'}) + \sum_{k=1}^J \sum_{i=1}^n \left[cap_i^k - p_i^{k'} \right] \\ \times (\beta_i^k - \beta_i^{k'}) \geq 0, \\ \forall (p, \beta) \in K^2. \end{aligned} \quad (7)$$

The above result follows from [4], page 287. Capacities have also been applied to links in various supply chain system-optimized problems and variational inequality formulations constructed; see, for example, [35] and [41].

2.2 The Capacitated User-Optimized (U-O) Problem

We now introduce the capacitated user-optimized version of the above S-O model. The new model extends the classical one introduced in [31] to include capacities.

The Capacitated Equilibrium Conditions

Mathematically, a multiclass population vector $p^* \in K^1$ is said to be U-O or, equivalently, a capacitated equilibrium, if for each class k , $k = 1, \dots, J$, and all locations i , $i = 1, \dots, n$:

$$U_i^k(p^*) \begin{cases} \geq \lambda^k, & \text{if } p_i^{k*} = cap_i^k, \\ = \lambda^k, & \text{if } 0 < p_i^{k*} < cap_i^k, \\ \leq \lambda^k, & \text{if } p_i^{k*} = 0. \end{cases} \quad (8)$$

From (8), one can see that locations with no population of a class are those with the lowest utilities; those locations with a positive population of a class, with the population not at the capacity for the location and class, will have equalized utility for that class and higher than the unpopulated locations of that class. Moreover, the equalized utility will be equal to an indicator λ^k . The indicator λ^k is, actually, the Lagrange multiplier associated with constraint (1) for k with the value at the equilibrium. Those locations with a class k at its capacity have a utility greater than or equal to λ^k .

A capacitated U-O solution p^* satisfies the VI: determine $p^* \in K^1$ such that:

$$\sum_{k=1}^J \sum_{i=1}^n -U_i^k(p^*) \times (p_i^k - p_i^{k*}) \geq 0, \quad \forall p \in K^1. \quad (9)$$

We now prove the equivalence of the solution to the capacitated equilibrium conditions (8) and the VI (9).

Indeed, it is easy to see that, according to (8), for a fixed k and i , the equilibrium conditions imply that:

$$\left[\lambda^k - U_i^k(p^*) \right] \times \left[p_i^k - p_i^{k*} \right] \geq 0, \quad \forall p_i^k : 0 \leq p_i^k \leq cap_i^k. \quad (10)$$

Observe that, if $p_i^{k*} = 0$, (10) holds true; if $p_i^{k*} = cap_i^k$, then (10) also holds; and (10) also holds if $0 < p_i^{k*} < cap_i^k$.

Summing now (10) over all k and all i yields:

$$\sum_{k=1}^J \sum_{i=1}^n [\lambda^k - U_i^k(p^*)] \times [p_i^k - p_i^{k*}] \geq 0, \quad \forall p \in K^1. \quad (11)$$

But, because of (1), (11) simplifies to precisely (9).

Furthermore, we now show that if p^* satisfies VI (9), then the p^* also satisfies the capacitated equilibrium conditions (8).

In (9), we set $p_i^l = p_i^{k*}$ for all $l \neq k$, which yields:

$$\sum_{i=1}^n -U_i^k(p^*) \times (p_i^k - p_i^{k*}) \geq 0, \quad \forall p_i^k : 0 \leq p_i^k \leq \text{cap}_i^k; \quad \sum_{i=1}^n p_i^k = P^k. \quad (12)$$

If there are two locations, say, r and s with positive populations not at their capacities, set for a sufficiently small $\epsilon > 0$:

$$p_r^k = p_s^{k*} - \epsilon; \quad p_s^k = p_r^{k*} + \epsilon$$

and all other p_i^k s equal to p_i^{k*} . Clearly, such a population distribution is also feasible. Substitution into (12) yields, after algebraic simplification:

$$(-U_r^k(p^*) + U_s^k(p^*)) \times (p_s^{k*} - p_r^{k*} - \epsilon) \geq 0. \quad (13)$$

Similarly, by constructing another feasible population pattern:

$$p_r^k = p_s^{k*} + \epsilon, \quad p_s^k = p_r^{k*} - \epsilon,$$

with all other $p_i^k = p_i^{k*}$, and substitution into (12) yields:

$$(U_r^k(p^*) - U_s^k(p^*)) \times (p_s^{k*} - p_r^{k*} - \epsilon) \geq 0. \quad (14)$$

Equations (13) and (14) can only hold true if:

$$U_r^k(p^*) = U_s^k(p^*)$$

which we call λ^k . Hence, the second condition in (8) has been established.

On the other hand, suppose that $p_i^{k*} \geq 0$ for all i , but $p_r^{k*} > 0$ and $p_s^{k*} = 0$. For a sufficiently small $\epsilon > 0$, construct $p_r^k = p_r^{k*} - \epsilon$ and $p_s^k = p_s^{k*} + \epsilon$, with all other p_i^k s equal to p_i^{k*} , and substitute these values into (12). After, algebraic simplification, we obtain:

$$(U_r^k(p^*) - U_s^k(p^*))\epsilon \geq 0,$$

hence,

$$U_r^k(p^*) \geq U_s^k(p^*)$$

and the third condition in (8) is verified.

Now, in order to verify that a solution to VI (9) also satisfies the top condition in (8), if for some location r , $p_r^{k*} = cap_r^k$, then we construct a feasible distribution pattern such that:

$$p_r^k = p_r^{k*} - \epsilon, \quad p_s^k = p_s^{k*} + \epsilon,$$

with $\epsilon > 0$ sufficiently small and all other $p_i^k = p_i^{k*}$. Substitution into (12), after algebraic simplification, yields:

$$U_r^k(p^*) \geq U_s^k(p^*)$$

and the conclusion follows. With the above arguments, we have shown that a capacitated equilibrium p^* is equivalent to the solution of the VI (9).

We now provide an alternative VI formulation of the capacitated equilibrium conditions. This result is immediate by making note of [31] demonstrating that the U-O human migration model (without capacities) is isomorphic to a traffic network equilibrium problem (cf. [14, 11]) and, hence, in the case of capacities, also isomorphic to a traffic network equilibrium problem with side constraints (see [28]) and with special structure.

Alternative Variational Inequality Formulation of the U-O Problem

The U-O solution satisfies the variational inequality problem: determine $(p^*, \beta^*) \in K^2$ such that:

$$\sum_{k=1}^J \sum_{i=1}^n [-U_i^k(p^*) + \beta_i^{k*}] \times (p_i^k - p_i^{k*}) + \sum_{k=1}^J \sum_{i=1}^n [cap_i^k - p_i^{k*}] \times (\beta_i^k - \beta_i^{k*}) \geq 0, \forall (p, \beta) \in K^2. \tag{15}$$

2.3 Illustrative Examples

We first present an uncapacitated example for which we provide U-O and S-O solutions. We then add capacities to the locations and report the new U-O and S-O solutions. There is a single class in the network economy and three locations. The total population is $P^1 = 120$, and the utility functions at the three locations are:

$$U_1^1(p) = -p_1^1 + 190, \quad U_2^1(p) = -p_2^1 + 200, \quad U_3^1(p) = -p_3^1 + 210.$$

The user-optimized solution is:

$$p_1^{1*} = 30.00, \quad p_2^{1*} = 40.00, \quad p_3^{1*} = 50.00,$$

yielding $\lambda^1 = 160$, since:

$$U_1^1(p^*) = U_2^1(p^*) = U_3^1(p^*) = 160.00.$$

The S-O solution, on the other hand, is:

$$p_1^{1'} = 35.00, \quad p_2^{1'} = 40.00, \quad p_3^{1'} = 45.00.$$

We now impose capacities as follows:

$$cap_1^1 = 60.00, \quad cap_2^1 = 60.00, \quad cap_3^1 = 30.00,$$

and solve for the U-O and S-O solutions.

The new U-O solution, satisfying VI (15), is:

$$p_1^{1*} = 40.00, \quad p_2^{1*} = 50.00, \quad p_3^{1*} = 30.00,$$

with Lagrange multipliers associated with the capacities of:

$$\beta_1^{1*} = 0.00, \quad \beta_2^{1*} = 0.00, \quad \beta_3^{1*} = 30.00.$$

The new S-O solution, satisfying VI (7), is:

$$p_1^{1'} = 42.50, \quad p_2^{1'} = 47.50, \quad p_3^{1'} = 30.00,$$

with Lagrange multipliers associated with the capacities of:

$$\beta_1^{1'} = 0.00, \quad \beta_2^{1'} = 0.00, \quad \beta_3^{1'} = 45.00.$$

Observe that the S-O solution is distinct from the U-O solution in both the uncapacitated and the capacitated versions.

Remark We now show how the optimal Lagrange multipliers can be utilized. For example, if one modifies the utility functions by reducing each of them by the value of the optimal Lagrange multiplier associated with the location and the class, then the same user-optimizing solution is obtained as the one for the problem with the corresponding capacities. Indeed, proceeding as above, we modify the utility functions as:

$$\tilde{U}_1^1(p) = -p_1^1 + 190 - 0 = -p_1^1 + 190,$$

$$\tilde{U}_2^1(p) = -p_2^1 + 200 - 0 = -p_2^1 + 200,$$

$$\tilde{U}_3^1(p) = -p_3^1 + 210 - 30 = -p_3^1 + 180,$$

and observe that the capacitated U-O solution $p_1^{1*} = 40.00$, $p_2^{1*} = 50.00$, and $p_3^{1*} = 30.00$ remains optimal.

Similarly, one can modify the utility functions in the same manner, but by using the optimal Lagrange multipliers for the S-O problem, to obtain the same S-O solution as for the problem with the capacities.

Hence, government decision-makers, in order to limit the population of certain (or all) classes at certain (or all) locations, can accomplish this through regulations corresponding to the capacities or by modifying the utility functions accordingly to yield the same result.

Now, we describe how subsidies (which may be viewed as a positive intervention) can, once imposed, make the capacitated S-O solution also a capacitated U-O one.

3 Subsidies to Guarantee the Capacitated S-O Solution Is Also a Capacitated U-O Solution

In [37], a procedure was introduced for the calculation of subsidies that, once applied to the locations with a positive population of a class under S-O, guaranteed that migrants operating under the U-O behavioral principle would select locations that were also optimal from a societal standpoint; that is, they were system-optimized.

Here we show that the same general construct is also applicable to capacitated problems of human migration.

The procedure is as follows. We first solve for the capacitated system-optimized solution p' satisfying VI (7) or, equivalently, VI (6). For each class k , we denote those locations with a positive population by k_1, \dots, k_{n_k} , where n_k is the number of locations in the network economy with a positive population of class k . We also introduce notation for subsidies associated with the different locations for each class denoted by class k by $(subsidy)_{k_1}, (subsidy)_{k_2}, \dots, (subsidy)_{k_{n_k}}$. We then enumerate those locations in a list as follows:

$$\begin{aligned} U_{k_1}^k(p') + subsidy_{k_1}^k &= \mu^k, \\ U_{k_2}^k(p') + subsidy_{k_2}^k &= \mu^k, \end{aligned} \tag{16}$$

and so on until:

$$U_{k_{n_k}}^k(p') + subsidy_{k_{n_k}}^k = \mu^k.$$

Note that μ^k is the incurred utility for class k after the subsidies are distributed for the class at the locations with positive populations of that class. Also, we can number those locations for that class with zero populations of that class (if there are any) as follows:

$$U_{k_{n_{k+1}}}^k(p') + \text{subsidy}_{k_{n_{k+1}}}^k \leq \mu^k,$$

and so on until:

$$U_{k_n}^k(p') + \text{subsidy}_{k_n}^k \leq \mu^k. \quad (17)$$

Expressions (16) and (17) reveal that the appropriate governmental authority chooses the μ^k for each class k and then the subsidy for each location for that class is determined by straightforward subtraction.

In order to select an appropriate μ^k , as noted in [37], for the uncapacitated case, the μ^k s can be set as $\max_{k_l; l=1, \dots, n_k} U_{k_l}^k(p')$. All thus calculated are nonnegative and, furthermore, all migrants enjoy the maximal utility for each class at all the populated locations. Also, for the subsidies associated with locations with no populations of a class k (see (17)), we set those subsidies zero.

Returning to the above simple example, we note that $\mu^1 = 180.00$ and the above subsidy formulae simplify to:

$$U_1^1(p') + \text{subsidy}_1^1 = \mu^1,$$

$$U_2^1(p') + \text{subsidy}_2^1 = \mu^1,$$

$$U_3^1(p') + \text{subsidy}_3^1 = \mu^1,$$

or

$$147.50 + \text{subsidy}_1^1 = 180.00,$$

$$152.50 + \text{subsidy}_2^1 = 180.00,$$

$$180.00 + \text{subsidy}_3^1 = 180.00,$$

which yields:

$$\text{subsidy}_1^1 = 32.50, \quad \text{subsidy}_2^1 = 27.50, \quad \text{subsidy}_3^1 = 0.00.$$

Observe that an application of the above subsidies modifies the utility functions as follows:

$$\tilde{U}_1^1(p) = -p_1^1 + 190 + 32.50, \quad \tilde{U}_2^1(p) = -p_2^1 + 200 + 27.50, \quad \tilde{U}_3^1(p) = -p_3^1 + 210 + 0.$$

Clearly, the S-O solution

$$p_1^{1'} = 42.50, \quad p_2^{1'} = 47.50, \quad p_3^{1'} = 30.00,$$

is at the same time U-O, since the utilities are equalized (and maximal) under this S-O pattern and, hence, migrants will select locations, although acting selfishly and individually, accordingly, because of the subsidies.

The above subsidies may be viewed as investments by government(s). As for the budgets, if an individual government experiences a budgetary shortfall, additional financing may be provided by a supra authority such as the World Bank, the United Nations, or, if in Europe, the European Union. Altemeyer-Bartscher et al. [1] have argued for closer cooperation among countries regarding migration crises and also advocated for an economic approach as to distribution of the migrants. Here, we provide a quantitative approach with explicit formulae for implementation.

As noted earlier, climate change as well as disasters may act as drivers of human migrations. Robinson et al. [49], for example, provide a machine learning approach to migration in the United States under sea level rise but emphasize that their approach is not yet ready for policy-making. They, as [5], consider sea level rise due to climate change and migration within a country – the United States. The latter authors observe that offering a subsidy (e.g., a partial buyout) can be effective if the government has a significantly lower discount rate than residents. However, they assume homogeneous residents, whereas we consider multiclass ones, and we also allow for multiple countries and not just regions within a country. For edited volumes on dynamics of disasters, see [26, 27]. Once a disaster or disasters strike, one would modify the fixed populations of the various classes in the economy, as need be, along with the utility functions and rerun the model(s), along with the subsidies. In the case of disasters, we can expect that populations will decrease and so would utility functions associated with locations that have been negatively impacted.

4 The Algorithm and Numerical Examples

We apply the Euler method of [16] for the solution of the capacitated network models of human migration. As discussed therein (see also [42]), the Euler method is induced by a general iterative scheme and was inspired by the theory of projected dynamical systems, whose set of stationary points coincides with the set of solutions to an appropriate variational inequality problem. The Euler method, in fact, can be viewed as a time discretization of the underlying continuous time trajectories of the projected dynamical system until a solution is achieved. It has been applied to numerous network problems, including supply chain ones (see [34]).

4.1 The Algorithm

For purposes of standardizing the mechanism, we utilize similar notation to that in [37] and put variational inequality (7) into standard form [33]: determine $X^{**} \in \mathcal{K} \subset \mathbb{R}^N$ such that:

$$\langle F(X^{**}), X - X^{**} \rangle \geq 0, \quad \forall X \in \mathcal{K}, \quad (18)$$

where $\langle \cdot, \cdot \rangle$ denotes the inner product in N -dimensional Euclidean space. $F(X)$ is a given continuous function such that $F(X) : X \rightarrow \mathcal{K} \subset \mathbb{R}^N$. \mathcal{K} is a closed and convex set.

We define the vector $X \equiv (p, \beta)$ and the vector $F(X)$ with elements $F_{k,i}^1(p, \beta) \equiv \sum_{l=1}^J \sum_{j=1}^n -\frac{\partial \hat{U}_j^l(p)}{\partial p_i^k}$ and $F_{k,i}^2(p, \beta) \equiv cap_i^k - p_i^k$; $k = 1, \dots, J$; $i = 1, \dots, n$. We define the feasible set as $\mathcal{K} \equiv K^2$ and $N = 2Jn$. Thus, VI (7) can be put into the standard form (18) with $X^{**} = (p', \beta')$. Similarly, VI (15) can also be put into standard form with X and \mathcal{K} as above and with the components of its $F(X)$ given by $-U_i^k(p, \beta)$, $cap_i^k - \beta_i^k$; $\forall k, \forall i$, and with $X^{**} = (p^*, \beta^*)$.

At iteration τ , the statement of the Euler method is:

$$X^{\tau+1} = P_{\mathcal{K}}(X^{\tau} - a_{\tau}F(X^{\tau})), \quad (19)$$

where $P_{\mathcal{K}}$ is the projection on the feasible set \mathcal{K} and F is the function that enters the variational inequality problem (18).

Dupuis and Nagurney [16] proved that, for convergence of the general iterative scheme, which induces the Euler method, the sequence $\{a_{\tau}\}$ must satisfy $\sum_{\tau=0}^{\infty} a_{\tau} = \infty$, $a_{\tau} > 0$, $a_{\tau} \rightarrow 0$, as $\tau \rightarrow \infty$. Specific conditions for convergence of the Euler method within many network-based models can be found in [42] and in [34] and the references therein.

The Euler method nicely exploits the special network structure of the models as depicted in Fig. 1 and allows for closed-form expressions at each iteration for the computation of the Lagrange multipliers associated with the capacity constraints. We solve the network subproblems of special structure, which are separable quadratic programming problems, using the exact equilibration algorithm (cf. [14, 33]). This algorithm yields the exact solution at each iteration for the populations.

4.2 Numerical Examples

The algorithm was implemented in FORTRAN and a Unix system at the University of Massachusetts Amherst used for the computations. The series $\{a_{\tau}\}$ in the algorithm was set to $1, \frac{1}{2}, \frac{1}{2}, \frac{1}{3}, \frac{1}{3}, \frac{1}{3}$, etc. with the convergence tolerance ϵ equal

to 10^{-5} . In other words, the algorithm was considered to have converged when the absolute value of each of the computed population values for each class at two successive iterations was less than or equal to .00001.

For continuity, and cross comparison purposes, the data for the uncapacitated examples was taken from [37], and to these we added capacities. For completeness, we report both the uncapacitated (solved in the paper above) and the capacitated versions, reported for the first time here.

In our numerical examples, the network economy consists of two classes of migrants and five locations.

Utility Function and Fixed Population Data

The fixed populations in the network economy of the two classes are, respectively:

$$P^1 = 1,000.00 \quad P^2 = 2,000.00.$$

The utility functions and the total utility functions for class 1 are:

$$U_1^1(p) = -2p_1^1 - .2p_1^2 + 2,000, \quad \hat{U}_1^1(p) = -2(p_1^1)^2 - .2p_1^2 p_1^1 + 2,000p_1^1,$$

$$U_2^1(p) = -3p_2^1 - .1p_2^2 + 1,500, \quad \hat{U}_2^1(p) = -3(p_2^1)^2 - .1p_2^2 p_2^1 + 1,500p_2^1,$$

$$U_3^1(p) = -p_3^1 - .3p_3^2 + 3,000, \quad \hat{U}_3^1(p) = -(p_3^1)^2 - .3p_3^2 p_3^1 + 3,000p_3^1,$$

$$U_4^1(p) = -p_4^1 - .2p_4^2 + 2,500, \quad \hat{U}_4^1(p) = -(p_4^1)^2 - .2p_4^2 p_4^1 + 2,500p_4^1,$$

$$U_5^1(p) = -2p_5^1 - .3p_5^2 + 4,000, \quad \hat{U}_5^1(p) = -2(p_5^1)^2 - .3p_5^2 p_5^1 + 4,000p_5^1.$$

The utility functions and the total utility functions for class 2 are:

$$U_1^2(p) = -p_1^2 - .4p_1^1 + 4,000, \quad \hat{U}_1^2(p) = -(p_1^2)^2 - .4p_1^1 p_1^2 + 4,000p_1^2,$$

$$U_2^2(p) = -2p_2^2 - .6p_2^1 + 3,000, \quad \hat{U}_2^2(p) = -2(p_2^2)^2 - .6p_2^1 p_2^2 + 3,000p_2^2,$$

$$U_3^2(p) = -p_3^2 - .2p_3^1 + 5,000, \quad \hat{U}_3^2(p) = -(p_3^2)^2 - .2p_3^1 p_3^2 + 5,000p_3^2,$$

$$U_4^2(p) = -2p_4^2 - .3p_4^1 + 4,000, \quad \hat{U}_4^2(p) = -2(p_4^2)^2 - .3p_4^1 p_4^2 + 4,000p_4^2,$$

$$U_5^2(p) = -p_5^2 - .4p_5^1 + 3,000, \quad \hat{U}_5^2(p) = -(p_5^2)^2 - .4p_5^1 p_5^2 + 3,000p_5^2.$$

We first recall the uncapacitated U-O and S-O solutions obtained in [37] and then report the capacitated solutions based on the new models constructed here. We also report the calculated subsidies in the more general capacitated case introduced in this paper. We provide two sets of examples.

4.2.1 Numerical Example Set 1

The uncapacitated U-O solution for the numerical example with the above data is:

Class 1 Uncapacitated U-O Population Distribution

$$p_1^{1*} = 0.00, \quad p_2^{1*} = 0.00, \quad p_3^{1*} = 167.31, \quad p_4^{1*} = 41.68, \quad p_5^{1*} = 791.01.$$

Class 2 Uncapacitated U-O Population Distribution

$$p_1^{2*} = 415.89, \quad p_2^{2*} = 0.00, \quad p_3^{2*} = 1,382.41, \quad p_4^{2*} = 201.69, \quad p_5^{2*} = 0.00.$$

The uncapacitated S-O solution is:

Class 1 Uncapacitated S-O Population Distribution

$$p_1^{1'} = 0.00, \quad p_2^{1'} = 0.00, \quad p_3^{1'} = 120.43, \quad p_4^{1'} = 314.39, \quad p_5^{1'} = 565.19.$$

Class 2 Uncapacitated S-O Population Distribution

$$p_1^{2'} = 606.48, \quad p_2^{2'} = 53.23, \quad p_3^{2'} = 1,076.35, \quad p_4^{2'} = 263.94, \quad p_5^{2'} = 0.00.$$

We now impose the following capacities on the locations for the classes in the above problem.

$$cap_1^1 = 500.00, \quad cap_2^1 = 500.00, \quad cap_3^1 = 500.00, \quad cap_4^1 = 500.00, \quad cap_5^1 = 200.00,$$

$$cap_1^2 = 500.00, \quad cap_2^2 = 500.00, \quad cap_3^2 = 400.00, \quad cap_4^2 = 500.00, \quad cap_5^2 = 500.00.$$

The capacitated U-O solution is:

Class 1 Capacitated U-O Population Distribution

$$p_1^{1*} = 0.00, \quad p_2^{1*} = 0.00, \quad p_3^{1*} = 500.00, \quad p_4^{1*} = 300.00, \quad p_5^{1*} = 200.00.$$

Class 2 Capacitated U-O Population Distribution

$$p_1^{2*} = 500.00, \quad p_2^{2*} = 226.67, \quad p_3^{2*} = 400.00, \quad p_4^{2*} = 500.00, \quad p_5^{2*} = 373.33.$$

The optimal Lagrange multipliers are:

Class 1 Capacitated U-O Lagrange Multipliers

$$\beta_1^{1*} = 0.00, \quad \beta_2^{1*} = 0.00, \quad \beta_3^{1*} = 280.00, \quad \beta_4^{1*} = 0.00, \quad \beta_5^{1*} = 1,388.01.$$

Class 2 Capacitated U-O Lagrange Multipliers

$$\beta_1^{2*} = 953.33, \quad \beta_2^{2*} = 0.00, \quad \beta_3^{2*} = 1,953.33, \quad \beta_4^{2*} = 363.33, \quad \beta_5^{2*} = 0.00.$$

One can see, from this example, that at all the locations with populations of a class at the capacity, there is an associated positive Lagrange multiplier. Also, it is clear that the capacitated U-O solution is quite distinct from the uncapacitated one. For example, all the locations have a positive population of class 2 under the capacitated solution. Moreover, in the uncapacitated case, location 5 is most attractive for class 1, whereas location 3 is most attractive for class 2. In contrast, in the capacitated case, location 3 is now most popular for class 1, whereas locations 1 and 4 are most popular (and at the capacities) for class 2.

The capacitated S-O solution is:

Class 1 Capacitated S-O Population Distribution

$$p_1^1 = 88.82, \quad p_2^1 = 0.00, \quad p_3^1 = 242.55, \quad p_4^1 = 468.63, \quad p_5^1 = 200.00.$$

Class 2 Capacitated S-O Population Distribution

$$p_1^2 = 500.00, \quad p_2^2 = 244.65, \quad p_3^2 = 400.00, \quad p_4^2 = 436.07, \quad p_5^2 = 419.29.$$

The optimal Lagrange multipliers are:

Class 1 Capacitated S-O Lagrange Multipliers

$$\beta_1^1 = 0.00, \quad \beta_2^1 = 0.00, \quad \beta_3^1 = 0.00, \quad \beta_4^1 = 0.00, \quad \beta_5^1 = 1,561.77.$$

Class 2 Capacitated S-O Lagrange Multipliers

$$\beta_1^2 = 925.30, \quad \beta_2^2 = 0.00, \quad \beta_3^2 = 2,057.33, \quad \beta_4^2 = 0.00, \quad \beta_5^2 = 0.00.$$

Under the uncapacitated S-O, location 5 is most attractive for class 1 and location 3 is for class 2. However, in the capacitated case, location 4 is best for class 1 and location 1 for class 2, with locations 3 through 5 also quite competitive.

We now report the calculated subsidies, which are obtained using the described procedure in Sect. 3. We note that $\mu^1 = 3,474.21$ and $\mu^2 = 4,551.50$ – these values represent the highest utility of each class at a location evaluated at the S-O solution, which are obtained for class 1 at location 5 and for class 2 at location 3. The calculated subsidies are:

Class 1 Subsidies

$$subsidy_1^1 = 1,751.85, \quad subsidy_2^1 = 1,998.67, \quad subsidy_3^1 = 836.76, \quad subsidy_4^1 = 1,530.05, \\ subsidy_5^1 = 0.00.$$

Class 2 Subsidies

$$subsidy_1^2 = 1,087.03, \quad subsidy_2^2 = 2,040.79, \quad subsidy_3^2 = 0.00, \quad subsidy_4^2 = 1,564.22, \\ subsidy_5^2 = 2,050.79.$$

4.2.2 Numerical Example Set 2

The data were as in the first numerical example set except now we considered a sizable decrease in the populations of each of the two classes due to a disaster. As argued in [37], this could occur in the form of a pandemic, that is, a healthcare disaster hitting the network economy. We note that the novel coronavirus outbreak that originated in Wuhan, China [51], was officially declared a pandemic by the World Health Organization on March 11, 2020 (cf. [7]). This coronavirus causes the disease known as Covid-19. The data in this example was as in Numerical Example 1, except that now we assumed that 50% of the population of each class has perished, that is,

$$P^1 = 500.00 \quad P^2 = 1,000.00.$$

The uncapacitated U-O solution for the numerical example with the above data is:

Class 1 Uncapacitated U-O Population Distribution

$$p_1^{1*} = 0.00, \quad p_2^{1*} = 0.00, \quad p_3^{1*} = 0.00, \quad p_4^{1*} = 0.00, \quad p_5^{1*} = 500.00.$$

Class 2 Uncapacitated U-O Population Distribution

$$p_1^{2*} = 0.00, \quad p_2^{2*} = 0.00, \quad p_3^{2*} = 1,000.00, \quad p_4^{2*} = 0.00, \quad p_5^{2*} = 0.00.$$

The uncapacitated computed S-O solution is:

Class 1 S-O Uncapacitated Population Distribution

$$p_1^{1'} = 0.00, \quad p_2^{1'} = 0.00, \quad p_3^{1'} = 47.98, \quad p_4^{1'} = 43.17, \quad p_5^{1'} = 408.85.$$

Class 2 S-O Uncapacitated Population Distribution

$$p_1^{2'} = 206.96, \quad p_2^{2'} = 0.00, \quad p_3^{2'} = 694.96, \quad p_4^{2'} = 98.08, \quad p_5^{2'} = 0.00.$$

As noted in [37], in the S-O solution, one sees a greater “spreading out” of the classes among the locations than in the U-O solution.

We kept the same capacities as in the first set. The Euler method now yielded the following solution:

The capacitated U-O solution for the numerical example with the above data is:

Class 1 Capacitated U-O Population Distribution

$$p_1^{1*} = 0.00, \quad p_2^{1*} = 0.00, \quad p_3^{1*} = 300.00, \quad p_4^{1*} = 0.00, \quad p_5^{1*} = 200.00.$$

Class 2 Capacitated U-O Population Distribution

$$p_1^{2*} = 0.00, \quad p_2^{2*} = 400.00, \quad p_3^{2*} = 0.00, \quad p_4^{2*} = 400.00, \quad p_5^{2*} = 200.00.$$

The optimal Lagrange multipliers are:

Class 1 Capacitated U-O Lagrange Multipliers

$$\beta_1^{1*} = 0.00, \quad \beta_2^{1*} = 0.00, \quad \beta_3^{1*} = 0.00, \quad \beta_4^{1*} = 0.00, \quad \beta_5^{1*} = 1,020.00.$$

Class 2 Capacitated U-O Lagrange Multipliers

$$\beta_1^{2*} = 0.00, \quad \beta_2^{2*} = 0.00, \quad \beta_3^{2*} = 940.00, \quad \beta_4^{2*} = 0.00, \quad \beta_5^{2*} = 0.00.$$

The capacitated computed S-O solution is:

Class 1 S-O Capacitated Population Distribution

$$p_1^{1'} = 0.00, \quad p_2^{1'} = 0.00, \quad p_3^{1'} = 124.08, \quad p_4^{1'} = 175.91, \quad p_5^{1'} = 200.00.$$

Class 2 S-O Capacitated Population Distribution

$$p_1^{2'} = 414.66, \quad p_2^{2'} = 0.00, \quad p_3^{2'} = 400.00, \quad p_4^{2'} = 185.34, \quad p_5^{2'} = 0.00.$$

The optimal Lagrange multipliers are:

Class 1 Capacitated S-O Lagrange Multipliers

$$\beta_1^{1'} = 0.00, \quad \beta_2^{1'} = 0.00, \quad \beta_3^{1'} = 0.00, \quad \beta_4^{1'} = 0.00, \quad \beta_5^{1'} = 1,144.49.$$

Class 2 Capacitated S-O Lagrange Multipliers

$$\beta_1^{2'} = 0.00, \quad \beta_2^{2'} = 0.00, \quad \beta_3^{2'} = 967.27, \quad \beta_4^{2'} = 0.00, \quad \beta_5^{2'} = 0.00.$$

We now report the subsidies that, when imposed, guarantee that the capacitated S-O solution obtained above for the second numerical example is also U-O. Here we had that $\mu^1 = 3,599.99$ and $\mu^2 = 4,575.18$.

Class 1 Subsidies

$$subsidy_1^1 = 1,682.92, \quad subsidy_2^1 = 2,099.99, \quad subsidy_3^1 = 844.07, \quad subsidy_4^1 = 1,312.97,$$

$$subsidy_5^1 = 0.00.$$

Class 2 Subsidies

$$subsidy_1^2 = 989.84, \quad subsidy_2^2 = 1,575.18, \quad subsidy_3^2 = 0.00, \quad subsidy_4^2 = 998.63,$$

$$subsidy_5^2 = 1,655.18.$$

5 Summary and Conclusions

Problems of human migration are issues of global concern and are presenting immense challenges to governments around the world. Multiple countries are dealing with different classes of migratory flows and the ensuing difficulties when faced with capacities at locations under their jurisdictions. Rigorous, appropriate policies may help to better reallocate migrants across suitable locations.

Historically, many of the mathematical models of human migration have utilized a network formalism and have assumed user-optimizing behavior, that is, that migrants select locations, which are best for themselves, as revealed through utility functions that depend on the population distributions among the locations of the different classes of migrants. However, such behavior may lead to costs to society and even reduced societal welfare.

Hence, in this paper, we build upon the recent work of [37], who proposed both system-optimized and user-optimized multiclass migration network models and demonstrated how incentives, in the form of subsidies, when applied, guarantee that the system-optimized solution, which maximizes the total utility in the network economy, becomes, at the same time, user-optimizing. Migrants, thus, under such subsidies, and acting selfishly and independently, would select locations to migrate to and locate at that are optimal from the system perspective.

In this paper, we propose a novel extension of that work, in the form of capacities at different locations associated with the classes of migrants. This brings a greater realism in capturing challenges faced by various governments who are dealing with refugees, asylum seekers, etc. For each U-O and S-O model, we provide alternative variational inequality formulations of the governing equilibrium/optimality conditions. We then utilize the variational inequality formulations with Lagrange multipliers associated with the multiclass capacity constraints to gain deeper insights into appropriate policies. We show that the Lagrange multipliers can be utilized to modify the utility functions so that the capacities are made implicit. Moreover, we show how, through the use of appropriately constructed formulae for subsidies, once applied, the system-optimized solution becomes, at the same time, user-optimized. This provides a more positive approach to the redistribution of human migrants and enhances societal welfare.

In addition, in this paper, we provide an effective computational procedure, which exploits the underlying special network structure of our models. The algorithm is implemented, and the solutions to a series of numerical examples are computed. We report the user-optimized and the system-optimized solutions, both uncapacitated and capacitated, along with the subsidies for the latter. Our theoretical framework can be applied in practice under different scenarios, along with sensitivity analysis, as, for example, in the case of disasters, when there are population changes and/or modifications to utility functions because of impacted infrastructure.

Acknowledgments The first two authors are grateful for the insights gained through participation in the Dynamics of Disasters conferences in Kalamata, Greece, and the very useful discussions.

The authors acknowledge the very helpful comments and suggestions provided by two anonymous reviewers on an earlier version of this paper.

References

1. Altemeyer-Bartscher, M., Holtemöller, O., Lindner, A., Schmalzbauer, A., Zeddies, G., 2016. On the distribution of refugees in the EU. *Intereconomics* 51(4), 220–228.
2. Bartenstein, B., McDonald, M.D., 2019. Exporting people: How Central America encourages mass migration. Bloomberg, July 19; available at: <https://www.bloomberg.com/news/articles/2019-06-19/migrant-crisis-at-border-how-central-america-encourages-exodus>
3. Beckmann, M., McGuire, C.B., Winsten, C.B., 1956. *Studies in the Economics of Transportation*. Yale University Press, New Haven, Connecticut.
4. Bertsekas, D.P., Tsitsiklis, J.N., 1989. *Parallel and Distributed Computation: Numerical Methods*. Prentice-Hall, Englewood Cliffs, NJ.
5. Bier, V.M., Zhou, Y., Du, H., 2019. Game-theoretic modeling of pre-disaster relocation. *The Engineering Economist*. DOI: 10.1080/0013791X.2019.1677837
6. Boyce, D.E., Mahmassani, H.S., Nagurney, A., 2005. A retrospective on Beckmann, McGuire and Winsten's *Studies in the Economics of Transportation*. *Papers in Regional Science* 84(1), 85–103.
7. Branswell, H., Joseph, A., 2020. WHO declares the coronavirus outbreak a pandemic. STAT. March 11; available at: <https://www.statnews.com/2020/03/11/who-declares-the-coronavirus-outbreak-a-pandemic/>
8. Cappello, G., Daniele, P., 2019. A variational formulation for a human migration model. In: Paolucci M., Sciomachen A., Uberti P., Editors, *Advances in Optimization and Decision Science for Society, Services and Enterprises*. AIRO Springer Series, vol 3. Springer Nature Switzerland, pp. 185–195.
9. Causa, A., Jadamba, B., Raciti, F., 2017. A migration equilibrium model with uncertain data and movement costs. *Decisions in Economics and Finance* 40, 159–175.
10. Chinchilla, L., Orozco, M., Pérez Bravo, T., Rodriguez, R., 2018. Do countries have enough capacity to handle migrants? *Latin American Advisor*, August 24. Available at: <https://www.thedialogue.org/analysis/do-countries-have-enough-capacity-to-handle-migrants/>
11. Dafermos, S., 1980. Traffic equilibrium and variational inequalities. *Transportation Science* 14(1), 42–54.
12. Dafermos, S.C., 1973. Toll patterns for multiclass-user transportation networks. *Transportation Science* 7(3), 211–223.
13. Dafermos, S., Sparrow, F.T., 1971. Optimal resource allocation and toll patterns in user-optimized transport networks. *Journal of Transport Economics and Policy* 5(2), 184–200.
14. Dafermos S.C., Sparrow, F.T., 1969. The traffic assignment problem for a general network. *Journal of Research of the National Bureau of Standards* 73B, 91–118.
15. Davis, K.F., D'Odorico, P., Laio, F., Ridolfi, L., 2013. Global spatio-temporal patterns in human migration: A complex network perspective. *PLOS ONE* 8(1), e53723.
16. Dupuis, P., Nagurney, A., 1993. Dynamical systems and variational inequalities. *Annals of Operations Research* 44, 9–42.
17. European Commission, 2019. Communication from the Commission on the European Parliament, the European Council and the Council. Progress report on the Implementation of the European Agenda on Migration. Brussels, Belgium, 6.3.2019 COM(2019) 126 final.
18. International Organization for Migration, 2019. *World migration report for 2020*. Geneva, Switzerland.

19. Isac, G., Bulavsky, V.A., Kalashnikov, V.V., 2002. *Complementarity, Equilibrium, Efficiency and Economics*. Kluwer Academic Publishers, Dordrecht, The Netherlands.
20. Jones, G., 2018. Italy will no longer be 'Europe's refugee camp', vows new government. *World News* June 4.
21. Kalashnikov, V., Kalashnykova, N., Rojas, R.L. Munos, M.M., Uranga, C., Rojas, A.L., 2008. Numerical experimentation with a human migration model. *European Journal of Operational Research* 189, 208–229.
22. Karagiannis, G.M., 2016. Emergency management perspective of the European migrant crisis. *Newsletter - special edition, The International Emergency Management Society*, issue 4, October, 12–24, Brussels, Belgium.
23. Kennedy, M., 2019. U.N. says more than 4 million people have left Venezuela. NPR; available at: <https://www.npr.org/2019/06/07/730687807/u-n-says-more-than-4-million-people-have-left-venezuela>
24. Kinderlehrer, D., Stampacchia, G., 1980. *An Introduction to Variational Inequalities and Their Applications*. Academic Press, New York.
25. Kitsantonis, N., 2019. Greek refugee camps are near catastrophe, Rights Chief warns. *The New York Times*, October 31.
26. Kotsireas, I.S., Nagurney, A., Pardalos, P.M., Editors, 2016. *Dynamics of Disasters: Key Concepts, Models, Algorithms, and Insights*. Springer International Publishing Switzerland.
27. Kotsireas, I.S., Nagurney, A., Pardalos, P.M., Editors, 2018. *Dynamics of Disasters: Algorithmic Approaches and Applications*. Springer International Publishing Switzerland.
28. Larsson, T., Patriksson, M., 1999. Side constrained traffic equilibrium models - analysis, computation and applications. *Transportation Research B* 33(4), 233–264.
29. Lawphongpanich, S., Hearn, D.W., Smith, M.J., Editors, 2006. *Mathematical and Computational Models for Congestion Charging*. Springer Science + Business Media, New York.
30. Mattiace, T., 2019. Mexico: Onset of migration crisis. *Global Risk Insights*, November 24. Available at: <https://globalriskinsights.com/2019/11/mexico-onset-of-migration-crisis/>
31. Nagurney, A., 1989. Migration equilibrium and variational inequalities. *Economics Letters* 31, 109–112.
32. Nagurney, A., 1990. A network model of migration equilibrium with movement costs. *Mathematical and Computer Modelling* 13, 79–88.
33. Nagurney, A., 1999. *Network Economics: A Variational Inequality Approach*, second and revised edition. Kluwer Academic Publishers, Dordrecht, The Netherlands.
34. Nagurney, A., 2006. *Supply Chain Network Economics: Dynamics of Prices, Flows and Profits*. Edward Elgar Publishing, Cheltenham, England.
35. Nagurney, A., 2010. Optimal supply chain network design and redesign at minimal total cost and with demand satisfaction. *International Journal of Production Economics* 128, 200–208.
36. Nagurney, A., Daniele, P., 2020. International human migration networks under regulations. *European Journal of Operational Research*, in press.
37. Nagurney, A., Daniele, P., Cappello, G., 2021. Human migration networks and policy interventions: Bringing population distributions in line with system-optimization. *International Transactions in Operational Research* 28(1), 5–26.
38. Nagurney, A., Daniele, P., Nagurney, L.S., 2020. Refugee migration networks and regulations: A multiclass, multipath variational inequality framework. *Journal of Global Optimization* 78, 627–649.
39. Nagurney, A., Pan, J., Zhao, L., 1992a. Human migration networks. *European Journal of Operational Research* 59, 262–274.
40. Nagurney, A., Pan, J., Zhao, L., 1992b. Human migration networks with class transformations. In: *Structure and Change in the Space Economy*. Lakshmanan, T.R., Nijkamp, P., Editors, Springer-Verlag, Berlin, Germany, pp. 239–258.
41. Nagurney, A., Yu, M., Qiang, Q., 2011. Supply chain network design for critical needs with outsourcing. *Papers in Regional Science* 90, 123–142.
42. Nagurney, A., Zhang, D., 1996. *Projected Dynamical Systems and Variational Inequalities with Applications*. Kluwer Academic Publishers, Boston, Massachusetts.

43. O'Connor, A., Batalova, J., Bolter, J., 2019. Central American immigrants in the United States. Migration Information Source, August 15. Available at: <https://www.migrationpolicy.org/article/central-american-immigrants-united-states>
44. OECD, 2019. How do OECD countries compare in their attractiveness for talented migrants? Migration Policy Debates, No. 19, May.
45. Pan, J., Nagurney, A., 1994. Using Markov chains to model human migration in a network equilibrium framework. *Mathematical and Computer Modelling* 19, 31–39.
46. Pan, J., Nagurney, A., 2006. Evolution variational inequalities and projected dynamical systems with application to human migration. *Mathematical and Computer Modelling* 43(5–6), 646–657.
47. Papadaki, S., Baniyas, G., Achillas, C., Aidonis, D., Folinias, D., Bochtis, D., Papangelou, S., 2018. A humanitarian logistics case study for the intermediary phase accommodation center for refugees and other humanitarian disaster victims. In: *Dynamics of Disasters: Algorithmic Approaches and Applications*, Kotsireas, I.S., Nagurney, A., Pardalos, P.M., Editors, Springer International Publishing Switzerland, pp. 157–202.
48. Parkinson, J., 2015. Which countries are in the best position to take migrants? BBC News Magazine, September 9. Available at: <https://www.bbc.com/news/magazine-34138831>
49. Robinson, C., Dilkina, B., Moreno-Cruz, J., 2020. Modeling migration patterns in the USA under sea level rise. *PLoS ONE* 15(1): e0227436. <https://doi.org/10.1371/journal.pone.0227436>
50. Sakuma, A., 2020. Damned for trying. Available at: <http://www.msnbc.com/specials/migrant-crisis/libya>
51. Shih, G., Denyer, S., Taylor, A., 2020. Worries grow that quarantine in China not enough to stem increasingly virulent coronavirus. *Washington Post*, January 27.
52. Stevis-Gridneff, M., 2020. Asylum seekers find a new route to Europe, flowing into a divided Cyprus. *The New York Times*, January 28.
53. UNHCR, 2020. Figures at a glance. Available at: <https://www.unhcr.org/en-us/figures-at-a-glance.html>
54. United Nations, 2017. Population facts. Department of Economic and Social Affairs, Population Division, New York, December; available at: https://www.un.org/en/development/desa/population/publications/pdf/popfacts/PopFacts_2017-5.pdf
55. United Nations Refugee Agency, 2015. The sea route to Europe: The Mediterranean passage in the age of refugees. July 1; available at: <https://www.unhcr.org/en-us/protection/operations/5592bd059/sea-route-europe-mediterranean-passage-age-refugees.html>
56. Wardrop, J.G., 1952. Some theoretical aspects of road traffic research. *Proceedings of the Institution of Civil Engineers, Part II* 1: pp. 325–378.

Land Property Data Logging on Blockchain Ledger



Stamatis Papangelou  and Zinos Alexios Charalampidis 

Abstract Occurrences of disaster lead to problems in information retrieval about damaged land properties as it is a time-consuming task, and one that entails a lot of bureaucracy. In this paper we will discuss a specific method using blockchain technology and specialized equipment to collect and register land property information. That information is critical for individuals, governments as well as insurance companies for evaluating risk associated with disasters. For reasons of data integrity and transparency, all of this information is available in a form on a public blockchain ledger.

Keywords Disaster management · Risk index · Geolocation information data · Blockchain

1 Introduction

There plenty of different methods to evaluate risk in the relevant literature. However, with the rapidly evolving risk evaluation technologies, many new problems that need to be solved are rising to the surface. As the risk indexes are getting more complex and technical, the processing environment is mirroring the same effects [17]. We assume that, in the near future, such indexes will have thousands or even millions of parameters in order to calculate more accurate and reliable outcomes [19]. In our current era, risk indexes are limited to wide geographical districts that may contain millions of properties on developed countries [15].

The goal of this paper is to suggest a platform and specific devices, so that future work on the subject can be done more effortlessly [10]. This short paper is a tool and a methodology of a platform that will produce, collect, store and process a significant volume of data in a publicly distributed platform named “blockchain” [4]. In Sect. 3, we will be discussing about risk evaluation methods and the literature

S. Papangelou (✉) · Z. A. Charalampidis
School of Science and Technology, International Hellenic University, Thessaloniki, Greece
e-mail: alexischar@protonmail.com

for risk-related indexes, while in Sect. 4, we describe a system that we use to retrieve, process and store land property data along with other information [13]. And finally, Sect. 5 describes how the blockchain technology can assist in data logging.

2 Motivation

Our ambition is to combine a very wide range of parameters associated with risk indexes to evaluate every disaster-prone property individually for all different types of disaster using a range of subindexes associated with the property itself. In order to produce such a big number of indexes, an even bigger sum of data and data sources are required. Using current risk indexes, which only provide information about very wide geographical districts, one is not able to generate specialized, area-specific, risk indexes. But with the technological evolution of big data and data analytics, we assume that in the near future, there will be sufficient data that, after being processed, will be able to generate several of the parameters needed. Therefore, the first step is building the base platform needed, so that when the data and parameters become available, they can be stored and processed. To do that we will search for a suitable data platform that can store data that can not be tampered with, then construct the pathways that these data and algorithmic outputs will follow and lastly suggest various ways to utilize existing data and methods to collect new ones. The platform that we believe is more suited for such a project is blockchain, and this will be described in the parts that follow.

3 Literature and Types of Risk

There are many types of risk that can affect a property, from wildfires to the humidity that can affect building foundations [26]. The current literature focuses on the risk related to natural disasters; however in order to build correct parametric models, in future researches, we need to acknowledge the importance of other types of disasters and investigate them as well. In this section we are going to analyse the literature concerning natural disasters, and we will be suggesting two more types of risks. Man-made disasters and disasters associated with the types of building construction [12].

3.1 *Natural Disasters*

A natural disaster is a major adverse event resulting from natural processes of the Earth; examples are floods, hurricanes, tornadoes, volcanic eruptions, earthquakes, tsunamis and other geological calamities. A natural disaster can cause loss of

life and damage in properties [14]. Data from naturally occurring disasters are commonly used to identify and evaluate disaster-related risk. The literature suggests various ways to examine and index natural hazard-related risk. Specifically Hakan-son [13] constructed a risk index to be used as a diagnostic tool for water pollution control purposes from a limited sediment sample of 13 Swedish lakes. Davidson [8] contributed on an earthquake-related disaster index along with Carreno [7]; he did a seismic risk approach, which expounded that risk estimation takes into account the expected physical damage, the number and type of casualties or economic losses, but also other social, organizational and institutional issues related to the development of communities that contribute to the creation of risk. The researchers mentioned above apply methods that contain significant parametric usage of variables to reflect aspects of such seismic risk, as it becomes clear in [7] where only 248 small statistical zones were used in Barcelona City. Carreno [6] proceeded with a similar approach to construct a risk management performance index in a more generic form called risk identification index (RMI). Pedussi [21] uses detailed parametric models to approach the subject of identifying natural risk using the expression below:

$$\ln(K) = \ln(C) + a \ln(PhExp) + a_1 \ln(V_1) + a_2 \ln(V_2) + \dots + a_r \ln(V_r) \quad (1)$$

where K = the number of people killed by a certain type of hazard; C = multiplicative constant; $PhExp$ = physical exposure, population living in exposed areas multiplied by the frequency of occurrence of the hazard; V_r = socio-economic variables; a_r = exponent of V_r , which can be negative(for ratio) [21].

But for simplicity reasons in our example, we are going to use the following weighted average of the time series of each of the variables:

$$V' = (V_{2005}K_{2005} + V_{2006}K_{2006} + \dots + V_nK_n)/K_{tot} \quad (2)$$

V' = weighted average of a given variable. V_n = value of the variable for the year n. K_n = number of recorded casualties for the year n. K_{tot} = total number of recorded casualties for all years [21].

The result of the above equation is an averaged value that is obtained from yearly values weighted according to the number of casualties in each year. This is the weighted average index that is used to provide results, stored in our smart contract. Moreover, Tsai [25], Islam [15], Orencio [19] and Shi [24] contribute in the subject with their approaches in different sectors. Data for cases like this are available from the UN [1], the Centre for Research on the Epidemiology of Disasters [22] and the Global climate risk index [9].

There are many models that we can apply and contain in our tool. Ideally, we want to include as much data as possible and utilize our information using a variety of indexes, so we can have more accurate and detailed outputs related to risk evaluation.

3.2 *Man-Made Disasters*

Moreover, there are also the man-made disasters [10], which are very hard to be evaluated mathematically and to be noticed. Anthropogenic hazards are hazards caused by human action or inaction; some examples are wars, terrorism, toxic chemicals and radioactive materials. As of right now, there are procedures to manage this risk but not to index it [24]. Ideally, we want to include such parameters in our parametric tool in our future research.

3.3 *Types of Construction*

To conclude, we also want to discuss the types of construction. Because our tool will be used for evaluating property risk, we believe that the type of structure and the materials that are used in building construction is a very important factor. To use as an example, let us assume we have two houses that are built using the same design and type of structure and both are located inside the same forest, with the only difference being that the walls of one of the houses are made from concrete and the other from wood. It is obvious that the house made from wood is much more likely to be burned on a wildfire that can occur in the forest, than the house made from concrete.

In our tool we don't yet use a specific way to model risk that can be found in types of construction. Our ambition is to be able in the near future to use all available construction aspects into a parametric model and add them to our tool. In this paper we will not cover a similar process, and we are going to use just a few parameters for simplicity. Those parameters are whether the property is an apartment building or a detached house, the type of foundation either concrete decking or footing and lastly the year of construction.

To summarize all of the above, it is clear that in our research, we encounter three main issues. First of all, there is a clear lack of data as regards disaster modelling. Second, there is no available literature in respect to man-made disaster modeling, nor for types of construction. And finally, only a small number of papers take a wide view on risk indexing; it is clear that an environment that combines parameters and variables from different disaster sectors does not exist.

4 System Design

The overall functional system we used to record data is the one seen below in Fig. 1.

It is comprised of the data acquisition device, the cloud storage and the interface to the smart contract as well as a web interface to retrieve any of the data we want to be accessible to the web.

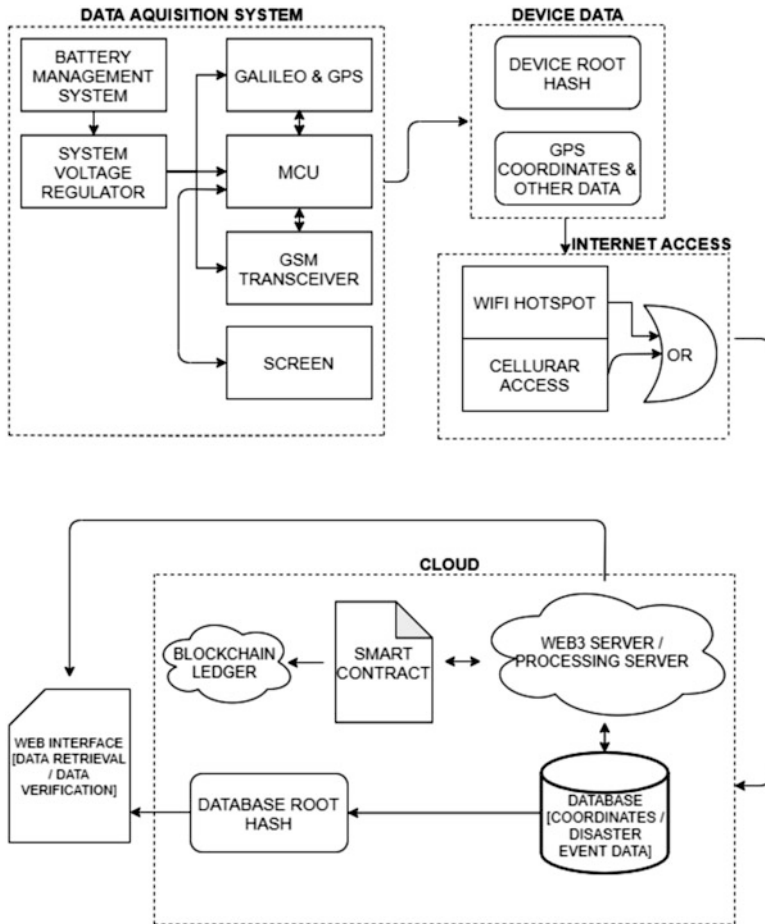


Fig. 1 Overall system design

4.1 Data Acquisition and Transmission

The data acquisition device used in our system to acquire geolocation information, as well as other identity- and construction-related data, can be as simple as a battery management system (BMS) to charge the batteries powering the portable device, along with a voltage regulator to supply nominal voltage to the microcontroller unit (MCU) (Figs. 2 and 3).

The MCU could optionally be Wi-Fi enabled and should be connected to a GSM modem which in turn can transmit and receive data on the Internet using the existing mobile network infrastructure, thus assuring Internet connectivity no matter where the device is located. To acquire geolocation information, a multi-constellation GPS receiver should be used to achieve high precision; some already commercially

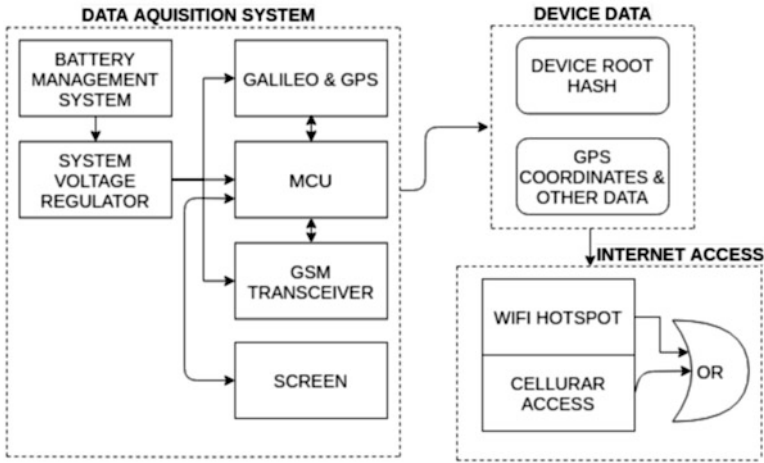


Fig. 2 Data acquisition and transmission block

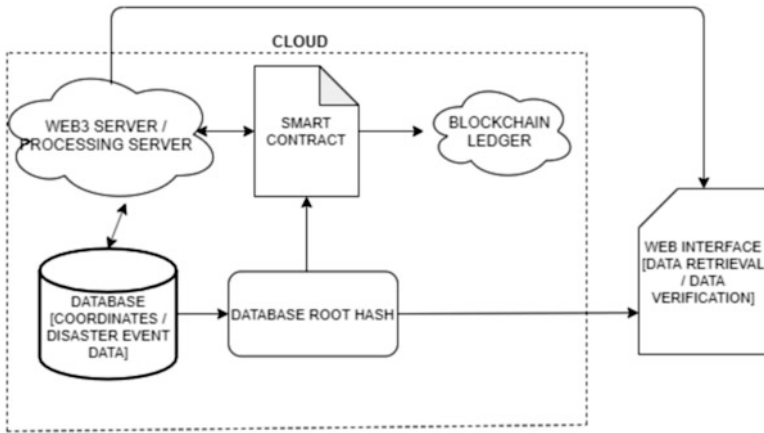


Fig. 3 Cloud structure

available receivers are achieving precision of 5 mm (RMS) in latitude and 8 mm (RMS) in longitude. Also, to acquire some user data and display information to the device user, a touchscreen is used. As described in Sect. 4, the data the device should publish on the database and to the smart contract are GPS and any other user input along with the root hash stored in the device.

4.2 Cloud

The transmitted data are then transferred to the cloud, to a web server that holds a database in order to store raw information such as property owner and GPS coordinates and is responsible to run a web3.js Ethereum interface. The web3.js is a collection of libraries used to interact with a remote Ethereum node [28], thus enabling us to send data directly to the smart contract on the Ethereum ledger.

This can store the risk index which is the output of the processing server based on algorithms shown in Section 3.1 (Pedussi, 2009) [21], along with the data transmitted by the device, such as the construction type, the foundation type and date of construction of a building, the database root hash, the device root hash, the name of the property owner and other information regarding buildings [18]. Furthermore, there is a function to compare whether the root hash of the server is the same as the root hash of the device. Finally, much of the data above can be made visible to the public through a web interface.

5 Blockchain Platform

Blockchain is an ordered list of records that are called blocks, which contain cryptographic stamps connected with every previous block and every information within the block [20]. A distributed digital ledger is used to record data transactions across a large number of computers, so that any record on the blockchain cannot be altered retroactively, without the alteration of all subsequent blocks [23].

Thus data stored in the blockchain or transactions logged by it are immutable and tamper-proof, given that vast computational resources are required to change just one single record [16, 11]. We chose to use a smart contract to save the root hash of data logged by the specific purpose device on the Ethereum blockchain while keeping the actual data generated by the device in an off-chain server for ease of access and cost efficiency described in 4.3 [2].

The root hash referenced above is the “top hash” of a Merkle tree comprised of all the data recorded on the field by the device [29]. The data include geolocation information about a property, risk indexes as well as ID information of the property owner and more [27].

Following the process above, a user, the smart contract itself or any custom programme can be assured that any data stored off-line in a server are integral and not tampered with [5].

A more in-depth explanation of the blockchain usage and application as well as a working example of the smart contract can be found in the website cited at [3].

6 Conclusion

With the growing number of parameters that can be employed to evaluate a disaster-related risk, it is necessary to use tools and technologies to store and process such information. We discussed some examples and methodologies of risk indexes that we can use in our tool and how blockchain can ensure risk evaluation transparency, along with a specific system to acquire data from the field as well as process such data on the cloud. We are confident that such a methodology can be used in future research as more data and index processing techniques become available.

References

1. <https://geodata.grid.unep.ch/>
2. <https://ethereum.github.io/yellowpaper/paper.pdf>
3. <https://github.com/alex-z-charalampidis/smart-contract-dod19>
4. Saveen A Abeyratne and Radmehr P Monfared. “Blockchain ready manufacturing supply chain using distributed ledger”. In: *International Journal of Research in Engineering and Technology* 5.9 (2016). Data Accessed in January 2019, pp. 1–10.
5. Georg Becker. “Merkle signature schemes, merkle trees and their cryptanalysis”. In: *Ruhr-University Bochum, Tech. Rep* (2008).
6. Martha Liliana Carreño, Omar D Cardona, and Alex H Barbat. “A disaster risk management performance index”. In: *Natural Hazards* 41.1 (2007), pp. 1–20.
7. Martha-Liliana Carreño, Omar D Cardona, and Alex H Barbat. “Urban seismic risk evaluation: a holistic approach”. In: *Natural Hazards* 40.1 (2017), pp. 137–172.
8. Rachel Davidson. “EERI annual student paper award a multidisciplinary urban earthquake disaster risk index”. In: *Earthquake Spectra* 13.2 (1997), pp. 211–223.
9. D Eckstein, V Künzel, and L Schäfer. *Global climate risk index 2018*. *Germanwatch*, 33. 2017.
10. Farin Fatemi et al. “Social vulnerability indicators in disasters: Findings from a systematic review”. In: *International journal of disaster risk reduction* 22 (2017), pp. 219–227.
11. Valentina Gatteschi et al. “Blockchain and smart contracts for insurance: Is the technology mature enough?”. In: *Future Internet* 10.2 (2018), p. 20.
12. Anne Goes and Jerry R Skees. *Financing natural disaster risk using charity contributions and ex ante index insurance*. Tech. rep. 2003.
13. Lars Hakanson. “An ecological risk index for aquatic pollution control. A sedimentological approach”. In: *Water research*, 14.8 (1980), pp. 975–1001.
14. Sven Harmeling. “Global Climate Risk Index 2009”. In: *Weather* (2008).
15. Mohammed Shariful Islam, Mohammad Shahidul Hasan Swapan, and Shamim Mahabubul Haque. “Disaster risk index: How far should it take account of local attributes?”. In: *International journal of disaster risk reduction* 3 (2013), pp. 76–87.
16. Hyong S Kim and Ke Wang. “Immutability measure for different blockchain structures”. In: *2018 IEEE 39th Sarnoff Symposium*. IEEE, 2018, pp. 1–6.
17. Sönke Kreft et al. “Global climate risk index 2014”. In: *Who suffers most from extreme weather events* 1 (2013).
18. Regio A Michelin et al. “SpeedyChain: A framework for decoupling data from blockchain for smart cities”. In: *Proceedings of the 15th EAI International Conference on Mobile and Ubiquitous Systems: Computing, Networking and Services*. 2018, pp. 145–154

19. Pedcris M Orencio and Masahiko Fujii. "A localized disaster-resilience index to assess coastal communities based on an analytic hierarchy process (AHP)". In: *International Journal of Disaster Risk Reduction* 3 (2013), pp. 62–75.
20. Kazım Rıfat Özyılmaz and Arda Yurdakul. "Work-in-progress: integrating low-power IoT devices to a blockchain-based infrastructure". In: *2017 International Conference on Embedded Software (EMSOFT)*. IEEE. 2017, pp. 1–2.
21. Pascal Peduzzi et al. "Assessing global exposure and vulnerability towards natural hazards: the Disaster Risk Index". In: *Natural Hazards and Earth System Sciences* 9.4 (2009), p. 1149.
22. Centre for Research on the Epidemiology of Disasters. "EM-DAT: the international disaster database". In: Centre for Research on the Epidemiology of Disasters Brussels. 2011.
23. Pradip Kumar Sharma, Mu-Yen Chen, and Jong Hyuk Park. "A software defined fog node based distributed blockchain cloud architecture for IoT". In: *Ieee Access* 6 (2017), pp. 115–124.
24. Peijun Shi et al. "World atlas of natural disaster risk". In: *World Atlas of natural disaster risk*. Springer, 2015, pp. 309–323.
25. Chung-Hung Tsai and Cheng-Wu Chen. "The establishment of a rapid natural disaster risk assessment model for the tourism industry". In: *Tourism Management* 32.1 (2011), pp. 158–171.
26. Hoang Tam Vo et al. "Blockchain-based data management and analytics for micro-insurance applications". In: *Proceedings of the 2017 ACM on Conference on Information and Knowledge Management*. 2017, pp. 2539–2542.
27. Shuai Wang et al. "An overview of smart contract: architecture, applications, and future trends". In: *2018 IEEE Intelligent Vehicles Symposium (IV)*. IEEE. 2018, pp. 108–113.
28. Web3. *web3.js - Ethereum Javascript*. Data Accessed in January 2019. Mar. 2019. <https://web3js.readthedocs.io/>.
29. Muhammad Saqib Niaz and Gunter Saake. "Merkle Hash Tree based Techniques for Data Integrity of Outsourced Data". In: *GvD*. (2015), pp. 66–71.

Universal Maximum Flow with Intermediate Storage for Evacuation Planning



Urmila Pyakurel and Stephan Dempe

Abstract The evacuation planning problem models the process of shifting residents from emergency areas (sources) to safe places (sinks) as quickly and efficiently as possible. Most of the flow over time models used in the evacuation planning are based on the flow conservation constraints, i.e., the inflow should be equal to the outflow on each node except at the sources and sinks. We investigate the universal maximum flow problem with intermediate storage, i.e., the inflow may be greater than the outflow on intermediate nodes which maximizes the number of evacuees leaving the emergency areas at each point of time. We propose efficient algorithms to solve the problem on two-terminal series-parallel and general networks. We also discuss the solution technique for the problem with arc reversal capability and compare these solutions without and with intermediate storage.

Keywords Evacuation planning · Network flow · Intermediate storage · Algorithms · Contraflow

1991 *Mathematics Subject Classification*. 2010 *Mathematics Subject Classification*. *Primary*: 90B10, 90C27, 68Q25; *Secondary*: 90B06, 90B20.

The first author acknowledges the support to her post doctoral research stay (November 2017 – October 2019) at TU Bergakademie, Freiberg, Germany and return fellowship (November 2019 – October 2020) of Alexander von Humboldt Foundation.

U. Pyakurel (✉)

Central Department of Mathematics, Tribhuvan University, Kathmandu, Nepal
e-mail: urmila.pyakurel@cdmath.tu.edu.np

S. Dempe

Fakultät für Mathematik und Informatik, TU Bergakademie Freiberg, Freiberg, Germany
e-mail: dempe@tu-freiberg.de

© Springer Nature Switzerland AG 2021

I. S. Kotsireas et al. (eds.), *Dynamics of Disasters*, Springer Optimization and Its Applications 169, https://doi.org/10.1007/978-3-030-64973-9_14

1 Introduction

After any type of disaster, we want to save the maximum number of evacuees as fast as possible from the emergency areas and send them to safer places. Due to the flow conservation constraints at each intermediate node of the evacuation network, the dynamic network flow models use only the bottleneck capacity to send the flow from sources to the sinks [4, 6]. They do not care about the excess capacity of intermediate nodes and a possible stay there. If leaving arcs from the sources have more capacity than the minimum cut capacity of the network, the models without intermediate storage do not utilize these arcs to send the possible excess flow. For example, suppose an emergency zone P has 50,000 evacuees and these should be evacuated as soon as possible from that zone. Let R be the safe zone to shift them, but there is no direct connection from P . There are some intermediate zones, let be denoted by Q , that has some capacities to hold an extra number of evacuees. The facility of transportation is available for 50,000 people per day from P to Q , but from Q to R , transportation allows only 40,000 people to travel per day. The existing network flow models send only 40,000 people from P to R , and the remaining 10,000 people should wait in the intermediate zone for the next day.

In this work, we investigate network flow models where intermediate storage is allowed. That means, the outflow from a source need not be equal to the inflow into a sink. The outflow can be larger. We propose a modification of the existing maximum flow models from this perspective. One aim is to use maximum arc capacity to push as much flow as possible out of the source. This modification can only be used if the total capacity of arcs leaving the source is greater than the bottleneck capacity of the network [8]. However, the intermediate nodes are not similar to the sink nodes. We just assume that the intermediate nodes have some capacities in which we can store the excess flow and utilize them as much as possible. In the example described above, by allowing intermediate storage for 10,000 people in the intermediate zones respecting their capacities, our model uses the excess capacity of the arcs from source P and shifts 50,000 people in one day. Moreover, we also assume that it is beneficial to push the flow as far from the sources as possible toward the sinks for more safety.

Pyakurel and Dempe [8] proposed the network flow model with intermediate storage and solved the maximum static flow and maximum dynamic flow problem in two-terminal networks. Moreover, they also claimed that the universal maximum flow (earliest arrival flow) with intermediate storage can be computed efficiently in a two-terminal series-parallel network. The universal maximum flow maximizes the leaving flow from the source at each point of time from the beginning. We propose a polynomial-time algorithm to solve the problem in the two-terminal series-parallel network in this paper. With arc reversal capability, the universal maximum contraflow problem is solved in these networks. Contraflow configuration of an evacuation network increases the outbound road capacities by reversing the direction of arcs that helps to increase the flow value reducing the traffic congestion [10].

The paper is organized as follows. In Sect. 2, we discuss basic terminology and mathematical models. We investigate the universal maximum flow with intermediate storage in Sect. 3. Section 4 presents an efficient algorithm to solve the universal maximum contraflow problem with intermediate storage. The paper concludes with Sect. 5.

2 Mathematical Model

To adopt the network flow models for evacuation planning, we consider a dynamic network $\mathcal{N} = (V, A, u, b, \tau, s, d, T)$ in which different numbers are assigned to the arcs as a nonnegative capacity $b : A \rightarrow \mathcal{Z}^+$, nonnegative cost $c : A \rightarrow \mathcal{Z}^+$, or transit time $\tau : A \rightarrow \mathcal{Z}^+$ and a capacity $u : V \rightarrow \mathcal{Z}^+$. We search for a network flow from sources (which implement risk nodes in evacuation planning problems) S to sinks (which are the safe nodes) D which have sufficient capacities. The given time horizon is T within which the evacuation process should be completed. It may be discretized into discrete time steps $\mathbf{T} = \{0, 1, \dots, T\}$ or can be considered as a continuous one $\mathbf{T} = [0, T]$. Let $s \in S$ be a single source and $d \in D$ be a single sink. Discarding the time function, the network $\mathcal{N} = (V, A, u, b, S, D)$ is a static network.

If we have a single arc $e = (s, d)$, it is a series-parallel network with source s and sink d . Let G_1 and G_2 be two series-parallel graphs with sources s_1 and s_2 and sinks d_1 and d_2 , respectively. Then, the combination $S(G_1, G_2)$ obtained by identifying d_1 with s_2 in the series composition is a series-parallel graph with s_1 and d_2 as its terminals. The graph $P(G_1, G_2)$ obtained by identifying s_1 with s_2 and also d_1 with d_2 in the parallel combination is a series-parallel graph with $s_1 (= s_2)$ and $d_1 (= d_2)$ as its terminals. Our dynamic network $\mathcal{N} = (V, A, u, b, \tau, s, d, T)$ is series parallel with single source s and single sink d .

Generally, we assume that no arcs enter the source nodes and no arcs exit the sink nodes so that $B_s = \emptyset$ and $A_d = \emptyset$ hold, where $B_v = \{e \mid e = (u, v) \in A\}$ and $A_v = \{e \mid e = (v, u) \in A\}$. However, in the case of contraflow configuration below, B_s and A_d are not empty in general. We have $|V| = n$ and $|A| = m$.

Neglecting the cost of the arcs, a static $s - d$ flow with intermediate storage $\phi : A \rightarrow R^+$ of value $\text{val}(\phi)$ in the objective function (1) satisfies the constraints (2–4) [8]:

$$\text{val}(\phi) = \sum_{e \in A_s} \phi_e = \sum_{e \in B_d} \phi_e + \sum_{v \in I: u_v \geq 0} \phi_v \tag{1}$$

$$\phi_v = \sum_{e \in B_v} \phi_e - \sum_{e \in A_v} \phi_e \geq 0, \quad \forall v \in I \tag{2}$$

$$b_e \geq \phi_e \geq 0, \quad \forall e \in A \tag{3}$$

$$u_v \geq \phi_v \geq 0, \quad \forall v \in I \tag{4}$$

Here, the function $\phi_v : I \rightarrow \mathcal{Z}^+$ is the amount of flow storage in the intermediate nodes.

If the total arc capacities leaving a source are greater than the minimum cut capacity of the network, then the formulation (1–4) gives the maximum static flow with intermediate storage.

Let $\psi : A \times \mathbf{T} \rightarrow \mathcal{R}^+$ be a dynamic flow in discrete time \mathbf{T} . The universal maximum flow problem with intermediate storage maximizes the objective function (5) with respect to $\psi_e(\sigma)$ for all $\theta \in T$ by satisfying the constraints (6–8):

$$\text{val}(\psi, \theta) = \sum_{e \in A(s)} \sum_{\sigma=0}^{\theta} \psi_e(\sigma) = \sum_{e \in B(d)} \sum_{\sigma=\tau_e}^{\theta} \psi_e(\sigma - \tau_e) + \sum_{v \in I, u_v > 0} \psi_v(\theta) \quad (5)$$

$$\psi_v(\theta) = \sum_{e \in B_v} \sum_{\sigma=\tau_e}^{\theta} \psi_e(\sigma - \tau_e) - \sum_{e \in A_v} \sum_{\sigma=0}^{\theta} \psi_e(\sigma) \geq 0, \quad \forall v \in I, \theta \in \mathbf{T} \quad (6)$$

$$b_e(\theta) \geq \psi_e(\theta) \geq 0, \quad \forall e \in A, \theta \in \mathbf{T} \quad (7)$$

$$u_v \geq \psi_v \geq 0, \quad \forall v \in I \quad (8)$$

Here, the function $\psi_v : I \times T \rightarrow \mathcal{Z}^+$ is the amount of flow storage in the intermediate nodes within time T .

If the flow is maximized in given time horizon T , then objective function (5) gives the maximum dynamic flow with intermediate storage by satisfying the constraints (6–8), [8]. Moreover, if the flow is not allowed to be stored at intermediate nodes, then the static and dynamic flow models are equivalent to the flow models of Ford and Fulkerson [6].

3 Flow over Time with Intermediate Storage

Based on the investigation conducted in [8], in this section, we discuss a solution technique for the universal maximum flow problems with intermediate storage. We present a polynomial-time algorithm to solve the problem in a two-terminal series-parallel network.

Definition 1 The universal maximum flow with intermediate storages is the earliest arrival flow in which outgoing flow from source is maximized at each point of time from the beginning and pushed flow as far as possible toward the sink allowing excess flow storage at intermediate nodes.

In the solution procedure (cf. Algorithm 1), we convert our network into a single-source multi-sink network in Step 1 and also fix the priority ordering in Step 2 as follows. We always give the first priority for the sink. But the priority of intermediate nodes is fixed according to their distances from the source. Let, for

$v \in V \setminus \{s\}$, $\text{dis}(s, v)$ be the shortest distance of node v with $u_v > 0$ from the source s with respect to the cost (time) that is obtained by using Dijkstra’s algorithm, [5] as we have $\tau_e \geq 0$ or $c_e \geq 0$. As our aim is to push the flow as far as possible from the source, the node with the longest distance, i.e., the maximum distance among the shortest distances, gets second priority and so on.

Then, a dummy shelter v' with dummy arc (v, v') having distance $c_{(v,v')} = 0$ and capacity $b_{(v,v')} = u_{v'} = u_v$ is added to each intermediate node $v \in I$ with capacity $u_v > 0$. Let the set of dummy shelters be denoted by I' . The dummy shelter v' is also a sink and gets the same priority as the node v . Thus, in Step 3, the given s - d network is modified into one with a single source and multiple sinks with updated parameters as $\mathcal{N}' = (V, A, b, u, c, s, D)$, where $V = V \cup I'$, $A = A \cup \{(v, v')\}$, and the multiple sinks $D := \{d\} \cup I'$. The parameters are modified as $b = b \cup \{b_{(v,v')}\}$, $u = u \cup \{u_{v'}\}$, and $c = c \cup \{c_{(v,v')}\}$. Let $\mathcal{S} = \{s\} \cup D$ with $|\mathcal{S}| = \delta$ be the set of terminals in the modified network in which we solve the lexicographically maximum dynamic flow problem (LMDFP) without intermediate storage using the polynomial-time algorithm of [7] in Step 4 of Algorithm 1. For the given time T and an ordered set of terminals, the LMDFP finds a feasible flow that lexicographically maximizes the flow entering each terminal with the given priority. By transforming the solution to one for the original network, we get the maximum dynamic flow with intermediate storage in two-terminal series-parallel network. As the obtained flow satisfies the earliest arrival property, i.e., a cumulative amount of flows reaching the sink in every considered time period and all preceding time periods of the considered one, it has to be maximal.

Algorithm 1: Universal maximum flow with intermediate storage

Input : An s - d series-parallel network $\mathcal{N} = (V, A, b, u, \tau, s, d)$

Output: The universal maximum flow with intermediate storage

- (1) Use the shortest path algorithm of [5] to find the minimum distances $\text{dis}(s, v)$ for all $v \in V \setminus \{s\}$ with $u_v > 0$.
 - (2) Give first priority to the sink d , second priority to the intermediate node v with longest distance from source with $u_v > 0$ and so on.
 - (3) Modify the network into single source and multi-sinks by creating dummy shelters I' . The resulting network is $\mathcal{N}' = (V, A, b, u, \tau, s, D)$, where $D = I' \cup \{d\}$.
 - (4) Compute priority-based maximum dynamic flow iteratively on the modified network.
 - (5) Transform the solution to the original network by removing dummy shelters and dummy arcs.
-

Theorem 1 *For an s - d series-parallel network, the maximum dynamic flow with intermediate storage can be solved in polynomial time complexity with Algorithm 1.*

As Pyakurel and Dempe [8] have presented, this is a polynomial-time algorithm to solve the maximum dynamic flow with intermediate storage in the two-terminal general network. The proof of the above theorem is similar but with improved complexity in the two-terminal series-parallel network.

Theorem 2 *The universal maximum flow with intermediate storage can be solved in $O(\delta \times (nm + m \log m))$ time complexity in the two-terminal series-parallel network.*

Proof As in [8] and Theorem 1, Algorithm 1 gives the maximum dynamic flow with intermediate storage in a two-terminal network. Due to the dummy shelters, the flow conservation at each node is satisfied. With the fixed priority ordering of nodes in D , Step 4 computes the dynamic flow via δ MCF computations using an algorithm of [7] in $O(\delta \times MCF(n, m))$ time, where δ gives the number of terminals, i.e., $\delta = |S|$, $|S| = \{s\} \cup D$ and $MCF(n, m)$ represents the time complexity of a single minimum cost flow computation MCF using the original network. A minimum cost circulation flow solution has minimum cost if and only if the corresponding residual network does not contain a cycle with negative cost [1]. The main advantage on a series-parallel network is that every cycle in the residual network has nonnegative cycle length. The minimum cost flow computation can be made in polynomial time $O(nm + m \log m)$ in s - d series-parallel network, [15]. Thus obtained maximum dynamic flow has the earliest arrival property, i.e., flow is maximized at every time point from the beginning, i.e., we have

$$\text{val}(\psi, \theta) = \sum_{e \in A(s)} \sum_{\sigma=0}^{\theta} \psi_e(\sigma) = \sum_{e \in B(d)} \sum_{\sigma=\tau_e}^{\theta \in T} \psi_e(\sigma - \tau_e) + \sum_{v \in I, u_v > 0} \psi_v(\theta).$$

This completes the proof. □

Example 1 Consider a two-terminal series-parallel network as in Fig. 1a in which $|v| = 7$ and $|A| = 16$. Let $I = \{x, y, u, w\}$ be the set of intermediate nodes with $u_v > 0$. Source s and sink d have infinite capacities. Intermediate nodes x, y, u , and w have capacities 20, 25, 15, and 10, respectively. Each arc has capacity and transit time function value. For example arc (s, y) has capacity 4 units and transit time 1 unit. That means, 4 units of flow can together travel along arc (s, y) with 1 unit transit time for each unit of flow. The minimum cut of this network is 5 and the maximum capacity outgoing from source is 9. As the capacity of outgoing arcs from the source is greater than the minimum cut, the dynamic flow with intermediate storage is possible.

First, we calculate the shortest distances of nodes in I from s . Using the shortest path algorithm, we get $\text{dis}(s, x) = 2$, $\text{dis}(s, y) = 1$, $\text{dis}(s, u) = 3$, and $\text{dis}(s, w) = 4$. The priority ordering is fixed as d, w, u, x, y , i.e., we maximize the flow to node d first; then to node w, u, x ; and last to node y . Then, by creating dummy shelters x', y', u' , and w' as well as dummy arcs with zero transit times and equal capacities as in respective intermediate nodes, we get the modified network as in Fig. 1c. Now we use the LMDF algorithm of [7] to calculate the minimum cost flow without intermediate storage at each sink. For this, we construct the super sink d^* and connect each sink with it assuming infinity capacity and zero transit time. Then we add an arc from d^* to s and compute the minimum cost flow circulation. Here

the minimum cost flow circulation is calculated by applying the greedy algorithm of [15]. That gives the universal maximum flow. Then the solution of dummy shelters is transformed in the respective intermediate nodes that give the universal maximum flow with intermediate storage. For $T = 6$, the universal maximum flow with intermediate storage is shown in Fig. 2:

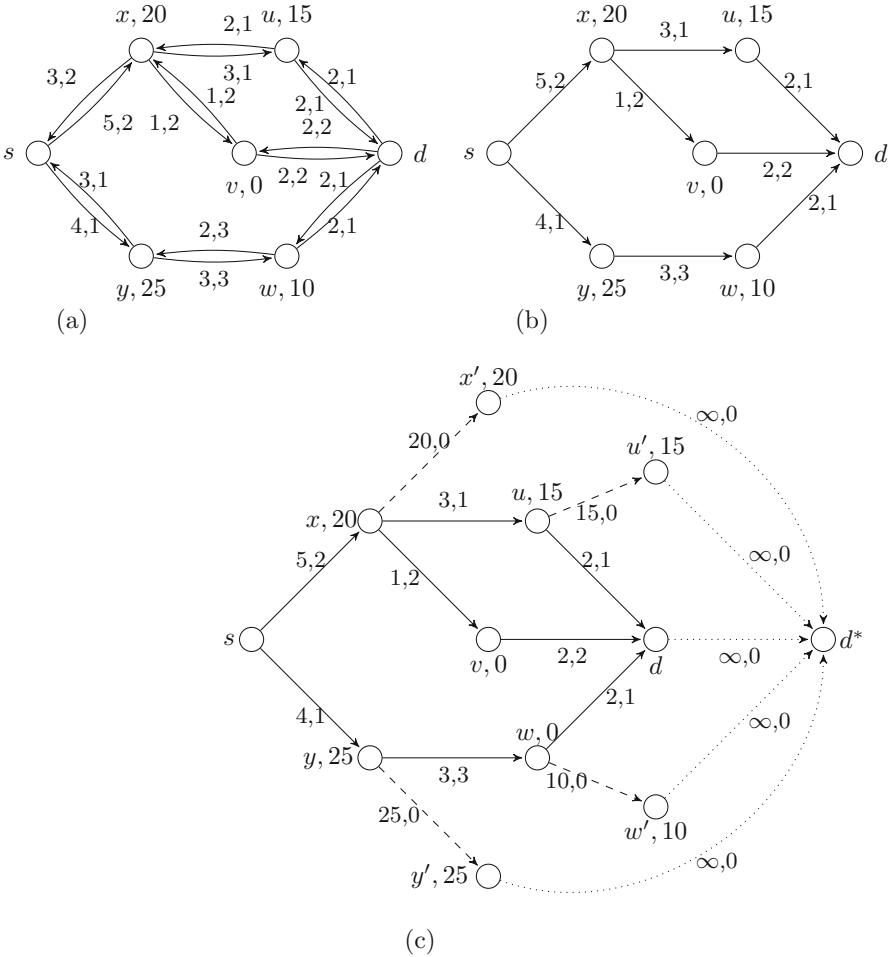


Fig. 1 (a) A two-way evacuation $s-d$ series-parallel network (b) One-way $s-d$ series-parallel network (c) Modified $s-D$ series-parallel network with super sink d^*

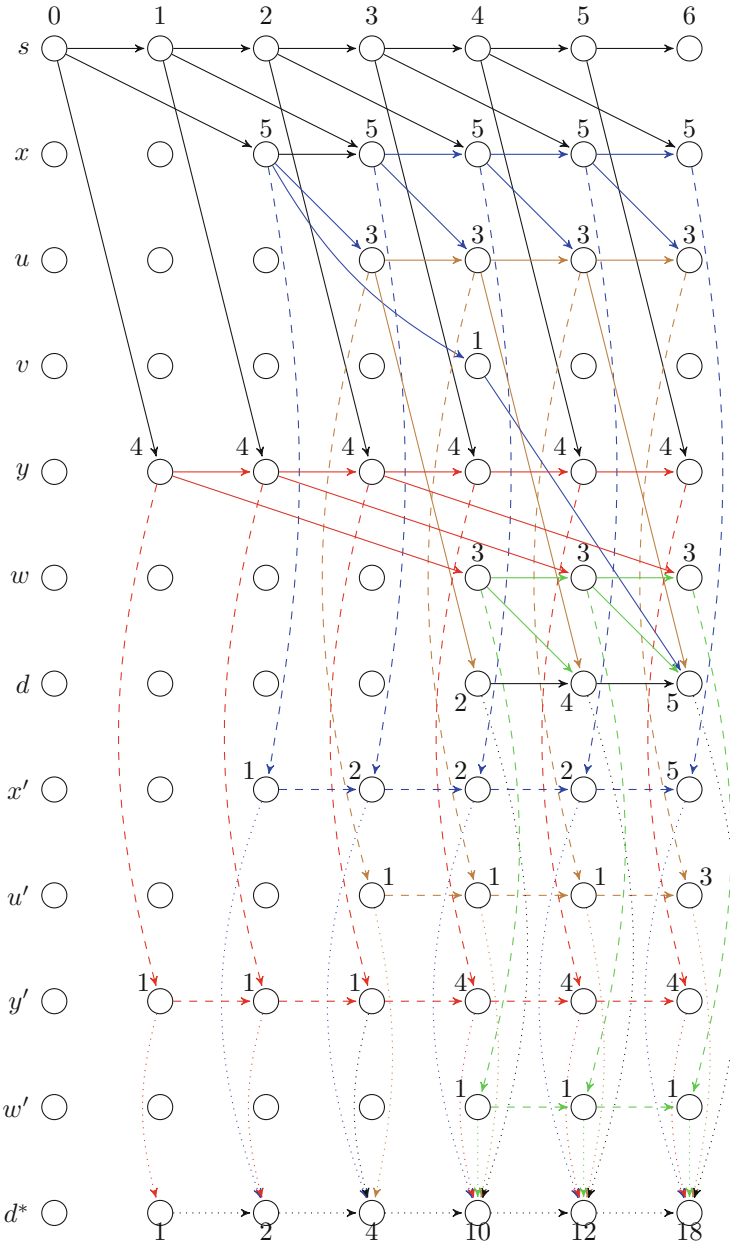


Fig. 2 Earliest arrival flow without intermediate storage in the time expanded network

On a s - d general network, the universal maximum flow with intermediate storage is obtained using the time expanded network and its complexity is pseudo-polynomial.

4 Contraflow over Time with Intermediate Storage

Due to the increasing number of large-scale disasters worldwide, the research in evacuation planning using a contraflow configuration technique for a transportation network is very important and useful. The contraflow approach aims at finding the ideal direction of the traffic flow resulting in increasing the outbound capacities of the arcs in the transportation network. That minimizes the traffic congestion and maximizes the flow so that evacuation time is also minimized, [2, 9, 10, 11, 12, 13, 14]. All contraflow models in literature have been designed without allowing the intermediate storage.

Pyakurel and Dempe [8] introduced the first network flow model with intermediate storage with arc reversal capability. They presented a polynomial-time algorithm that solves the maximum dynamic contraflow problem with intermediate storage on a two-terminal network for a given time horizon T . In this section, we introduce the universal maximum contraflow (UMCF) problem with intermediate storage in which outgoing flow from source is maximized at every time point from the beginning. However, our network for the problem is a two-terminal series-parallel network.

Definition 2 Given an s - d series-parallel network $\mathcal{N} = (V, A, b, u, \tau, s, d, T)$ with symmetric transit times, the universal maximum contraflow with intermediate storage is the earliest arrival contraflow in which outgoing flow from source is maximized at each point of time and pushed as far as possible toward the sink allowing excess flow storage at intermediate nodes with arc reversal capability.

The UMCF problem without intermediate storage has been solved with a strongly polynomial-time algorithm in a two-terminal series-parallel network, [3, 9]. To solve the UMCF with intermediate storage on the two-terminal series-parallel network, we adopt their solution technique to find s - d UMCF and push maximum flow value using maximum capacity away from the source. In the procedure, we construct an auxiliary network in which the two-way capacities of each arc are added to obtain the resulting capacity and transit time is taken as constant. Then, for each intermediate node $v \in I$, the shortest distance $d(s, v)$ from source s is computed and the priority ordering is fixed as in Sect. 3. For each node v with $u_v > 0$, we construct a dummy shelter v' at zero distance with capacity $b_{(v,v')} = u_v = u_{v'}$ having same priority ordering as in v so that the network becomes a modified auxiliary network. In this network, we compute the MCCF with single sink d having first priority and obtain MDF without intermediate storage. Then, we update the remaining capacities of the network and compute the MCCF for the dummy shelter v' with second priority respecting the node capacity $u_{v'}$. Again we update the arc capacities of the network and solve another MCCF problem for the dummy sink with third priority and so on as in [7]. However, we take the time bound of [15] to compute the MCCF for s - d series-parallel network. Then the obtained priority-based MDF solution is transformed into an auxiliary network by removing the dummy shelters that gives the MDF at the sink d and storage at intermediate nodes. Moreover, the obtained

MDF solution has maximal value leaving the source at each time point from the beginning. Thus, it is the UMF with intermediate storage on the auxiliary network. As we are doing the contraflow configuration for the single-sink network, the UMF at d on the auxiliary network is equivalent to the UMCF for the original network \mathcal{N} as in [3, 9]. The intermediate storage does not change the UMCF solution for the original network with a single sink d . We use Algorithm 2 to find the UMCF with intermediate storage on two-terminal series-parallel networks.

Algorithm 2: Universal maximum contraflow with intermediate storage

Input : An s - d series-parallel network $\mathcal{N} = (V, A, b, u, \tau, s, d, T)$

Output: The universal maximum contraflow with intermediate storage

- (1) Construct the corresponding auxiliary network $\bar{\mathcal{N}}=(V, E, \bar{b}, u, \bar{\tau}, s, D, T)$, where the capacities and transit times are defined as

$$b_{\bar{e}} = b_e + b_{e'}$$

$$\tau_{\bar{e}} = \begin{cases} \tau_e & \text{if } e \in A \\ \tau_{e'} & \text{otherwise} \end{cases}$$

with the reversal of an arc $e = (v, w)$ as denoted by $e' = (w, v)$.

- (2) Solve Steps (1–3) of Algorithm 1 and obtain the modified network $\bar{\mathcal{N}}' = (V, A, b, u, \tau, s, D, T)$
 - (3) Compute the LMDF without intermediate storage on the auxiliary network $\bar{\mathcal{N}}'$ within the time bound of [15].
 - (4) Decompose the obtained flow in Step 3 into paths and removable cycles.
 - (5) Remove the dummy shelters and transform the solution on auxiliary network that gives the priority-based MDF with intermediate storage.
 - (6) Reverse the arc $e' \in A$ up to the capacity $\phi_e - b_e$ if and only if $b_e < \phi_e$, b_e is replaced by 0 whenever $e \notin A$.
 - (7) For the original network, it is equivalent to the UMCF with intermediate storage for single sink d .
-

Theorem 3 *The UMCF with intermediate storage can be computed in polynomial time complexity on s - d series-parallel network.*

Proof Steps 1, 2, 3, 4, 5 and 7 of the algorithm are feasible. Now, it is enough to show that only Step 6 is well defined to prove the feasibility of Algorithm 2. As Step 4 does not contain any cycle, there is either a flow along arc $e = (v, w)$ or $e' = (w, v)$ but never in both arcs in Step 6. This proves that the flow is not greater than the reversed capacities on all arcs at all time units. Thus, Step 6 is also feasible.

Now, Algorithm 2 gives an optimal solution as follows. For the given s - d series-parallel network, the contraflow configuration is performed as in Step 1 at zero time, and it is fixed for all time periods. In the auxiliary network $\bar{\mathcal{N}}$, shortest distance $\text{dis}(s, v)$ for all $v \in V \setminus \{s\}$ is computed, the priority ordering is fixed, and the modified auxiliary network $\bar{\mathcal{N}}' = (V, A, \bar{b}, u, \bar{\tau}, s, D, T)$ is constructed by creating dummy shelters as in Algorithm 1. With dummy shelters, the modified

auxiliary network is a multi-sink network with fixed priority ordering. We use the algorithm of [7] within the time bound of computing minimum cost flow circulation using the greedy algorithm of [15] and compute the priority-based MDF without intermediate storage on the multi-sink network which is obtained in polynomial time complexity. The dummy shelters are removed, and the solution is transformed into the s - d auxiliary network that gives the MDF for single sink d with intermediate storage which is equal to the UMF with intermediate storage. According to [3, 9], every universal maximum dynamic flow without intermediate storage on s - d auxiliary network is equivalent to the universal maximum dynamic contraflow without intermediate storage on given s - d network. As we use the excess arc capacity to transship the flow from s to intermediate nodes, the s - d UMCF does not change by allowing intermediate storage. This completes the proof. \square

Example 2 We consider Fig. 1a as an input network. According to Algorithm 2, we construct the auxiliary network of \mathcal{N} using Step 1 as in Fig. 3 in which we add two-way arc capacities, but the transit time remains fixed. Then in the auxiliary network, we calculate the shortest distance, fix priority ordering, and create dummy shelters as in Example 1. Then we compute the MDF in given priority orderings without intermediate storage, e.g., by computing the minimum cost flow circulation using the greedy algorithm of [15]. The priority-based MDF on a modified auxiliary network is equal to the UMF on an auxiliary network without intermediate storage. Transforming the solution in the original network, we get the UMCF solution with intermediate storage. With contraflow configuration, total of 22 units reach the sink, 3 units stay at w , 8 units stay at u , 18 units stay at x , and 25 units stay at y . As

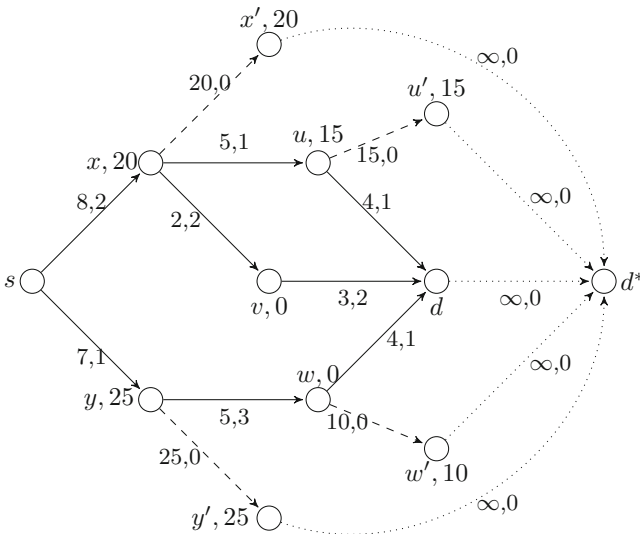


Fig. 3 Auxiliary modified network

node y has 25 capacity, path $s - y$ carries only 5 units flow at time 6. Thus, the number of flow units leaving the source is significantly increased with contraflow configuration.

In both cases, i.e., without contraflow and with contraflow, the obtained universal maximum flow solution with intermediate storage is more practicable in comparison to the solution without intermediate storage.

5 Conclusions

We have investigated the network flow models with intermediate storage and introduced the universal maximum flow problem with intermediate storage in two-terminal series-parallel network. We have presented a polynomial-time algorithm to solve the problem. Moreover, with the arc reversal capability, we have introduced the universal maximum contraflow problem with intermediate storage and solved it with a polynomial-time algorithm in a two-terminal series-parallel network.

References

1. R. K. Ahuja, T.L. Magnati, T. and J.B. Orlin, (1993). *Network flows: theory, algorithms and applications*. Prentice Hall, Englewood Cliffs, New Jersey.
2. A. Arulsevan, (2009). *Network model for disaster management*. Ph.D. Thesis, University of Florida, USA.
3. T.N. Dhamala and U. Pyakurel (2013). Earliest arrival contraflow problem on series-parallel graphs. *International Journal of Operations Research*, **10**, 1–13
4. T.N. Dhamala, U. Pyakurel and S. Dempe (2018). A critical survey on the network optimization algorithms for evacuation planning problems. *International Journal of Operations Research (TW)*, **15**(3), 101–133.
5. E. W. Dijkstra (1959). A note on two problems in connexion with graphs. *Numerische Mathematik*, **1**(1), 269–271.
6. L.R. Ford and D.R. Fulkerson (1962). *Flows in networks*. Princeton University Press, Princeton, New Jersey.
7. B. Hoppe and E. Tardos (2000). The quickest transshipment problem. *Mathematics of Operations Research*, **25**, 36–62.
8. U. Pyakurel and S. Dempe (2019). *Network flow with intermediate storage: Models and algorithms*. Preprint, 2019, TU Bergakademie Freiberg.
9. U. Pyakurel and T.N. Dhamala (2015). Models and algorithms on contraflow evacuation planning network problems. *International Journal of Operations Research*, **12**, 36–46.
10. U. Pyakurel and T.N. Dhamala (2017). Continuous dynamic contraflow approach for evacuation planning. *Annals of Operation Research*, **253**, 573–598.
11. U. Pyakurel, T.N. Dhamala and S. Dempe (2017). Efficient continuous contraflow algorithms for evacuation planning problems. *Annals of Operations Research (ANOR)*, **254**, 335–364.
12. U. Pyakurel, H.N. Nath and T.N. Dhamala (2018). Efficient contraflow algorithms for quickest evacuation planning. *Science China Mathematics*, **61**(11), 2079–2100.

13. U. Pyakurel, H.H. Nath and T.N. Dhamala (2018). Partial contraflow with path reversals for evacuation planning. *Annals of Operations Research*, <https://doi.org/10.1007/s10479-018-3031-8>.
14. S. Rebennack, A. Arulsevan, L. Elefteriadou and P.M. Pardalos (2010). Complexity analysis for maximum flow problems with arc reversals. *Journal of Combinatorial Optimization*, **19**, 200–216.
15. S. Ruzika, H. Sperber and M. Steiner (2011). Earliest arrival flows on series- parallel graphs. *Networks*, **10**, 169–173.

A General Framework and Control Theoretic Approach for Adaptive Interactive Learning Environments



Alexander Streicher, Rainer Schönbein, and Stefan Wolfgang Pickl

Abstract From a system's theoretical point of view, adaptive learning systems (ALS) for education and training contain in their core – in a simplified form – closed feedback control loops in which the control is determined by the measured users' performance. Improving this performance can increase the learning outcome, especially for critical disciplines such as education or training for disaster risk management. However, for this special form of intelligent (e-learning) assistance systems, learning theories and behavioral models have to be considered, e.g., game flow theory, cognition models, or learning models. The research question is how adaptive interactive learning environments (ILE) such as serious games and computer simulations can be characterized and analyzed to determine optimal adaptation strategies. Adaptive learning environments should adapt to the context-related needs of the user in order to ensure and optimize learning success, especially for disaster management training. This contribution presents a concept for an interoperable, adaptive ILE framework which follows control theory and its models, contributing to the state of the art for adaptive games or simulations in disaster risk management.

Keywords Adaptivity · Assistance systems · Interactive learning environments · Modeling of human performance · Closed-loop feedback

1 Introduction

Effective assistance systems for education and training try to improve the users' learning experience. One key factor in effective training and tutoring is to motivate

A. Streicher · R. Schönbein
Fraunhofer IOSB, Karlsruhe, Germany
e-mail: alexander.streicher@iosb.fraunhofer.de; rainer.schoenbein@iosb.fraunhofer.de

S. W. Pickl (✉)
Universität der Bundeswehr München, Neubiberg, Germany
e-mail: stefan.pickl@unibw.de

the users. In contrast to external motivational factors (e.g., social or economic pressure to succeed), intrinsic motivation can sustainably optimize learning outcomes [28]. One way to increase user motivation is to utilize the principles from digital game-based learning. Further optimization can be achieved through personalized learning in which adaptive learning systems (ALS) adapt to the individual needs of the user [34]. This is typically referred to as intelligent tutoring systems (ITS), cf. Woolf [36]. They can be regarded as a special form of intelligent assistance systems for learning. A special form of adaptive learning systems is found in interactive learning environments (ILE) such as computer simulations and serious games. The latter are digital learning games with a characterizing or “serious” goal – in the case of digital learning games, education, and training, cf. Dörner et al. [12]. Particular challenges lie in modeling and analysis. In the four-phase adaptivity process by Shute et al. [30], our focus is on the analysis phase and the learner model or, more generally, user model. This contribution deals with the modeling and analysis of adaptive ILE (aILE). The research question is how aILE such as serious games and computer simulations can be characterized and analyzed to determine optimal adaptation strategies.

The problem statement originates in our application area, which is adaptive e-learning for professional aerial and satellite image interpretation. It is a discipline which is also of help for disaster response tasks such as search-and-rescue operations (S&R). Figure 1 shows an example S&R application with a quadrocopter looking for buried victims and a mobile learning app for operators training. Image-based intelligence systems have become increasingly important for emergency and security services [8, 18], e.g., for dynamic disaster response training. To provide rapid and targeted assistance in case of disaster, the emergency services and security forces depend on up-to-date and location-relevant information of the current situation in the field. Combined sensor systems with all kinds of sensor platforms, e.g., robots and balloons, can support emergency services. An example

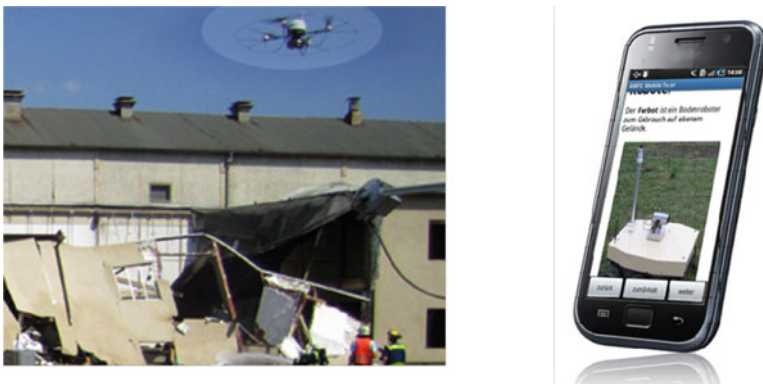


Fig. 1 (left) Application of a quadrocopter for aerial image intelligence in a disaster scenario. (right) Smartphone with mobile assistant to support the action force in the field

of a relevant application of such combined information systems is the remote sensing of damaged reactors at the Fukushima nuclear power plant disaster. Another example is the training of disaster scenarios for emergency services. Scientists and rescue teams test new technologies to assist emergency services and to help protect the people in real-world settings. The interpretation of aerial and satellite images poses a wide range of challenges because of different imagery sensor types, difficult image material, and unknown objects or situations that are hard to interpret. Professional image interpretation is done in various fields, ranging from the microscopic level in medicine, e.g., diagnostics in histopathology, to the macroscopic level of aerial or satellite images, e.g., civilian applications like search-and-rescue, agriculture, oceanography, or military intelligence [26]. Special face-to-face training courses blended with technology-enhanced learning tools, such as e-learning courses, simulations, and serious games, ensure that image analysts are qualified to a high standard. Adaptive assistance systems support the users in this.

2 Related Work

2.1 *Disaster Management and Educational Serious Gaming*

As can be seen in the comprehensive literature review by Solinska-Nowak et al. [31], serious games, i.e., games with a characterizing goal [12], are widely applied to disaster management. The benefits arise from their hands-on or experiential learning experience which strengthens knowledge acquisition and activates learning, as depicted by Kolb [17].

The characterizing goal of serious games for disaster management typically concerns the character of disaster itself – real disasters are not for game entertainment. Often this aspect already fulfills the “serious” aspect. However, there are combinations of other serious aspects as well, such as education and training, or learning. For the latter the term educational serious games is typically used [12]. In our work we focus on this very combination of serious gaming, education and disaster management, and adaptivity to further increase the intrinsic motivation and learning outcome [34].

The literature review from Solinska-Nowak et al. [31] lists various examples for serious gaming for disaster management. Such examples comprise serious games on disaster risk reduction to raise awareness about geohazards [21] or [15]; or games on natural resource management [4]; on climate or climate change [27].

Regarding the topic of adaptive educational serious games for disaster management, only a very limited number of matching publications can be found. The search terms “disaster management” and “serious game” and (adaptive or adaptivity or personalization) show only a handful of matching results, “adaptive” or “adaptivity” being the limiting factor.

Arnold et al. [2] focus on an adaptivity for a serious game for disaster management. They describe a storyboarding approach combined with a user model to implement an adaptive behavior.

Oulhaci et al. [24] present an adaptive approach with a multi-agent system which addresses humanlike behavior of non-player characters (NPC) in a game for crisis management.

Capuano et al. [6] show an adaptive game approach to teach school students how to behave in case of natural disasters.

From a system theoretic perspective, control theory has long been an active, well-established, and vastly applied field of research [19, 3]. One of its main problems studied is adaptive control [3, 5]. A comprehensive literature review can be found in the book by Chalam [7], which highlights its importance for various fields of application, including electrical and electronic engineering, chemistry, mechanics, aerospace, biomedicine, shipping, transport, and power plant engineering. While there is adaptivity in e-learning (e.g., [36, 35]), little is to be found on the transfer from systems theory to e-learning. Our work contributes to this aspect, to benefit from the combination of both worlds. We apply adaptive control theory to our models of adaptivity in e-learning.

2.2 *Systems Theory and E-learning*

Advantages can arise when two disciplines are combined – in the combination lies the strength. In this case, the established methods of systems theory [19, 7] are transferred to e-learning and there especially to adaptive learning systems. In both disciplines there are approaches to adaptive systems. In systems theory, it is the adaptive control systems that adapt to dynamic changes in environmental parameters at runtime [3, 16]. Similarly, in e-learning it is the adaptive learning systems that adapt to the dynamic behavior of the user. While there are established and proven adaptive systems in systems theory and control engineering for decades (e.g., [19]), this is not yet the case with e-learning. In control engineering, adaptive control systems that are standardized, tested, and certified in engineering terms can be used interoperably in similar applications, thanks to generic modeling. For example, adaptive altitude control systems for aircraft are so similar that they can easily be exchanged at the same interfaces if the underlying flight characteristics are modeled identically. In adaptive learning systems, there are no uniform interfaces or models with regard to inputs and outputs. More recent approaches use the usage tracking standard protocol *Experience API* (xAPI) for the acquisition of input data [34]. There is no standard yet for adaptive responses. Here, a transfer of the approaches from control engineering can show the directions. The added values can be found in the definition of the interfaces as well as in the modeling. It is also possible to learn from the development history and identify dead ends and wrong directions at an early stage. Another point is that one should try to transfer the robustness aspects like dealing with unmodeled dynamics or uncertainties. The theory of adaptive

control is quite vast and incorporates robustness in many settings [3, 29]. Adaptive learning systems must also be robust to dynamic inputs in terms of reliability and correctness. In control engineering critical situations that necessitate robust reaction can arise immediately, for example, the automatic control of airplanes to prevent dangerous situations such as stalling. However, the consequences of adaptive assistance systems in e-learning can be rather long-term, for example, the wrong training of action patterns, which are difficult to relearn.

2.3 Adaptive Assistance in E-learning

Adaptivity for education and training has long been an active research topic, generally seen as intelligent tutoring systems [23, 36], and also in specialized forms for serious gaming [14, 34]. To achieve an adaptive behavior, AI methods such as data mining and machine learning are used in all adaptivity phases, cf. Frutos-Pascual and Zapirain [14], and, as stated by Yannakakis [37], AI for decision-making and player experience modeling (PEM) are key research areas. Cruz et al. [10] show how the well-established theory of flow is used for player-centered game adaptivity. In respect to our generic modeling approaches, Mäses et al. [20] present a similar approach to define user performance metrics and scores. On completeness, the more technical aspects of interoperable adaptivity frameworks and their related work have already been described in other contributions from the authors, e.g., Streicher et al. [33].

Regarding the transfer of systems theory to ALS, in particular control theory and adaptive control, no related literature has been found, to the best of our knowledge.

3 Adaptive Control for Adaptive Learning Environments

As learning efficacy is directly linked to high intrinsic motivation, one possibility to keep the users motivated is to engage them to continuously participate in the (e-learning) programs. For educational serious games, one can try to keep up high immersion levels by keeping the users in the so-called flow channel [9]; Fig. 2 depicts this and how adaptivity comes into play. An adaptive learning system should control the ILE to keep the users in the flow channel, i.e., by automatically adapting the game to fit the users' skills and competencies. This balance between skill and competence is typically called the flow channel [11, 9].

Fig. 2 AI to control the flow channel alignment (based on the original three-dimensional model by Csikszentmihalyi et al. [11])

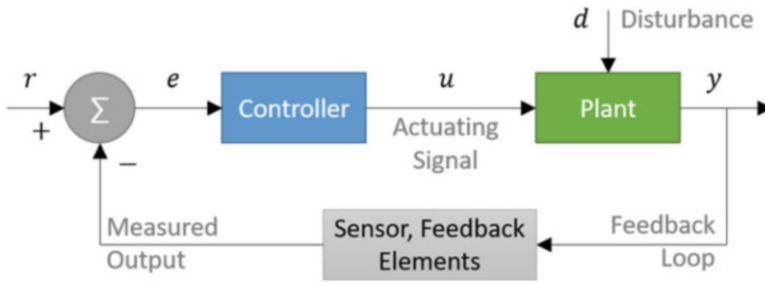
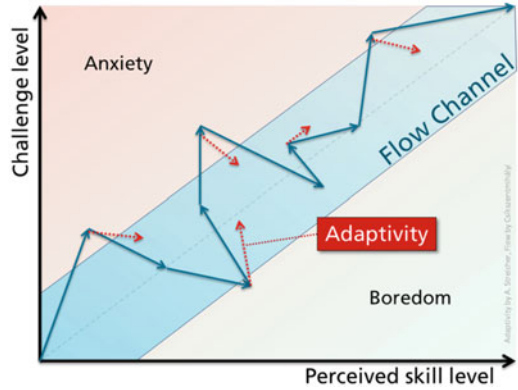


Fig. 3 Closed-loop feedback control system

3.1 Control Systems

Taking this to the broadest sense, the ALS measures how the users interact with the system and modifies it in a way that the next inputs produce certain expected outputs [19]. This perfectly fits the description for general (linear) closed-loop feedback control systems where the output y is fed back as feedback to the input r (see the block diagram for a negative feedback closed-loop control system; Fig. 3). The controller issues actuating signals u to the process or plant which gives the output y . A comparator function produces an error signal $e = r - y$ as the difference between the input and the feedback signal.

3.2 Control Systems from a Learner’s Perspective

This control system model can also be seen differently from the learner or e-learning perspective where the learning outcome of the users should be “controlled.” Figure 4 depicts this transfer to the learner perspective: the “system under control” could be seen as the learner, and the controller is the ILE which should influence the

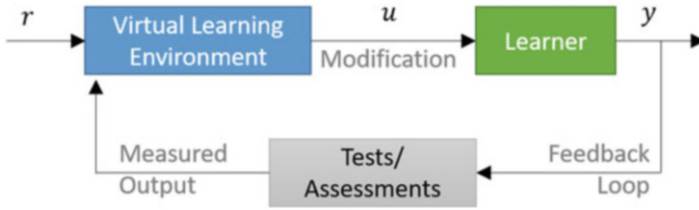


Fig. 4 Learner perspective for a closed-loop feedback control system for e-learning

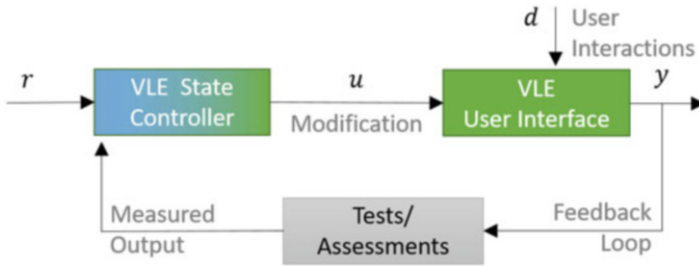


Fig. 5 System perspective for a closed-loop feedback control system for e-learning

learning outcome. In the feedback loop, we measure the learner’s performance (e.g., assessments) and issue feedback elements to the ILE.

3.3 Control Systems from System Perspective

Since we are interested in the system theoretic perspective, we can use the control system model and apply it to ILE systems, so the ILE itself becomes the system under control; see Fig. 5. From a software design view, an ILE has a controlling back end to adjust the game state, as well as a user interface for presentation and user interaction. The actuating signal u can be seen as the dynamic elements in a game, e.g., virtual consoles, NPCs, resources, etc.

3.4 Ideal Path Control Framework

But, normally human learning cannot be measured and controlled in deterministic ways. Hence nonlinear and learning-based adaptive control must be considered [25]. With human learning in the loop, we typically deal with complex, nonlinear processes which motivates the use of adaptive control theory [3]. In adaptive control the controller must adapt to initially uncertain or varying parameters. This perfectly fits the idea of ALS – at the beginning we deal with the so-called cold-start problem

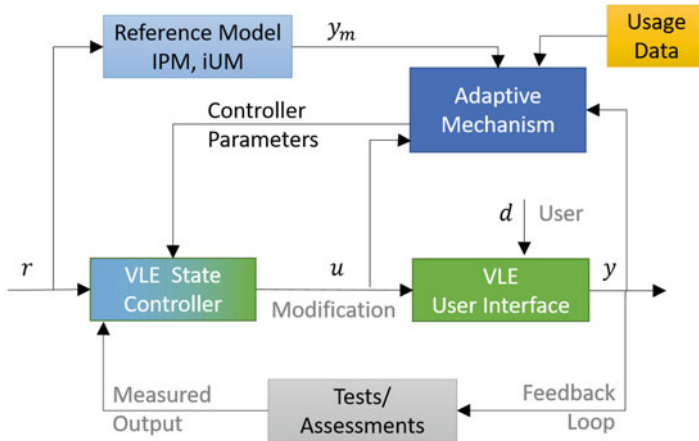


Fig. 6 Model reference adaptive control (MRAC) for adaptive interactive learning environments

because no information on the user is available. Typically ALS start with assessing the users' knowledge level by initial questionnaires or tests to classify the user, e.g., stereotyping the user as beginner, intermediate, or expert. Over time ALS must adapt to parameter changes, e.g., change of playing pace, performance, or motivation (cf. Sect. 1).

To define the closed-loop performance, we need a reference model as basis for deviation estimation, i.e., a model to characterize the users' playing behavior. One approach in adaptive control is model reference adaptive controller (MRAC) systems [3, 22]. We propose to see the reference model as an "ideal path" through an ILE, as suggested with the ideal path model (IPM) [33]. The IPM is basically a "ground-truth" how an ideal interaction through a game would look like, "ideal" meaning an optimal sequence of interactions to play through a game without unnecessary detours. Based on the game mechanics, there can be just one or multiple ideal paths. Of course, a beginner would not play a game as straightforward as an expert; thus, the deviations from IPM would be very different for the beginner and for the expert (Fig. 6).

The IPM [33] is intended to improve the adaptive control of ILE by more accurately assessing performance and the need for help based on player interaction. The IPM is particularly useful in combination with additional sensor data observing the users' behavior while interacting with an assistance system, for example, gaze or eye tracking. Eye tracking can provide insights into the cognitive states of users by tracking their visual attention. A typical example would be that attention is directed to the first area of interest by moving the fovea to that point. Once the movement is complete, the feature is inspected with higher attention before moving on to the next area of interest [13]. This gaze data can make an adaptive system more robust: a high correlation between gaze direction and pointing coordinates (mouse clicks or touch events) could indicate a high level of attention by the user.

To evaluate the attention level with respect to goal orientation, the IPM has been developed as a reference model. This fits perfectly to the MRAC approach and its reference model. The reference model serves as a reference for comparisons, e.g., to evaluate the deviation of users during a game. Combined with a metric, this allows the calculation of a distance value, the ideal path score (IPS), which reflects the user’s goal-orientedness. In a forthcoming contribution, this theoretical framework will be validated by assessing a suitable performance parameter.

3.5 Ideal Path Model (IPM)

The ideal path model (IPM) describes all necessary steps to achieve the goals of the game without unnecessary detours. Essentially, it is a sequence of episodes and interactions in an ILE that leads most directly to the next goal [33]. In an adventure game, for example, the ideal path would be the optimal passage, i.e., the optimal sequence of interactions from the start of the game to the end of the game. The building blocks of IPM comprise (Fig. 7):

1. Scene manifestations, which capture the current state of a scene. New scene states develop when the user interacts with the scene.
2. Interaction elements (IE), which are all game elements with which a player can interact.
3. Ideal path through the sequence of all scene manifestations and interaction elements, which can be seen as a reference model.
4. Actual path which reflects the actual sequence of steps a player has taken to interact with the game.
5. A metric which defines a distance $d_i : M \times M \rightarrow \mathbb{R}$ or deviation from an ideal path to an actual path.

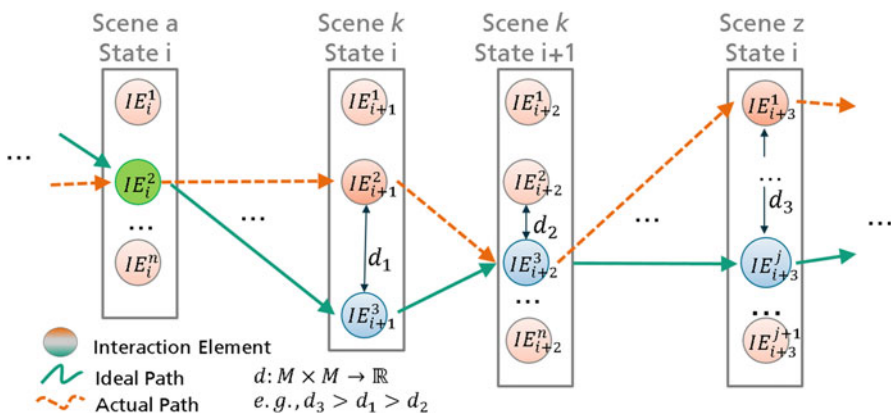


Fig. 7 Ideal path model with scene states, interaction elements, and distances

3.6 *Ideal Path Score (IPS)*

The ideal path score (IPS) supports the calculation of the users' progress, i.e., to calculate a performance score how well the used plays a game. It is a metric defined on the IPM and described the distance between an ideal path and an actual path. The score is normalized to $[-1; 1]$ to be invariant for different game genres or different users.

- $IPS = 1$ means a perfect move, congruent with an ideal path.
- $IPS = 0$ is a move without significant progress.
- $IPS = -1$ is a degrading move (negative progress), e.g., a move in the complete opposite direction.

For ILE with continuous moves, the IPS could be in $\{x | x \in \mathbb{R}, -1 \leq x \leq 1\}$. While the ideal path model is generic and can be modeled independently of the game, the IPS and its metrics are typically game-specific. In step-by-step games, for example, this could be a string similarity distance; or in a 3D shooter-type game, the metric could be a distance between waypoints.

3.7 *Ideal Path Model Creation*

A scene can have multiple manifestations for each possible interaction that a user can perform. The IPM can be built manually or automatically by recording the steps that an “optimal player” would take [32]. The recording of both the ideal path and all actual paths can be created using the data format *Experience API* (xAPI) [32]. The xAPI protocol records the experiences of the user while using an (e-learning) system. In its very core, xAPI is based on the W3C standard *activity streams*, so basically it is a (typically chronological) sequence of actions a user undertakes while using a software – such as an ILE – which includes an xAPI or activity stream tracker. Collections of such activity statements are used to form the ideal or actual paths through a ILE. It is worth mentioning that there is no fixated definition on the granularity of the events being tracked; it could range from micro-level mouse click tracking (lots of events) to macro-level tracking of whole usage episodes (very few events). Typically, for the e-learning or serious gaming context, one records meaningful learning experiences as xAPI statements, such as the start or end of a session or the completion of an assessment task, e.g., “John completed the assessment of image interpretation task 5.3.” Using xAPI all data can be stored in an xAPI-compliant database, a so-called learning record store (LRS).

3.8 Technical Concept

Following the generic input-processing-output model from systems theory, the input is the captured user interaction with the ILE, e.g., with a computer simulation or a (serious) game. To achieve easy applicability and interoperability, we propose to use the e-learning usage tracking standard *Experience API* (xAPI) which is based on the W3C standard *activity streams* [1]. The captured xAPI statements with the triple structure actor-verb-object act as measurement input to our adaptive learning system (ALS). We store these triples in a graph database. This offers several advantages, e.g., efficient analysis of relations (path finding, cluster detection, social network analysis, etc.) and flexibility due to the absence of fixed data models (it is a NoSQL database); or it brings with an easy and naturally understandable visualization as graphs for visual analysis.

3.9 Application

To apply control theory, we first need to define the involved processes and signals. We use the authors' proposed ALS architecture, as depicted in Fig. 8 [33]. It consists of three main parts: (1) the ILE; (2) a controlling interface which collects user interaction data and also modifies the ILE; and (3) the adaptivity controlling system including an interpretation engine for analysis and an influence engine for selecting the best adaptation strategy. The signals include the user interaction tracking data and the adaptation control messages. In general, as depicted in Fig. 9, an ALS

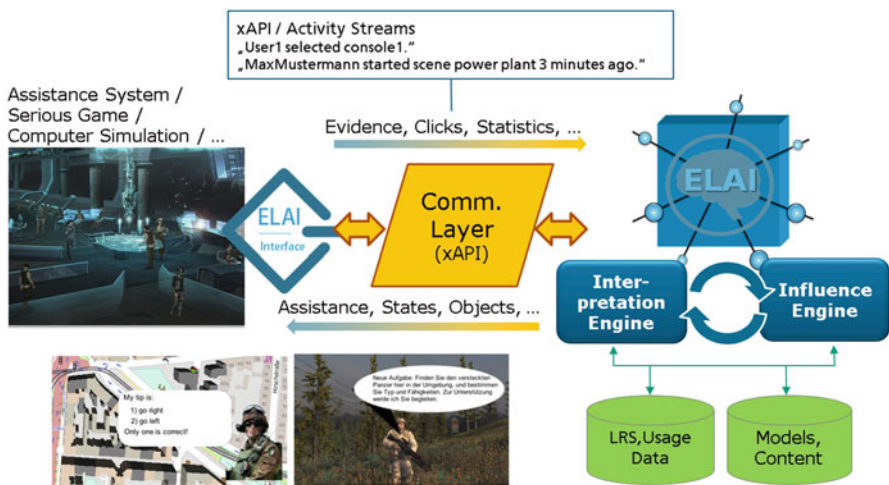


Fig. 8 Software architecture *E-learning AI* (ELAI) for adaptive interactive learning environments

Fig. 9 General scheme for adaptivity

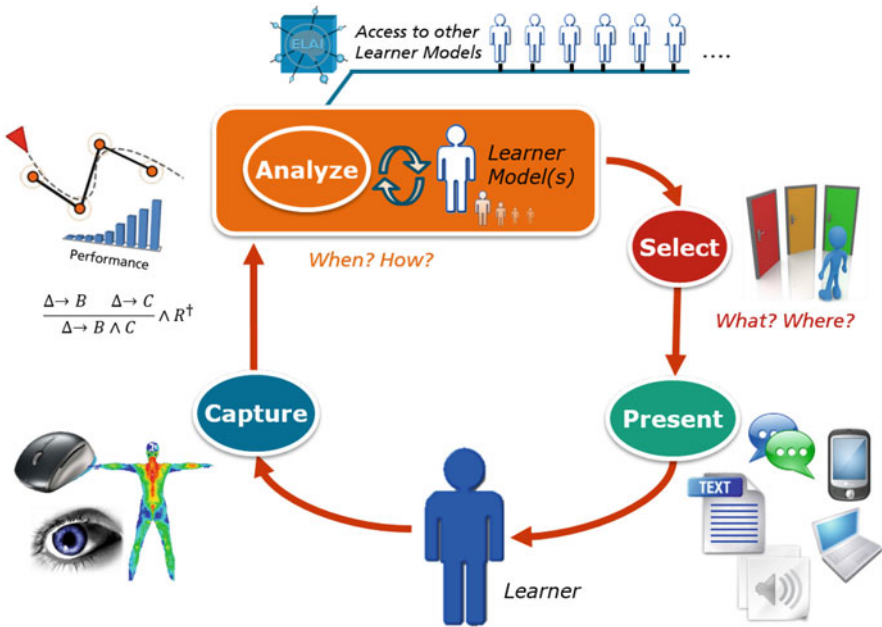
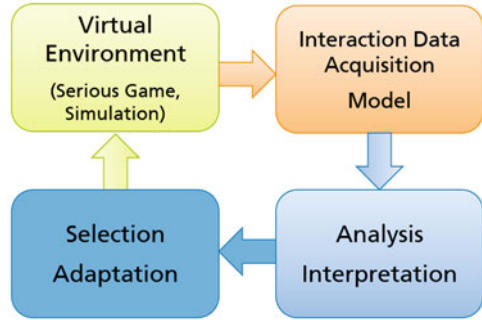


Fig. 10 Extended 4-phased adaptivity cycle

follows the scheme of (1) using an ILE like a serious game; (2) acquiring data from the ILE and on the user (a human tutor would observe the student); (3) interpreting that data with reference to models on the student, domain or teaching (like a human tutor); and (4) selecting appropriate adaptation strategies like recommending relevant learning material or modifying the ILE by dynamic difficulty adjustments. In the following and for process structuring of our adaptivity system, we follow an extended four-phased adaptivity cycle. It basically extends the model from Shute et al. [30] by combining the analysis phase and the learner models (from the current user and also from other users) (Fig. 10).

When applying control systems theory to our ALS architecture, we can see the ILE as the signal model which is to be controlled. Over time this model changes because it is being adapted to the user or, more precisely, toward the user model. Similar to the previous control system from the system perspective (Sect. 3.3, Fig. 5), we have the basic structure of an ILE back-end controller and a controlled ILE user interface. This is depicted in Fig. 6. The input r is the ILE in its current state; the output y is the next (adapted) state. In relation to MRAC, the reference model is the previously mentioned IPM plus a user or student model which takes as input the current state r and outputs a model of the desired output y_m . For the IPM this could be the next interaction element to take; for the user model, it could be information on suggested concepts (e.g., from player experience model or individualized knowledge tracing model). Inputs to the adaptive mechanism are the next state y , the reference models y_m , and also usage tracking data. Additionally the usage information should also contain assessment results. The controller parameters are when and how to adapt, e.g., given a virtual agent as one possible feedback mechanism, the adaptive mechanism controls the parameters the point in time this virtual agent should show up. This aspect will be elaborated in a forthcoming contribution.

4 Conclusion & Outlook

Disaster risk management (DRM) can benefit from applying serious games as motivational and engaging tools to foster disaster response competencies [31]. Whereas serious games for DRM are an active research topic [31], the number of *personalized or adaptive* interactive learning environments (aILE) is limited. The objective here is to benefit from adaptive serious gaming also for disaster risk management. This contribution presents the transfer of adaptive control to adaptive learning systems (ALS) with special focus on interactive learning environments like educational serious games (also known as digital game-based learning) or computer simulations. The general idea is to adapt systems theory and control theory to the control processes of ALS. An adaptive system must react to the user – it measures how the users interact with the system and modifies it in a way that the next inputs produce certain expected outputs. Since we deal with complex systems with nonlinear and stochastic processes, we propose to adopt adaptive control theory with reference models (MRAC). For aILE we use an ideal path model as a reference model for adaptive control.

The next steps are to detail the needed user modeling and the system's control parameters. For the former we propose to use flexible models consisting of semantic triple data structures and graph models; for the latter (control parameters), we follow the idea of using an ideal path model as reference model to detect deviations and to modify parameter ensembles derived from the theory of flow. Of further research interest is the applicability of multiple models as well as fuzzy adaptive control systems.

References

1. Advanced Distributed Learning (ADL): Experience API (xAPI) Specification, Version 1.0.1. Tech. rep., Advanced Distributed Learning (ADL) Initiative, U.S. Department of Defense (2013)
2. Arnold, S., Fujima, J., Karsten, A., Simeit, H.: Adaptive Behavior with User Modeling and Storyboarding in Serious Games. In: 2013 International Conference on Signal-Image Technology Internet-Based Systems. pp. 345–350 (2013)
3. Åström, K., Wittenmark, B.: Adaptive Control: Second Edition. Dover Books on Electrical Engineering, Dover Publications (2013)
4. Barreteau, O., Page, C.L., Perez, P.: Contribution of simulation and gaming to natural resource management issues: An introduction: Simulation & Gaming (2007). <https://doi.org/10/bj4x74>, <https://journals.sagepub.com/doi/10.1177/1046878107300660>
5. Benosman, M.: Learning-Based Adaptive Control: An Extremum Seeking Approach – Theory and Applications. Butterworth-Heinemann (Aug 2016)
6. Capuano, N., Mangione, G.R., Pierri, A., Lin, E.: Engaging e-learning for Risk Management: The ALICE Experience in Italian Schools. In: 2013 Seventh International Conference on Complex, Intelligent, and Software Intensive Systems. pp. 367–372 (2013). <https://doi.org/10.1109/CISIS.2013.67>
7. Chalam: Adaptive Control Systems: Techniques & Applications. Routledge (2017)
8. Chamasemani, F.F., Affendey, L.S.: Systematic review and classification on video surveillance systems. International Journal of Information Technology and Computer Science(IJITCS) **5**(7), 87 (2013)
9. Chen, J.: Flow in Games (and Everything else). Communications of the ACM **50**(4), 31–34 (Apr 2007)
10. Cruz, C.A., Ramirez Uresti, J.A.: Player-centered game AI from a flow perspective: Towards a better understanding of past trends and future directions. Entertainment Computing **20**, 11–24 (May 2017)
11. Csikszentmihalyi, M., Abuhamdeh, S., Nakamura, J.: Flow and the Foundations of Positive Psychology. Springer Netherlands (2014)
12. Dörner, R., Göbel, S., Effelsberg, W., Wiemeyer, J. (eds.): Serious Games – Foundations, Concepts and Practice. Springer International Publishing, Cham (2016)
13. Duchowski, A.T.: Eye Tracking Methodology: Theory and practice. Springer Nature (2007). <https://doi.org/10.1145/1117309.1117356>
14. Frutos-Pascual, M., Zapirain, B.G.: Review of the Use of AI Techniques in Serious Games: Decision Making and Machine Learning. IEEE Transactions on Computational Intelligence and AI in Games **9**(2) (2017)
15. Gampell, A., Gaillard, J.C.: Stop Disasters 2.0: Video Games as Tools for Disaster Risk Reduction. International Journal of Mass Emergencies and Disasters **34**(2) (2016), <https://researchspace.auckland.ac.nz/handle/2292/32960>
16. Ioannou, P., Sun, J.: Robust Adaptive Control. Courier Corporation (Sep 2013)
17. Kolb, D.: Experiential Learning: Experience as the Source of Learning and Development. Prentice Hall (1984)
18. Lagerstrom, R., Arzhaeva, Y., Szul, P., Obst, O., Power, R., Robinson, B., Bednarz, T.: Image Classification to Support Emergency Situation Awareness. Frontiers in Robotics and AI **3** (2016). <https://doi.org/10/ggqf53>
19. Landau, I.D., Lozano, R., M’Saad, M., Karimi, A.: Adaptive Control: Algorithms, Analysis and Applications. Springer Science & Business Media (Jun 2011)
20. Mäses, S., Hallaq, B., Maennel, O.: Obtaining Better Metrics for Complex Serious Games Within Virtualised Simulation Environments. In: European Conference on Games Based Learning. pp. 428–434. Academic Conferences Intern. Ltd. (2017)

21. Mossoux, S., Delcamp, A., Poppe, S., Michellier, C., Canters, F., Kervyn, M.: Hazagora: Will you survive the next disaster? – A serious game to raise awareness about geohazards and disaster risk reduction. *Natural Hazards And Earth System Sciences* **16**(1), 135–147 (2016). <https://doi.org/10.5194/nhess-16-135-2016>, <https://lirias.kuleuven.be/435182>
22. Nguyen, N.T.: *Model-Reference Adaptive Control: A Primer*. Springer (Mar 2018)
23. Nkambou, R., Azevedo, R., Vassileva, J. (eds.): *Intelligent Tutoring Systems, Lecture Notes in Computer Science*, vol. 10858. Springer (2018)
24. Oulhaci, M.A., Tranvouez, E., Fournier, S., Espinasse, B.: A MultiAgent Architecture for Collaborative Serious Game applied to Crisis Management Training: Improving Adaptability of Non Player Characters. *EAI Endorsed Trans. Serious Games* (2014). <https://doi.org/10.4108/sg.1.2.e7>
25. Pons, L., Bernon, C., Glize, P.: Scenario control for (serious) games using self-organizing multi-agent systems. In: 2012 IEEE International Conference on Complex Systems (ICCS). pp. 1–6. IEEE, Agadir, Morocco (Nov 2012)
26. Roller, W., Berger, A., Szentes, D.: Technology based training for radar image interpreters. In: 2013 6th International Conference on Recent Advances in Space Technologies (RAST). pp. 1173–1177. IEEE (Jun 2013)
27. Rumore, D., Schenk, T., Susskind, L.: Role-play simulations for climate change adaptation education and engagement. *Nature Climate Change* **6**(8), 745–750 (2016). <https://doi.org/10/f85gkp>, <https://www.nature.com/articles/nclimate3084>
28. Sampayo-Vargas, S., Cope, C.J., He, Z., Byrne, G.J.: The effectiveness of adaptive difficulty adjustments on students' motivation and learning in an educational computer game. *Computers & Education* **69** (Nov 2013)
29. Sastry, S., Bodson, M.: *Adaptive Control: Stability, Convergence, and Robustness*. Prentice-Hall Advanced Reference Series (Engineering) (1994)
30. Shute, V., Zapata-Rivera, D.: Adaptive educational systems. *Adaptive technologies for training and education* **7**(1), 1–35 (2012)
31. Solinska-Nowak, A., Magnuszewski, P., Curl, M., French, A., Keating, A., Mochizuki, J., Liu, W., Mechler, R., Kulakowska, M., Jarzabek, L.: An overview of serious games for disaster risk management – Prospects and limitations for informing actions to arrest increasing risk. *International Journal of Disaster Risk Reduction* **31**, 1013–1029 (2018). <https://doi.org/10/gff4sn>, <http://www.sciencedirect.com/science/article/pii/S2212420917304090>
32. Streicher, A., Bach, L., Roller, W.: Usage Simulation and Testing with xAPI for Adaptive E-Learning. In: 14th European Conference on Technology Enhanced Learning, EC-TEL 2019. pp. 692–695. Springer, Delft (2019)
33. Streicher, A., Roller, W.: Interoperable Adaptivity and Learning Analytics for Serious Games in Image Interpretation. In: *Data Driven Approaches in Digital Education: 12th European Conference on Technology Enhanced Learning, EC-TEL 2017, Proceedings*. vol. 10474 LNCS, pp. 598–601. Springer International Publishing, Tallinn, Estonia (2017)
34. Streicher, A., Smeddinck, J.D.: Personalized and Adaptive Serious Games. In: R. Dörner et al. (ed.) *Entertainment Computing and Serious Games: International GI-Dagstuhl Seminar 15283, Dagstuhl Castle, Germany, July 5–10, 2015, Revised Selected Papers*, pp. 332–377. Springer International Publishing, Cham (2016)
35. Van Eck, R.: Building Artificially Intelligent Learning Games. In: Gibson, D., Aldrich, C., Prensky, M. (eds.) *Games and Simulations in Online Learning: Research and Development Frameworks*, pp. 271–307. IGI Global (2007)
36. Woolf, B.P.: *Building Intelligent Interactive Tutors*. Morgan Kaufmann (2009)
37. Yannakakis, G.N.: Game AI revisited. In: *Proceedings of the 9th Conference on Computing Frontiers – CF '12*. p. 285. ACM Press, Cagliari, Italy (2012)

A Simulation Model for the Analysis of the Consequences of Extreme Weather Conditions to the Traffic Status of the City of Thessaloniki, Greece



Georgios Tsaples, Josep Maria Salanova Grau, Georgia Aifadopoulou, and Panagiotis Tzenos

Abstract Natural disasters such as flooding and snow blizzards have evolved from a relatively rare event to a recurring concern for stakeholders, policy makers, and citizens. A special place in this debate is held by the transportation infrastructure; it provides services crucial to a society, and it can yield positive effects to the overall economy due to its interrelation with the urban activities. Finally, due to the increasing trend of urbanization, people are having an increasing dependence on urban transportation.

Consequently, extreme weather conditions could severely impact not only the operation of the transportation infrastructure (network and means) but also the economic activity of a city. Hence, there is the need for a framework that will allow decision-makers, on the one hand, to monitor in real time the status of the transportation network and on the other hand offer them insights on how a critical event, such as a flooding, could affect it before it does.

The purpose of this paper is to present such a tool that allows for efficient and effective monitoring of the status of the transportation network and crisis management in the case of a flooding.

To achieve the objective, two methodological frameworks will be combined: data analytics and simulation. Floating car data (FCD) from a fleet of taxis in the city of the Thessaloniki offer a glimpse on the status of the transportation network. The KPIs that are produced from the data are used as an input to a simulation model. The model has been developed with the methodology of system dynamics, because it allows for the adequate representations of complex systems (such as the transportation infrastructure), it offers a top-down view on the behavior of the system over time, and it can be easily communicated to non-experts.

The model also simulates the physical process of rain and snow, and the user can define how much rain and snow and at which times of the day it will fall. The water accumulates in the road network affecting the speed of the vehicles, and the larger

G. Tsaples (✉) · J. M. S. Grau · G. Aifadopoulou · P. Tzenos
Hellenic Institute of Transport, Thessaloniki, Greece
e-mail: gtsaples@certh.gr; jose@certh.gr; gea@certh.gr; ptzenos@certh.gr

the amount of water the more difficult it is for the sewage system to remove it, thus resulting in flooding roads.

Several scenarios were simulated, mainly trying to capture the dynamics of sudden rainfall and flooding. The results illustrate that there is a disproportional delay between the time that the rain stops and the time it is required for the system to bounce to an equilibrium.

Keywords System dynamics · Simulation · Flooding · Crisis · Urban transportation

1 Introduction

The city of Thessaloniki, Greece, is regularly suffering from flooding that makes traffic conditions dire and hinders the movement of passengers. The latest such event occurred on September of 2019 [6] when the streets flooded from an extreme and intense downpour. The event was not unique; similar situations happened on May of 2018. Furthermore, the event is limited neither in the city of Thessaloniki nor in the country of Greece. For example, Italy suffers from floods that cause traffic chaos and material damages and injuries [7], while human loss was the devastating effect of the catastrophic flood in Texas [22].

Thus, extreme weather conditions – such as flooding or snow blizzards – that were once considered events of low probability [17] have become a recurring concern for local authorities, high-level policy makers, and citizens alike [10].

A special place in this concern is held by the urban transportation sector due to its inherent importance; it provides services crucial to a society, and it can yield positive effects to the overall economy due its interrelation with the urban activities [1, 14]. This importance increases due to the increasing trend of urbanization, which will result in more and more people being dependent on an efficient urban transportation system [13].

Hence, there is the need for an extra level of preparedness since the ongoing climate change will result in more and more extreme weather conditions; decision-making on an urban environment needs to change from reactive to proactive and embrace crisis management as its core framework, in order to deal with potential consequences before, during, and after an extreme weather event [3].

The purpose of this paper is to present a decision support tool that allows for efficient and effective monitoring of the status of the transportation network and crisis management planning in the case of a flooding. To achieve the objective of the paper, a simulation model is developed and combined with real-time floating car data from a fleet of taxis in the city of Thessaloniki.

The rest of the paper is organized as follows: General information on such critical events, the methodology, and the simulation model structure are presented. Following in the next section, results are described and analyzed, while conclusions and future research directions are presented in the final part of the document.

2 Methodology

A flooding can be considered a crisis in general, in the sense that it may occur suddenly and with intensity, it requires one or more rapid decisions to avoid negative consequences, and there is no knowledge whether these particular decisions will have a negative or positive effect [17]. Thus, decision-making in such a context becomes even more complex than normal since the environment and the decisions are interrelated and subsequent changes may occur due to the decisions or independently [5, 9, 16].

Moreover, the complexity increases due to the inherent nature of the transportation system (or any urban system for that matter). It entails a large number of components that are connected causally, it involves different time scales and feedback loops, and finally, at its core it depends on the human behavior.

Thus, simulation can aid decision-makers with grasping the full scale of such a system and how it may be affected by a flood. Simulation models are representations of reality, which:

- Offer such insights
- Help decision-makers to gain experience in a consequence-free environment
- Allow the experimentation of different scenarios
- Can account for different perspectives [24]

Consequently, a search was performed in scientific databases using the terms “simulation,” “transportation system,” and “flooding” in different combinations and synonyms. The search was further refined by studying the abstract of the results to check for relevance with the subject matter. The final set includes the following papers.

Kermanshah et al. [12] used GIS data with a network science approach to simulate flooding scenarios and their effects for the city of Chicago. Armenia et al. [2] used system dynamics enhanced with a user interface to create an interactive learning environment to train managers on how a flooding can affect the energy, transportation, and telecommunication system of a city.

Jordan et al. [11] similarly used system dynamics, however including in their research the interrelation between the road and rail networks of an urban environment. The authors used simulation to estimate the times of appropriate closure and the subsequent costs of these closures on crossings and routes in case of a flood.

Armenia et al. [3, 4] used system dynamics to research the effects of critical events (including floods and terrorist attacks) on an urban transportation system and the domino effects that it might generate on the business community. Zhu et al. [25] on the other hand investigated the system from a bottom-up approach and, by using an agent-based model, investigated how drivers’ behavior is affected by a flood and used the area of Lishui, China, as a reference.

Song et al. [19] used the qualitative branch of system dynamics, i.e., causal loop diagrams to research causal relations and resilience in the urban environment of Busan, Republic of Korea, among its various sectors. Yang et al. [23] utilized GIS

data to identify how large-scale floods in the Arakawa River of Tokyo can affect inter-firm transactions in the area. Finally, Pyatkova et al. [15] used a microscopic traffic model to gain insights on the traffic disruption and its effects under different flooding scenarios.

No claim is made that the above research is exhaustive, nonetheless several interesting findings can be seen. First, the interactions between floods and the transportation system have not been extensively studied so far; a conclusion also held by Pyatkova et al. [15]. Furthermore, system dynamics is the methodology used in the majority of the papers, while only recently, with the increasing availability of data and advancements in computational power, (big) data are considered as a viable tool for this type of research. Consequently, the current paper contributes to the literature by offering a simulation model that combines big data and system dynamics to investigate the effects of different flooding scenarios in the city of Thessaloniki, Greece. It should also be noted that the simulation model relies on and expands the model developed by Armenia et al. [2].

2.1 System Dynamics

System dynamics [8, 20] is a computer-based methodology that uses ordinary differential equations to model the behavior of systems over time. It relies on the framework of systems thinking [18] to generate insights into how this behavior might be altered if different policies are applied to it [21].

The methodology offers further advantages as it can incorporate randomness, which characterizes the behavior of all transportation systems. Moreover, it can simulate the so-called soft variables – variables that are not easily quantified such as those associated with human behavior. Thus, system dynamics assumes that if the structure of the system under study is captured accurately enough, then the insights that will be provided by the simulation can be more helpful than a deterministic analysis. Finally, the qualitative arm of the methodology (causal loop diagrams) can be used as a communication tool to illustrate the decision-making process to non-experts.

2.2 Model Structure

The simulation model that was developed in the context of the paper combines data analytics and system dynamics simulation. Floating car data (FCD) from a fleet of taxis in the city of the Thessaloniki offer a glimpse on the status of the transportation network. The data are analyzed and two types of KPIs are produced: firstly, metrics such as average speed (real-time information from the taxis, aggregated) for the entire road network of the city, volumes of vehicles (inferred by combining average speed from the taxis and historical data), and a traffic KPI defined as the volume of

vehicles in (every) part of the road network compared to the theoretical capacity of that particular part. Furthermore, the above KPIs can be combined to investigate the trends on a longer time horizon, which results in an origin-destination matrix for the various geographical zones of the city.

The KPIs that are produced from the data are used as an input to a simulation model. The simulated urban environment is divided into geographical zones, each of which has internal characteristics such as population density, area of the road network and its characteristic, public transport stops, extent of the sewage system, available parking spaces, etc. Thus, the simulated model accounts only for public means (mainly buses) and private transportation (cars, taxis) since the city of Thessaloniki does not yet have a metro network.

The KPIs from the data determine the behavior of the simulation model. The origin-destination matrix determines how people move among the various zones; the average speed and vehicles volumes determine the status of the road network and what remains from the population is using public means of transport. Furthermore, the model allows for the closing of roads in each geographical zone and the introduction or withdrawal of public vehicles. This allows for the dynamic allocation/movement of people: depending on the level of service of each available transport mode, a passenger may choose buses – if the service level is adequate – or use a private vehicle. The use of system dynamics also allows the incorporation of “soft factors” in that determination, factors such as habit, comfort, etc. As a result, the focus of the model is on the structure of the transportation system and how it determines the overall behavior. Figure 1 illustrates the main elements of the transportation part of the model.

In more detail, each geographic zone in the model entails a road network that is formed by major (large capacity of vehicles per kilometer) and minor (small capacity of vehicles per kilometer) roads. Important elements of the road network are those points that connect the zones. They can be considered as focal points

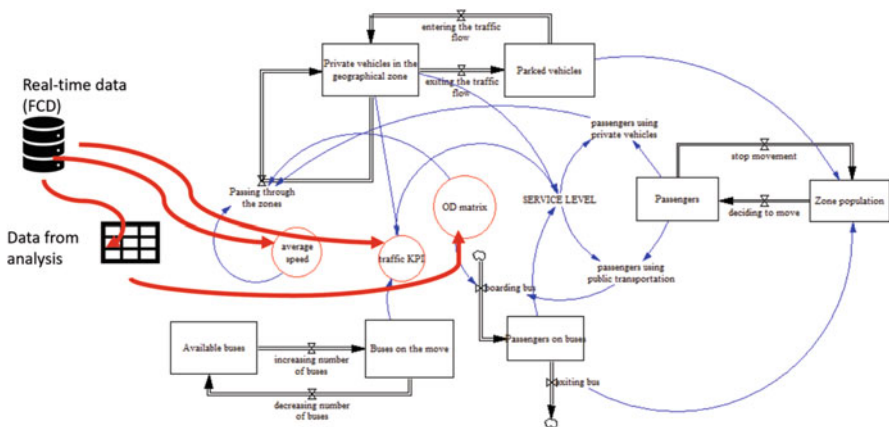


Fig. 1 General structure of the simulation model

in the network and their determination was performed manually with the map of the city. As a result, the movement of cars among the zones is determined by the origin-destination matrix (generated by the floating car data), the zone capacity (determined by the roads), and the percentage of cars that can pass per minute through the focal points.

Once inside the zone, a percentage of cars is moving to go to another zone, while the rest are looking for a parking place inside the zone. The parking capacity of each zone was determined by the available data from the municipality of Thessaloniki, multiplied by a random factor. Hence, vehicle movement is dynamic and dependent only by the internal structure of the model. This dynamic model allows the emergence of new behavior if, for example, new origin-destination matrices are generated by the FC data, due to an unexpected event.

Up until the development of the model, the city of Thessaloniki did not yet have a metro/subway network, and public transportation was performed only by buses. Thus, the buses' movement in the model is similar to that of the private vehicles.

Regarding the socio-demographic aspect of the model, each zone has a population, percentage of which travels either for leisure or business among the various zones. Data from the city of Thessaloniki was chosen as a reference case. Figure 2 below illustrates the travel demand derived from data from CERTH-HIT.

As it can be expected, two peaks are observed in the beginning of the day and early in the afternoon, coinciding with the general times that people move to and from their place of work. However, the figure below does not separate between the types of activity that might result in a trip. For that reason, in the context of the model, the above graph was separated into two, one for people that travel for business and one for people traveling for leisure (Fig. 3).

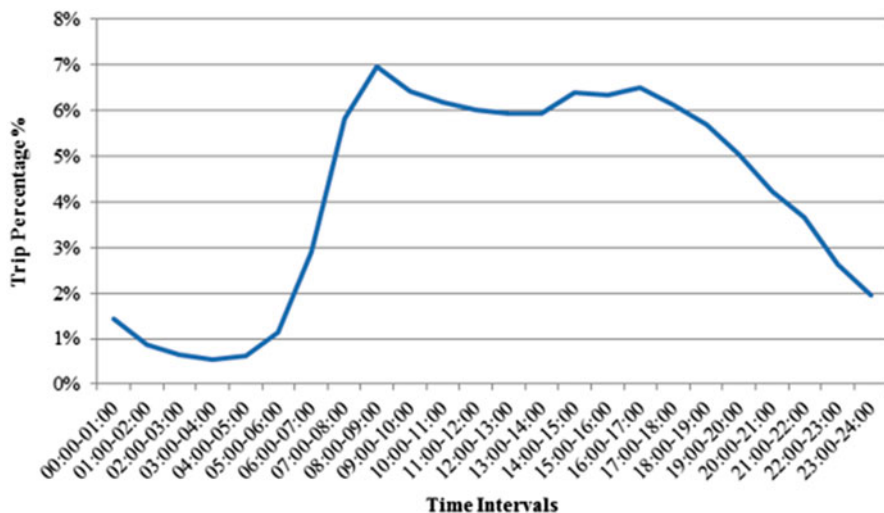


Fig. 2 Travel demand for the city of Thessaloniki

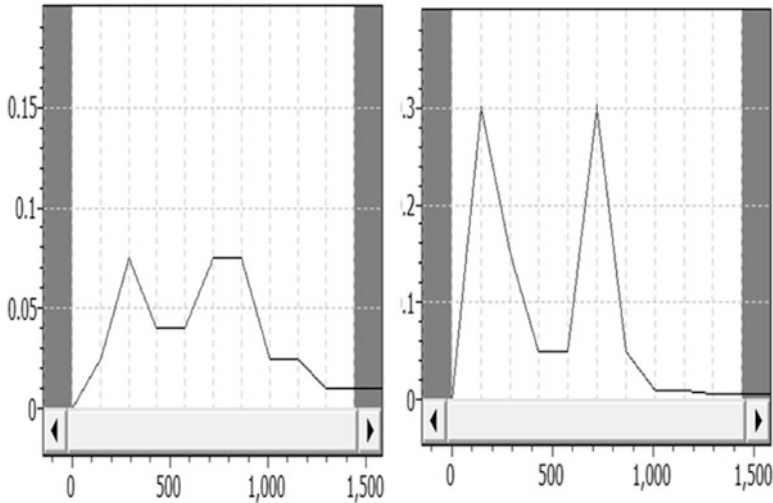


Fig. 3 Travel demand in the model for passengers traveling for leisure (left) and business (right)

Finally, the simulated passengers choose what means of transport they will use based on the utility of each one; the following factors are normalized to form the utility:

- Habit: a random number between 0 and 1.
- Road accessibility: counting the number of roads that are open compared to the sum of all roads in the zone.
- Perception of traffic KPI: a delayed number that is generated by the FCD.
- Parking availability: a delayed number that is generated by the number of empty parking spots compared to the total parking spots of a zone (multiplied to a random number).
- Comfort: a qualitative factor between 0 and 1. For private transportation it is a fixed number (above 0.5), while for public transportation it is calculated by the number of passengers on buses divided by their total capacity.
- Frequency of buses: it is used only when the utility of public transportation is calculated.

As a result, the choice of transport mean is dynamic and internal in the model, and it is decided by the current state of the system during the simulation steps. Finally, the model is simulated for 72 h.

In conclusion, the model attempts to capture the dynamics of the transportation sector of Thessaloniki during 3 (working) days. The model is assisted by data gathered from the city, but every “choice” that affects the overall behavior is decided internally based on the status of the model.

3 Results

The simulated model is tested under two different scenarios: In the first one (Scenario 1), the rain starts falling during the morning hours of the first day; it lasts for only a few hours and it stops. In the second scenario (Scenario 2), there is heavy rain from the beginning of the simulation that lasts for 1 full day. Figure 4 illustrates how the different types of rain are simulated in the model. The vertical axis depicts the mm of rain, while the duration is depicted at the horizontal axis.

Finally, the simulated city is separated into 15 zones, but for reasons of clarity only the results from zone that corresponds to the city center will be displayed.

3.1 Scenario 1 Results

The simulated result of the first “type of rain” is that the water level does not exceed an (hypothetical) alarm threshold that is used in the model to signal when the roads start to gather water. As a result, the water level on the road network persists – although at low levels – for the entire period of the simulation time, but it does not create significant problems (Fig. 5).

The result from that (persistent) low level of water is that the traffic is high during the hours that the demand for travel is high and falls otherwise (Fig. 6). This result does not differ from the “business as usual” scenario where there is no rain.

However, the travel times become slower which results in smaller periods of low traffic KPI (illustrated with the black circles on Fig. 6). The low water levels on the road network force the cars and buses to travel at lower speeds; thus more time is

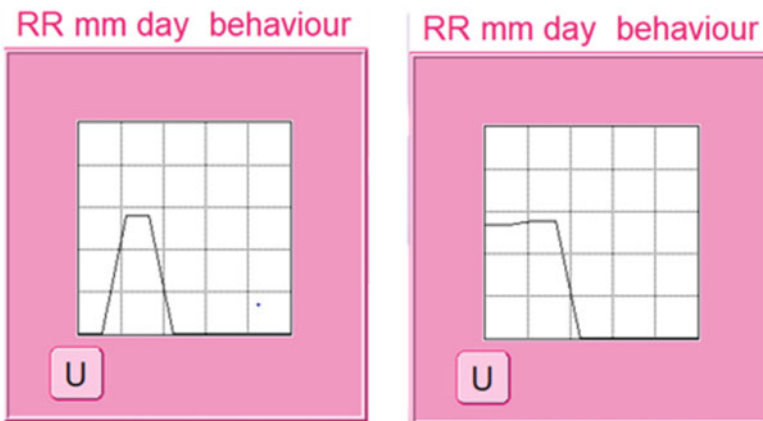


Fig. 4 Scenario 1 (left); Scenario 2 (right)

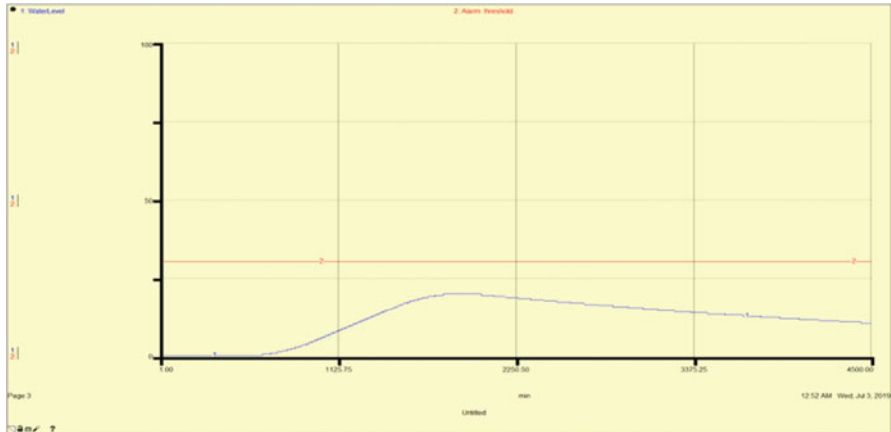


Fig. 5 Water level on the road network compared to the alarm threshold

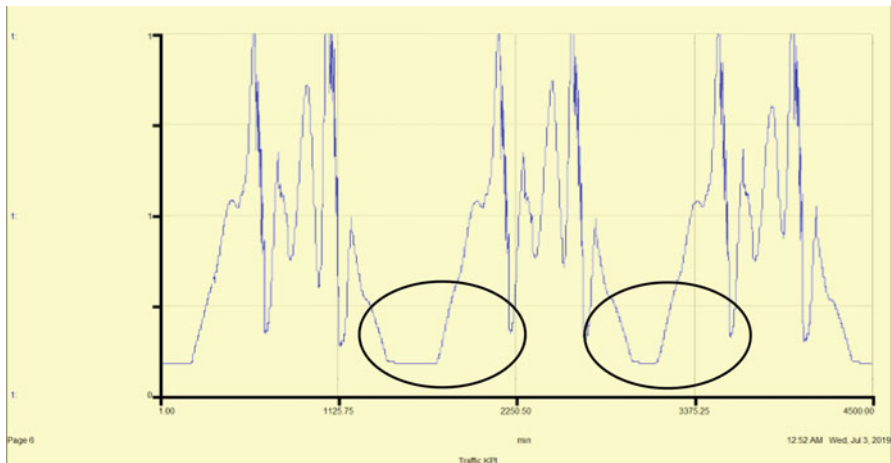


Fig. 6 Traffic KPI for zone 1 of the model (city center)

required to go from their origin to their destination. Consequently, more cars remain on the road for more time, which results in smaller periods of low traffic.

In conclusion, a “light” rain does not have significant effects on the transportation sector apart from larger periods of traffic. What is interesting is that the effects do not occur during the rain but persist after it has stopped.

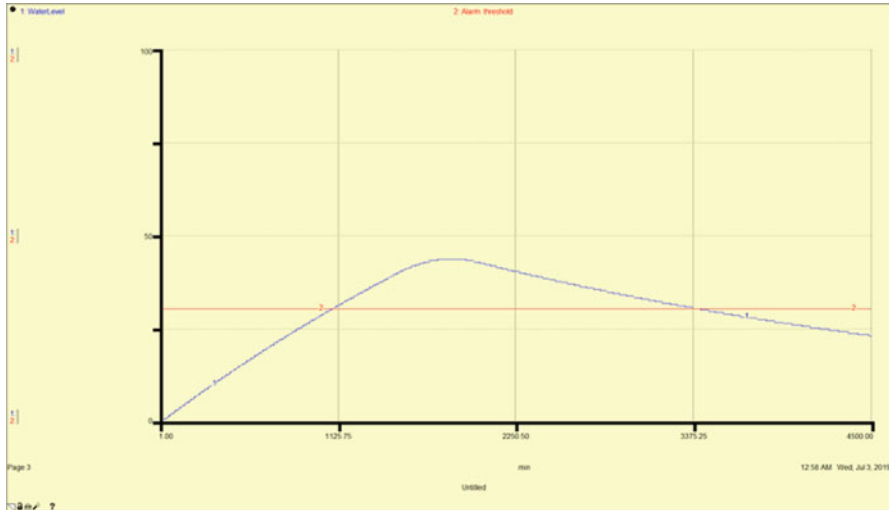


Fig. 7 Water level on the road network compared to the alarm threshold for Scenario 2

3.2 Scenario 2 Results

In the second scenario, “heavy” rain falls from the beginning of the simulation. This results in the water level being above the alarm threshold and the road network suffers from flooding. Figure 7 illustrates that the water level remains in high levels long after the rain has stopped and only at the latest stages of the simulation time it falls beneath the threshold. However, even then it is relatively high and, in any case, higher than any time of the first scenario.

The higher levels of water result in almost a standstill on the road network of zone 1. The network reaches almost its full capacity; similar to the first scenario, this occurs after the rain has stopped falling. Figure 8 illustrates the two scenarios that were simulated along with the “business-as-usual” scenario. The pink line of Scenario 2 shows that the traffic remains at alarmingly high levels until the end of the simulation time due to the water levels that take time to fall beneath the alarm threshold.

Compared to Scenario 1 (red line in Fig. 8), which resembles the basic scenario (blue line), Scenario 2 has the most severe effects on the road network, and since there is no subway, the effects do not concern only private transportation but public transportation as well. To illustrate the effect on buses, Fig. 9 below maps the service level of buses for the three scenarios.

The basic scenario (blue line) and Scenario 1 (red line) have similar results, with the service level being at its lowest during the peak of travel demand. Variations between the two results can be attributed to the slightly longer travel times that are observed in Scenario 1. However, in Scenario 2 the service level reaches the lowest

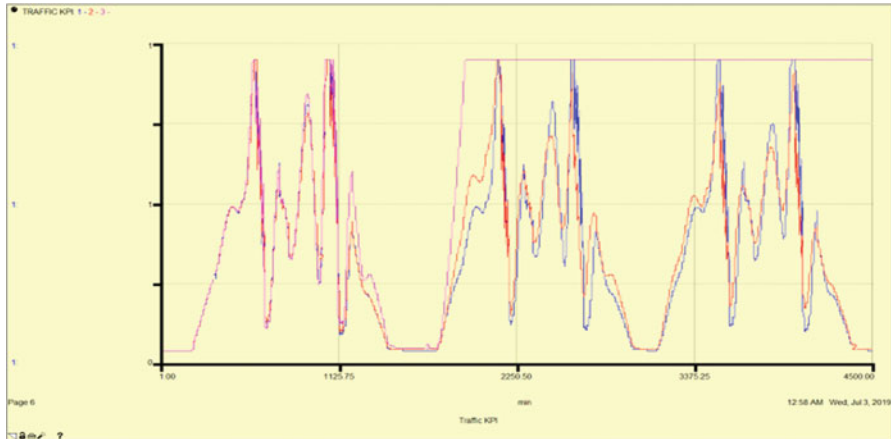


Fig. 8 Traffic KPI for business-as-usual scenario (blue), Scenario 1 (red), Scenario 2 (pink)

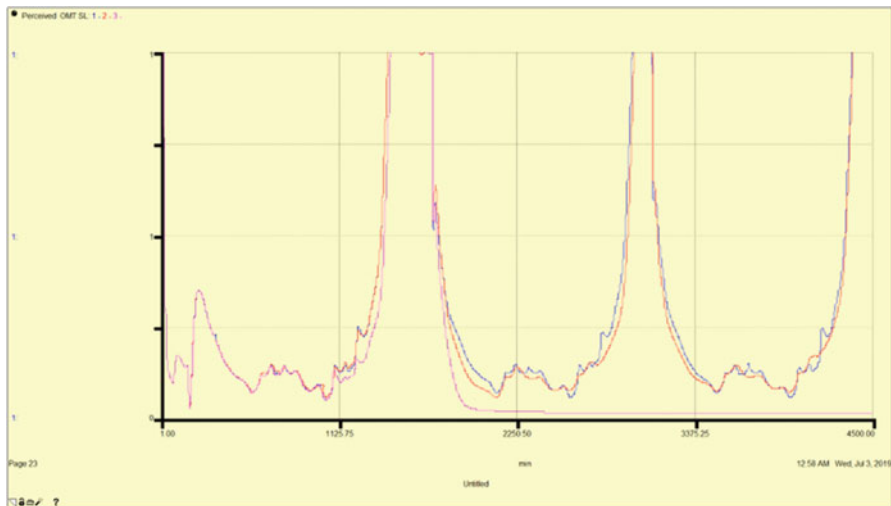


Fig. 9 Public transport service-level KPI for business-as-usual scenario (blue), Scenario 1 (red), Scenario 2 (pink)

point (for all three scenarios) and does not rebound to normal values during the remaining of the simulation time.

In conclusion, for both scenarios the most interesting results stem from the delay between the rain and the manifestation of the effects on the transportation network. Due to the slow descent of the water levels, the effects take time to manifest and to fade out completely. Comparing it with the real situation that occurred in Thessaloniki in 2018, the model reproduces the situation in the roads of the city

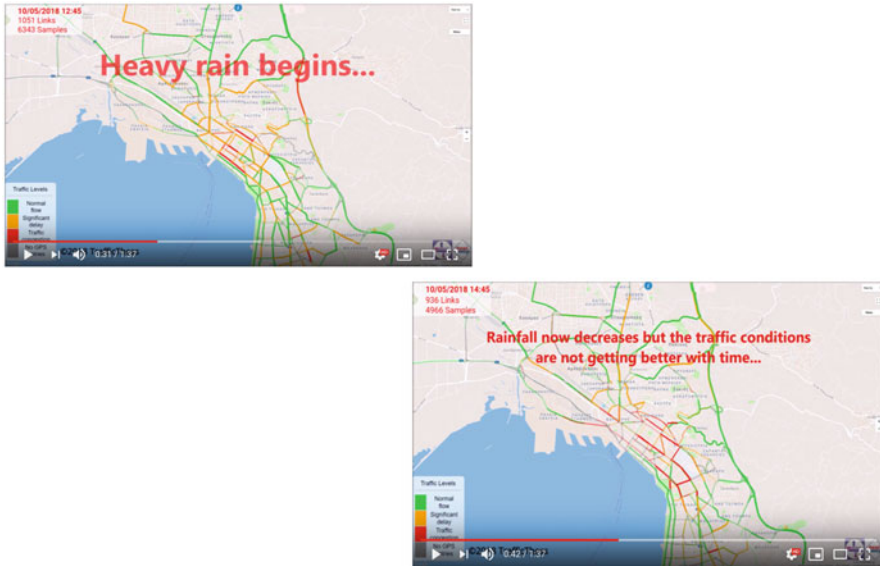


Fig. 10 How the flooding was captured by real-time data

center; despite the decrease in the amount of rain, the traffic conditions were not improving with time (Fig. 10).¹

4 Conclusions

Floods in urban environments are becoming increasingly common phenomena around the world every year. Their consequences on the transportation sector can be severe and last for days, with the potential to create domino effects to other sectors and even lead to human losses. As a result, policy makers need to integrate their decision-making process regarding the transportation sector in a crisis management framework. This shift will assist them in reaching effective decisions before, during, and after a crisis (flood).

The purpose of this paper was to assist policy makers by proposing a simulation model that can act as a decision support tool and provide insights on the monitoring of the transportation sector during a flood. The model uses data from a fleet of taxis in Thessaloniki, Greece, as input and captures the dynamics of passenger movement in an internal way.

¹<https://www.youtube.com/watch?v=uX0o1kax8sU>

The model was tested for two different scenarios that simulate different types of rain. The results indicate that the consequences can be seen long after the rain has stopped and can last for long periods resulting in a transportation system with extremely low level of service and in a state of disequilibrium.

Future directions of the current research include the studying of the effects to other zones of the simulated city, how the effects can move from one zone to another, etc., in other words, increasing the robustness of spatial dimension of the model. Furthermore, potential policies and countermeasures can be tested in the model and provide insights on which work (along with where in the city they work better) and which produce counter-intuitive results. Finally, a user interface and more interactive and intuitive graphical results would increase the communication value of the model and allow it to be used by non-experts. Finally, validation and verification efforts will continue to be indispensable parts of any direction that the model will follow.

References

1. Abbas, K. A. (1990). The use of system dynamics in modeling transportation systems with respect to new cities in Egypt. *System*, 17.
2. Armenia, S., Tsaples, G., & Carlini, C. (2015). Interactive learning environments for crisis management through a system dynamics approach. *Proceedings of the 15th European Academy of Management (EURAM) Conference*. 66. EURAM.
3. Armenia, S., Tsaples, G., & Carlini, C. (2018). Critical Events and Critical Infrastructures: A System Dynamics Approach. *Lecture Notes in Business Information Processing*, 313, 55–66.
4. Armenia, S., Tsaples, G., Carlini, C., Volpetti, C., Onori, R., & Biondi, G. (2017). A system dynamics simulation tool for the management of extreme events in urban transportation systems. *International Journal of Critical Infrastructures*, 13(4), 329–353.
5. Edwards, W. (1962). Dynamic decision theory and probabilistic information processings. *Human factors*, 4(2), 59–74.
6. eKathimerini. (2019, September 20). *Heavy rainfall provokes floods in Thessaloniki*. Retrieved September 23, 2019, from <http://www.ekathimerini.com/244733/article/ekathimerini/news/heavy-rainfall-provokes-floods-in-thessaloniki>
7. Euronews. (2014, November 16). Retrieved September 23, 2019, from <https://www.euronews.com/2014/11/16/heavy-rains-wreak-havoc-along-swiss-italian-border>
8. Forrester, J. (1997). Industrial dynamics. *Journal of Operational Research Society*, 48(10), 1037–1041.
9. Gonzalez, C., Vanyukov, P., & Martin, M. (2005). The use of microworlds to study dynamic decision making. *Computers in human behavior*, 21(2), 273–286.
10. Hinssen, P. (2010). *The New Normal*. Mach Media NV.
11. Jordan, P., Nathan, R., Weeks, W., Waskiw, P., Herron, A., Cetin, L., . . . Russell, C. (2015). Estimation of flood risk for linear transport infrastructure using continuous simulation modelling. *36th Hydrology and Water Resources Symposium: The art and science of water* (p. 1441). Engineers Australia.
12. Kermanshah, A., Karduni, A., Peiravian, F., & Derrible, S. (2014). Impact analysis of extreme events on flows in spatial networks. *IEEE International Conference on Big Data (Big Data)* (pp. 29–34). IEEE.
13. Miller-Hooks, E., Zhang, X., & Faturechi, R. (2012). Measuring and maximizing resilience of freight transportation networks. *Computers & Operations Research*, 39, 1633–1643.

14. Nowacki, G. (2014). Threat assessment of potential terrorist attacks to the transport infrastructure. *TransNav: International Journal of Marine Navigation and Safety of Sea Transportation*, 8.
15. Pyatkova, K., Chen, A., Butler, D., Vojinović, Z., & Djordjević, S. (2019). Assessing the knock-on effects of flooding on road transportation. *Journal of environmental management*, 244, 48–60.
16. Qudrat-Ullah, H., & Karakul, M. (2007). Decision making in interactive learning environments towards an integrated model. *Journal of decision systems*, 16(1), 79–99.
17. Sayegh, L., Anthony, W., & Perrewé, P. (2004). Managerial decision-making under crisis: The role of emotion in an intuitive decision process. *Human Resource Management Review*, 14(2), 179–199.
18. Senge, P. (2006). *The fifth discipline: The art and practice of the learning organization*. Broadway Business.
19. Song, K., You, S., & Chon, J. (2018). Simulation modeling for a resilience improvement plan for natural disasters in a coastal area. *Environmental pollution*, 242, 1970–1980.
20. Sterman, J. (2000). *Business Dynamics: Systems Thinking and Modeling for a Complex World*. Boston: Irwin/McGraw-Hill.
21. Tsaples, G., & Armenia, S. (2016). Studying pension systems and retirement age: a simple system dynamics model for a complex issue. *International Journal of Applied Systemic Studies*, 6(3), 258–270.
22. Villarreal, M. (2019, September 20). *CBS News*. Retrieved September 23, 2019, from <https://www.cbsnews.com/news/imelda-death-toll-rises-from-catastrophic-floods-texas-today-2019-09-20/>
23. Yang, S., Shibasaki, R., Ogawa, Y., Ikeuchi, K., & Akiyama, Y. (2018). Estimation of the economic impact of large-scale flooding in the Tokyo metropolitan area. *IEEE International Conference on Big Data (Big Data)* (pp. 3191–3200). IEEE.
24. Zhang, P., & Peeta, S. (2011). A generalized modeling framework to analyze interdependencies among infrastructure systems. *Transportation Research Part B: Methodological*, 45(3), 553–579.
25. Zhu, J., Dai, Q., Deng, Y., Zhang, A., Zhang, Y., & Zhang, S. (2018). Indirect damage of urban flooding: Investigation of flood-induced traffic congestion using dynamic modeling. *Water*, 10(5), 622.